IRON OXIDE REDUCTION
WITH FLUX ADDITIONS

A thesis
presented for the degree of
Doctor of Philosophy
of the
University of London
and for the Diploma of the Imperial College

by

HYOUNG-KY SHIN

John Percy Reseach Group
Department of Metallurgy and Materials Science
Imperial College of Science and Technology
London S.W.7 2BP

April 1984

ABSTRACT

The reduction of Carol Lake iron ore concentrates has been studied with and without additions of the fluxing agents, lime, magnesia and dolomite. Flux additions in the range from 1 to 5 wt.% were investigated in the temperature range 950-1100^{o}C. The major interest of this study relates to the kinetics of reduction to iron for which a thermogravimetric technique was used. The morphology of reduced and partially reduced specimens was studied using optical and electron microscopic techniques. The phases present in each specimen are characterised by X-ray diffraction technique. In addition, the surface area of several typical samples was measured by the B.E.T. technique.

Most of the present work has concentrated primarily on the kinetics of reduction and the morphology of phases with the major interest in understanding the variation of reduction with time and temperature in terms of rate processes and morphology of the reduced oxide and flux additions.

The rate of reduction increased with increasing reduction temperature and the concentrate powder reduced at a lower rate than compacts especially at low temperature due to stronger sintering, while swelling and cracking occurred with the compacts.

The formation of fayalite was observed in most of the specimens except those with lime and dolomite additions.

The major effect of lime additions on reduction is the formation of a liquid phase. At low temperatures, the reduction rate decreased markedly due to the blockage of pores while a slight increase in rate was observed at high temperatures. For 5% CaO additions, a small increase in reduction rate is observed due to the presence of CaO in solid solution in the wustite phase.

Magnesia additions gave faster rates at all temperatures than the iron ore compacts or those with lime additions and increasing the amount of magnesia also increased the rate of reduction. Magnesioferrite formed during sintering and precipitation of hematite occurred during cooling preferentially on sub-grain-boundaries or in a specific crystallographic direction. Significant carbon deposition occurred in the specimens before complete reduction is achieved. Magnesiowustite reduced more rapidly than wustite due to the ease of iron nucleation over the whole surface.

Dolomite additions produced effects which can be related to both lime and magnesia. A liquid phase was formed during sintering and mainly consisted of augite. The magnesioferrite which was crystallized from the liquid phase was reduced from the surface of the grains forming a thick iron shell and the concentration of MgO in the grains increased considerably due to the diffusion of MgO. Upon wustite formation at 1100^{o}C, the formation of another liquid in the CaO-MgO-SiO_2 system is observed and produces similar effects to the corresponding liquid in the lime system.

CONTENTS Page

LIST OF FIGURES

Page

Page

Page

Page

LIST OF TABLES

Page

LIST OF PLATES

Page

Page

CHAPTER 1

INTRODUCTION

CHAPTER 1

INTRODUCTION

There are many systems of practical importance in metals and materials processing operations where a solid phase is made to react with a gas mixture, one or more components of which participate in the reaction. In the reduction of iron oxides with carbon monoxide and hydrogen or their mixtures, the mathematical formulation of a so called general rate equation is considered not to explain the overall reaction phenomena completely. Because of the apparent complexity of the rate process, further more, there are large number of variables, including the nature and flow rate of the reducing gas, the chemical composition and physical properties of the ore, the temperature of reaction, all of which can affect both the mechanism and kinetics of reduction.

The study of foreign oxide additions to iron ore was carried out to improve our knowledge of burden characteristics in blast furnace operation. The advantage of adding finely crushed calcium compounds to sinter mixtures was first recognized in Sweden(59) and has been applied to pellets, producing so called self-flux sinter and self-flux pellets instead of acid pellets. These improvements can result in a remarkable reduction of fuel ratio on blast furnace operation.

Throughout the world, lack of high purity iron ore forces the use of hematite containing high alumina as a burden material. Generally, high alumina in iron ore makes highly viscous slags and more flux material is needed to reduce this harmful property. Alumina additions are known to cause degradation during low temperature reduction. MgO additions are typical additions to cure these effects and is considered to improve the high temperature reduction characteristics. However the use of dolomite or serpentine as an MgO source leaves some doubt related to the reduction behaviour as it was postulated that this kind of flux material can not give satisfactory results for reducibility and mechanical or thermal properties of the burden material in practical performance.

The program of study in this laboratory has concentrated on the isothermal reduction of one material; Carol Lake hematite which was chosen on account of its relatively high hematite content(96%) coupled with a good resistance to swelling and cracking during reduction. Investigations were initially limited to the reduction of hematite to magnetite or iron in carbon monoxide-carbon dioxide and hydrogen-water vapour mixtures.

In contrast with the extensive information now available on reduction of Carol Lake iron ore, the reduction of this iron ore with flux additions, which is the subject of the present investigation, has received little attention.

Such a study would yield valuable information on the

influence of flux materials on the kinetics and structural changes. In addition, a comparison between the reduction behaviour in these systems would make a valuable contribution to industrial knowledge.

Accordingly, a survey of the literature is made, followed by experiments using a thermogravimetric technique. The reduced samples are examined using optical microscopy and the phases are identified using X-ray diffraction and electron probe microanalysis.

CHAPTER 2

LITERATURE SURVEY

CHAPTER 2

LITERATURE SURVEY

2.1. INTRODUCTION

The behaviour during reduction of iron oxide indicates that the total process is extremely complex. While iron oxide reduction with gas mixtures has been studied very extensively during the past three decades, the detailed reaction mechanism is not understood completely. By the efforts of recent workers(6,11,12,15,16), interpretation of reduction mechanisms has become more clarified both theoretically and practically.

2.2. IRON OXIDE

Iron has three oxides, hematite(Fe_2O_3), magnetite (Fe_3O_4) and wustite (Fe_xO). Magnetite and wustite exist within certain variable concentration ranges.
Fig. 2.1 shows the diagram according to Darken and Gurry(53). The oxide phases in equilibrium with different gas mixtures of $CO-CO_2$ are shown in Fig. 2.2, which gives the equilibrium relationship for Fe-O-C (9).
Wustite has a cubic lattice of the NaCl type and is unstable below 570°C, when it decomposes eutectoidally into α- iron and magnetite :

$$4FeO = Fe_3O_4 + Fe$$

However, it is easy to undercool wustite and maintain it in a metastable state(1). The range of existence of

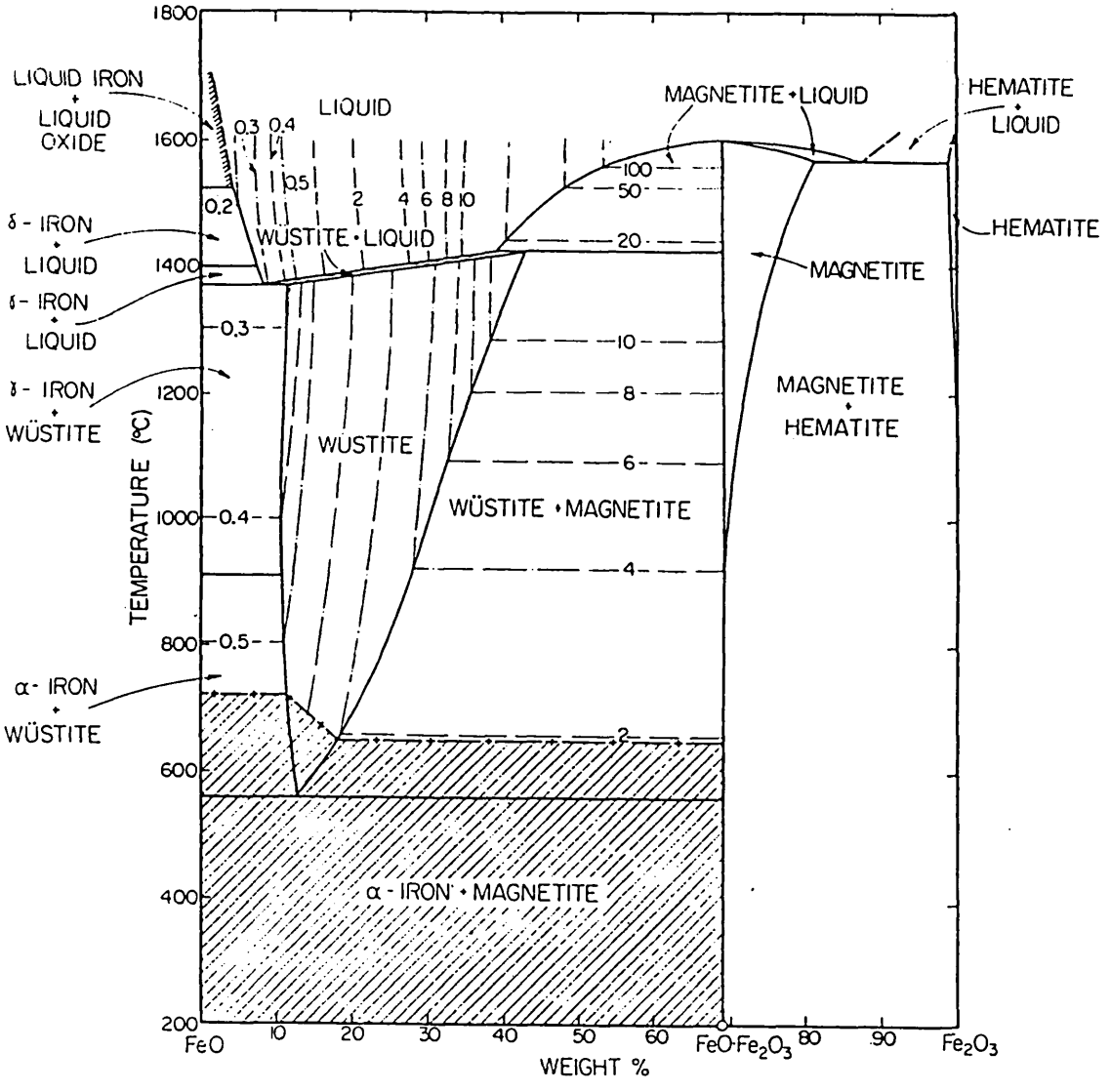

Fig.2.1 Iron-oxygen system (53).

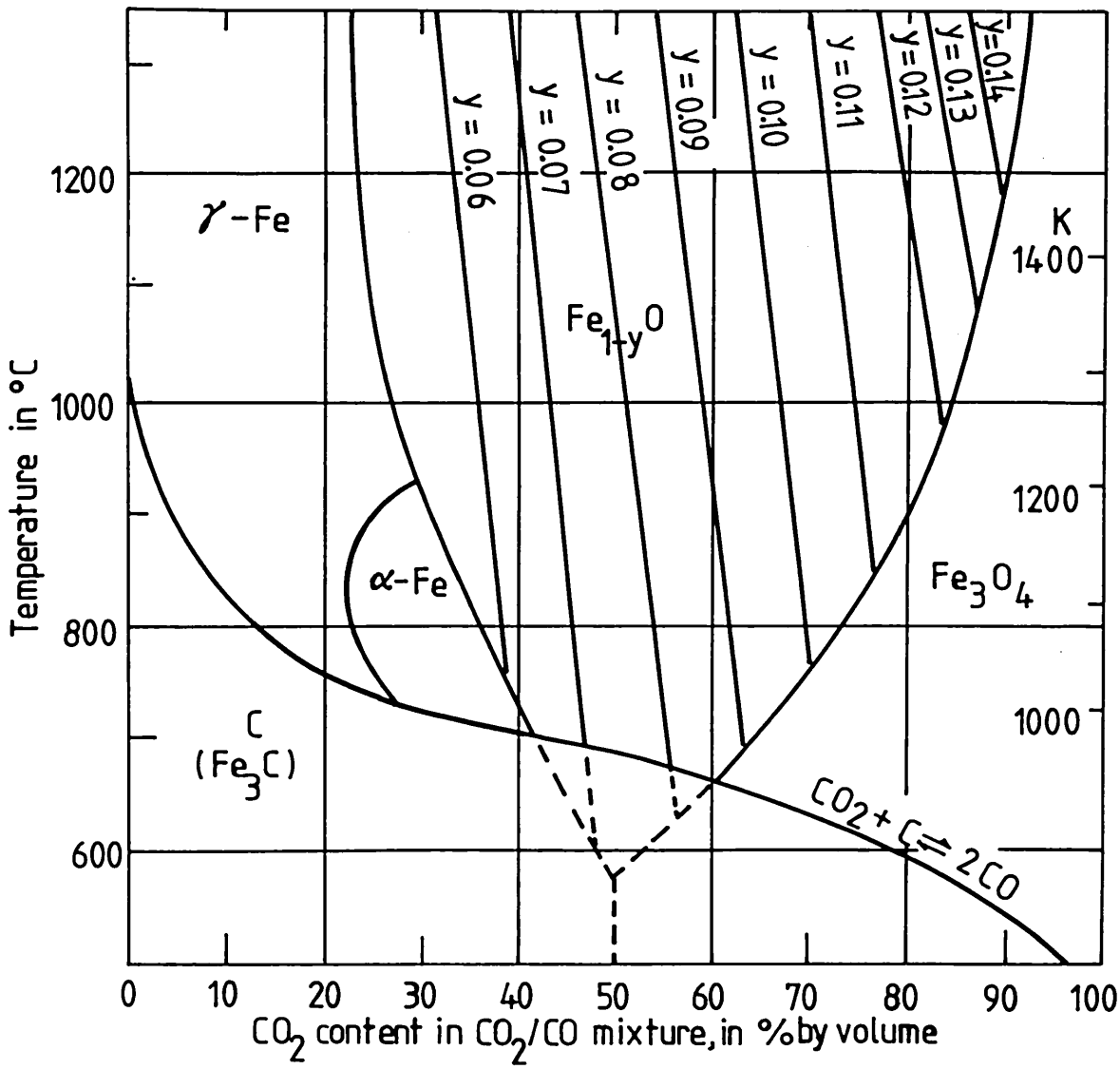

Fig. 2.2 Equilibria between iron, wustite, magnetite, carbon dioxide and carbon (9).

wustite is fairly large but does not include the stoichiometric compound FeO, the oxide always has a higher oxygen content with the iron lattice containing 5-11% vacancies. The lattice parameter varies linearly with oxygen content, from 4.3010 to 4.2816 Å (9). Magnetite also has a cubic lattice of the reverse spinel type. It has a close packed cubic lattice of O^{2-} ions with the smaller Fe^{2+} and Fe^{3+} ions distributed in the various interstices. This oxide also shows a gradually decreasing lattice parameter with increasing oxygen, indicating the presence of vacant cationic lattice points. Hematite exists in two modifications with different lattices: α- Hematite is of the rhombohedral corundum type and γ- Hematite is, like magnetite, a cubic spinel type. It is obtained by dehydration of γ- FeOOH below 500°C, or by oxidation of magnetite below 400°C (1). Transformation of α- Hematite to γ- Hematite has not been observed and it appears that γ- Hematite is a metastable phase formed only during dehydration or oxidation(1).

2.3. REDUCTION OF IRON OXIDE

The reduction of iron oxides and various iron ores has been investigated many times(1-16). However there have been great differences of opinion in the literature as to whether the reduction of iron oxide is controlled by a diffusion process(2) or by a reaction process(1,5). The most common reducing agents used in iron oxide reduction process are carbon monoxide, hydrogen and mixtures of these two gases. The reduction of hematite represents a complex system. The reduction takes place through the

series $Fe_2O_3/Fe_3O_4/FeO/Fe$ above the temperature (570^oC) where wustite is stable. For a transformation according to the reduction :

$$Fe_nO_m + mCO = nFe + mCO_2$$

$$Fe_nO_m + mH_2 = nFe + mH_2O$$

Bogdandy illustrates the reduction sequences schematically using porous lump iron ore(9). The progress of reaction of nonporous solid iron oxide with gaseous reactants was studied by many workers(1,5). It can be represented by the unreacted core model. The reaction occurs at a sharp face or within a narrow region between the unreacted core and the product layer. The product may or may not be porous. In either case, the gaseous reactant must be able to penetrate through the product layer in order for the reaction to proceed to completion.

2.3.1. REDUCTION BY CARBON MONOXIDE

The reduction of ferric oxide to iron using carbon monoxide, takes place in three stages at temperatures above 570^oC. But at lower temperatures below 570^oC, it is generally thought that iron oxide reduction takes place in two stages. The magnetite produced in the first stage is reduced to iron by passing the wustite stage:

$$1/4Fe_3O_4 + CO = 3/4Fe + CO_2$$

By calculating the free energy change for each reaction (Table 2.1), the equilibria can be calculated. Fig.2.2 shows three curves for these reactions and also contains the curve showing the $CO-CO_2$ composition at equilibtium

TABLE 2.1 THERMODYNAMIC PROPERTIES OF IRON OXIDES AND SOME SELECTED COMPOUNDS (9,86)

(Free energy of formation)
cal.

T^oC	FeO	Fe_3O_4	Fe_2O_3	CO
927	-44450	-174600	-122200	-52150
1027	-42900	-167400	-116400	-54350
1127	-41400	-160300	-110600	-56250

T^oC	CO_2	CaO	MgO	$MgFe_2O_4$
927	-94650	-122400	-112600	-3030
1027	-94700	-119900	-109500	-3000
1127	-94750	-117250	-106850	-2950

T^oC	$Ca_2Fe_2O_5$	QUARTZ	CRISTOBALITE	VITREOUS GLASS
927	-12090	-158400	-158450	-152200
1027	-12330	-154150	-154250	-148100
1127	-12530	-150100	-150200	-144000

T^oC	$CaMg(SiO_3)_2$
927	-35820
1027	-36490
1127	-36630

for the reaction: $CO_2 + C = 2CO$ commonly known as the Boudouard reaction. At temperatures above about 1000°C, the reaction is essentially complete. That is the gas phase is 100% CO. This means that carbon dioxide can not exist to any great extent at temperatures above 1000°C in the presence of carbon. This might suggest that carbon monoxide can not reduce iron oxide at temperatures above 1000°C with carbon deposition occurring. However, reduction does take place and this appears to be due to the reduction reaction and carbon deposition taking place separately(31).

2.3.2. REDUCTION BY HYDROGEN

The reduction of iron by hydrogen is much the same as reduction by carbon monoxide. That is, the reduction takes place in three stages at temperatures above 570°C and two stages below 570°C. In the system Fe-H-O, there is no reaction involving hydrogen similar to the Boudouard reaction that complicates this system. Therefore the reduction of magnetite and wustite at temperatures below 650°C and 700°C are thermodynamically feasible(31).

2.3.3. REDUCTION BY CARBON MONOXIDE AND HYDROGEN MIXTURES

This system is more complex not only beacuse the reactions are not restricted to those between the gaseous and solid phases but also due to reactions between the gaseous phases. Therefore, whatever P_{CO_2}/P_{CO} ratio is in equilibrium with a solid phase must be in equilibrium with a definite composition of hydrogen and water vapour

according to the reaction:

$$CO_2 + H_2 = CO + H_2O$$

Recently many workers studied this kind of reduction because of its practical interest(21).

2.4. REDUCTION KINETICS OF IRON OXIDE

For obvious technological reasons, the kinetics of reduction of iron oxides has become the subject of intensive experimental and theoretical investigation during recent years. Continuing efforts to construct mathematical models(32,33) to describe the kinetics of reaction between a gas stream and a granular bed of solid particles have demonstrated the necessity of a thorough understanding of the reaction kinetics of a single particle within the system as a prerequisite to the construction of physically significant models for a complex reaction system.

2.4.1. INFLUENCE OF VARIOUS PROPERTIES ON THE REDUCTION RATE

Some of the rate determining steps in iron ore reduction are associated with the nature of the reaction system and the contact between the reacting phases while others are associated with the nature of the ore. The latter determines the ease with which oxygen can be removed from the iron oxides in the ore by the reducing gases. This property of an ore is often referred to as the reducibility. In turn, the properties of an ore which determines its reducibility are particle size,shape,density,porosity, crystal structure and composition. All of these properties influence the relative amount of reactive surface

area of the iron oxides exposed to the reducing gases(36).

a) Porosity of iron ore

Joseph(24) carried out reducibility tests on several natural ores and the results of some of his experiments show that the porosity of iron ore particles is one of the most important factors controlling reducibility. Joseph's work showed that the reducibility, expressed as the reciprocal of the time required for 90% reduction, varied directly with the porosity.

b) Structural change of iron ore during reduction

In reduction of iron oxides by CO or H_2, the external volume of the sample often changes considerably. The volume changes during stepwise reduction of 4mm cubes of Fe_2O_3 and Fe_3O_4 in CO or CO-CO_2 mixtures were reported by Edstrom(1). In the formation of magnetite from hematite, two distinct microstructures, porous growth magnetite and lath magnetite produced by mechanism resembling discontinuous precipitation and a shear mechanism respectively were observed(27).

In the transformation of magnetite to wustite, the oxygen lattice remains unchanged while iron diffuses to fill the vacant sites in the iron lattice. This can be accomodated with only a small increase in volume(1). The lack of expansion of magnetite during reduction as starting material causes the formation of a dense layer of metallic iron surrounding remnants of wustite which cut off access of the reducing gas to the oxide and practically prevents

complete removal of oxygen(28).

Other structural changes which occur during reduction, excepting those which are a direct result of the chemical change in the iron oxide mentioned above, are sintering, swelling, softening and cracking.

Sintering

This behaviour may be of particular importance in the reduction of iron oxides where sintering of the porous metal product layer may markedly reduce the overall rate of reduction by limiting access of the reactant gas(36). Activation energies for sintering are high(36); that is, the rate of sintering increases rapidly with increasing temperature and the lowest reduction observed at 650^{o}C(17) is regarded as due to sintering of the iron layer.

Swelling

Most iron ores and pellets swell to some extent during reduction but some exhibit what has become known as a "catastrophic" swelling(34). The swelling results in the production of a mass of metallic wires or whiskers, rather than the fairly dense sponge of the normal reduction, and causes severe problem in blast furnace operation. According to Bleifuss(40), catastrophic swelling involved in the reduction of calcioferrous ores is due to the formation of a surface layer of lime saturated with iron. Normal swelling is probably caused by the crystallographic transformations, that occur during reduction(7).

Softening

As far as the effect on gas-solid reactions are concerned,

softening may be considered as an extreme form of sintering(36). At softening temperatures, pores must close extremely rapidly, which in turn prevents diffusion of gaseous reactant into the solid and thus severely hinders the reaction(54,57,58,76,78).

Cracking

Cracking of the solid is usually undesirable for gas-solid reaction systems carried out on an industrial scale, because the reactant breakage may cause operational difficulties. However, cracking of ore may increase the overall rate of reaction by reducing the diffusional resistance(2,36).

c) Degree of oxidation and reducibility test

The chemical composition of the raw material has great influence on the reduction(4). Even a small change in the degree of oxidation influences the reducibility considerably. All stages of iron oxide reduction can be graded in terms of increasing difficulties:

Fe_3O_4(from Fe_2O_3)----FeO (least difficult)

Fe_3O_4(as charged)---FeO

FeO(from Fe_2O_3)------Fe

FeO(from Fe_3O_4)-----Fe (most difficult)

The reducibility of an iron ore can be determined experimentally in many ways. Most reducibility measurements are made by the thermogravimetric methods. Some workers use 90% reduction, others use as low as 50%, whichever is most suitable for the particular process(31).

d) Carburization during reduction

The oxygen removed from the oxide can be measured by a method measuring loss-in-weight during reduction. But with CO it is impossible to calculate the oxygen removed directly. At 1000°C and higher with Fe_2O_3 as the original material, carbon deposition is significant after 80% of of the oxygen has been removed(1). At higher temperatures than 1100°C, carburization dose not proceed until the reduction degree exceeds 90%(20). In addition, iron carbide (Fe_3C), commonly called cementite, can be formed by the reaction.

$$3Fe + 2CO = Fe_3C + CO_2$$

Like carbon deposition, the above reaction is also favoured by low temperatures and high carbon monoxide concentrations. Okura(18) reported that the rate of carbon deposition on iron powder reduced at low temperature is larger than that reduced at high temperatures and the weight of carbon deposited is proportional to the specific surface area.

2.4.2. REDUCTION KINETICS OF IRON ORES

Concerning the reacting surface exposed to the reducing gases there are other factors that affect the rate of reduction of iron oxides. The first to be considered is the rate of heat and mass transfer across the gas-flow boundary layer at the outer surface of the solid phase. When the reaction rate is controlled by this phenomenon, it is known as "Boundary Layer Control". Secondly the rate of diffusion of the reducing gas inward and the product gas outwards through the reduced iron layer can control the rate of reduction of iron oxides. This phenomenon is generally associated with large ore particles, and known as "Gaseous

Diffusion Control" or "Iron Pore Control". Thirdly the chemical reaction at the wustite-iron interface is believed by McKewan(1,5) to be rate controlling. When this is the case, the rate of reduction per unit area of remaining iron oxide surface is found to be constant with time. This mechanism is reffered to as "Interfacial Reaction Control" or "Phase Boundary Reaction Control".

When both gas diffusion control and interfacial reaction control combine to influence the rate of reduction, the mechanism is reffered to as "Mixed Control"(6,11).

All of the above factors include other factors such as nucleation and crystal growth in the iron phase(27), the presence of impurities, partial pressure of reducing and product gases(1), the presence of inert gases(31) and temperature which can contribute to the rate controlling step in the reduction of iron oxides and these have been investigated by many workers(1,22,23).

a) Boundary layer control

In boundary layer control, the overall reduction rate is controlled by the rate of diffusion of gas and or heat through a boundary layer of stagnant gas that builds up around each particle(36). Therefore the rate of diffusion of gas through this layer is proportional to the gas concentration gradient across the layer.

b) Phase boundary reaction control

When counter-diffusion of the reducing gas and the product gas in the reduced outer iron layer is sufficiently fast, the concentration of the reducing gas at the reacting

surface is effectively the same as its concentration at the particle surface. McKewan(10) developed a mathematical model in support of this mechanism based on the assumption that the reaction rate is proportional to the surface area of the reaction interface.

c) Gaseous diffusion control

A mathematical model of gaseous diffusion control for a spherical particle has been proposed by Spitzer et al.(6) and Ross et al.(7). During the early stages of reduction, where the iron layer is non-existent or very thin, the phase boundary reaction controls the reduction rate, but gaseous diffusion control takes over as the iron layer thickens(7,17,35). During the final stages of reduction other factors can become the predominant controllong influence(16).

d) Mixed control

Mixed control has been proposed by several experimenters (6,7,13) to reconcile the complexities and conflicting results obtained with the simpler mechanisms. Under these conditions, Ross(7) proposed a generalized rate equation. The relative importance of these two contributory factors (transportation of gases and phase boundary reaction) is of course a function of the nature of ore(31) to be reduced.

e) Solid state diffusion

The rate minimum, which has often been observed in the reduction of certain iron ores, can be related to the recrystallization of iron which slows down the reduction of

wustite which is surrounded by recrystallized iron and cause a change from a process controlled by the phase boundary reaction to one controlled by solid state diffusion(40).

Regarding mass transport through dense solid oxide layers, Wagner(50) has postulated that diffusion in oxides may be interpreted as migration processes of ions and electrons. Edstrom(56) studied the solid state diffusion phenomenon in the reduction of dense magnetite in which the same parabolic data were obtained as those in the oxidation of iron.

f) Activation energy

To estimate the reaction rate, an "Arrhenius plot" is conveniently used and some experimental results have been interpreted using the temperature variations of reaction rate.

The activation energy of a reaction controlled phase boundary reaction was reported as 15.2 Kcal(2,5), 14.9 Kcal(2) and for solid state diffusion as 47.8 Kcal(49) and 52 Kcal (48).

2.5. FORMATION AND GROWTH OF NUCLEI DURING REDUCTION

The formation of solid reaction products in the reduction of metal oxides is a process in which the formation of a nucleus is necessary. The problem of nucleation of the product phase becomes more important as the particle size of the ore is reduced since at high reaction rates the ore may be transformed by the growth of a single nucleus(44). Hayes and Grieveson(27) studied the formation of magnetite from hematite and for the situation where the nucleation

frequency of the new phase is high compared with the rate of growth of the nuclei, complete coverage of the surface occurs with an approximately uniform porous layer.

2.6. INTRAPARTICLE TEMPERATURE OF IRON OXIDE DURING REDUCTION

In the kinetic analysis of the reduction process of iron oxide specimens, it is generally assumed for simplicity in mathematical modelling that the temperatures of the reaction space and the specimen being metallized are equal. The influence of heats of reaction of the gaseous reducing agent on the temperature inside iron oxide pellets depends on the reduction stages and temperature(25). In the gaseous reduction by hydrogen or carbon monoxide, the rise in temperature inside the sample at the beginning of the process is less pronounced than its subsequent decrease(19). The initial porosity of the sample has different effects on reduction rate(31,36) and the temperature distribution throughout the sample(19).

2.7. THE EFFECT OF FOREIGN OXIDE ADDITIONS ON REDUCTION OF IRON OXIDE

The study of foreign oxides in iron ore as additives was carried out for the purpose of improving burden characteristics in blast furnace operation. The advantages of adding finely crushed calcium compounds to sinter mixes were first recognized in Sweden(59) and this has been applied to pellets the so called self-flux sinter and pellet instead of acid ones.

Throughout the world, lack of high purity iron ore forces

the use of hematite containing high alumina which makes highly viscous slags and more flux material is needed to reduce this harmful property. Some kinds of alumina are known to cause degradation during low temperature reduction(55,60). MgO additions are typical solutions for these effects and are considered to improve high temperature characteristics (54,61). All these relationships between foreign oxides and iron oxide are complicated and all are interrelated with each other. Recently, systematic stduies have been carried out by several workers(37,38,39,47).

2.7.1. MINERAL PHASES CHANGES DURING SINTERING

Mineral phase changes during sintering of iron ore with some foreign oxides vary with many factors, such as temperature, amount of foreign oxide, particle size and distribution.

Comprehensive studies dealing with the Ca-Fe-Si-O system were carried out by Phillips and Muan(45), the Ca-Fe-O system by Edstrom(62), Turkdogan(46) and Rosenberg et al. (51). The Si-Fe-O system, particulary the formation of fayalite was studied by Baldwin(41) concerning the aspects of the formation of fayalite with or without other oxides. In the system MgO-FeO-Fe_2O_3, many works(83,84,87) have been done as it forms a basis for the study of the various solid solution phases in the systems Mg-Fe-Si-O and Fe-Mg-Ti-O. Recently the study of dolomite or serpentine additions as flux materials in iron ore has been investigated(77-80).

CaO and SiO_2

Lime can react with hematite during sintering of pellets, prior to their reduction, formimg the calcium ferrites (37-39) $2CaO\ Fe_2O_3$, $CaO\ Fe_2O_3$ or $CaO\ 2Fe_2O_3$. Lime can also form solid solutions with wustite(63) and magnetite(82). The system Fe-Ca-O has been described by many authors. An important part of it, the sub-system $FeO-Fe_2O_3-CaO$ at 1100^oC was described by Reijen(37).

Practically, commercial iron ore has a lot of foreign oxides as impurities, mainly silica. When CaO is added to iron ore, the mineralogical composition will be iron oxide, calcium ferrite, crystalline slag and glassy slag(66,69).

The process of mineral formation of mixtures of fine powder consisting of hematite, lime and quartz was studied by some workers(42,66). In a series of experiments with CaO, SiO_2 and Fe_2O_3, no reaction products were detected at 1300^oC in the mixtures of $CaO-SiO_2$, $SiO_2-Fe_2O_3$, except transformation of high quartz from low quartz. In the system SiO_2-Calcium Ferrite($CaO\ Fe_2O_3$, $CaO\ 2Fe_2O_3$), no reaction products were found at 1150^oC, but at 1200^oC SiO_2 disappeared with the formation of a silicate and calcium ferrite phase(66). Fig. 2.3 shows a schematic diagram of the mineral formation processes of mixtures in the $Fe_2O_3-CaO-SiO_2$ system(69) while Fig. 4.17 shows the phase diagram(64) of this system.

Fig 2.4 shows the phase relation of $FeO-Fe_2O_3-SiO_2$(64).

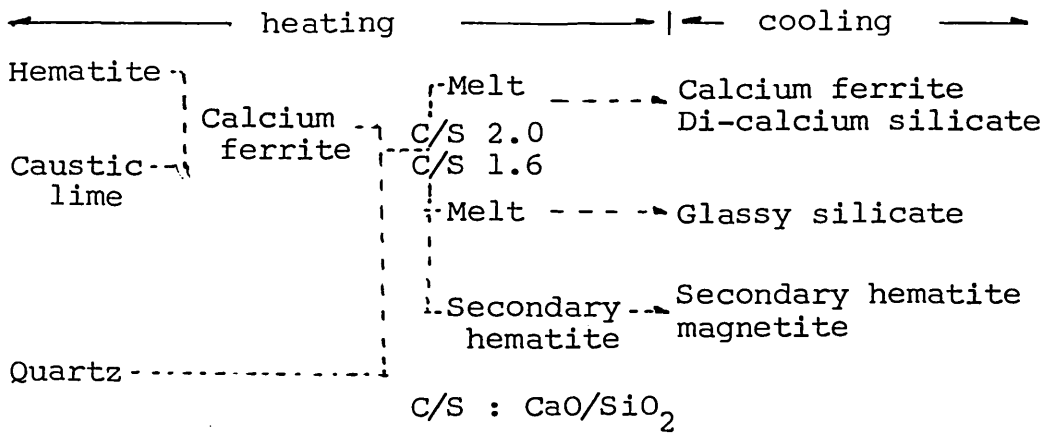

Fig 2.3 Schematic diagram of mineral formation of mixtures of 80% Fe_2O_3-CaO-SiO_2 system(69)

MgO

The mineral phase change observed on adding MgO to iron oxide is the formation of magnesio-ferrite. MgO in iron oxide forms magnesio-ferrite by solid-solid reaction between iron oxide and MgO during the heating process(54,55). This phase has the same crystal structure as magnetite where Fe^{2+} in the spinel phase is completely or partially substituted with Mg^{2+} ions(65). Thus MgO stabilizes magnetite during sintering. In the presence of CaO or SiO_2, great changes in the amount of mineral phases were observed (67). At 1200°C calcium ferrite and magnesio-ferrite increased with increasing amounts of MgO. At 1250-1300°C the increase of magnesio-ferrite was particularly significant.

Al_2O_3 and others

The other minor elements such as Al_2O_3, TiO_2, MnO and sodium containing hematite were considered to form a multi-component magnetite(68). Detailed information about formation of mineral phases with iron oxide is not known.

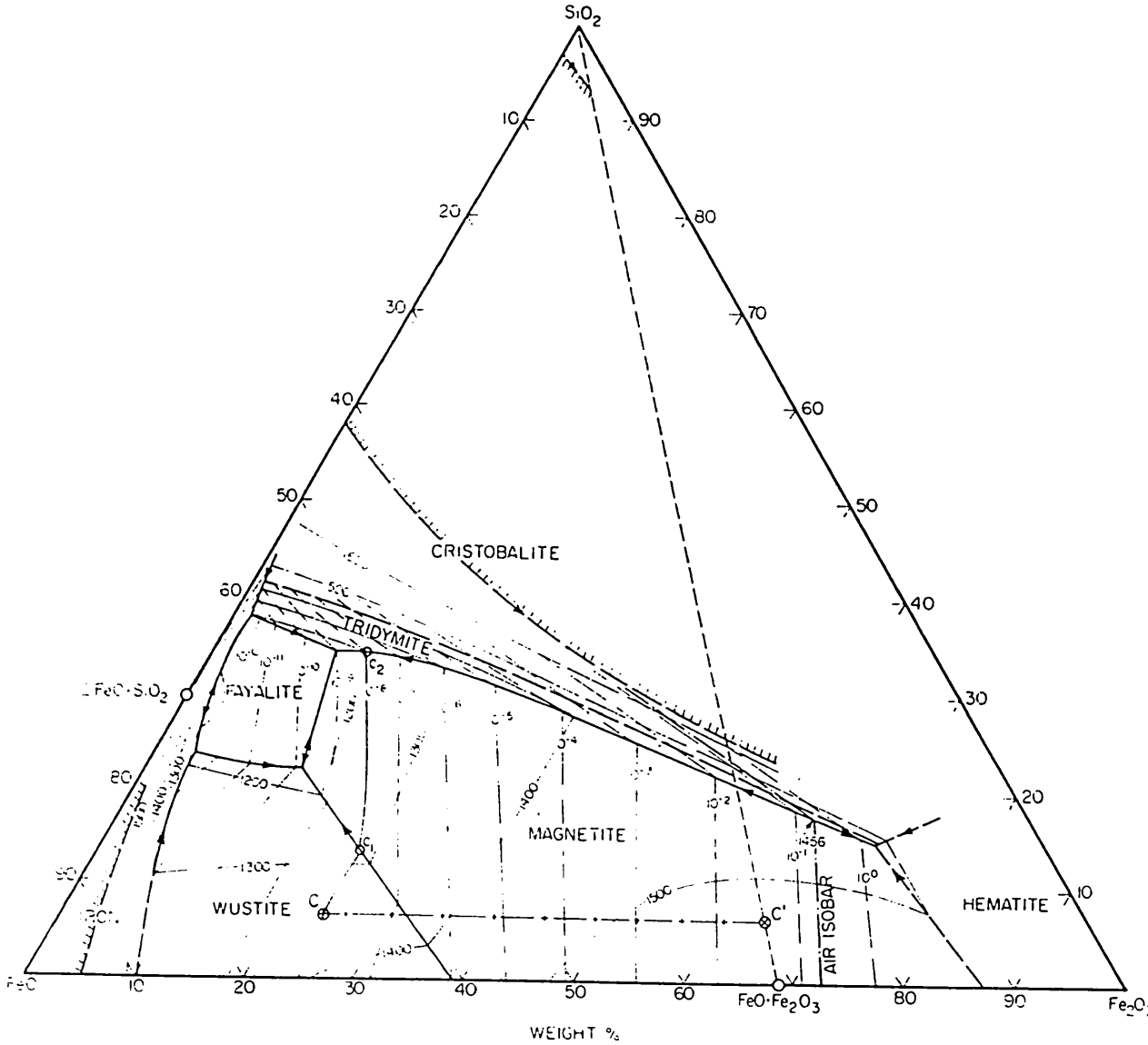

Fig 2.4 Phase diagram of the system $FeO-Fe_2O_3-SiO_2$ (64)

2.7.2. THE EFFECT OF FOREIGN OXIDES ON REDUCTION

CaO

The influence of lime on the reducibility of iron oxides has been investigated extensively. Some authors(17,39) found an accelerating effect, for which sometimes a maximum at a CaO content of 1% is found(17), while others found retarding effects(55). Turkdogan(38) postulated the negligible effect of lime on the reducibility as the calciumferrites formed during sintering are easily decomposed during reduction. Reijen et al(37) studied the effect of lime on reduction rate by applying the hot kerosene method and found no difference. Ross(39) added calcium carbonate to hematite and explained the accelerating effect by the mechanism: $2CaO + 3FeO = Fe + 2CaO\ Fe_2O_3$ The dicalcium ferrite formed will yield iron and calcium oxide during reduction and the regenerated calcium oxide will dissociate more wustite. From thermodynamic considerations, it can be shown that such a mechanism is impossible.

SiO_2

Baldwin studied the formation and decomposition of fayalite and found that formation of fayalite can occur during the reduction of iron ores above 800°C when ferrous oxide and silica are present in the absence of lime(41). Fig. 2.4 shows the phase diagram of the system Fe-Si-O. Geasy et al.(42) claimed that fayalite was not formed when the silica is present as crystalline particles. The particle size of the silica also affects the reduction rate (38) and the formation of fayalite always accompanied the retardation of the final stage of reduction(42).

MgO

Some recent studies(70,73) reported that the reduction rate with MgO additions varies with CaO/SiO_2 ratio and the reduction mechanism of MgO containing iron oxide is controlled by oxygen diffusion in the metallic iron shell (55). The reducibility of the pellelts with added $MgCO_3$ (29) arises from the increase of MgO content because the resultant increase in porosity greatly improves the reducibility, although magnesioferrite in the pellets has been reported to(30) reduce the rate (see Fig.2.5,2.6).

Others

Khalafalla(71) studied the reducibility of iron oxide containing alkali and alkaline earth metal oxides and found a strong accelerating effect. Koch(72) reported that K_2O containing iron oxide accelerates the reduction rate. This kind of acceleration factor was decribed by the authors in terms of lattice disturbance effects(42,71) or lowering the nonstoichiometry of wustite(52).
Effects of gaseous sulfides on the rate of reduction of iron oxide were studied and the reduction rate was observed to be greatly decreased(26).

2.8. SOFTENING AND MELTING BEHAVIOUR

The softening properties of an ore play an important role in the permeability and reducibility in the stack of the blast furnace. It is generally considered that a good ore should not melt at too low temperature in order

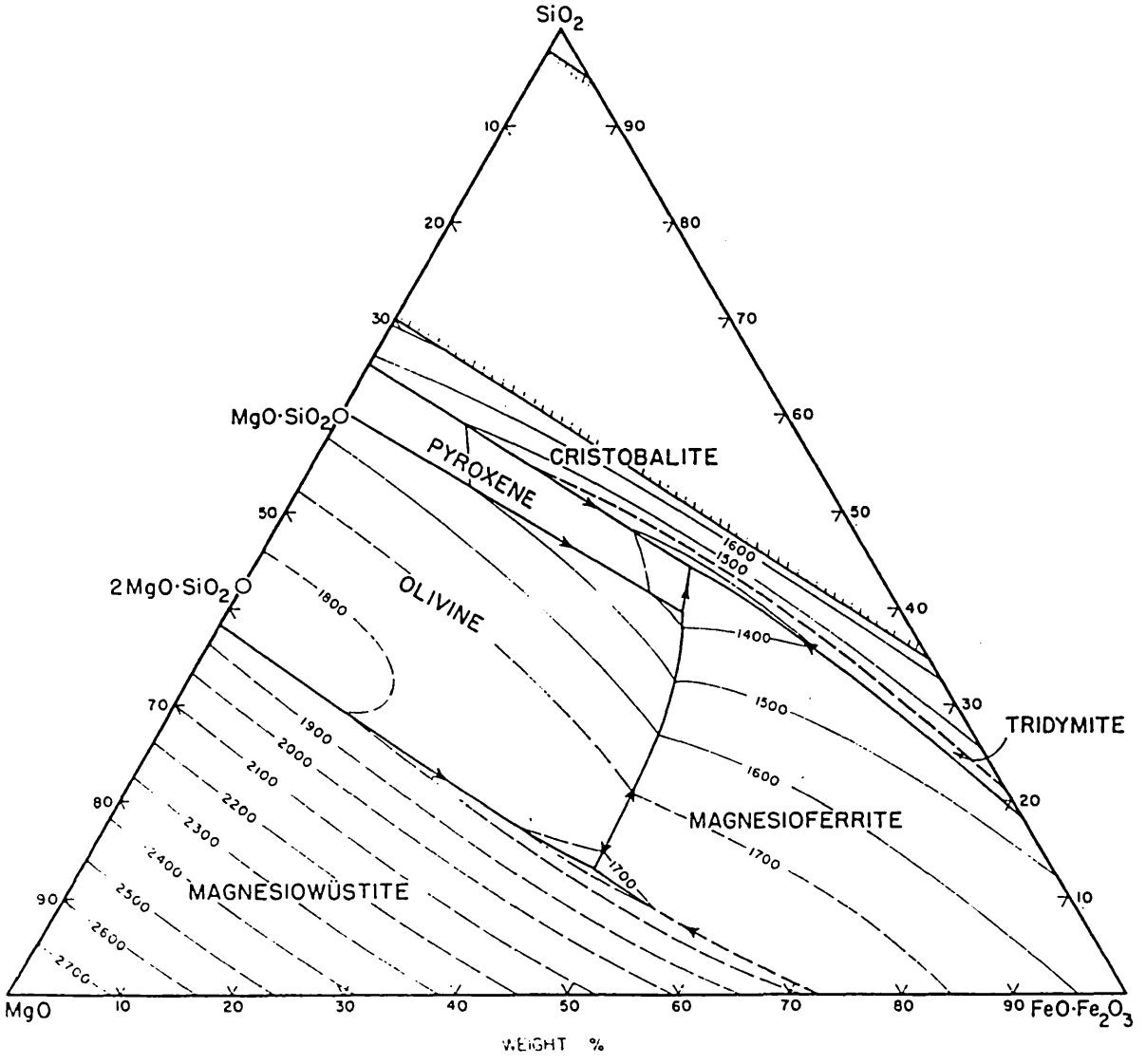

Fig. 2.5 Phase diagram for the system MgO-iron-SiO_2 in air (64)

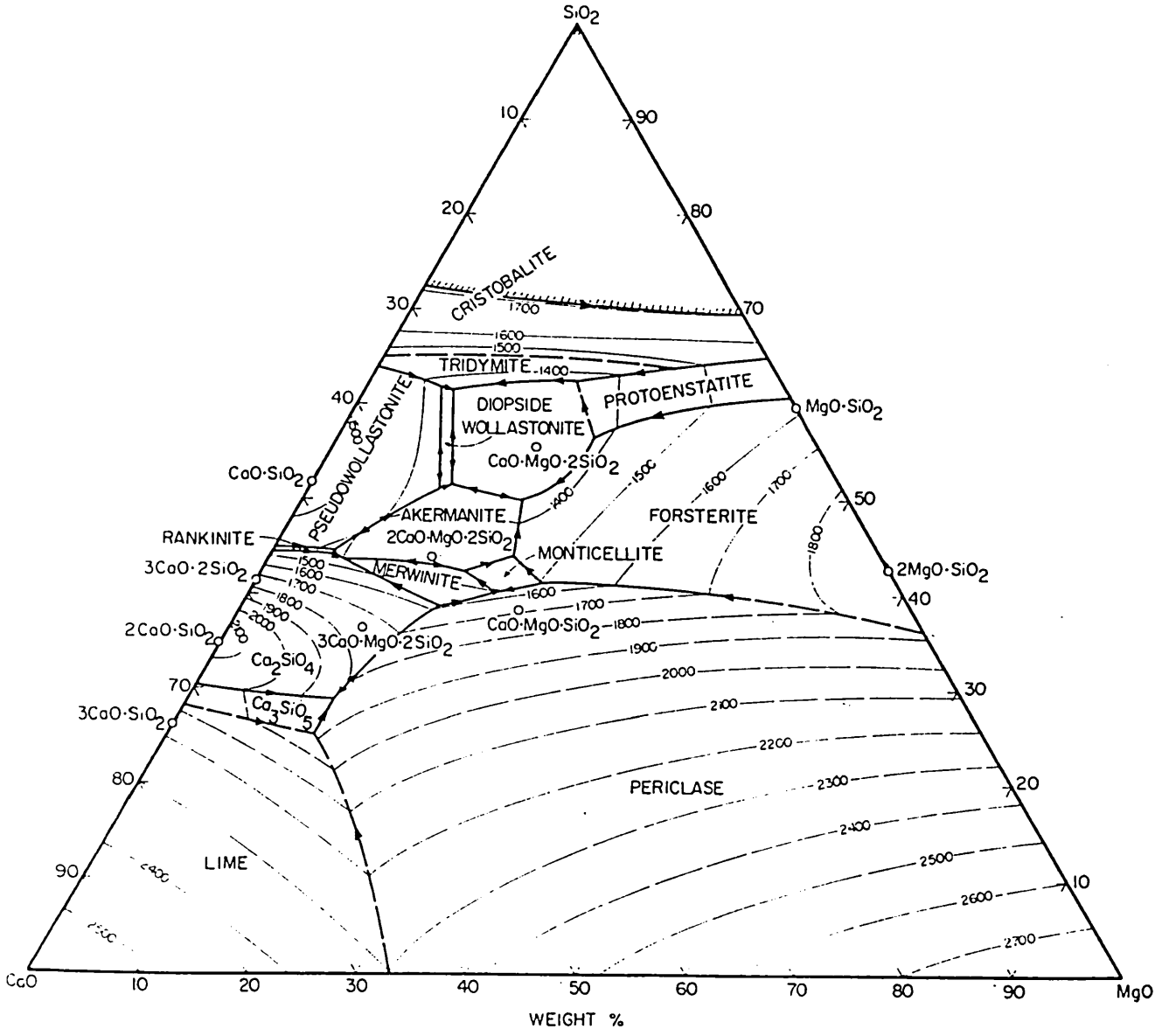

Fig 2.6 Phase diagram of the system CaO-MgO-SiO_2 (64)

not to degrade during reduction.

After quenching and dissecting a working blast furnace in Japan, they found that there has a great difference between operating conditions and shape of the cohesive zone(30,54). Some workers(43) have developed gas flow models by changing the thickness of the cohesive zone. Recently many studies have been carried out to improve the high temperature characteristics by adding MgO sources to iron ore(54,70).

2.8.1. SOFTENING TEST

To study the softening behaviour of iron ore, C.R.M. has developed(57,58) a softening test.

Principle

An ore, sinter or pellet sample is partly prereduced and then packed into a heat resistant steel crucible, which is placed inside a furnace under a given pressure. The softening start and finish temperatures are defined as those corresponding to shrinkage of 1 and 25%, respectively of the initial height of the specimen. The softening behaviour is characterized by two curves giving the dependence of the softening start and finish temperatures on the degree of reduction.

Choice of the test conditions

In order to get good reproducibility of the test results, it is generally accepted by I.R.S.I.D and J.I.S that the conditions of gas, pressure, temperature and shape of sample are important.

2.8.2. THE SOFTENING AND MELTING BEHAVIOUR OF IRON ORE AND THE INFLUENCE OF FOREIGN OXIDES ADDITION

The influence of several factors on softening temperature was studied(58,70), especially :

chemical composition

the degree of reduction

Influence of chemical composition on the softening behaviour

The softening behaviour after reduction of an iron ore is normally worse than it was before reduction. On the other hand, the softening mechanism in the reduced and unreduced state exhibits a number of similarities. The relationships between softening start(T_1) and finish(T_2) temperatures, on the one hand, and the total iron content, Fe_t, basicity index CaO/SiO_2 and initial state of oxidation at.O/at.Fe, on the other hand, were studied(58) statistically using various kinds of sinter.

$$T_1 = 685 + 1.23Fe_t + 280 \frac{at.O}{at.Fe} + 70.3 \frac{CaO}{SiO_2}$$

$$T_2 = 733 + 299 \frac{at.O}{at.Fe} + 91.5 \frac{CaO}{SiO_2}$$

However, within the range of chemical compositions given in commerical iron ores, sinter and pellets, the influence of minor elements such as TiO_2,Mn,MgO or alkali metals on the melting temperatures of the compounds which cause softening is so small that it cannot be detected statistically to any degree of significance. After the above equations were established, C.R.M studied the cases for the increase in softening temperatures with increasing

iron content, basicity index CaO/SiO_2, and initial state of oxidation at.O/at.Fe. The softening start and finish temperatures of several sinters having similar iron contents degree of oxidation have been plotted(58) as a function of basicity index CaO/SiO_2.

These results indicate that the softening temperature increases fairly rapidly with increasing basicity index. It is known that iron can be combined with SiO_2 and CaO, either in the form of fayalite from FeO or calcium ferrite from Fe_2O_3. In Fig. 4.18, the $FeO-CaO-SiO_2$ ternary diagram, it is seen that the minimum temperature of fusion lies near 1100°C in the case of the composition: FeO;46%, SiO_2;37%, CaO;17%, corresponding to a basicity index of 0.46.

This temperature of 1100°C corresponds to the minimum softening start temperature determined by the C.R.M test on hard burned sinters with a CaO/SiO_2 index near 0.5. On the other hand, for a given FeO content, it can be considered that the softening temperature will increase as the basicity index of the gangue rises beyond a value in the neighbourhood of 0.46 and this agrees with the results of Willems(74). Concerning medium to highly oxidized iron the melting temperatures rise progressively from 1200°C to 1250°C when the basicity index and the Fe_2O_3 content dissolved in the gangue increase simultaneously, coinciding with the softening start temperatures of highly oxidized sinters shown in the figures(58).

Accordingly, the impurity content such as CaO, SiO_2, Al_2O_3,

MgO,MnO, or even P_2O_5,Na_2O and K_2O may also play an important role on softening behaviour. This shows the influence of the addition of alkali oxides on the softening temperatures of hematite. In the case of ores, the softening mechanism is even more complex, since the structure of the gangue including porosity and its texture may play a role(78), in addition to the overall chemical composition(76).

Influence of the degree of reduction on the softening behaviour

Since the materials charged into the blast furnace soften only after being partially reduced, it is necessary to determine the influence of this factor(54). Decker et al(57,58) suggested that the temperature is related to the nature of gangue(basicity) in ore and to the initial degree of oxidation, which depends for a large part the reduction mode and the amount of wustite present at each moment to form, low-melting phases with SiO_2. Further, the sticky fusion range of partly reduced ores diminishes when the basicity index increases.

CHAPTER 3

EXPERIMENTAL

CHAPTER 3

EXPERIMENTAL

3.1. INTRODUCTION

Thermogravimetry together with optical microscopy, X-ray diffraction and electron probe microanalysis were employed to study the reduction behaviour of iron oxide with additions and identify the phases and morphology of the iron produced. The apparatus employed for the thermogravimetric study was essentially that used previously by Gupta(85). Some modifications however were made to meet the special requirements of this investigation.

3.2. APPARATUS

Fig3.1 is a schematic diagram of the apparatus. It consisted of a furnace, a quartz reaction tube and linear variable differential transformer - L.V.D.T.- for monitoring the weight change of the sample. Gas flow rates were measured with an orifice flow meter and rotameter.

Furnace and Reaction Tube

The furnace and reaction tube are illustrated schematically in Fig. 3.2 . The furnace consisted of a mullite tube, 65mm I.D. x 5mm thick x 350mm long, wound with Kanthal A-1 wire of 30 ohms resistance. A layer of Kaowool, 115mm thick, served as the insulation. The furnace was mounted on two guides so that it could be raised and lowered around the reaction tube. The entire assembly was supported on an angle

iron frame. The temperature of furnace was controlled using a Eurotherm controller connected to a Pt/Pt-13% Rh thermocouple placed adjacent to the furnace windings. Typical temperature profiles in the furnace, with the reaction tube in position are shown in Fig 3.3 . A constant temperature region ($\pm$ 1^{o}C), 50mm long, was obtained which proved adequate for the reduction experiments.

The reaction vessel was made of quartz in two parts. The upper section was connected by a cone and socket joint, and the lower portion consisted of two concentric tubes, 34mm and 55mm I.D. with an inlet and an outlet for the gas, as shown in Fig 3.2 . A bed of alumina chips, 30mm deep, ensured that adequate preheating and uniform distribution of the gas before it reached the sample. The upper part of the reaction tube had a disc with two holes, 5 and 3mm diameter, which allowed entry for the suspension wire for the sample and the thermocouple respectively. This disc prevented the outgoing gas from entering the housing of the L.V.D.T. . This section of reaction tube, which was held in position by a split brass sleeve, was water cooled.

L.V.D.T. and Sample Suspension

The weight of the sample undergoing reduction was determined from the voltage output of the L.V.D.T. connected to a chart recorder (with two pens). The L.V.D.T. shown in Fig 3.4 was enclosed in a steel box and mounted on a water-cooled mild steel plate. A flow of 300 mls/min of nitrogen gas through the box maintained a constant temperature and prevented the entry of hot gases from the reactor during experiments. The L.V.D.T. was calibrated by measuring

its output for a series of known weights suspended from it. The calibration was linear and is shown in Fig 3.5 .

3.3. MATERIAL

In the present investigation Carol Lake iron ore concentrates from Canada was used. Chemical analysis of this material by Pohang Iron and Steel Company in Korea is given in Table 3.1 . This table also shows the analysis of iron ore powder (oxidized at 650^{o}C in air for 24 hours) and shows that a small amount of Fe^{2+} remains. The presence of ferrous iron was not detected by X-ray analysis.

In most experiments, oxidized iron ore was used as the starting material. The size distribution of the oxidized iron ore powder shows that more than 75% weight fraction of the sample was less than 75 μm in diameter, see table 3.2 .

3.4. PREPARATION OF COMPACTED SPECIMENS

All briquettes were made in a 6.35mm inner diameter cylindrical mould, using a pressure of 5000 psi. without any binder. Each briquette weighed about 1 gram and its length was about 8.7mm . The briquettes were sintered in a furnace at a temperature of 1300^{o}C in air for 24 hours after the required temperature had been attained. The temperature of the furnace was controlled by a Eurotherm controller. The specific gravity of the sample was measured after scaling the surface with a thin film of Araldite and the results are shown in Table 3.3 . The briquettes which contain weight fractions of 1% , 2% and 5% of CaO , MgO , Thrislington Dolomite and Whitewell Dolomite were also produced in a similar manner. Both specpure CaO and MgO were obtained from

Key to Fig 3.1

a	Gas valve
b	Three way stop cock
c	Rotameter
d	Capillary flow meter
e	Drying tower containing Mg-perchlorate
f	Soda-asbestos for CO_2 elimination
g	movable vertical tube furnace
h	Reaction tube
i	L.V.D.T
j	to recorder
k	"
l	to gas burner (air)
m	Platinum basket and suspension wire
n	Thermocouple
o	Mixing tower
p	Furnace for oxygen removal (Cu gauze)

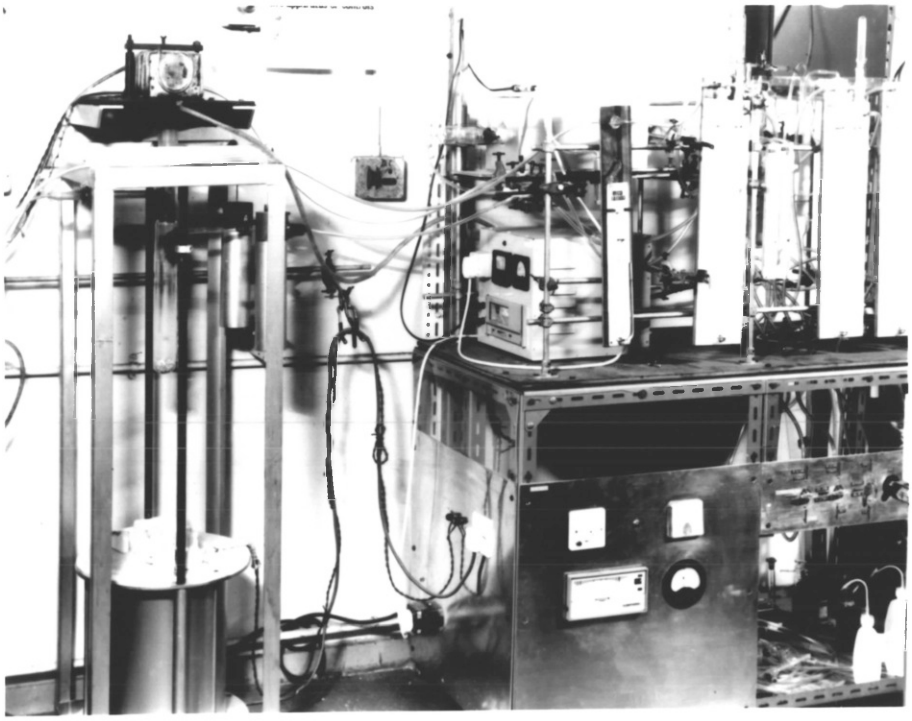

Front view of the Apparatus

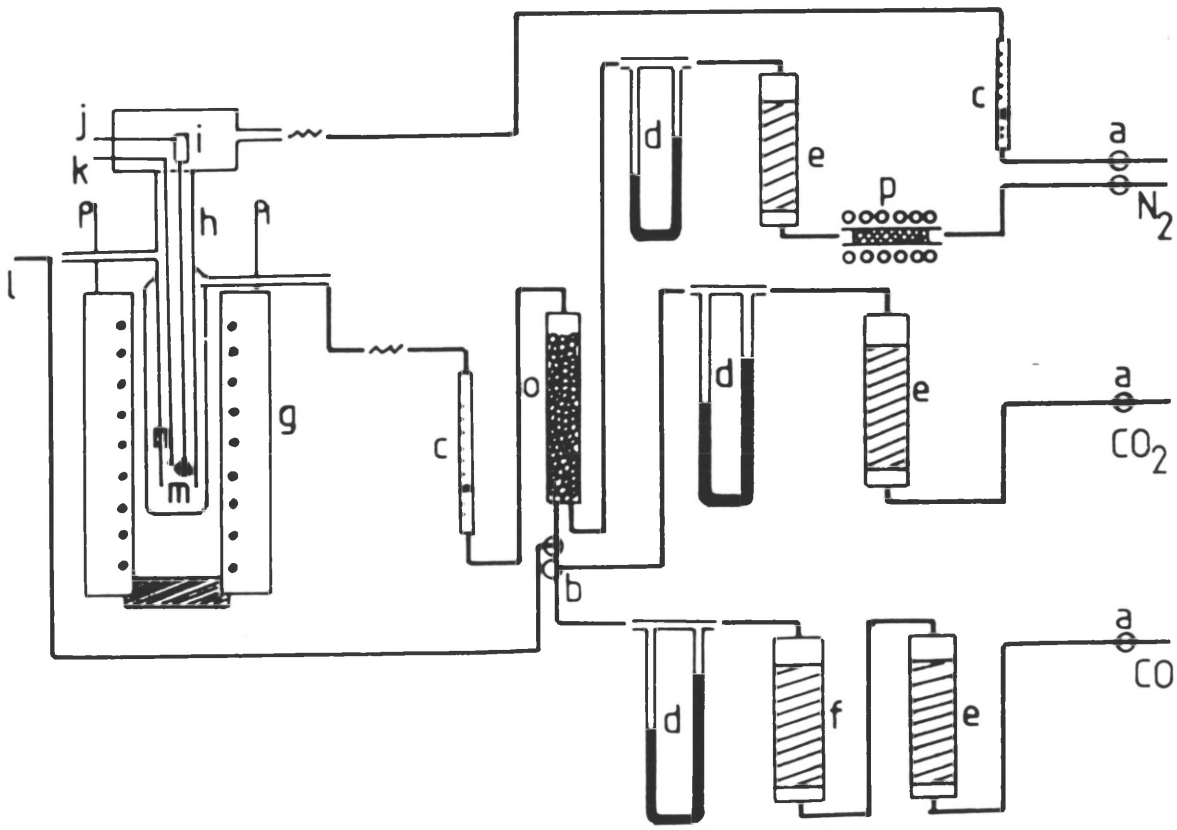

Fig.3.1 Schematic diagram of the apparatus

Key to Fig 3.2

A	Sample thermocouple
B	Split brass sleeve
C	Alumina chips
D	Quartz disc
E	Water cooling
F	Angle-iron frame
G	Guide line
H	Counter weight
I	Gas inlet
J	Cone and socket joint
K	Kaowool packing
L	Sample suspension
M	Mullite tube
O	Gas outlet
P	Plug
R	Quartz reaction tube
S	Sample
W	Furnace winding
Z	Power supply

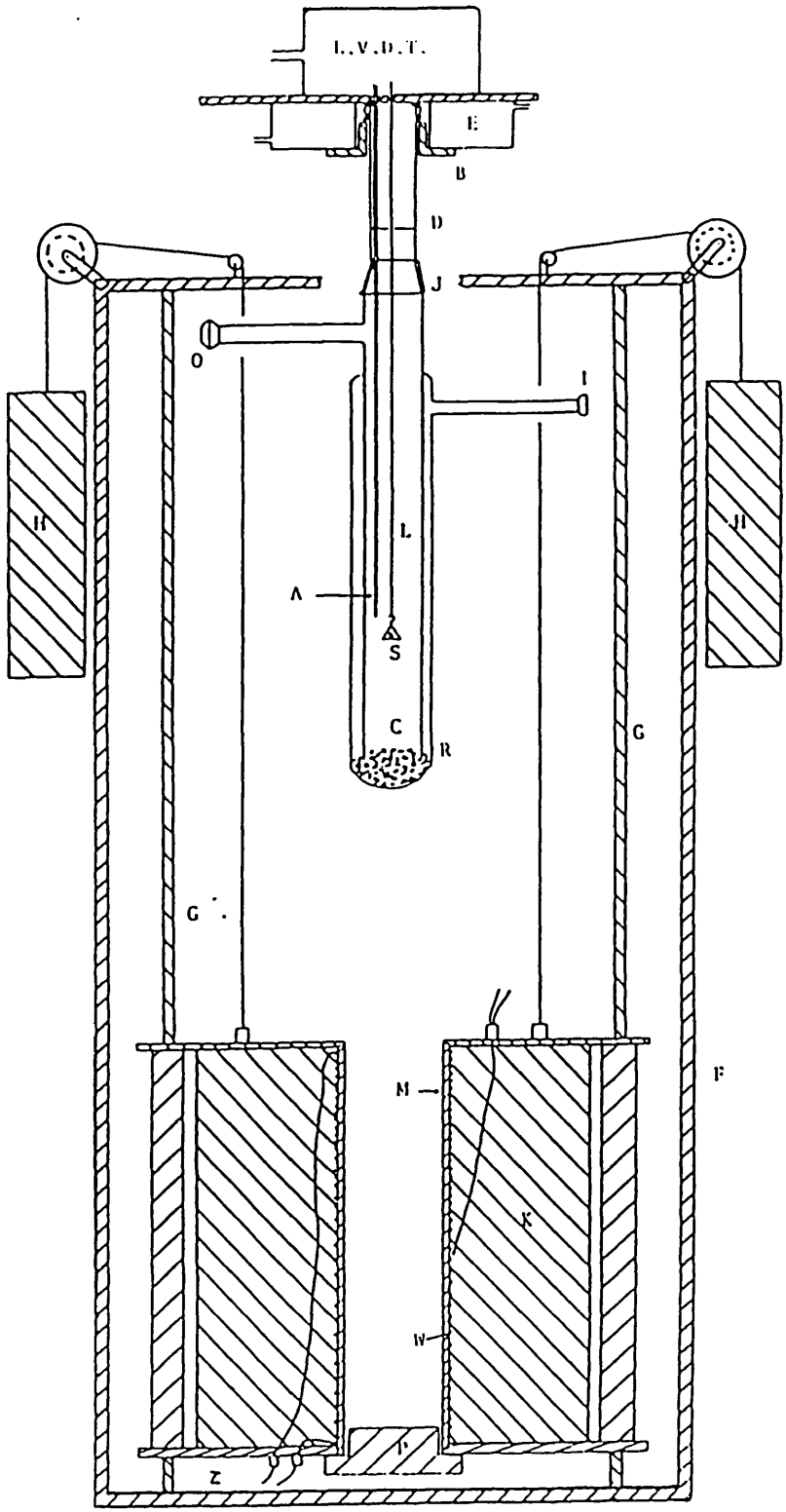

Fig. 3.2 Furnace and Reaction tube.

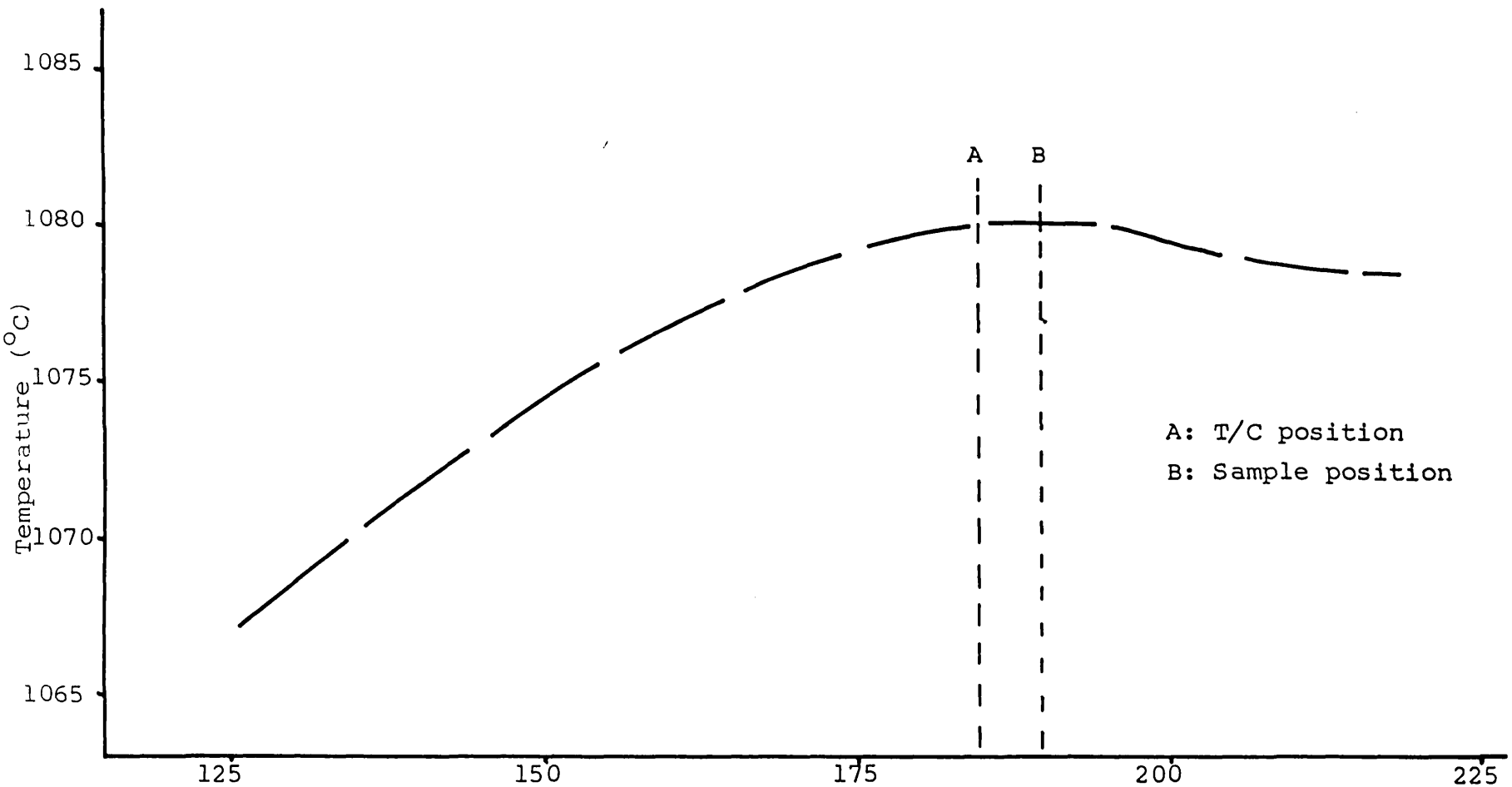

Fig. 3.3 TEMPERATURE PROFILE ALONG THE LENGTH OF THE FURNACE

BDH Chemicals Ltd. and the two types of Dolomite were provided from STEETLEY MINERALS (see Table 3.4). These oxide powders were held in the furnace at 1000°C for 1 hour to eliminate the possible existence of CO_2 or H_2O and other volatile matter.

3.5. PROCEDURE FOR REDUCTION EXPERIMENTS

The reduction experiments were carried out in two stages. Each sample was reduced to the Wustite region with CO 50, CO_2 50% mixtures at various temperatures (Reduction temperatures employed for these experiments are 950, 1050 and 1100°C. In some cases, 850°C was also used for several specimens). After pretreatment, the reduction experiments were carried out in a high purity (99.99%) CO gas atmosphere at various temperatures (950, 1050 and 1100°C and occasionally at 850°C). Reduction experiments were carried out at these temperatures on specimens which had been pretreated at 950, 1050 and 1100°C. This is schematically illustrated in Fig 3.6 . The gas was dried by passing through a column of magnesium perchlorate and subsequently a column of soda asbestos to eliminate CO_2. Prior to the attainment of the reaction temperature, N_2 gas was passed through the apparatus as inert gas. Nitrogen was also purified by passing through a furnace containing copper gauze. This copper gauze was kept at 550°C to eliminate oxygen from the nitrogen.

The gas flow rate in all experiments was adjusted to 2 l/min (Preliminary experiments with various gas flow rates confirmed that 2 l/min was above the critical flow rate to eliminate gas starvation, see Fig 3.7).

Key to Fig 3.4

A	Amature of the L.V.D.T.
B	Zero adjustment
C	Alumina adopter
D	Platinum wire and hook
E	Perspex holder
F	L.V.D.T. support
G	Rubber pad
H	L.V.D.T. box
I	Water inlet
J	Rubber " O " ring
K	Split brass sleeve
L	Electrical leads
N	Argon gas inlet
O	Water outlet
P	Mild steel plate
R	Quartz reaction tube
S	Seal
T	Thermocouple

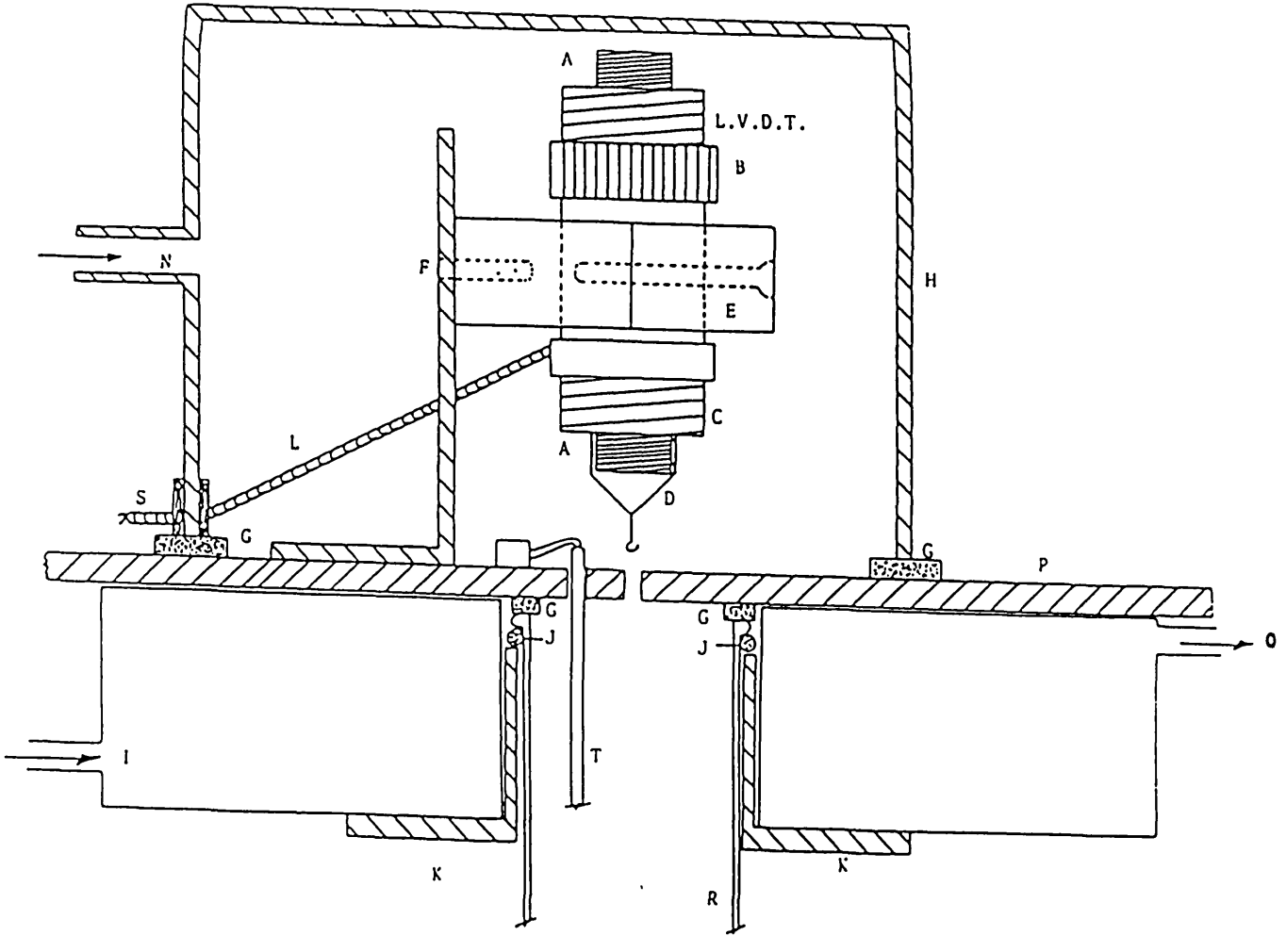

Fig. 3.4 L.V.D.T. and mounting

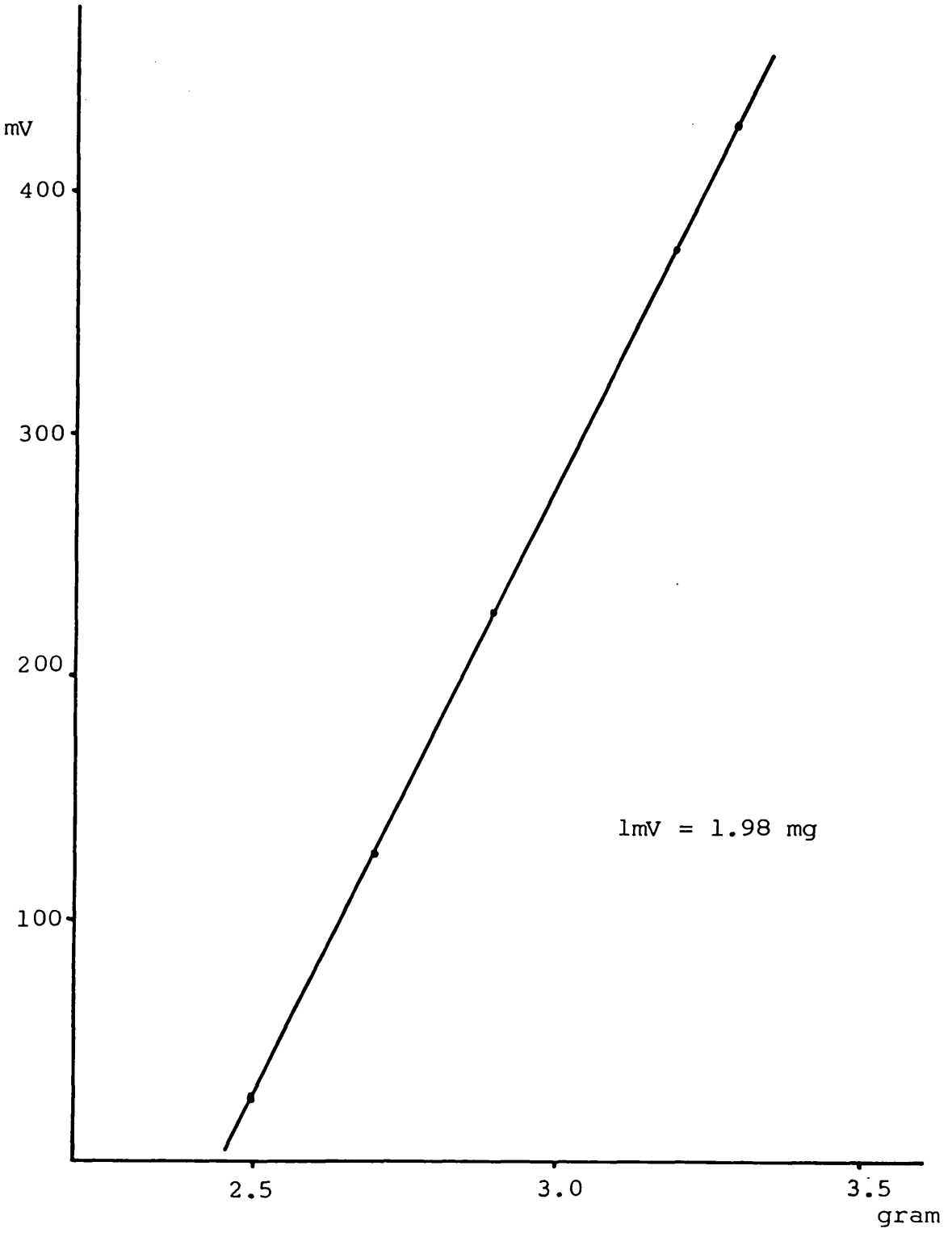

Fig. 3.5 CALIBRATION OF L.V.D.T.

TABLE 3.1

Chemical composition of Carol Lake iron ore

	Iron ore concentrates	Oxidized ore
T . Fe	65.62	65.16
Fe^{2+}	6.53	0.44
SiO_2	4.48	4.73
CaO	0.2	0.2
MgO	0.6	0.5
Al_2O_3	0.2	0.2
Mn	0.29	0.28
P	0.011	0.01
S	Tr.	Tr.

TABLE 3.2

Particle size distribution of Carol Lake iron ore

Diameter (μm)	Wt. fraction of sample
+300	0.09(%)
-300 +210	0.16
-210 +150	0.82
-150 +104	5.0
-104 + 75	16.33
- 75 + 53	19.77
- 53	57.83

The prepared sample was kept on a platinum pan or basket - this depended on the state of specimen - and then suspended in the constant temperature zone of the reaction tube from the armature of the L.V.D.T. by a platinum chain. The weight of the sample and temperature of the specimen were automatically recorded throughout an experiment. After reduction the furnace was lowered and the reduced sample was cooled in a nitrogen atmosphere to prevent re-oxidation of the reduced specimen.

To obtain rapid cooling, a special cooling system consisting of spiral copper pipe containing holes directed towards the reaction tube and an air compressor was used. The pressure of the compressed air for the cooling system was maintained at 100psi to give a homogeneous cooling rate. With this system, the cooling rate of 400^{o}C/min could be obtained down to 150^{o}C .

The representative samples were taken for X-ray diffraction, optical microscopic examination, electron- probe microanalysis (Quantitative EDX analysis and Digital X-ray mapping) and surface area measurements (B.E.T).

3.6. X-RAY DIFFRACTION (X.R.D)

The phases present in each of the samples whether reduced or unreduced were determined by X-ray powder diffraction using a Guinier focussing camera with monochromatized Co K_{α} radiation (Metallurgy department) or Cu K_{α} radiation (Chemistry department).

Guinier focussing camera has been found to give, by a simple and rapid procedure, results satisfactory for most

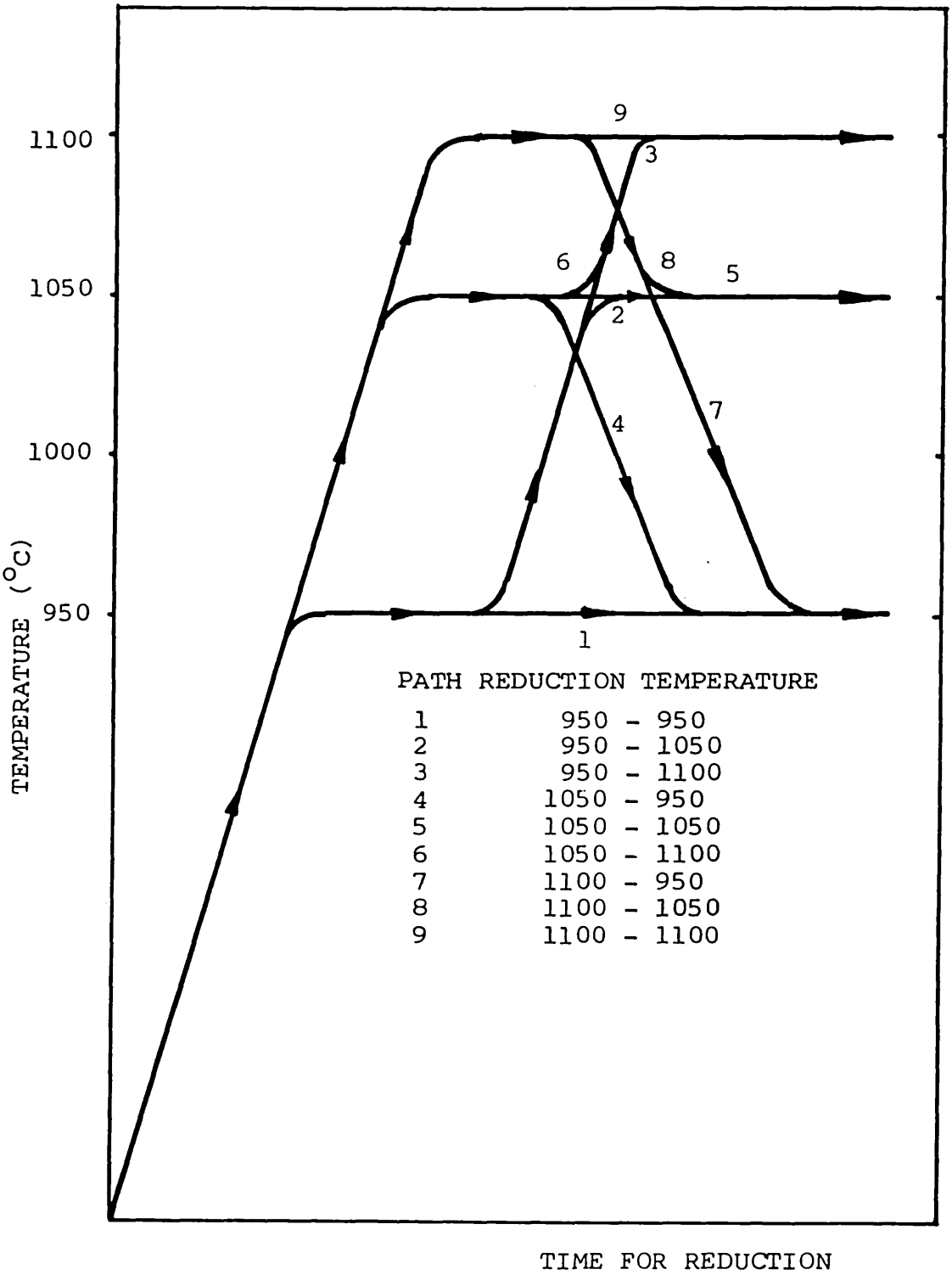

Fig. 3.6 SCHEMATIC DIAGRAM OF REDUCTION PROCEDURE

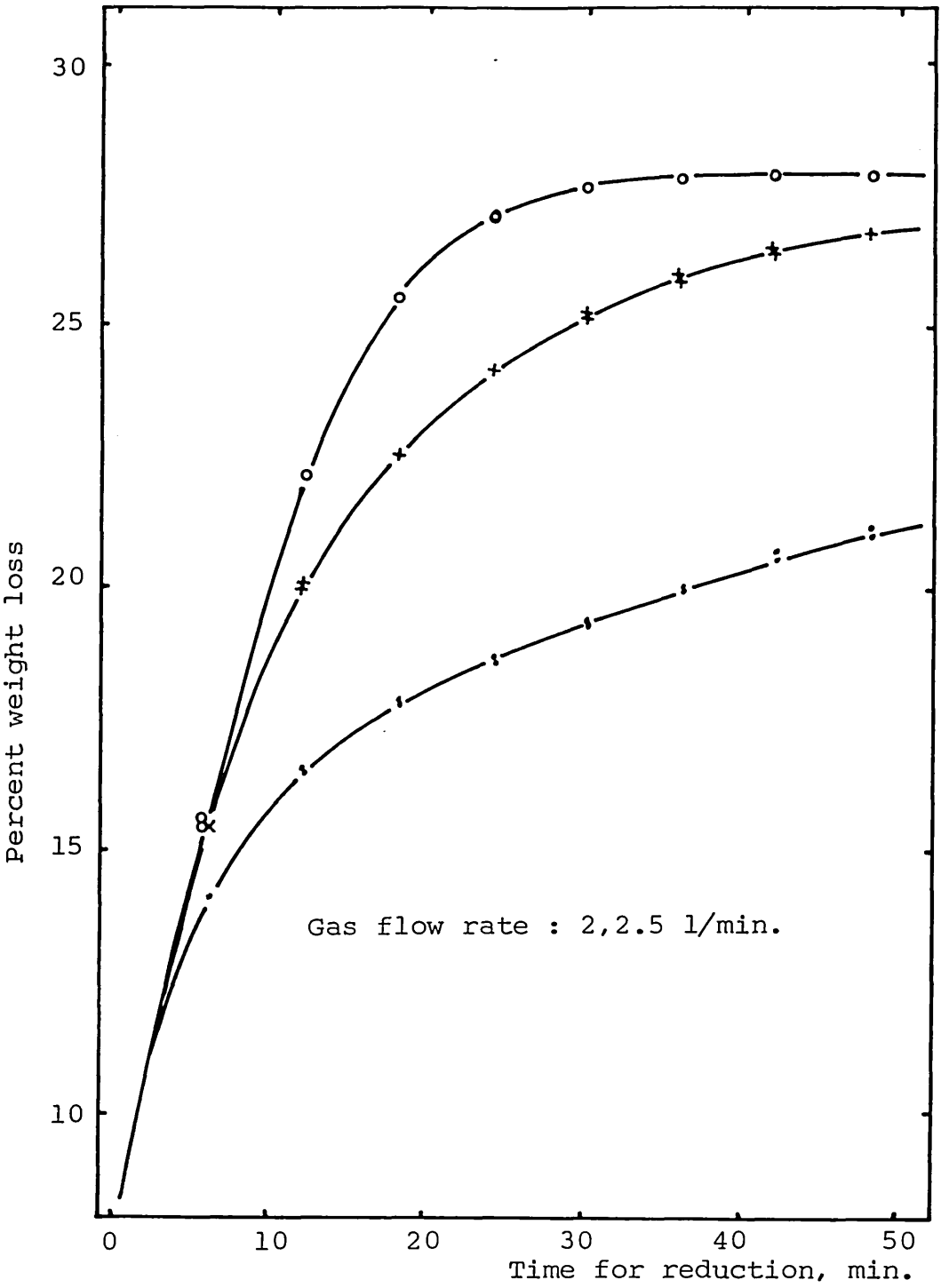

Fig. 3.7- The effect of gas flow rate on the rate of reduction.
Reduced at 950,1050 and 1100°C with wustite produced at 950°C (compacts without addition).

TABLE 3.3

SPECIFIC GRAVITY OF SINTERED SAMPLE

Sample	S.G(g/cm^3)	Porosity
Non addition	4.74	1.25%
1% CaO	4.46	
2% "	4.16	
5% "	4.04	
1% MgO	4.33	
2% "	4.16	
5% "	3.92	
1% Thrislington Dolomite	4.21	
2% "	4.02	
5% "	3.74	
1% Whitewell Dolomite	4.30	
2% "	4.08	
5% "	3.86	

@ Porosity was Calculated from the powder state of each sample.

TABLE 3.4

CHEMICAL ANALYSIS OF DOLOMITE USED AS ADDITIVES

	Thrislington Dolomite	Whitewell Dolomite
SiO_2	0.8	1.0
Al_2O_3	2.4	0.5
Fe_2O_3	1.0	1.0
CaO	61-63	55-57
MgO	35-37	39-41
CaO/MgO	1.72	1.4

needs. X-ray diffraction photography of four different samples can be taken simultaneously on the same film which allows a quick comparison. The exposure time was 2.5 hours in all cases (30 KV, 20mA).

3.7. OPTICAL MICROSCOPY

For optical microscopy, sample were mounted in "Metset" mounting resin. The specimens were ground on silicon-carbide papers to 800 grade and then polished with 7 μm, 3 μm, 1 μm and 1/4 μm "Hyperz" diamond compounds. The optical microscope used for the specimen was Reichert MeF II Inverted Photographic Microscope.

3.8. ELECTRON PROBE MICROANALYSIS

The same samples which were investigated for optical microscopy were used for electron probe microanalysis. The qualitative analysis was done by Digital X-ray mapping method using DIGIMAP disc and each ion in the specimen was displayed on the screen and the distribution of ions was taken picture for comparison. The quantitative analysis was carried out as point analysis for small areas ($\leq$10 μm) and area analysis for relatively big areas ($\geq$10 μm). ZAF 4 programmed disc was used for the quantitative EDX analysis and electron microscope used was Jeol JSM 35CF. The results were recalculated as oxides form related to the whole phases determined by the X.R.D .

3.9. SURFACE AREA

Surface area before and after reduction was measured by using B.E.T (Brunner Emmet Teller) technique for the

some selected specimens. This B.E.T technique for the Krypton adsorption isotherm at liquid nitrogen temperature (-195°C) was determined by the Equation for multilayer adsorption and this is given by

$$\frac{P}{V\ (Po-P)} = \frac{1}{C\ Vm} + \frac{C-1}{C\ Vm} \cdot \frac{P}{Po}$$

where C : constant for a given gas-solid system.

V : amount of Krypton (ml at STP per gm) adsorbed at the pressure P.

Po : the saturation vapour pressure of Krypton at -195°C

Vm : the volume required to complete monolayer.

A plot of left hand side of the equation against P/Po gives a straight line up to 0.32. Knowing the value of Vm from the slope and the intercept, the surface area was computed taking the cross-sectional area for the Krypton to be $0.185 \times 10^{-14} cm^2$.

The symbol used for the kinetic analysis

- • : reduction at 950°C
- × : reduction at 1050°C
- o : reduction at 1100°C

CHAPTER 4

RESULTS AND DISCUSSION

CHAPTER 4

RESULTS AND DISCUSSION

4.1. INTRODUCTION

In the present work, the reduction characteristics of six different groups of samples were investigated. The samples consisted of Carol Lake iron ore concentrate in both powder and compacted form and compacts with CaO, MgO and two types of natural dolomite were studied as examples of flux additions.

For each flux, additions of 1,2 and 5% by weight were investigated. The Carol Lake iron ore, which consisted of α- hematite with 4 weight percent α- Quartz as the major impurity, was reduced in powder and compact forms to establish basic data for comparison. A total of 450 kinetic experiments were carried out at temperatures of 950, 1050 and 1100^{o}C.

In each case, the reduced and partially reduced samples were examined using X-ray diffraction(XRD), optical microscopy and electron probe microanalysis(EPMA).

4.2. IRON ORE POWDER AND COMPACTS WITHOUT ADDITION

Natural Carol Lake iron ore concentrate was reduced in both powder and compact forms. The results for the reduction of iron ore powder at temperatures 950, 1050 and 1100^{o}C are shown in Fig 4.1-3 . These experimental results are presented in terms of percent weight loss versus time of reduction. The percent weight loss is defined as follows:

$$\% \text{ weight loss} = \frac{\text{weight loss at time t}}{(\text{weight of sample before reduction} - \text{weight of additive material})} \times 100$$

The figures also illustrate the excellent reproducibility of these measurements. Each experiment will be described by a two temperature notation (950-1100) which indicates the temperature used for hematite to wustite reduction followed by the temperature used for wustite reduction to iron. In the case of flux additions, an additional notation is used which indicates the flux material being added and its concentration placed after the temperature notation, such as (950-1100)·CaO 2%.

4.2.1. EFFECT OF TEMPERATURE

The effect of temperature on the rate of reduction of wustite to iron is illustrated in Fig 4.1-3 (powder without addition) and Fig 4.4-6 (compacts without addition). As expected, it is seen that the higher the temperature the faster the overall rate of reduction. In the case of powder specimens at 1100^{o}C , 99.5% of reduction was achieved within 30 minutes while 90% and 70% reduction were observed at 1050^{o}C and 950^{o}C respectively in this time. In Fig 4.2, the overall rate of reduction at each temperature decreases and the difference between reduction rates at (1050-1100)·P and (1050-1050)·P becomes larger while the difference between the reduction rates at (1050-1050)·P and at (1050-950)·P are more or less the same as that between those of for (950-1050)·P and (950-950)·P . The reduction rate at (1100-950)·P indicates an initial rate which decreases

until 30 minutes have elapsed and then shows a linear rate of reduction.

In the reduction of iron ore compacts, the reduction rate at (950-1050)· C does not show the decrease in initial rate expected with temperature (see Fig 4.4). Investigation of the samples after reduction showed the occurrence of significant swelling (or cracking) in the samples (this phenomenon is mainly caused during reduction from hematite to wustite). It is suggested that this cracking is necessary for the high initial reduction rate due to an increase in surface area and ease of ingress of gas. For reduction at (950-1100)· C , fast reduction is observed for 12 minutes and thereafter a linear rate of reduction occurs. In contrast, the reduction at (950-1050)· C shows the expected gradual decrease in rate until 15 minutes have elapsed. The reduction at (950- 950)· C also shows rate of reduction which decreases with time (see Fig 4.4). In Fig 4.5 and Fig 4.6 , the reduction rates at 1050°C are seen to be slightly slower when compared with the reduction rate at (950-1050)· C , due to the absence of cracking. It should be noted that these results are reproducible and consistant-severe cracking of the compacts was only noticed with samples treated at (950-1050)· C condition.

4.2.2. EFFECT OF WUSTITE PREPARATION TEMPERATURE

As seen in Fig. 4.1-3, the wustite preparation temperature affects the reduction rate significantly. When the wustite is produced at low temperatures, the reduction to iron by carbon monoxide is observed to be faster at each

subsequent reduction temperature. At 950°C, the reduction rate to iron is observed to decrease for higher temperatures of wustite production. Although the reduction rate at (1050-1050)· P is less than the reduction rate at (950-1050)· P, it is similar to that of at (1100-1050)· P. Similar observation are made for reduction at 1100°C. Thus, it can be seen that the temperature at which wustite is formed has a considerable effect on the rate of the subsequent reduction to iron. Wustite formed at the lowest temperature is most easily reduced.

As seen in Fig , 4.4-6, the effect of the temperature of wustite formation on the rate of iron formation is much less marked than for powder specimens for final reduction at 1100°C. For reduction to iron at 1050°C, the production of wustite at 1050°C or 1100°C seems to have no effect. However for final reduction at 950°C, the lowest reduction rate is observed for wustite formed at 1050°C.

4.2.3. EFFECT OF GAS COMPOSITION

Fig. 4.7 shows the effect of gas composition on a plot of percent weight loss against reduction time at 950°C for wustite samples produced at 950°C (CO/CO_2= 1) with iron ore powder. As expected, it is seen that the composition of the reactant gas affects the initial rate of reduction significantly and then all reduction rates become linear.

4.2.4. IDENTIFICATION OF THE PHASES PRODUCED BY REDUCTION

The phases present in the natural iron ore were α-hematite, magnetite and α- Quartz. However, the mate-

rial used in these experiments was obtained by the oxidation of this powder at 650°C in air for 24 hours and the phases present were α- hematite and α- Quartz. Chemical analysis showed the presence of a negligible quantity of ferrous ions. The phase changes occurring during reduction at the three temperatures studied were determined for samples reacted for 1 hour.

The XRD results of samples reduced at 950, 1050 and 1100°C in CO/CO_2 = 1 atmosphere for the preparation of wustite showed the presence of wustite, α- Quartz and α- Cristobalite. The intensity of the X-ray reflexions indicated an increase in the α- Cristobalite content for increasing reduction temperatures.

The XRD results are shown in Table 4.1 (Powder) and Table 4.2 (Compacts). On the basis of the chemical composition of the ore, 27.94% weight loss would correspond to 100% reduction of the oxidized iron ore. It is evident, however, that 1 hour is sufficient for total reduction at 1050°C and 1100°C, while at 950°C only about 75% reduction was accomplished.

Wustite

During reduction of hematite to wustite, the hematite transformed to wustite completely within 15 minutes as confirmed by XRD. No other iron oxide phases were observed. Following reduction from wustite to iron, wustite was still observed depending on the degree of reduction and, in all cases, the intensity of wustite reflexions agreed well with the degree of reduction.

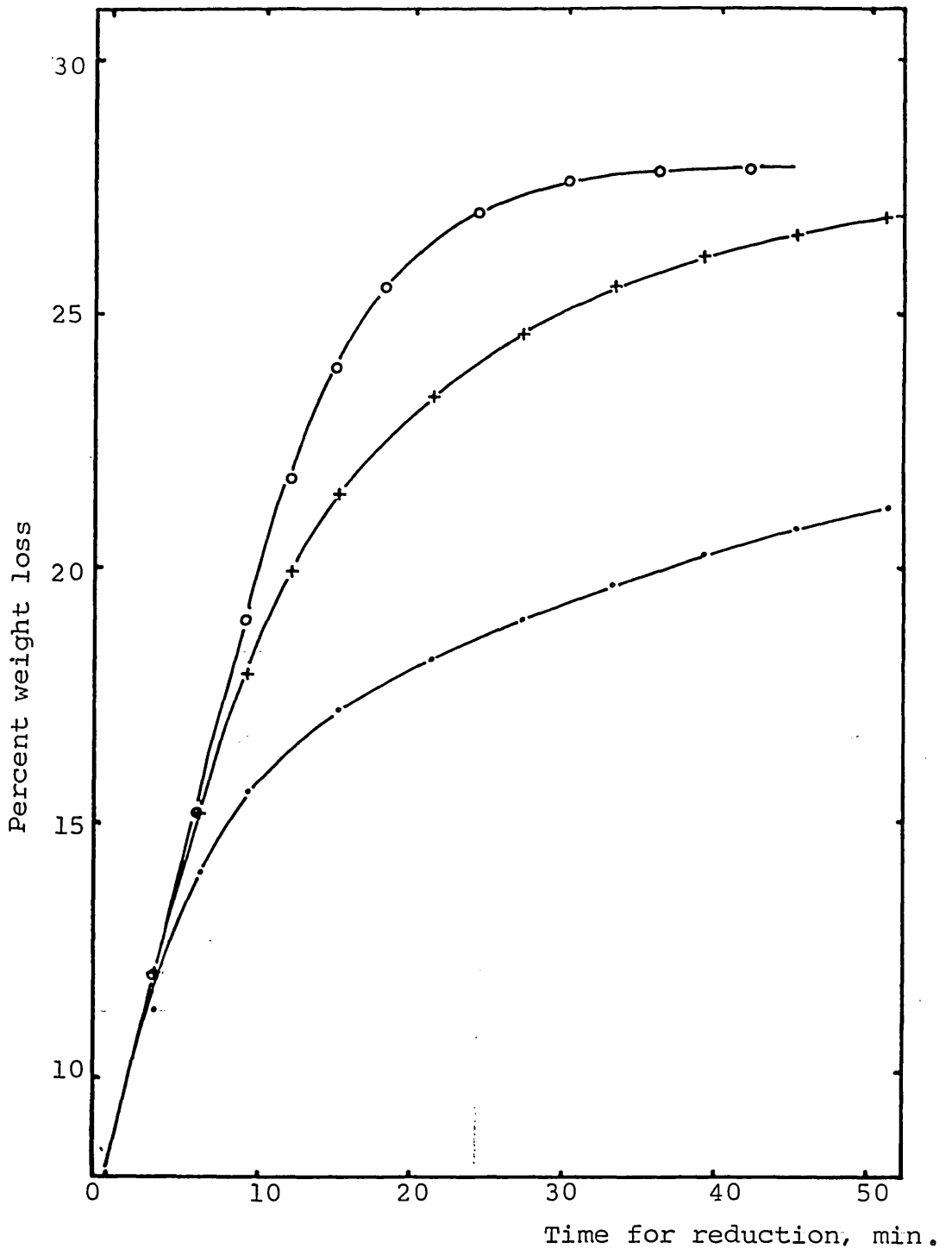

Fig. 4.1- The effect of temperature at 950, 1050 and 1100°C on reduction of wustite powder pre-reduced at 950°C without additions.

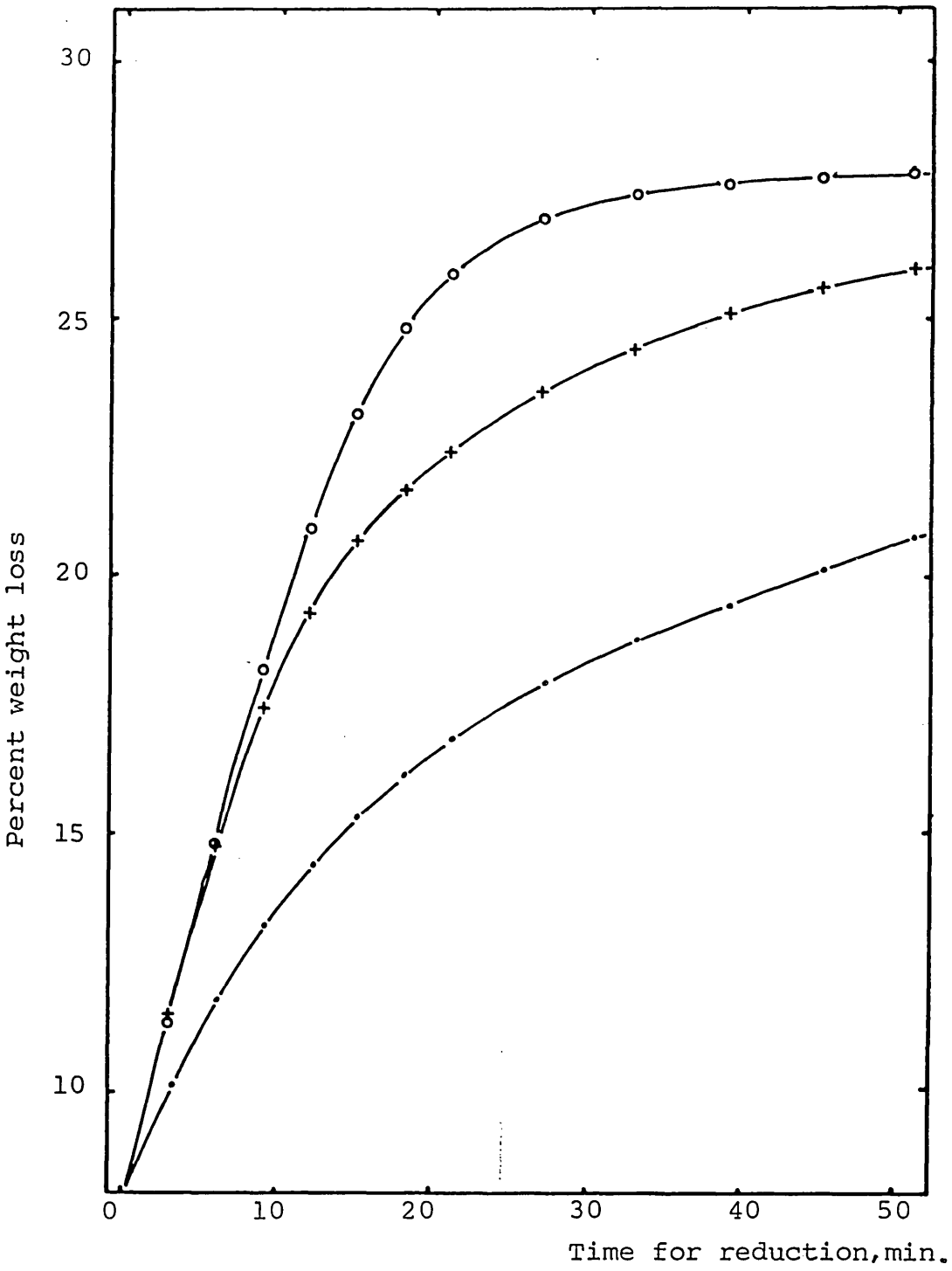

Fig. 4.2- The effect of temperature at 950,1050 and 1100°C on reduction of wustite powder pre-reduced at 1050°C without additions.

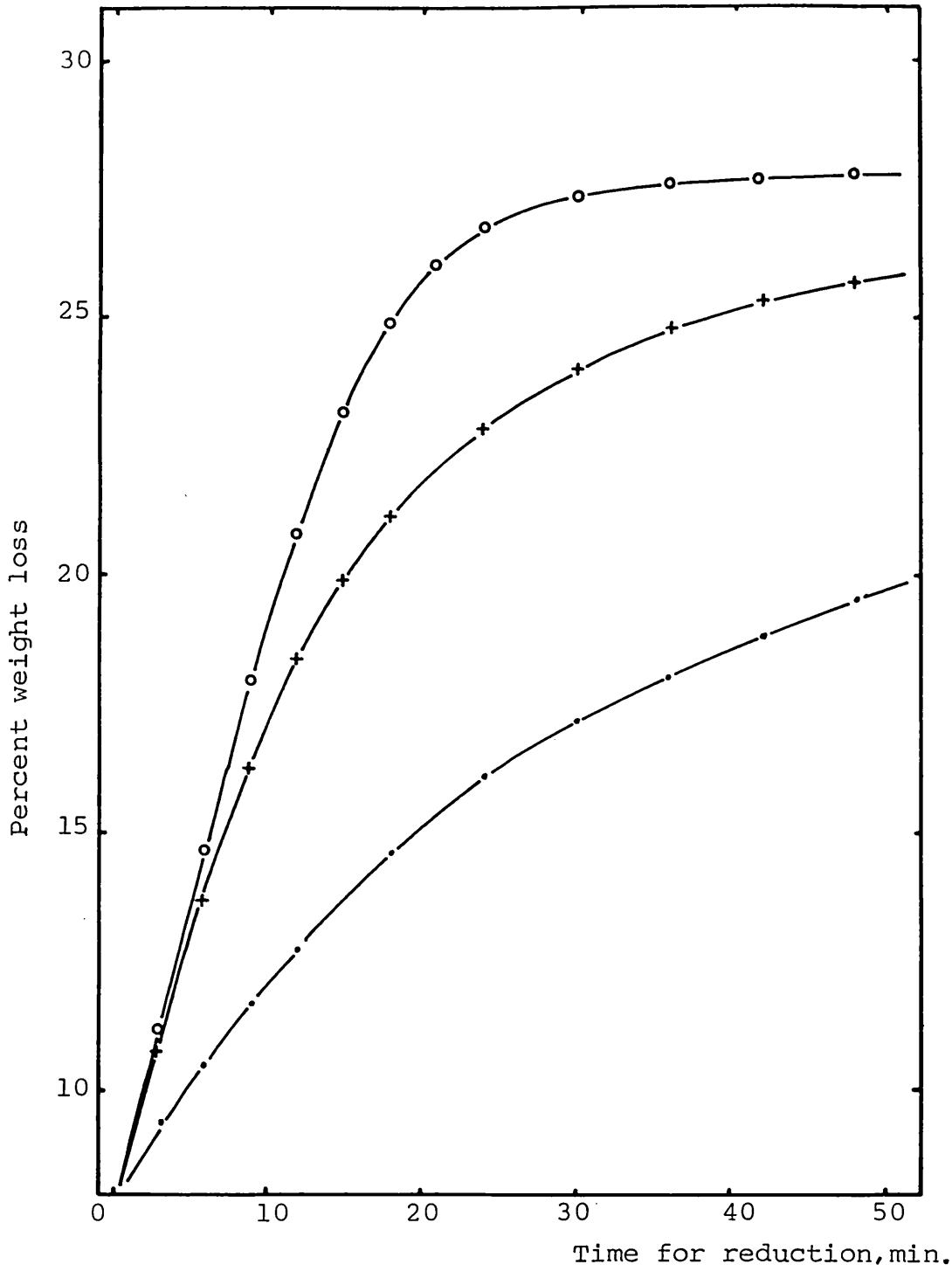

Fig. 4.3- The effect of temperature at 950, 1050 and 1100°C on reduction of wustite powder pre-reduced at 1100°C without additions.

Iron

In every sample, iron (α- iron), was observed and the intensity of iron reflexions was very strong.

Fayalite ($Fe_2 SiO_4$)

The formation of fayalite seems to be very temperature sensitive. Fayalite was observed only after high temperature reduction with powder samples (1100°C) and for compacts (1050, 1100°C). To study the rate of fayalite formation wustite formation was continued for 1 hour and 2 hours. The composition of the reducing gas was also varied i.e. $CO/CO_2 = 1$ and $CO/CO_2 = 7/3$ (very close to the iron phase boundary at 1100°C, see Fig 2.3). Fayalite formed at this temperature in both gas compositions but was not observed with ($CO/CO_2 = 1$ at 950°C) even after 1 hour.

With these powder specimens, fayalite was only observed for reduction conditions (950-1100), (1050-1100) and (1100-950), (see Table 4.1) i.e. some heat-treatment at 1100°C seemed to be essential. However, with the compacted specimens, the fayalite was observed in almost every specimen, an exception being(950-950)·C . The intensity of fayalite is related to the percent weight loss (degree of reduction) of the sample.

α- Quartz and α- Cristobalite

The silica was observed in the starting material (oxidized iron ore powder) as α- Quartz, and α- Cristobalite was not identified. After reduction, α - Quartz was observed

in every sample (powder and compacts). The intensity of α- Quartz reflexions (Table 4.1 , 4.2) shows a gradual decrease with increasing reduction temperature, while the intensity of α- Cristobalite decreases with increasing reduction temperature for powder (see Table 4.1).
The intensity of α- Cristobalite after reduction is always stronger in compacted samples than with powder, cf Table 4.1 and 4.2.

Cementite

Cementite was observed in every reduced powder samples even in the presence of wustite (e.g. 75% of reduction). However, with compacted specimens, (1050-950)· C and (1100-950)· C , no cementite was observed with degrees of reduction of 64.5% and 77.7% respectively. The intensity of the cementite reflexions was stronger for higher reduction temperatures with powders but was less consistant with compacts.

4.2.5. STRUCTURAL CHANGES DURING REDUCTION

The microstructures of Carol Lake iron ore powder and the wustite particles produced at 950°C in CO/CO_2 = 1 atmosphere are shown in Plate 1.a and Plate 1.b respectively. The wustite grains contain internal cracks and the iron structures seems to be directly related to these cracks after reduction (see Plate 1.c). Plate 2 shows the microstructure at various temperatures of iron produced

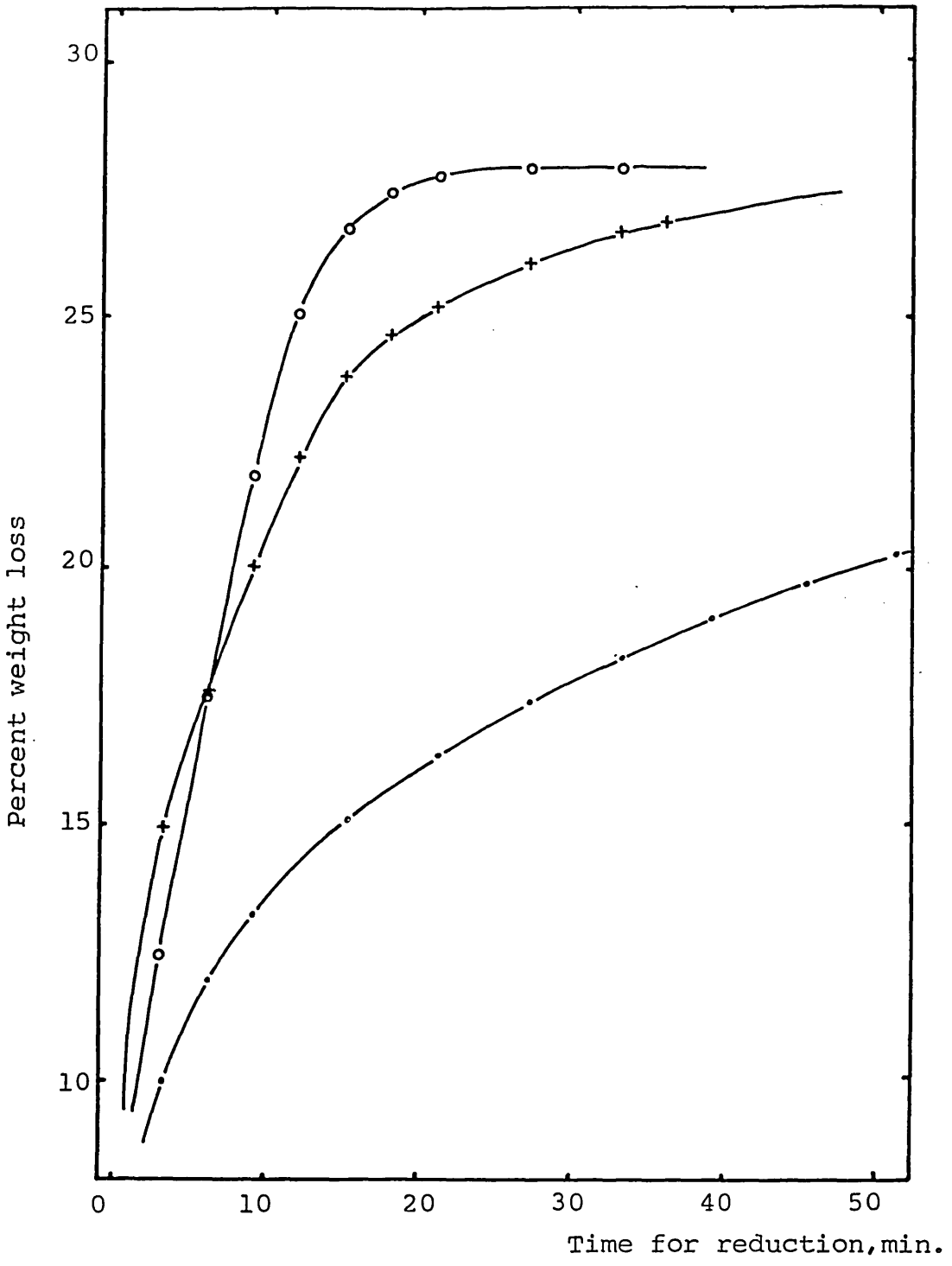

Fig. 4.4- The effect of temperature at 950, 1050 and 1100°C on reduction of wustite compacts pre-reduced at 950°C without additions.

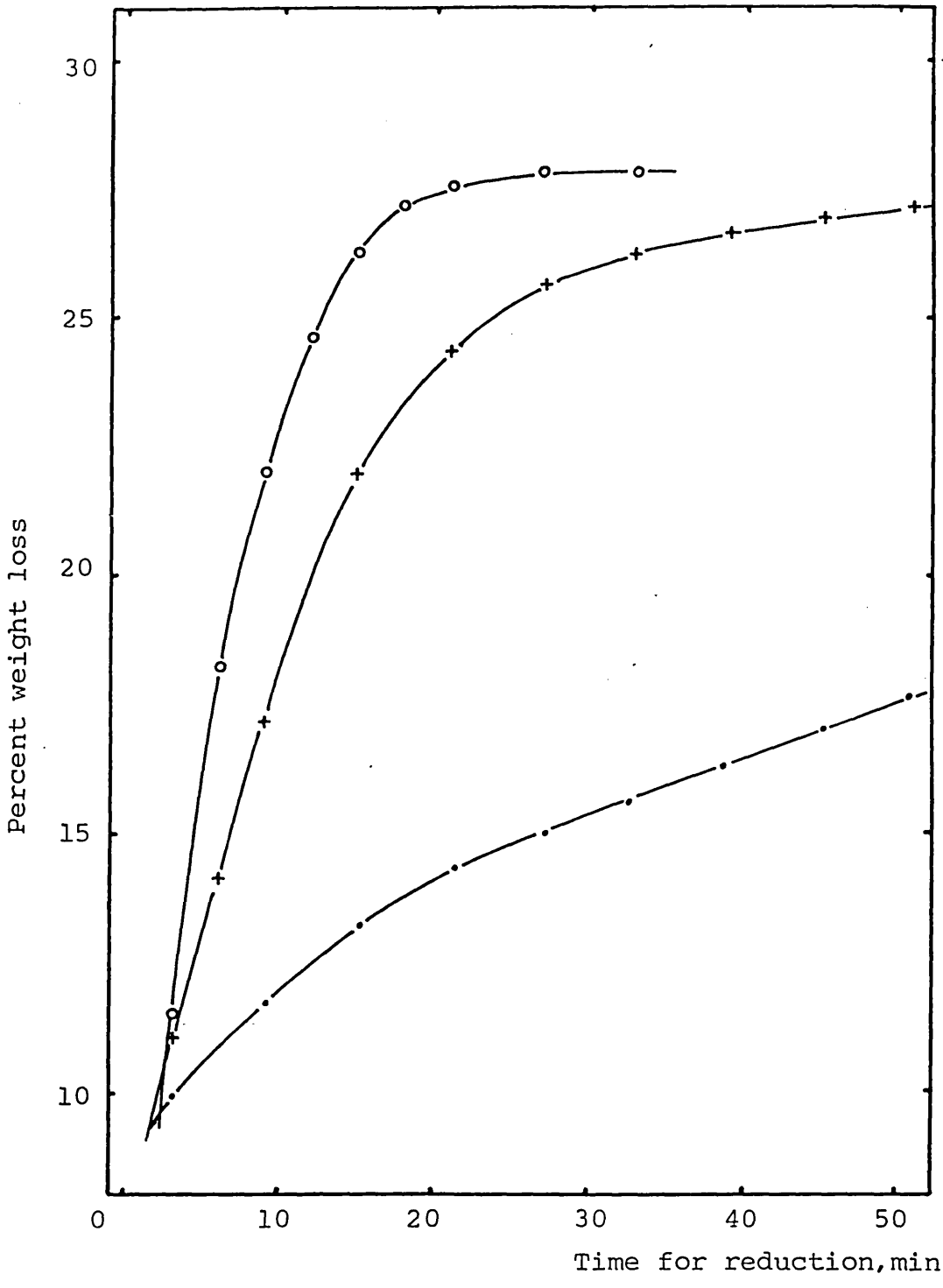

Fig. 4.5- The effect of temperature at 950, 1050 and 1100°C on reduction of wustite compacts pre-reduced at 1050°C without additions.

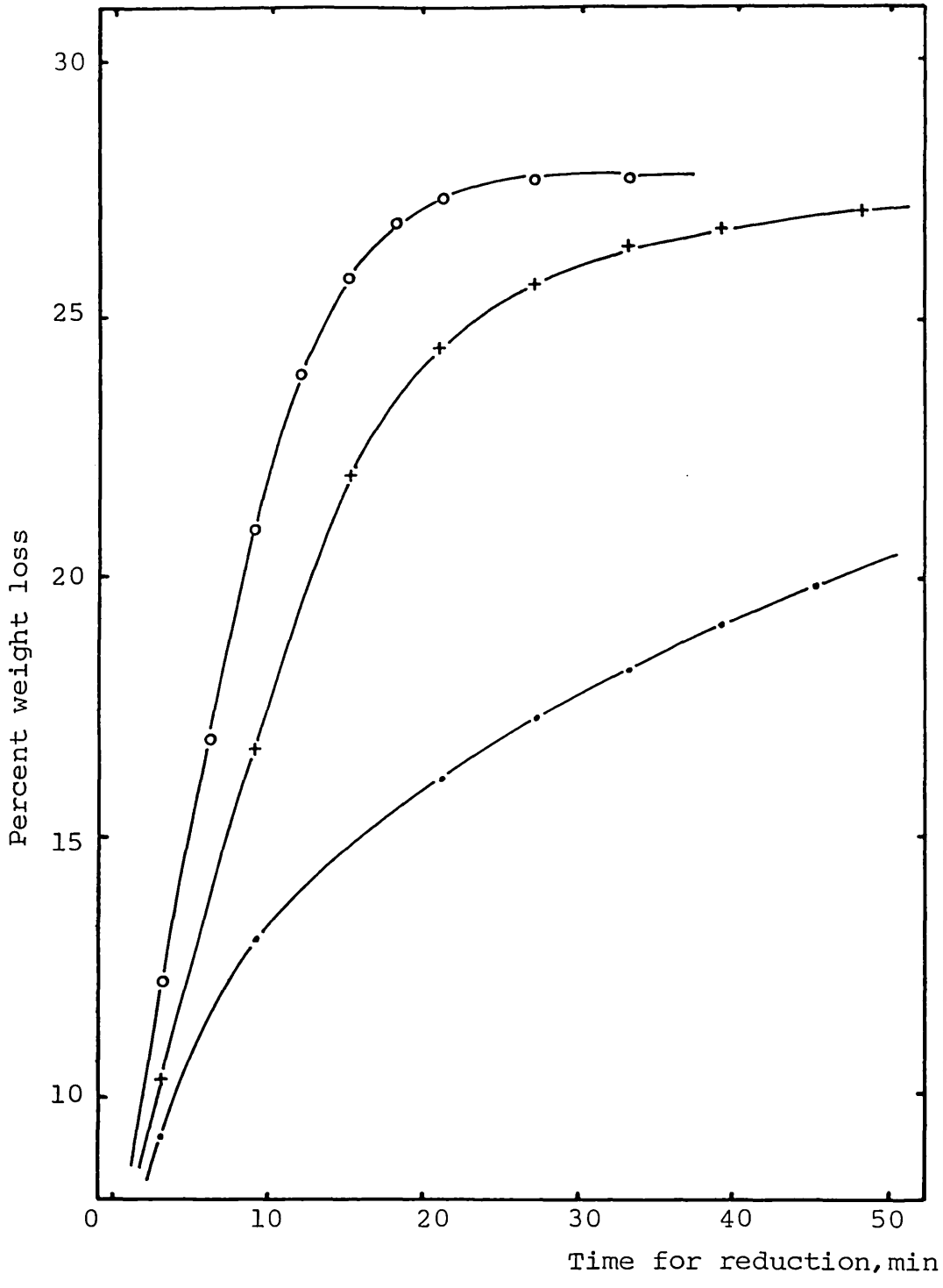

Fig. 4.6- The effect of temperature at 950, 1050 and 1100°C on reduction of wustite compacts pre-reduced at 1100°C without additions.

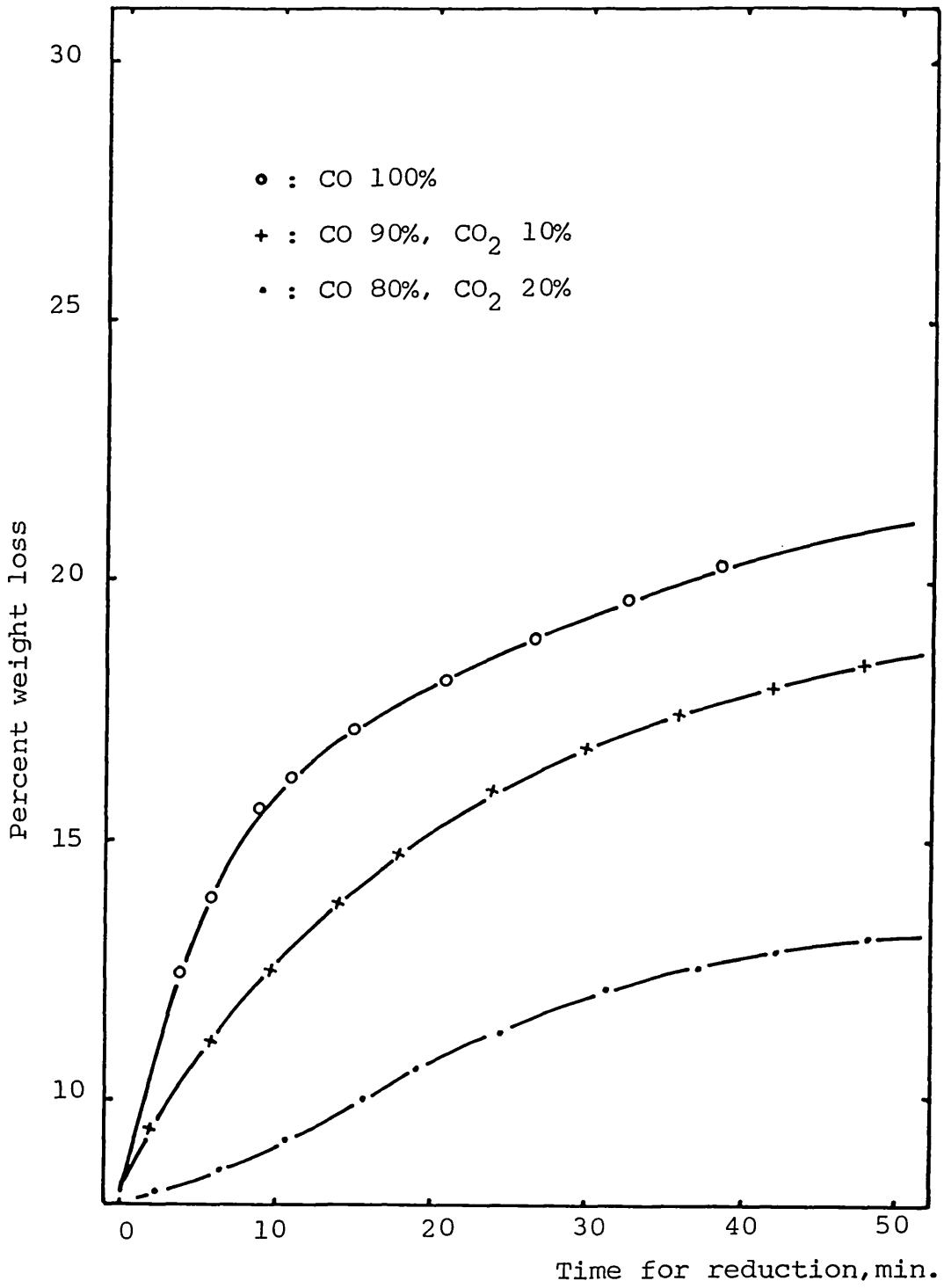

Fig. 4.7- The effect of gas composition on the reduction at (950-950)·Compact.

from wustite made at 1100°C. While the individual grains consist of unreduced wustite surrounded by the thick iron layer (relatively large particles) they show the partial progress of sintering from outside. Plate 4.a shows the microstructure of hematite (compacted and sintered at 1300°C in air for 24 hours) revealing considerable sintering of particles. After reduction of this compact at (950-1100)·C , the structure of iron seems to fall within two types. Plates 4.b and c show some iron grains with a microporous structure surrounded by a thick iron shell and small particles with an iron structure. Plate 3 shows the microstructure of a whole compact reduced at (1100-1100)·C. This illustrates that the gas penetrates through the specimen from the beginning and reduction occurred in the center even at 25% of reduction. Plate 5 shows significant changes in the structure of the iron with reduction temperature. Plate 6 and Table 4.3 illustrate the distribution of elements and the results of EPMA respectively. The numbers in Plate 6 I, II show the analysed points of EPMA and it demonstrates that the silica particles remain unreacted or only partially reacted from the surface (Plate 6.I , II). However the silica particles shown in Plate 6 II shows that a small amount of FeO (4% by weight) had reacted with a silica particle and the iron is distributed in a kind of heterogeneous segregation. The concentration of silica in the microporous iron structure is very low for both examples.

4.2.6. DISCUSSION

As expected, it is seen that the higher the temperature of reduction, the faster the overall rate of reduction. However the reduction rate at low temperature depends on the type of wustite reacted. The reduction rate at (950-950)·P, (1050-950)·P and (1100-950)·P shows a gradual decrease and it is considered that sintering is more likely to occur at higher temperatures of wustite formation. After production of wustite, the powder samples were observed to be sintered more at the higher temperature, while cracking(or swelling) was observed in the compacts at every temperatures. When iron oxide particles sintered, access of the reducing gas becomes more difficult and the reduction rate shown in Fig. 4.1-3 (reduction temperature 950^{o}C) essentially agrees with this interpretation. However the phenomenon illustrated in the previous section that the reduction rate at high temperature is independent of the type of wustite seems to indicate the domination of the temperature effect on the rate of reduction overcoming the sintering effect. At higher temperatures (950-1050, 1050-1050, 1100-1050), it has been shown that the reduction rate is mainly dependent on the reduction temperature and at the later stages on the formation of fayalite. So the experiments were carried out to discover the rate of formation of fayalite at 950,1050 and 1100^{o}C for 1 and 2 hours in the CO/CO_2= 1 mixture.

At 950^{o}C, there was virtually no fayalite as determined by XRD, while at 1050 and 1100^{o}C, fayalite line were observed regardless of reduction time (1 or 2 hours).

This phenomenon indicates that the formation of fayalite can occur during reduction at the higher temperatures (1050, 1100°C) in the presence of wustite.

The amount of silica in the iron ore is 4% and moreover a higher concentration of silica (as α- Quartz) was observed in the size range + 150 μm. Unreacted individual silica particles have been observed by microscopy (Plate 6 I,II). This could explain why fayalite did not form in every powder sample whilst fayalite appeared in every compact (due to the closer compacting and sintering).

Another reason for the low rate of reduction at low temperature could be the blockage of pores by a liquid phase (fayalite). Whereas, the highest temperature (1100°C) used for reduction was far below the melting temperature of iron oxide and silica, the liquidus temperature of fayalite is close to this temperature. When the reduction of iron proceeds at low temperature, the liquid phase made at high temperature would freeze onto the pores and the access of reducing gas would be difficult.

The microstructure of iron after reduction has two distinct morphologies. During the preparation of wustite, this phase becomes fragile (Plate 1.b) and cracks are observed inside the particles. When this wustite is reduced to iron, the nucleation of iron occurs from the surface of the particles and is also associated with the cracks.

In this case, complete reduction could be obtained due to the greater surface area presented for reduction.

TABLE 4.1

XRD ANALYSES OF REDUCED SAMPLES OF IRON ORE POWDER WITHOUT ADDITIONS.

REDUCTION PROCEDURE	REDUCTION		PHASES IDENTIFIED
	% Wt.LOSS	TIME, MIN.	
950-950	24.2	60	Fe:VS, W:W, Q:M, C:VW
950-1050	26.9	60	Fe:VS, W:VW, Q:MW, C:VW, CR:VW
950-1100	27.9	42	Fe:VS, Q:W, FS:VW, C:W, CR:VW
1050-950	24.6	60	Fe:VS, W:MW, Q:W, C:W, CR:VW
1050-1050	27.0	60	Fe:VS, W:W, Q:W, C:VW, CR:W
1050-1100	27.9	52	Fe:VS, Q:VW, FS:VW, C:W, CR:VW
1100-950	21.0	60	Fe:VS, W:MW, Q:MW, FS:W, C:VW, CR:VW
1100-1050	26.6	60	Fe:VS, W:W, Q:MW, C:W, CR:W
1100-1100	27.8	60	Fe:VS, Q:MW, C:W, CR:W

@ ORDER OF INTENSITY:VS,S,MS,M,MW,W,VW,VVW

Fe : α- Iron

Q : α- Quartz

CR : α- Cristobalite, SiO_2

FS : Fayalite, Fe_2SiO_4

W : Wustite

C : Cementite, Fe_3C

TABLE 4.2

XRD ANALYSES OF REDUCED SAMPLES OF IRON ORE COMPACTS WITHOUT ADDITIONS.

REDUCTION PROCEDURE	REDUCTION		PHASES IDENTIFIED
	% Wt.LOSS	TIME, MIN.	
950-950	21.0	60	Fe:VS, W:S, Q:M, C:VW, CR:MS
950-1050	27.1	57	Fe:VS, W:MW, Q:M, C:W, FS:VW, CR:MS
950-1100	27.94	24	Fe:VS, Q:W, FS:VVW, C:VW, CR:M
1050-950	18.03	60	Fe:VS, W:S, Q:W, FS:W, CR:MW
1050-1050	27.4	60	Fe:VS, Q:MW, FS:VVW, C:VW, CR:M
1050-1100	27.94	27	Fe:VS, Q:W, FS:VVW, C:VVW, CR:M
1100-950	21.7	60	Fe:VS, W:S, Q:MW, FS:MW, CR:MS
1100-1050	27.3	60	Fe:VS, W:MW, Q:W, FS:VW, C:VVW, CR:W
1100-1100	27.7	33	Fe:VS, Q:MW, FS:VVW, C:VW, CR:MS

@ ORDER OF INTENSITY:VS,S,MS,M,MW,W,VW,VVW

Fe : α- Iron
Q : α- Quartz, SiO_2
CR : α- Cristobalite
FS : Fayalite, Fe_2SiO_4
W : Wustite
C : Cementite, Fe_3C

Another type is the reduction of relatively large wustite particles. During reduction, nucleation occurrs only from the surface and forms thick iron shell (γ- iron becomes saturated with carbon due to carbon deposition and diffusion into the iron) and further reduction could only proceed with carbon diffusing through the iron shell. The microporous structure is then developed by reaction of unreduced wustite with this carbon while the iron shell maintains its shape and CO is produced in the grains (Consideration of the gaps observed between iron shell and unreduced wustite support such an agreement). This change in mechanism is associated with the change in the weight loss with time curves especially at 950° and 1050°C where a significant reduction in rate is observed after fast initial reaction. The apparent linear portions of the curves at 950°C are also in agreement since steady state diffusion through a constant iron shell would produce linear weight loss with time.

Transformation of silica during reduction

α- Cristobalite was identified in most of the reduced samples (powder or compacts). Because of kinetic reasons, the transformation to cristobalite was hardly expected to occur in these experiments(especially at these temperatures). Some workers(75) report that the transformation of α- Quartz to α- Cristobalite takes 200 hours at 1500°C. Several experiments with iron ore compacts were carried out to investigate the formation of α- Cristobalite. When a wustite sample was prepared under the normal conditions used

TABLE 4.3 EPMA RESULTS.

NO.	COMPOSITION (Wt.%)						REMARKS
	Fe	FeO	CaO	SiO_2	MgO	MnO	
1	0	6.39	0.84	94.42	0.15	0.19	PLATE 6 I)
2	98.91	0	0	0.57	0.18	0.34	"
3	0	4.74	1.21	93.75	0.11	0.19	PLATE 6 II)
4	97.10	0	0	1.57	0.36	0.97	"
5	99.46	0	0.11	0.25	0	0.17	"

in this work i.e. within a period (15-20 minutes), no cristobalite was identified. However, when these samples were maintained in the same conditions for 1 hour or 2 hours, some transformation of α- Quartz to α- Cristobalite occurred other experiments with different gas composition (CO/CO_2 = 7/3, at 950,1100^{o}C) also produced α- Cristobalite. These results illustrate that the transformation to α- Cristobalite can be caused to occur in the presence of iron oxide (especially wustite). The gas composition (reducing atmosphere adapted for these experiments) did not affect the transformation since no transformation was identified by maintaining α- Quartz in a CO/CO_2 = 1 atmosphere at similar temperatures.

α - Cristobalite and fayalite

In the study of the intensities of XRD films, the relationship between (α- Quartz - Fayalite) and (Fayalite-α- Cristobalite) is rather difficult to understand.

PLATE 1

Micro-structure of a)hematite grains of natural Carol Lake Iron Ore powder, b)Wustite grains reduced with CO/CO_2=1 at 950°C (reduced from a)) and c)iron reduced at (950-1050)· powder.

a)

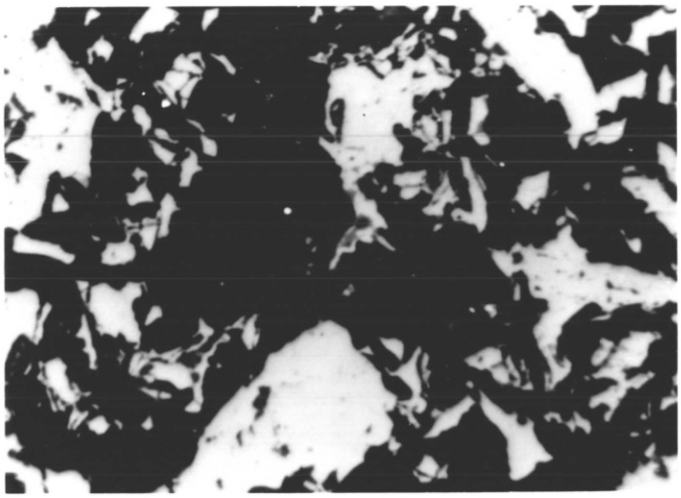

white : hematite
dark grey and
black : resine.

x 320

b)

light grey:wustite
black : resine
(voids)

x 320

c)

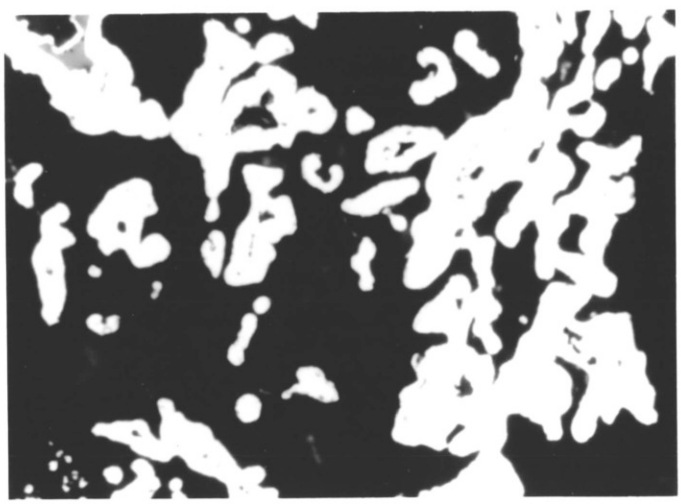

white : iron
light grey:wustite
black : resine
(voids)

x 320

PLATE 2

Micro-structure of iron reduced at a) (1100-950) · P, b) (1100-1050)· P and c) (1100-1100)· P .

a)

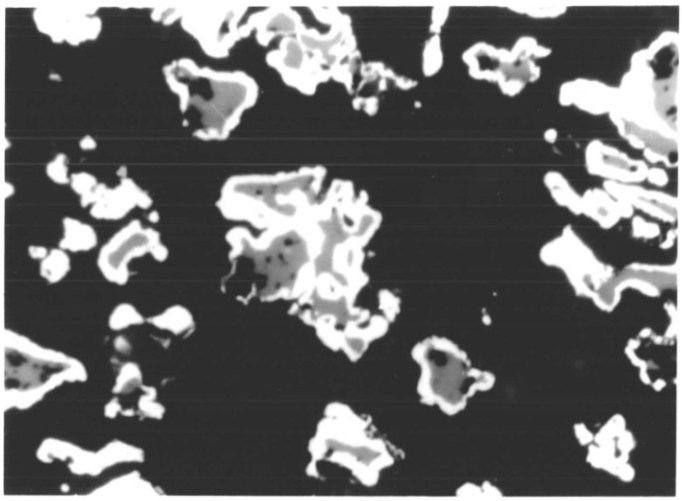

white : iron
light grey:wustite
black : voids

x 320

b)

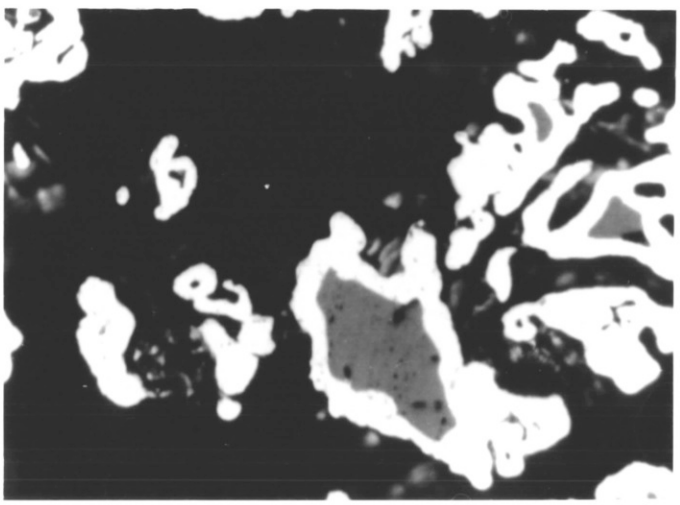

white : iron
light grey:wustite
black : voids

x 320

c)

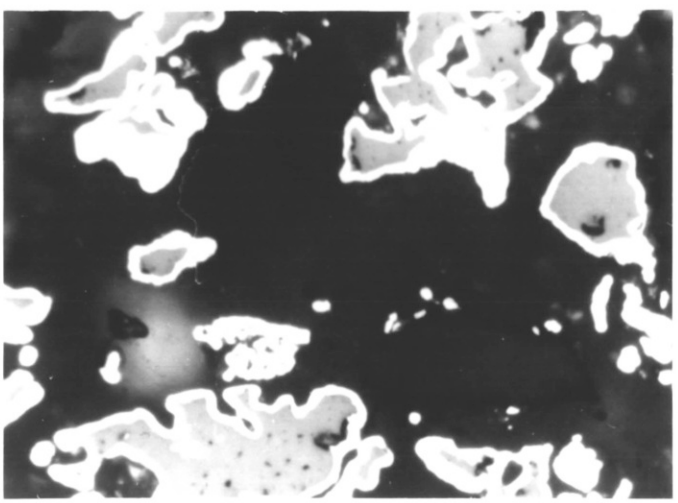

white : iron
light grey:wustite
black : voids

x 320

PLATE 3

Continuous photomicrographs of iron ore compacts reduced at (1100-1100)·C , showing a)25% of reduction , b)50% of reduction and c)75% of reduction proceeded respectively. white(iron), light grey(wustite), dark grey(silica) and black(voids). x 57

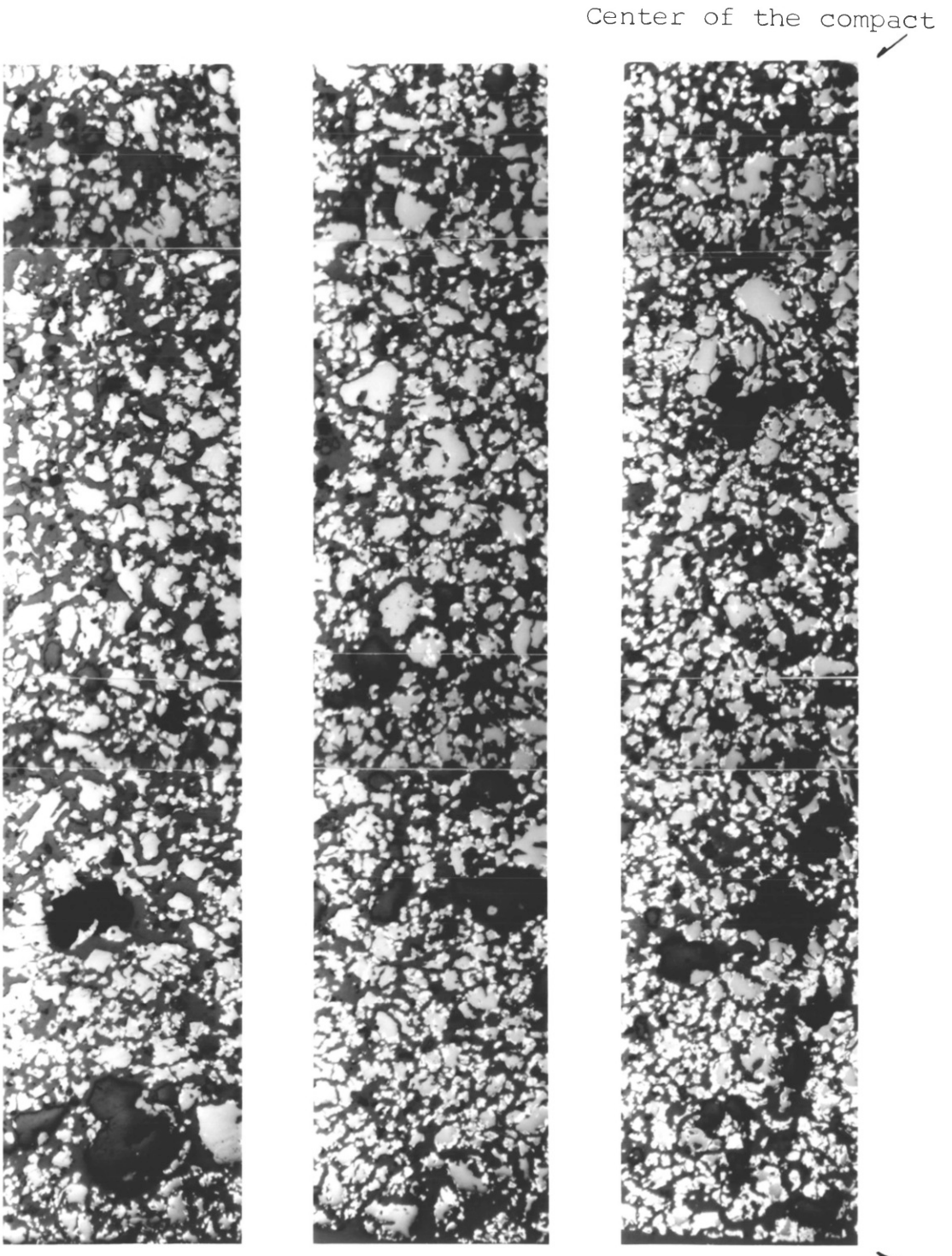

PLATE 4

Micro-structure of a)hematite grains of iron ore compact sintered at 1300°C for 24 hours in air and iron reduced at b) (950-1100)·C and (950-1100)·C .

a)

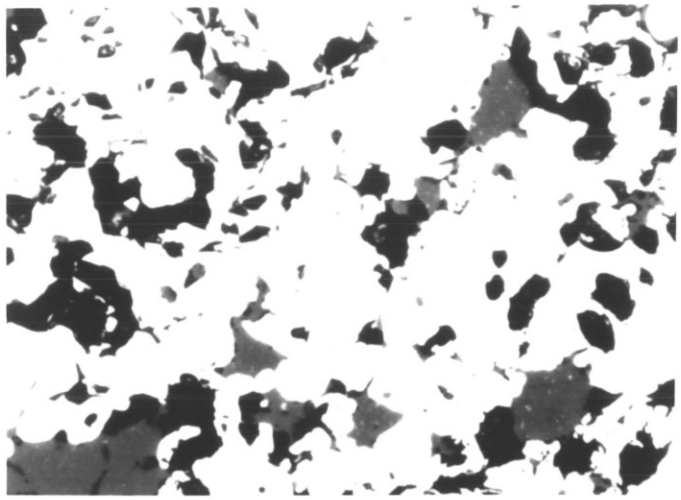

white : hematite
grey : α- Quartz
black : voids

x 320

b)

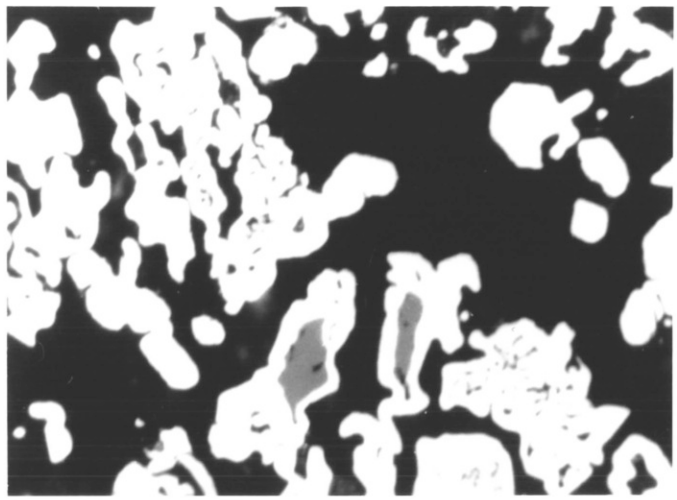

white : iron
light grey : wustite
black : voids

x 320

c)

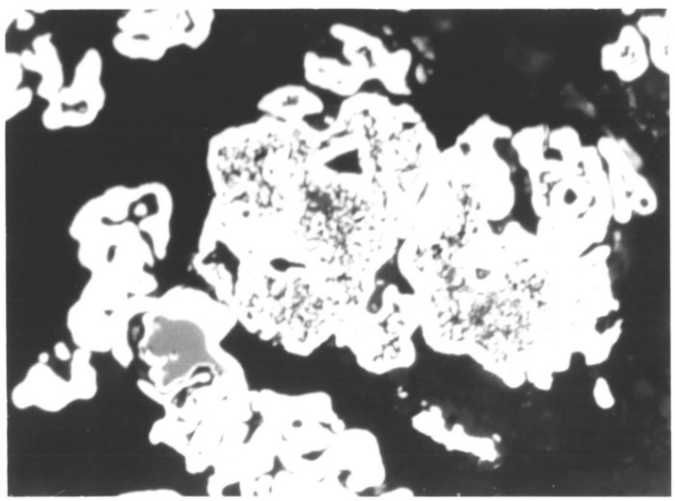

white : iron
light grey : wustite
black : voids

x 320

PLATE 5

Micro-structure of iron reduced at a) (1050-950)·C , b) (1050-1050)·C and c) (1050-1100)·C .

a)

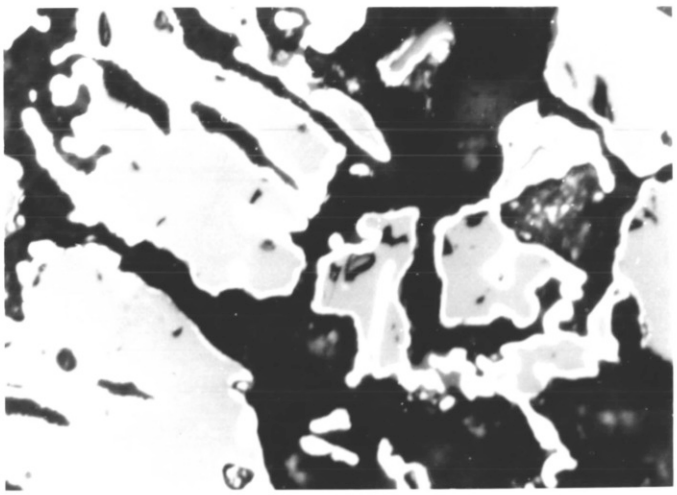

white : iron
light grey : wustite
dark grey : α - Quartz
black : voids

x 320

b)

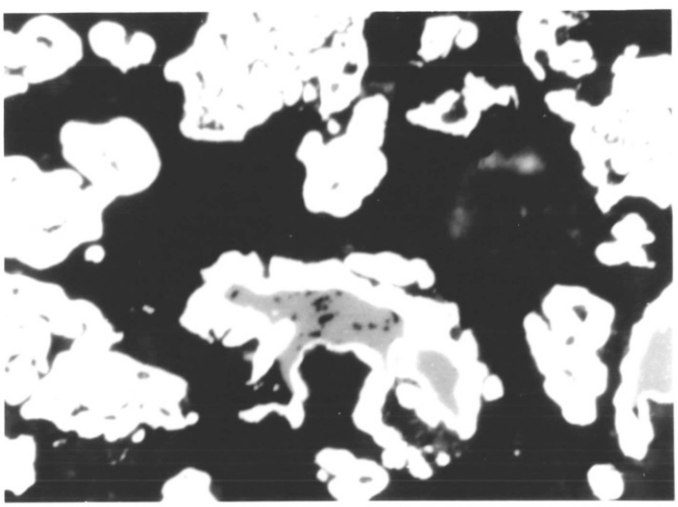

white : iron
light grey : wustite
black : voids

x 320

c)

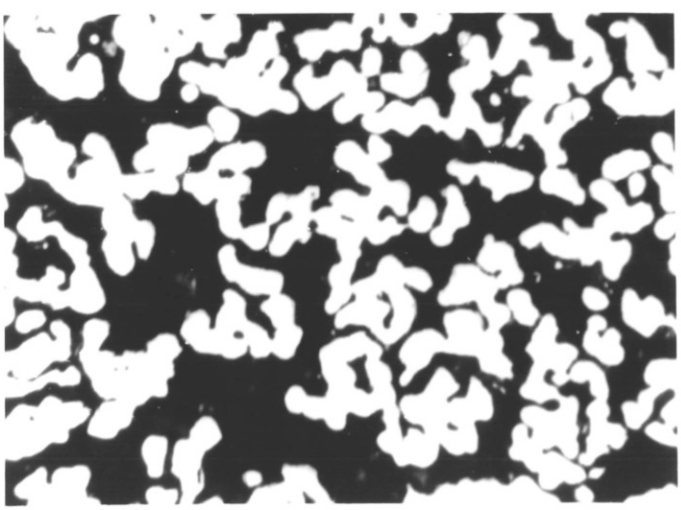

white : iron
dark grey : α - Quartz
black : voids

x 320

PLATE 6

Digital X-ray mapping of iron reduced at I) (1100-1100)·C and II) (1050-1100)·C .
EPMA displays of I) and II) for a)structure of iron grains, b)iron and c)silicon.

I)

a)

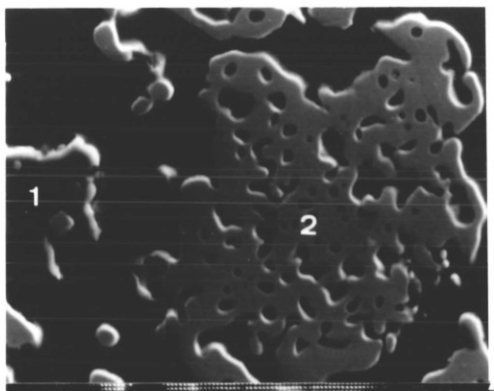

1 : α- Quartz(dark grey)with wustite(grey) and iron particles(white)

2 : iron

b)

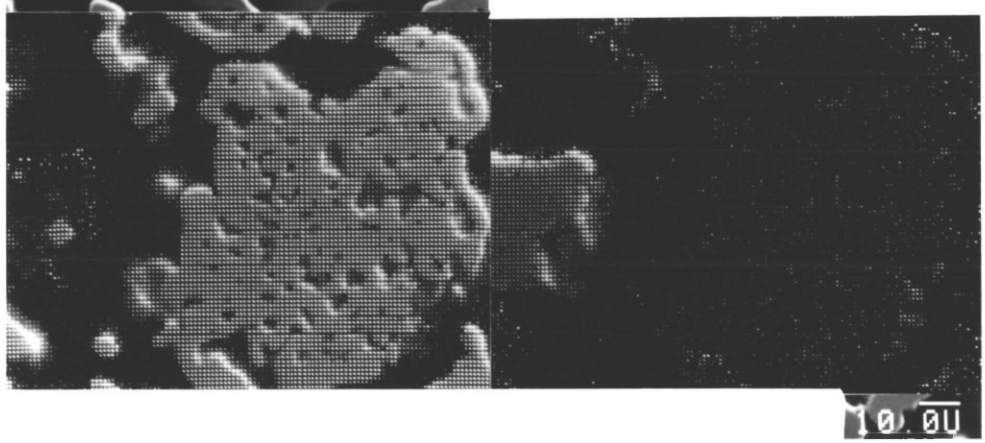

c)

II)

a)

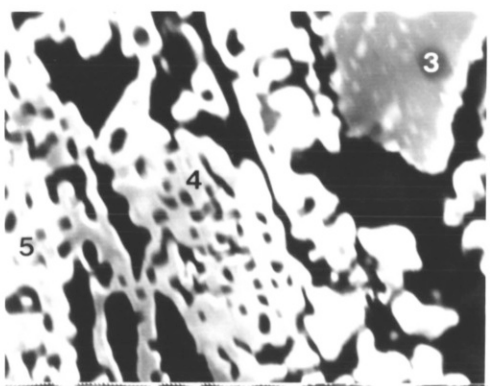

3 : α- Quartz(grey) with iron particles(white)

4 : iron

5 : iron

b)

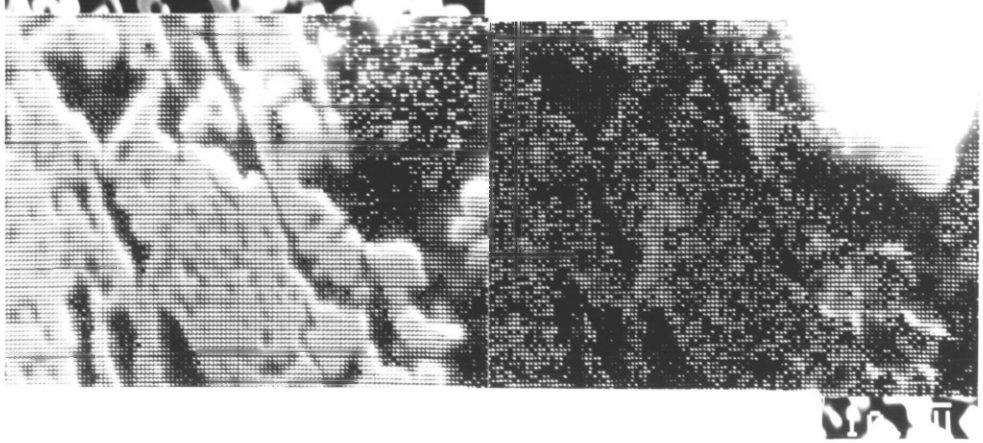

c)

Since fayalite formation is followed by the consumption of α- Quartz, it is obvious that the increase of the intensity of fayalite must be accompanied by a decrease in the intensity of α- Quartz. However it is interesting to note that the cristobalite patterns are particularly weak with powder specimen where very little fayalite is formed. With compacts where fayalite forms reasonably easily, cristobalite patterns are much stronger.

Thus, it appears that the formation of cristobalite when fayalite is reduced explains this difference. However, since cristobalite is also observed in the absence of fayalite, the situation is obviously complex.

4.3. IRON ORE COMPACTS WITH CaO ADDITIONS

CaO additions to sintered compacts were prepared as described in Chapter 3 and were reduced with a gas mixture of composition CO 50% CO_2 50% from hematite to wustite at 950, 1050 and 1100°C. These reduced wustite samples were further reduced with 100% CO atmospheres, at 950, 1050 and 1100°C. All these results are compared with the results for specimens without addition in an attempt to understand the role of CaO addition to the iron ore.

4.3.1. EFFECT OF TEMPERATURE

Fig . 4.8-16 shows that percent weight loss versus reduction time at 950, 1050 and 1100°C with wustite and each different amount of CaO addition. Once again, as expected, these results show that increasing the temperature increases the reduction rate.

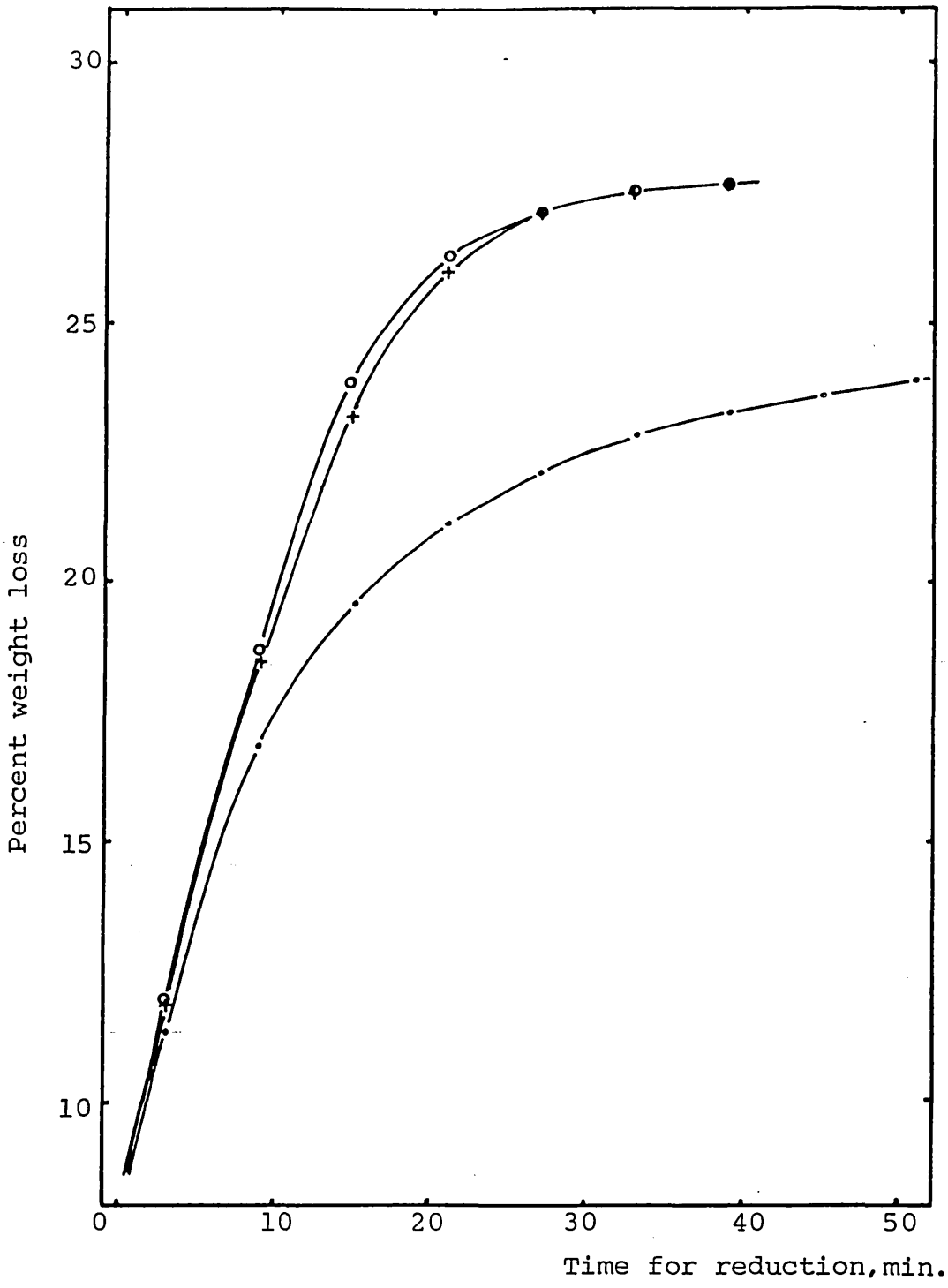

Fig. 4.8- The effect of temperature at 950, 1050 and 1100°C on reduction of wustite compacts pre-reduced at 950°C with CaO 1% additions.

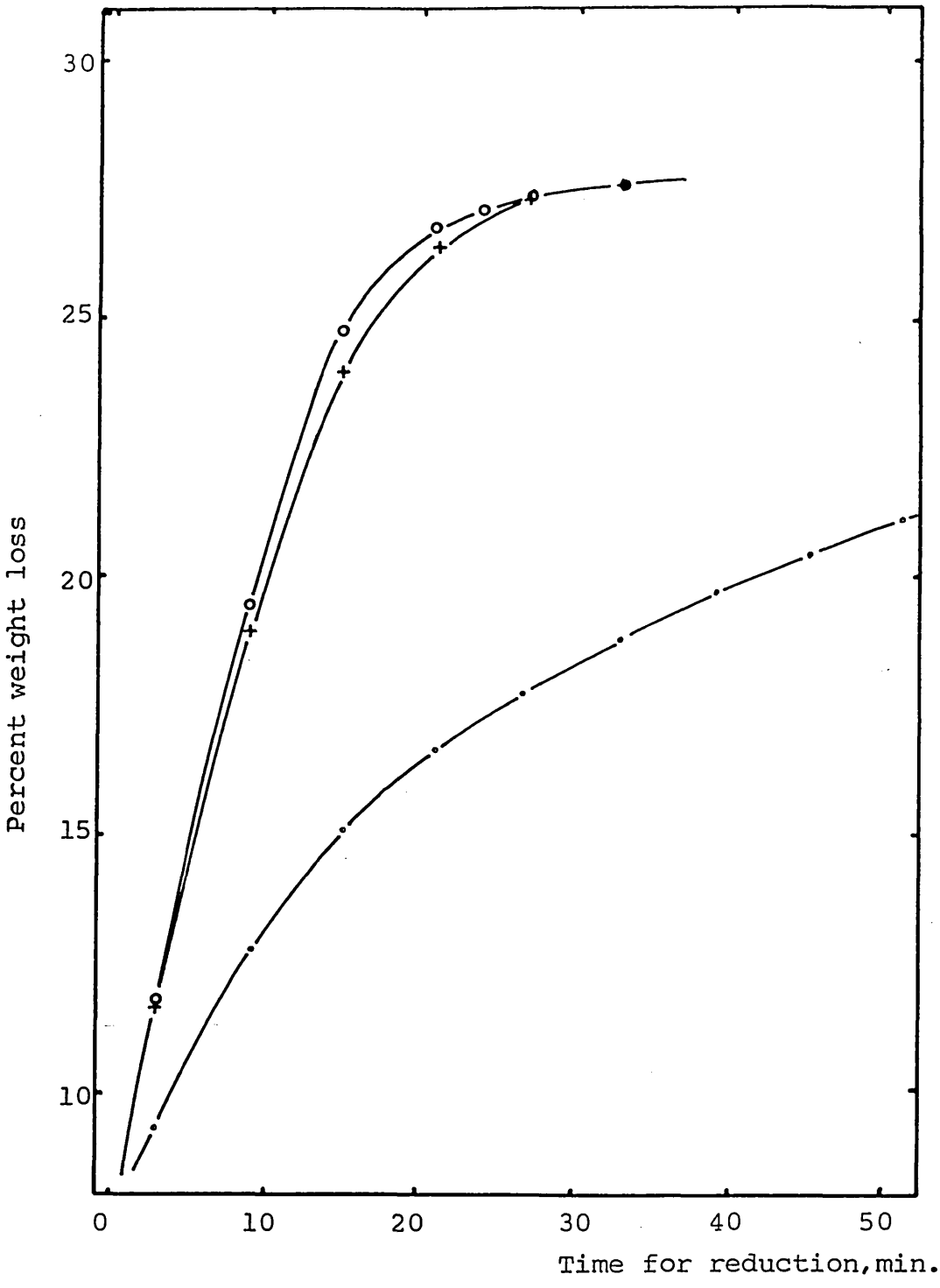

Fig. 4.9- The effect of temperature at 950, 1050 and 1100°C on reduction of wustite compacts pre-reduced at 1050°C with CaO 1% additions.

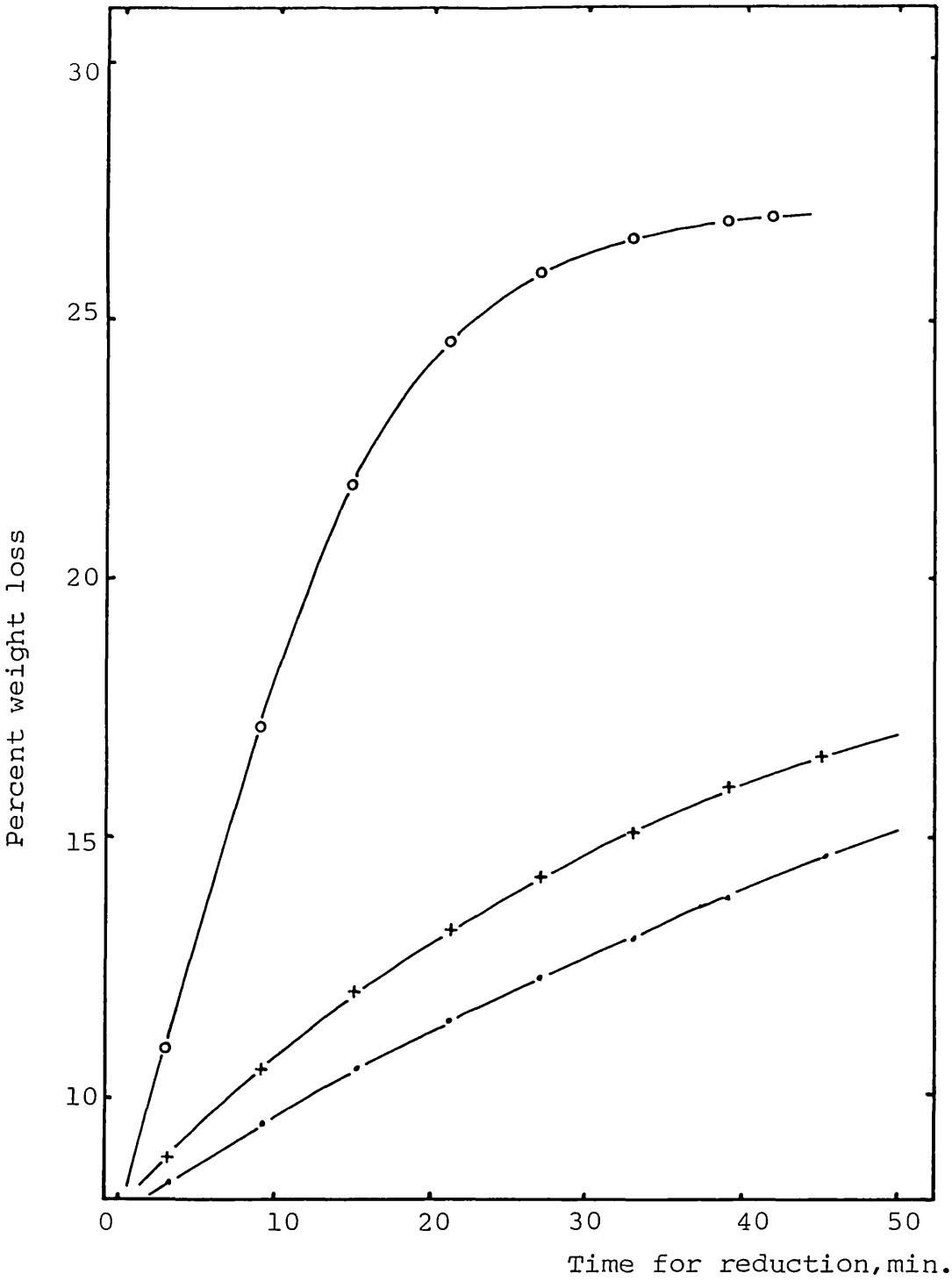

Fig. 4.10- The effect of temperature at 950, 1050 and 1100°C on reduction of wustite compacts pre-reduced at 1100°C with CaO 1% additions.

1% CaO

With the CaO addition, no effect of temperature on the reduction to iron at 1100°C and 1050°C was observed with the wustite made at low temperatures(950,1050°C). However it may be suggested that the reduction rate decreased slightly with increasing temperature of wustite production, but it is considered that this is probably within the limits of error. The low temperature reduction to iron at 950°C, as seen in Fig . 4.8-10, shows a remarkable decrease in rate with increasing temperature of wustite production.

In Fig. 4.10 for wustite formation at 1100°C, the reduction rates showed marked difference from the other 1% CaO addition results indicating that the process occurs in a completely different way. The reduction of 1% CaO addition reduced at (1100-1050) shows a dramatic decrease in rate and is not significantly different to the reduction rate at (1100-950)· CaO 1%.

CaO 2% addition

Samples with CaO 2% addition show a similar behaviour to 1% CaO addition samples.

The reduction rate at (1050-1050)· CaO 2% shows a rather slower rate of reduction than the 1% sample (see Fig 4.12).

CaO 5% addition

In Fig . 4.14-16 show the effect of temperature on the rate of reduction. CaO 5% addition samples display different reduction characteristics compared to 1 and 2% CaO addition

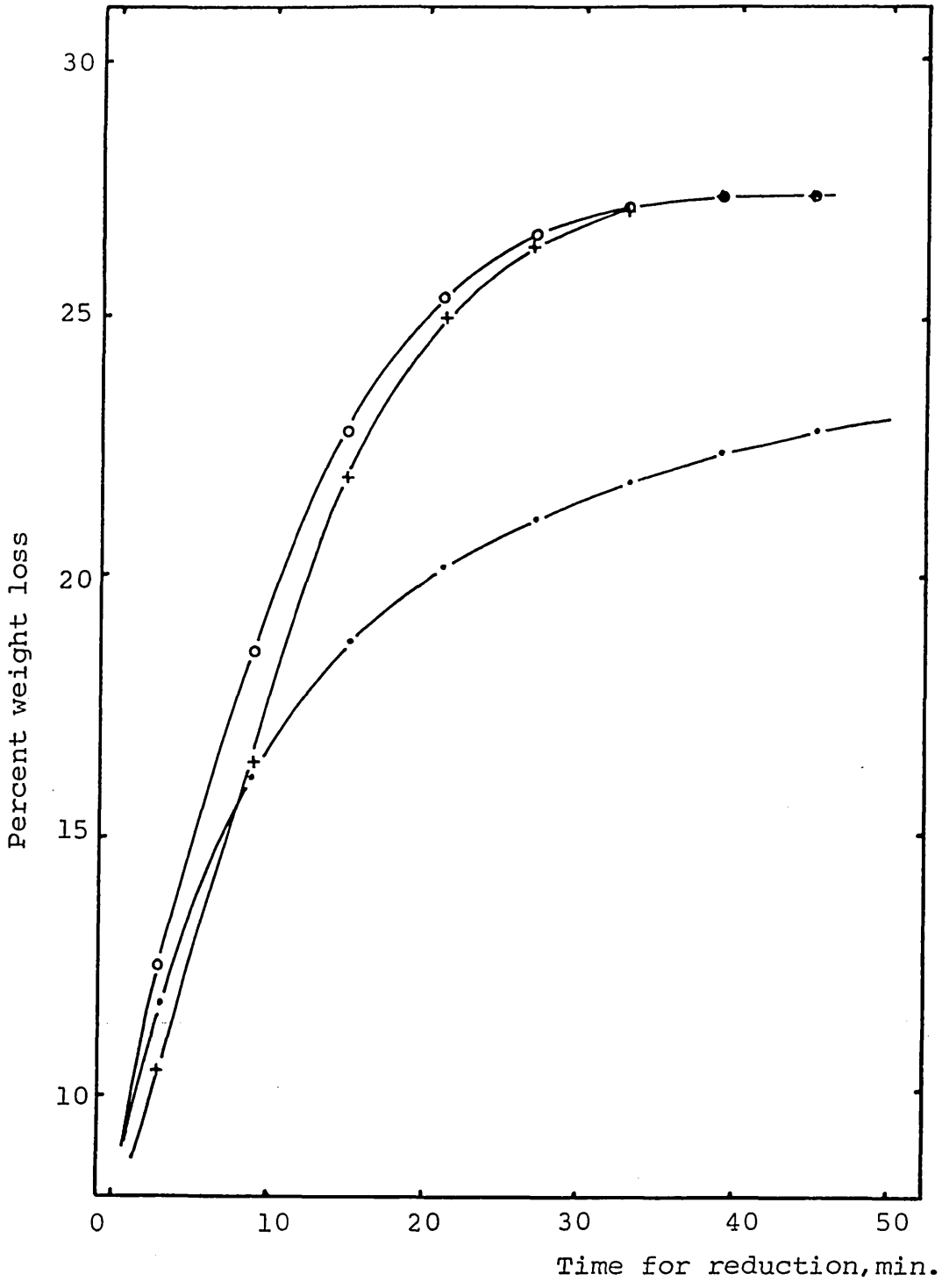

Fig. 4.11- The effect of temperature at 950, 1050 and 1100°C on reduction of wustite compacts pre-reduced at 950°C with CaO 2% additions.

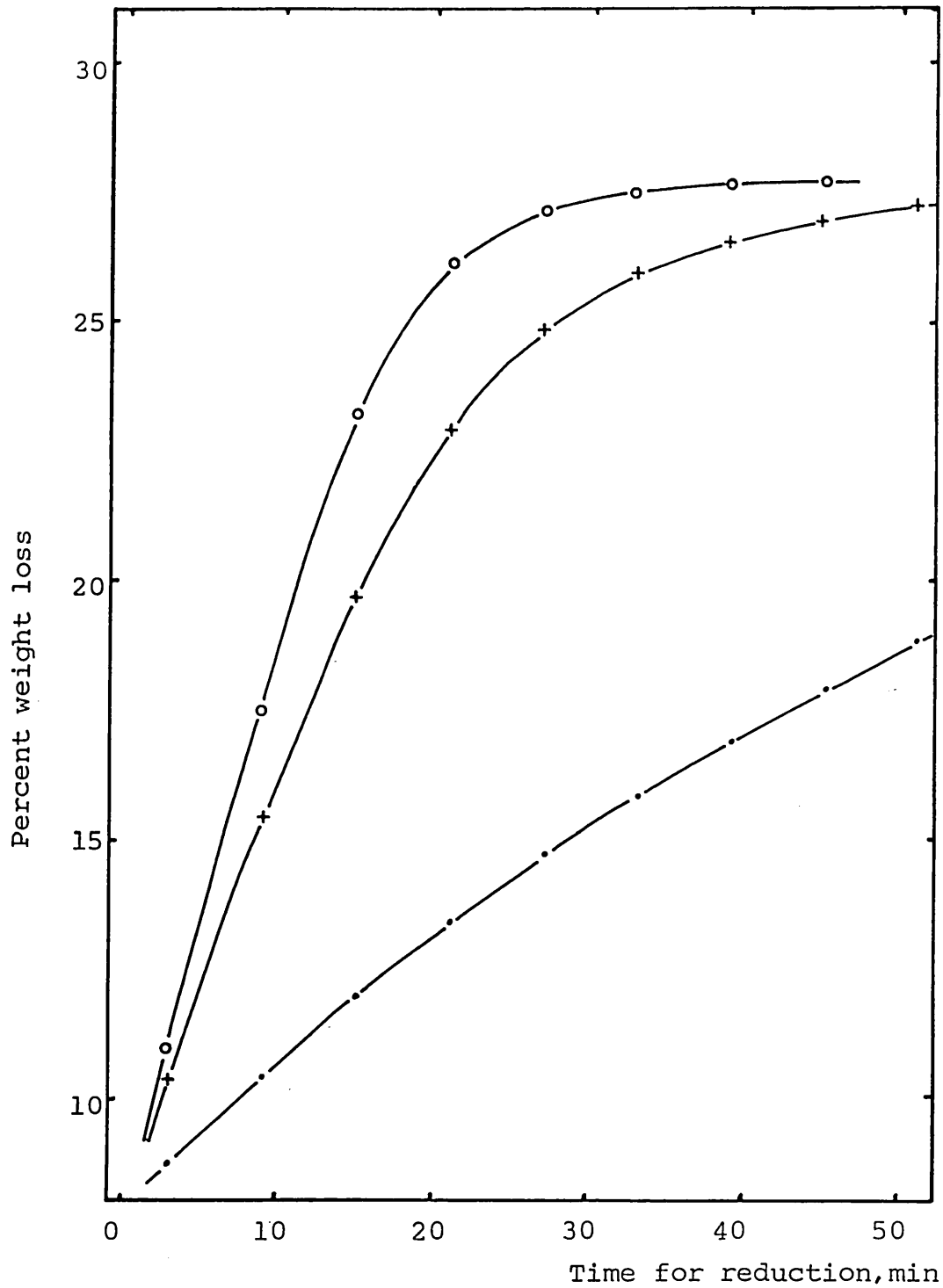

Fig. 4.12- The effect of temperature at 950, 1050 and 1100°C on reduction of wustite compacts pre-reduced at 1050°C with CaO 2% additions.

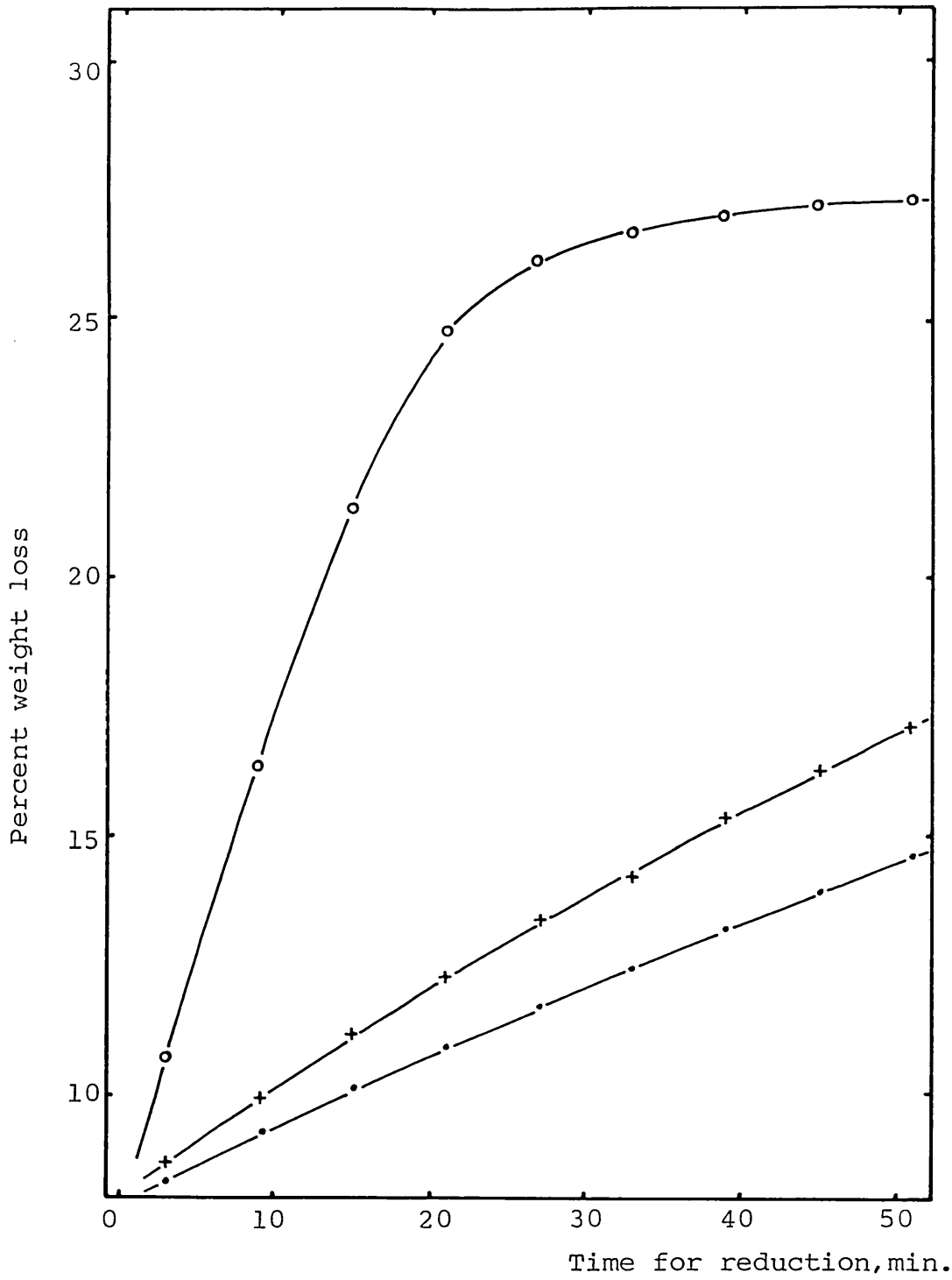

Fig. 4.13- The effect of temperature at 950, 1050 and 1100°C on reduction of wustite compacts pre-reduced at 1100°C with CaO 2% additions.

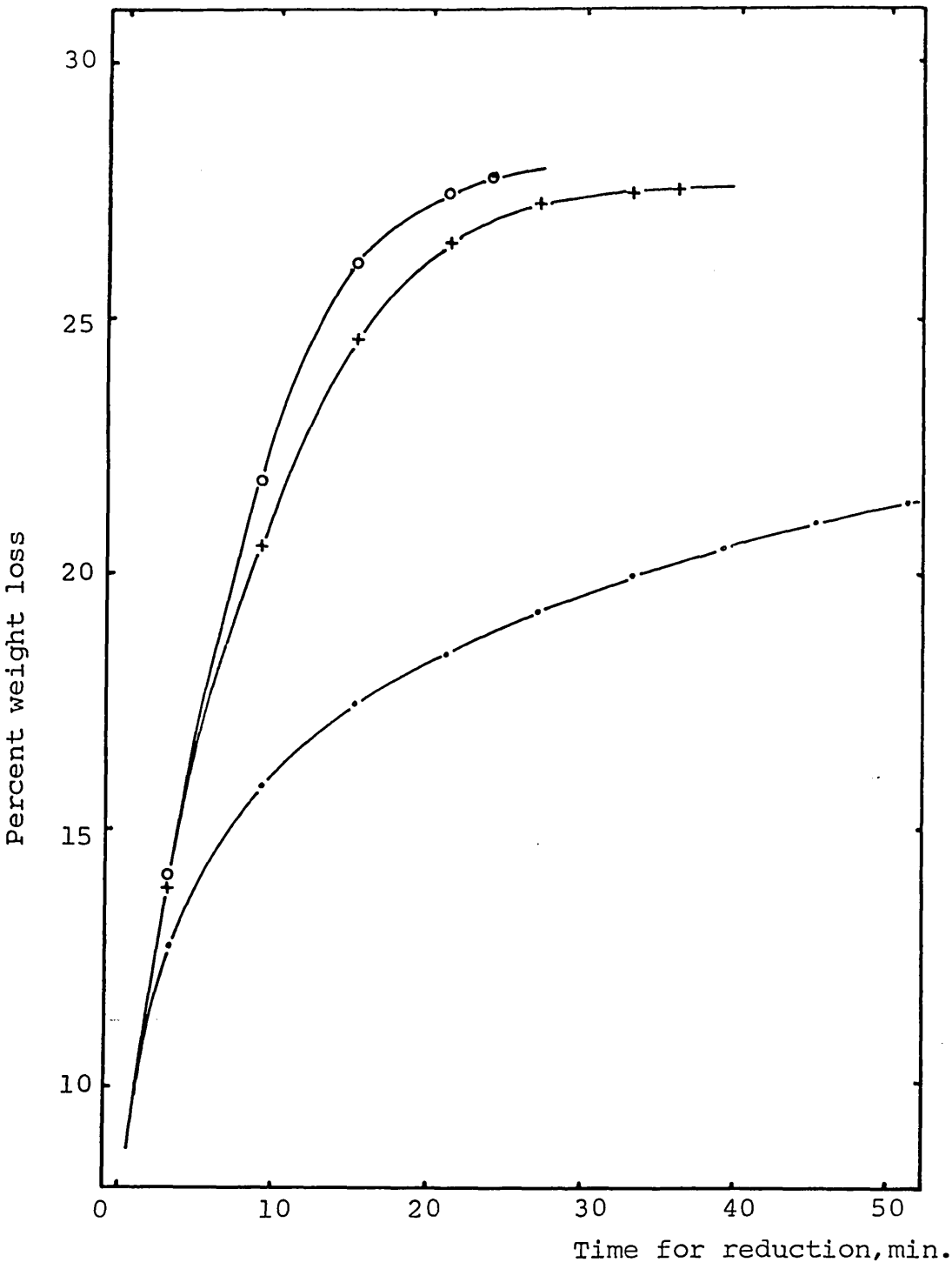

Fig. 4.14- The effect of temperature at 950, 1050 and 1100°C on reduction of wustite compacts pre-reduced at 950°C with CaO 5% additions.

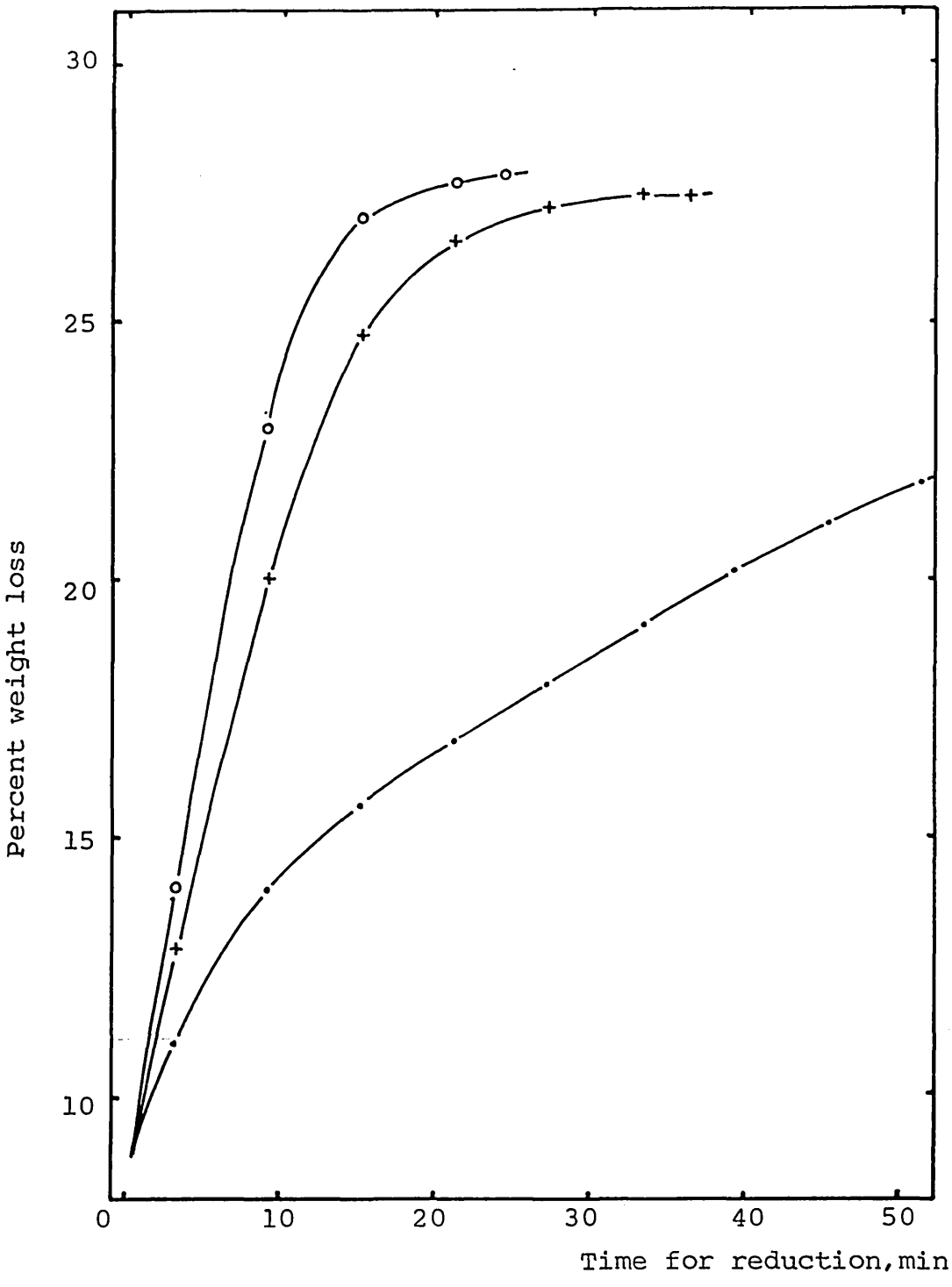

Fig. 4.15- The effect of temperature at 950, 1050 and 1100°C on reduction of wustite compacts pre-reduced at 1050°C with CaO 5% additions.

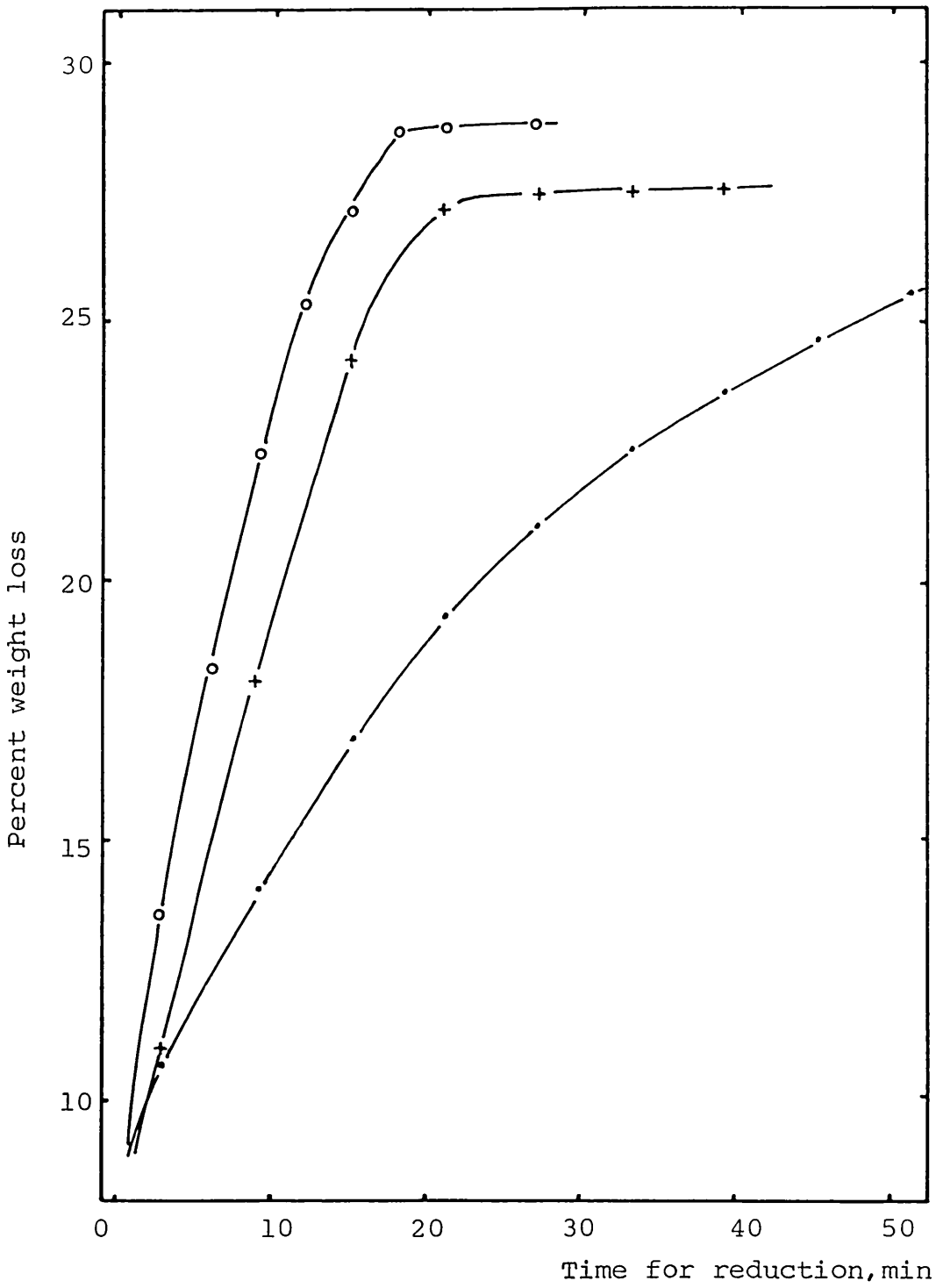

Fig. 4.16- The effect of temperature at 950, 1050 and 1100°C on reduction of wustite compacts pre-reduced at 1100°C with CaO 5% additions.

and are similar to the non-addition compacts especially at low temperature reduction. However, the increase of reduction rate for samples pretreated at 1100°C (see Fig. 4.16) is quite significant.

4.3.2. THE EFFECT OF WUSTITE PREPARATION TEMPERATURE

In low temperature reduction with 1% CaO addition, the reduction decreases significantly with increasing temperature of wustite production. However the reduction rate at (1050-1050)· CaO 1% and at (950-1050)· CaO 1% is consistent from beginning to end. The reduction at (1100-1050)· CaO 1% indicates that the mechanism of reduction is quite different compared with the reduction of wustite produced at lower temperatures.

When 2% of CaO was added to the compacts, similar effect are seen for the type of wustite during low temperature reduction (950°C) to the 1% CaO addition.

Fig . 4.14-16 show the effect of wustite on the rate of reduction at each temperature with 5% CaO additions. The overall characteristics of the reduction rate resembles the rate curves for compacts without addition. At low temperature, the rate of reduction at (950-950)·CaO 5% is higher than (1050-950)·CaO 5%. However the rate at (1100-950)· CaO 5% shows a much higher rate than (950-950)· CaO 5%.

The initial rate at the beginning of the reduction is very high at (950-950)· CaO 5% while the rate is much lower at (1050-950)· CaO 5% and (1100-950)· CaO 5%. At high temperature(1100°C), the reduction rate increases with

increasing the temperature for wustite preparation while the reduction rate decreases at 1050°C.

4.3.3. EFFECT OF AMOUNT OF CaO ADDITION

Fig. 4.8 , 4.11 and 4.14 show the effect of the amount of CaO addition on the rate of reduction with the wustite produced at 950°C. These results show quite clearly that the reduction rate decreases with increasing amount of CaO addition at 950°C. However the reduction at higher temperatures (1050, 1100°C) varies in a totally different manner. The reduction rate decreases slightly by increasing the amount of CaO from 1 to 2% CaO. However, the rate increases again to a higher value with 5% CaO additions. When the wustite is produced at 1050°C or 1100°C, a similar relationship is observed with reduction temperature.

4.3.4. IDENTIFICATION OF PHASES AFTER REDUCTION

The phases present during reduction with CaO additions were iron, wustite(partially reduced specimens only), Fayalite(Fe_2SiO_4), Cementite(Fe_3C), Wollastonite($CaO{\cdot}SiO_2$) and Kirschsteinite($CaO{\cdot}FeO{\cdot}SiO_2$).

However the main difference observed during reduction in different experiments were related to the phases fayalite, wollastonite and kirschsteinite.

By the XRD results, the phases in the starting materials (sintered compacts) were hematite and wollastonite. These results revealed that all the α- Quartz in the iron ore has reacted with CaO.

Wollastonite ($CaSiO_3$)

Wollastonite was observed in every sample after reduction

of 1% CaO addition specimens and the intensity of this phase was similar in all specimens. With 2% CaO additions it is noticed that the intensity of wollastonite in the XRD film decreased as the reduction temperature increases. However a completely different relationship is observed when 5% of CaO was added to the compacts. The intensity of wollastonite increased with increasing reduction temperature.
At this stage, these results appear to very confusing.

Kirschsteinite ($CaO \cdot FeO \cdot SiO_2$)

This phase was identified only in the compacts with CaO 5% additions. The intensity of the kirschsteinite phase varies with the degree of reduction. The intensity of kirschsteinite weakens with time of high temperature reduction and even disappeared for times in excess of those required to give theoretical weight loss. However, it was shown that complete reduction of kirschsteinite was very difficult at low temperatures (Table 4.6).

Fayalite (Fe_2SiO_4)

Fayalite was identified even in the presence of CaO in the case of 1 and 2% of CaO additions.
The intensity of fayalite was observed to decrease with increasing reduction temperature in most cases.

α - Cristobalite ($CaO \cdot SiO_2$)

α - Cristobalite was identified when the iron was completely reduced at (1100-1100)·CaO 1% even in the presence of wollastonite. In the case of CaO 2% additions, more α - Cristobalite was observed in every sample except (950-950)·CaO 2% and (1100-1100)·CaO 2%. In general, the

TABLE. 4.4

XRD ANALYSES OF REDUCED SAMPLES OF IRON ORE COMPACTS WITH CaO 1% ADDITIONS.

REDUCTION PROCEDURE	REDUCTION		PHASES IDENTIFIED
	% Wt.LOSS	TIME, MIN.	
950-950	24.5	60	Fe:VS, W:MW, FS:W, C:M, CS:VVW
950-1050	27.6	38	Fe:VS, FS:VW, C:M, CS:VVW
950-1100	27.8	39	Fe:VS, FS:VVW, C:VVW, CR:W, CS:VVW
1050-950	22.6	60	Fe:VS, W:MS, FS:MW, C:MW, CS:VVW
1050-1050	27.7	39	Fe:VS, FS:W, W:VVW, C:VVW, CS:VVW
1050-1100	27.3	39	Fe:VS, FS:VVW, C:VVW, CS:VVW
1100-950	15.9	60	Fe:VS, W:M, FS:VVW, C:VVW, CS:VVW
1100-1050	17.2	60	Fe:VS, W:S, FS:VVW, C:MW, CS:VVW
1100-1100	27.1	50	Fe:VS, W:W, FS:W, C:VVW CR:VVW, CS:VVW

@ ORDER OF INTENSITY:VS,S,MS,M,MW,W,VW,VVW

Fe : α- Iron

C : Cementite, Fe_3C

CS : Wollastonite, $CaSiO_3$

FS : Fayalite, Fe_2SiO_4

CR : α- Cristobalite, SiO_2

W : Wustite

TABLE 4.5

XRD ANALYSES OF REDUCED SAMPLES OF

IRON ORE COMPACTS WITH CaO 2% ADDITIONS.

REDUCTION PROCEDURE	REDUCTION		PHASES IDENTIFIED
	% Wt.LOSS	TIME, MIN.	
950-950	24.4	60	Fe:VS, W:MW, FS:VVW, C:MW, CS:MW
950-1050	27.1	45	Fe:VS, C:W, CS:MW, FS:W, CR:VW, Q:VVW
950-1100	27.7	45	Fe:VS, CS:VW, FS:VW, C:VVW, CR:VVW, Q:VW
1050-950	20.4	60	Fe:VS, W:S, FS:VW, C:VW, CR:W
1050-1050	27.4	60	Fe:VS, W:MW, FS:VVW, C:W, CR:MW
1050-1100	27.7	45	Fe:VS, FS:VVW, C:MW, CR:MW
1100-950	16.3	60	Fe:VS, W:M, FS:VVW, CS:VW, CR:VW
1100-1050	17.9	60	Fe:VS, W:W, FS:VVW, C:VW, CS:W, CR:VW
1100-1100	27.5	60	Fe:VS, C:MW, FS:VW, CS:W

@ ORDER OF INTENSITY:VS,S,MS,M,MW,W,VW,VVW

Fe : α- Iron

FS : Fayalite, Fe_2SiO_4

CR : α- Cristobalite, SiO_2

Q : α- Quartz, SiO_2

CS : Wollastonite, $CaSiO_3$

W : Wustite

C : Cementite, Fe_3C

TABLE.4.6

XRD ANALYSES OF REDUCED SAMPLES OF IRON ORE COMPACTS WITH CaO 5% ADDITIONS.

REDUCTION PROCEDURE	REDUCTION		PHASES IDENTIFIED
	% Wt.LOSS	TIME, MIN.	
950-950	22.0	60	Fe:VS, W:M, CS:VW, C:VW, CFS:VW
950-1050	27.5	36	Fe:VS, C:W, CS:VW, CFS:VW
950-1100	27.8	26	Fe:VS, C:MW, CS:W, CFS:VVW
1050-950	23.2	60	Fe:VS, C:VVW, W:MW, CS:VW, CFS:VW
1050-1050	27.5	36	Fe:VS, C:W, CS:VW, CFS:VW
1050-1100	27.7	24	Fe:VS, C:MW, CS:W, CFS:VVW
1100-950	26.6	60	Fe:VS, C:W, CS:VVW, CFS:VW
1100-1050	27.1	39	Fe:VS, C:W, CS:VW, CFS:VVW
1100-1100	27.6	21	Fe:VS, C:W, CS:W

@ ORDER OF INTENSITY:VS,S,MS,M,MW,W,VW,VVW

Fe : α- Iron W : Wustite

CS : Wollastonite, $CaSiO_3$

CFS : Kirschsteinite, $CaO \cdot FeO \cdot SiO_2$

C : Cementite, Fe_3C

intensity of this phase was observed to be stronger with increasing reduction temperature.

Cementite (Fe_3C)

The formation of cementite was observed in every sample with CaO additions and the intensity identified from XRD showed stronger lines when compare with the compacts without additions. This phase was present even with wustite (55% of reduction achieved) and the intensity was stronger at lower temperature.

4.3.5. STRUCTURAL CHANGES DURING REDUCTION

The main difference in microstructures of iron after reduction with CaO additions was liquid phase formation. Plate 7 shows the microstructure of hematite grains of iron ore compacts with 1% CaO (a), 2% CaO (b) and 5% CaO (c) sintered at 1300°C for 24 hours in air. The hematite particles were severely attacked by the CaO and the liquid phase formed around the hematite grains was $CaO \cdot SiO_2 \cdot Fe_2O_3$ in the pseudo-wollastonite phase field as identified from phase diagram (see Plate 12, Fig. 4.17 and Table 4.7) which reveals a liquidus temperatures of 1300°C.

Plate 8 shows the microstructure of samples reduced at various temperatures. The unreduced wustite shown in Plate 8a is completely surrounded by an iron shell and this iron penetrates into the wustite. For reduction at 1050°C, the iron structure (completely reduced in this picture, Plate 8b) seems to be made up of small fragrants sintered together. Some small particles of iron are also observed in the liquid phase regions. At 1100°C, the iron particle size appears much bigger and all the iron is sintered to-

gether with liquid phase regions located around the iron. The microstructure of iron reduced at (1100-950)·CaO 1% (Plate 9a) is quite different to that of (950-950)·CaO 1%. The unreduced wustite was surrounded by iron, however the shape of iron is much closer to the structure shown in Plate 8c. Plate 9b also shows similar iron formation for 2% CaO additions to that of Plate 9a.

Plate 10 and Plate 11 also show a similar mode to those seen in Plate 8 and 9 depending on the temperature of wustite production.

The thickness of the iron layer shown in the picture c of Plates 8,9,10 and 11 grows gradually according to the increasing temperature at which wustite was produced and also with increasing the amount of CaO (1 to 2%) addition.

The digital X-ray mapping shown in Plate 12 II displays the element (Fe,Ca,Si) distribution of the reduced sample (reduced at (1100-1050)·CaO 2%). It shows that the CaO distributes homogeneously in the unreduced wustite while SiO_2 is present only in the liquid phase.

Plate 13c shows the microstructure of iron reduced at (950-950)·CaO 5%. This iron structure gave the appearance of small grains with voids associated with them. Plate 14a also shows a similar structure to that illustrated in Plate 13c. Plate 14b and c shows the gradual sintering of the iron structure according to the reduction temperature and the iron structure formed in the outer grains is similar to the structure shown in Plate 9b.

Plate 15 and 16 show the analytical points of EPMA analysis and also displays the qualitative analysis by X-ray digimapping. The distribution of silicon as silica and calcium

KEY TO PLATE 7-16

PLATE 7 showing hematite grains attacked by calcium silicate and precipitation of hematite from the liquid phase during cooling.

PLATE 8 c) shows that this iron was reduced from the liquid phase of $CaO-FeO-SiO_2$.

PLATE 9 b) shows the same iron structure around the wustite grains.

PLATE 13 a) the surface of wustite shows very porous structure.

b) the cementite(dark area) and ferrite (white).

PLATE 7

Micro-structure of hematite grains of iron ore compacts with a) 1% CaO, b) 2% CaO and c) 5% CaO addition, sintered at 1300°C for 24 hours in air.

a)

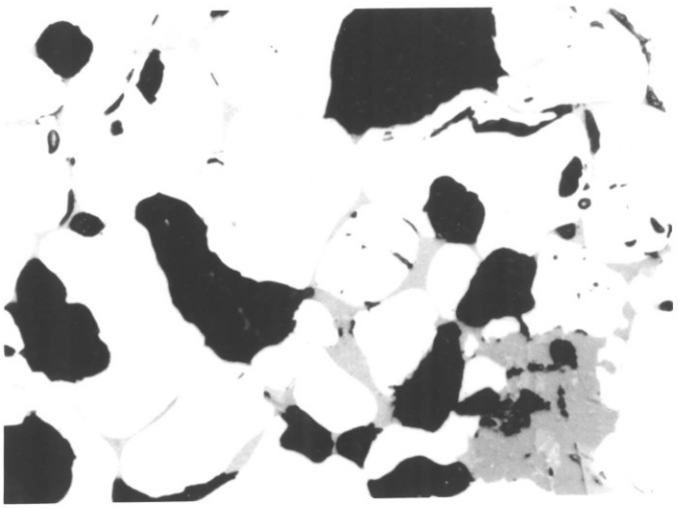

white : hematite
light grey : magnetite
dark grey : wollastonite
black : voids

x 320

b)

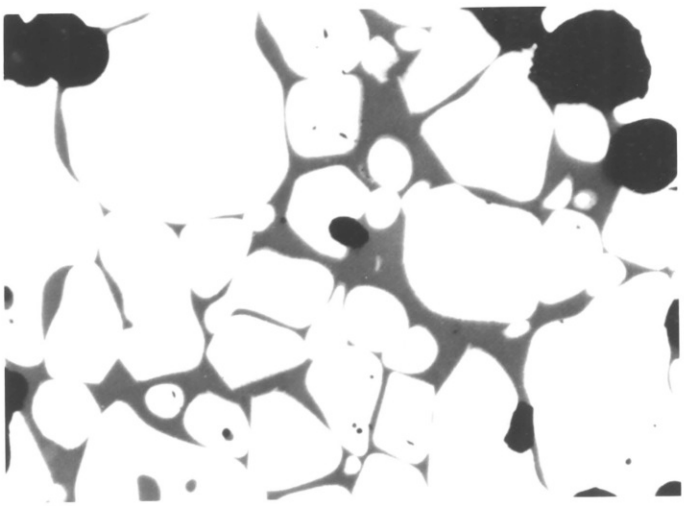

white : hematite
grey : wollastonite
black : voids

x 320

c)

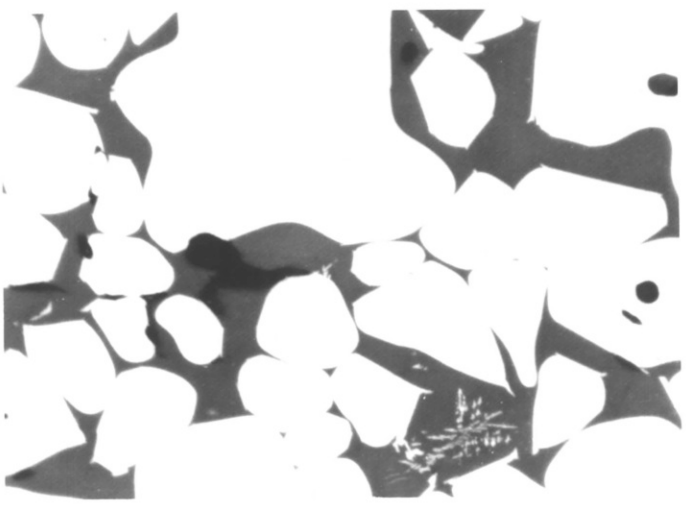

white : hematite
grey : wollastonite
black : voids

x 320

as calcium oxide in the reduced iron shows very small concentrations while iron also is distributed in the liquid phase with SiO_2 and CaO. Fig. 18 shows the positions of analysed point by EPMA in the CaO-FeO-SiO_2 diagram. This indicates that the composition varies according to the amount of CaO additions and the phases identified by the analysis is pseudo-wollastonite, wollastonite (both phases were identified as wollastonite by XRD) and olivine (as kirschsteinite by XRD).

4.3.6. DISCUSSION

The optical microscopy indicated the presence of a liquid phase in the materials sintered in air at 1300°C. This liquid was undoubtedly realted to the CaO-SiO_2-Fe_2O_3 system. The XRD observations clearly indicated the presence of wollastonite for all CaO additions.
This result suggests that the liquid formed at 1300°C must be associated with the pseudowollastonite phase field.
With the low concentrations of CaO 1% and 2%, this liquid composition must lie at or near the silica saturated region of the phase diagram because of the SiO_2 : CaO ratios present in the compacts. Upon cooling this liquid would probably partially crystallise and produce wollastonite, fayalite and silica, in general agreement with the XRD results.
With 5% CaO addition, the higher CaO : SiO_2 ratio in the pellet would produce a liquid near the Rankinite phase field. Upon cooling, once again recrystallization would occur and upon reduction, this composition lies almost exactly in the Kirschsteinite-Wollastonite two phase field.
Once again excellent agreement is observed with the XRD

PLATE 8

Micro-structure of iron reduced at a) (950-950)• CaO 1% , b) (950-1050)• CaO 1% and c) (950-1100)• CaO 1%.

a)

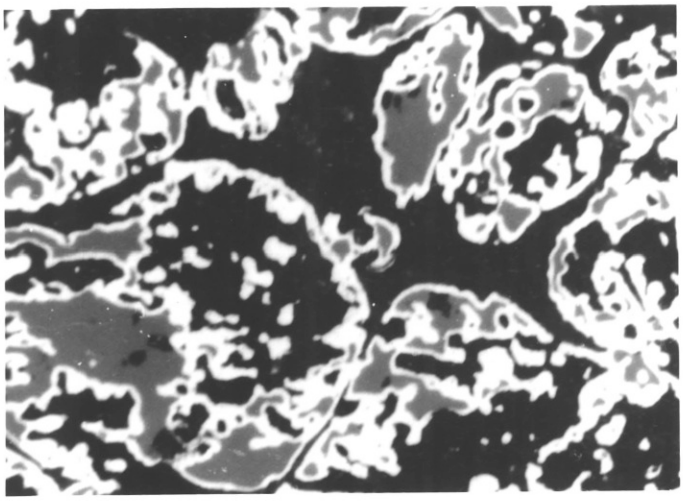

white : iron
light grey : wustite
dark grey : wollastonite
black : voids

x 320

b)

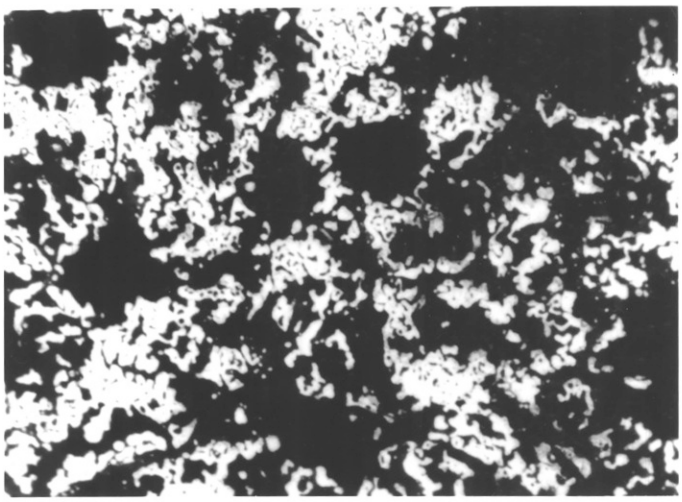

white : iron
dark grey : wollastonite
black : voids

x 320

c)

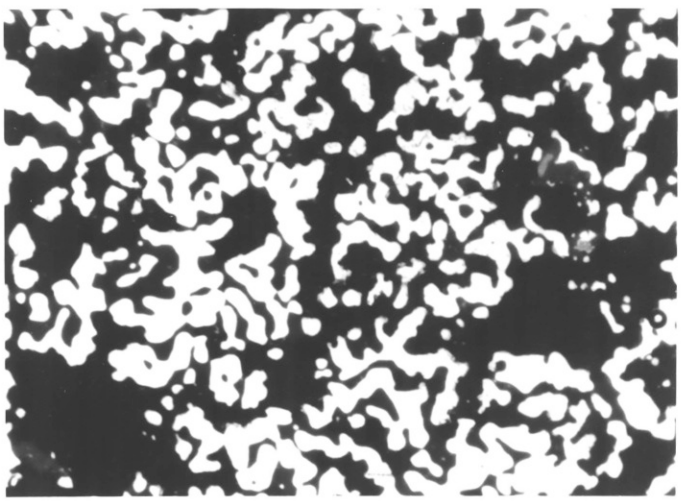

white : iron
dark grey : wollastonite
black : voids

x 320

PLATE 9

Micro-structure of iron reduced at a) (1100-950)·CaO1% , b) (1100-1050)·CaO 1% and c) (1100-1100)·CaO 1% .

a)

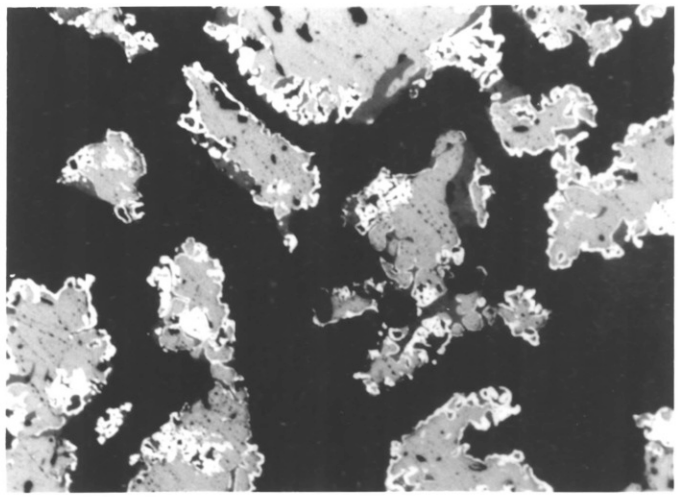

white : iron
light grey : wustite
dark grey : wollastonite
black : voids

x 320

b)

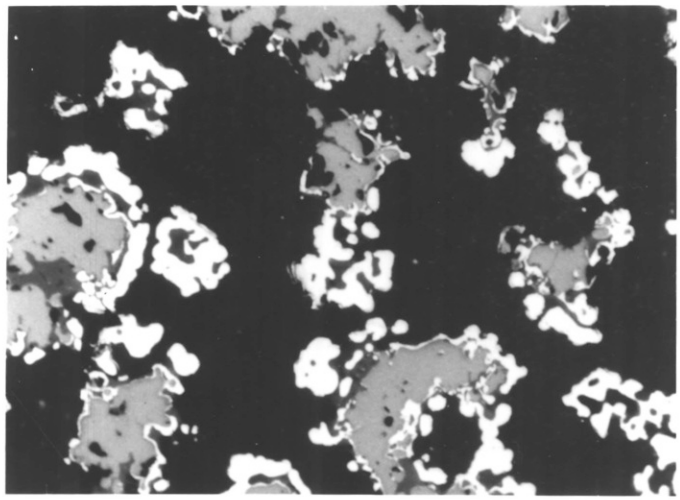

white : iron
light grey : wustite
dark grey : wollastonite or kirschsteinite
black : voids

x320

c)

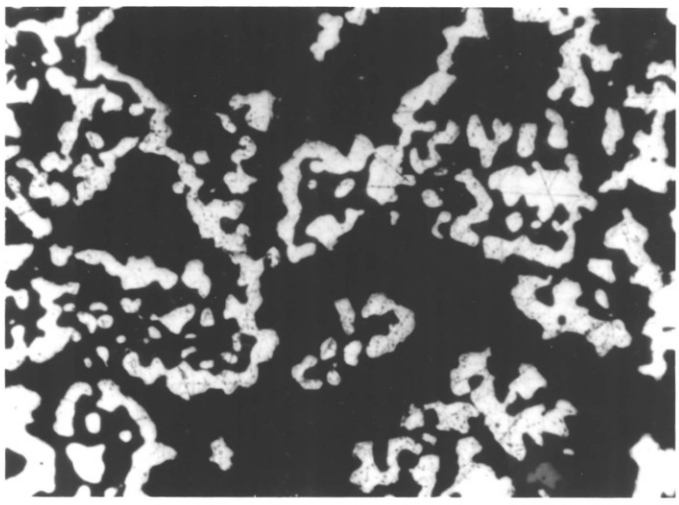

white : iron
dark grey : wollastonite
black : voids

x 320

PLATE 10

Micro-structure of iron reduced at a) (950-950)·CaO 2%, b) (950-1050)·CaO 2% and c) (950-1100)·CaO 2% .

a)

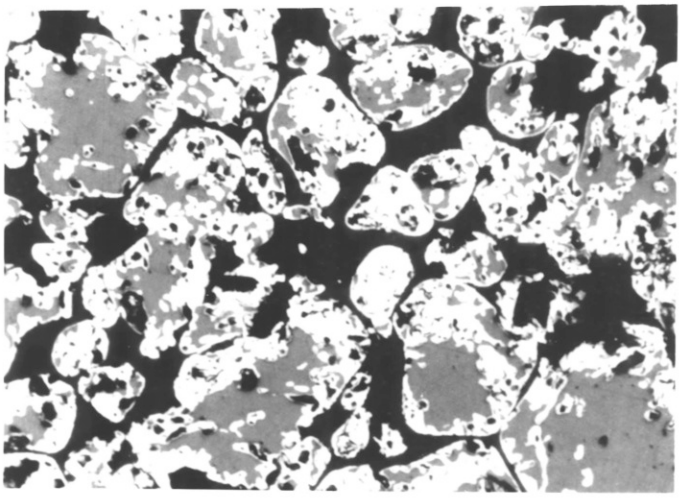

white : iron
light grey : wustite
dark grey : wollastonite
black : voids

x 320

b)

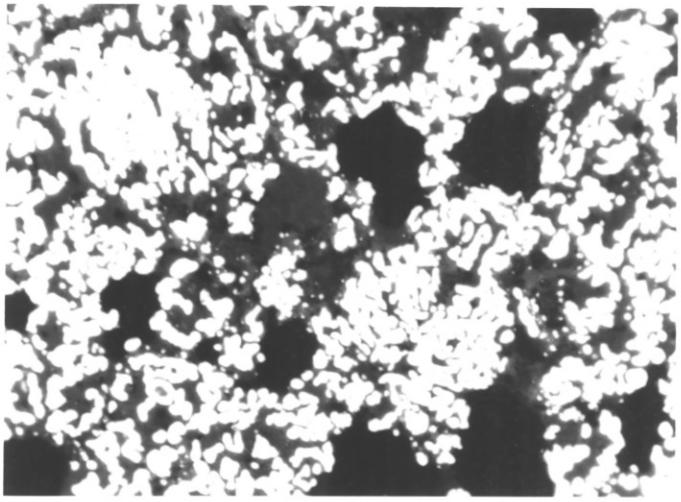

white : iron
dark grey : wollastonite
black : voids

x 320

c)

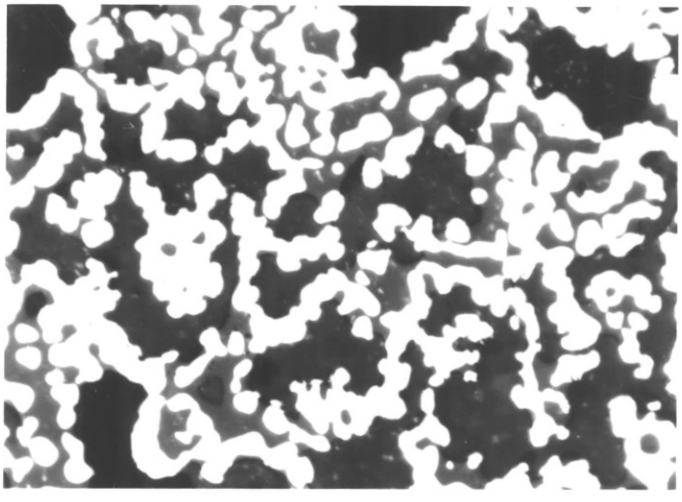

white : iron
dark grey : wollastonite
black : voids

x 320

PLATE 11

Micro-structure of iron reduced at a) (1100-950)·CaO 2% , b) (1100-1050)·CaO 2% and c) (1100-1100)·CaO 2% .

a)

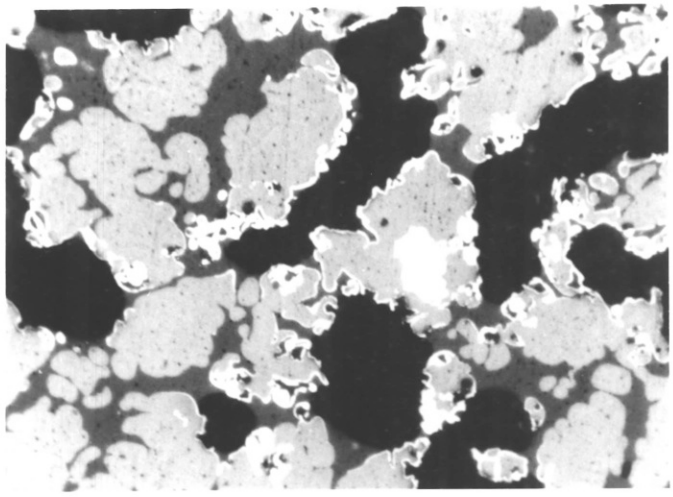

white : iron
light grey : wustite
dark grey : wollastonite
black : voids

x 320

b)

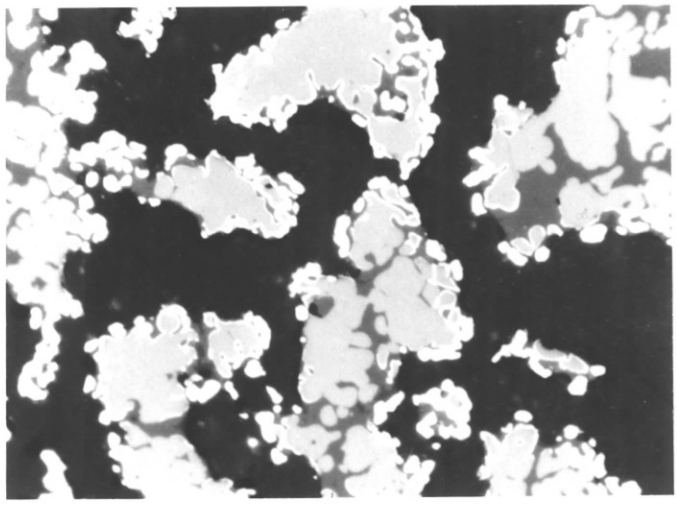

white : iron
dark grey : wollastonite
black : voids

x 320

c)

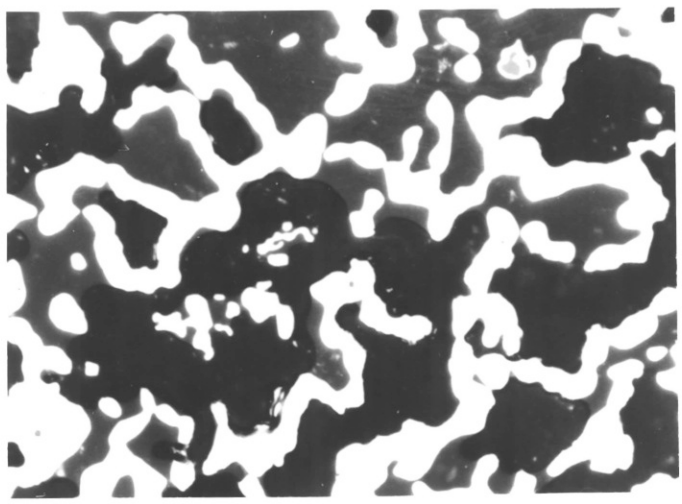

white : iron
dark grey : wollastonite
black : voids

x 320

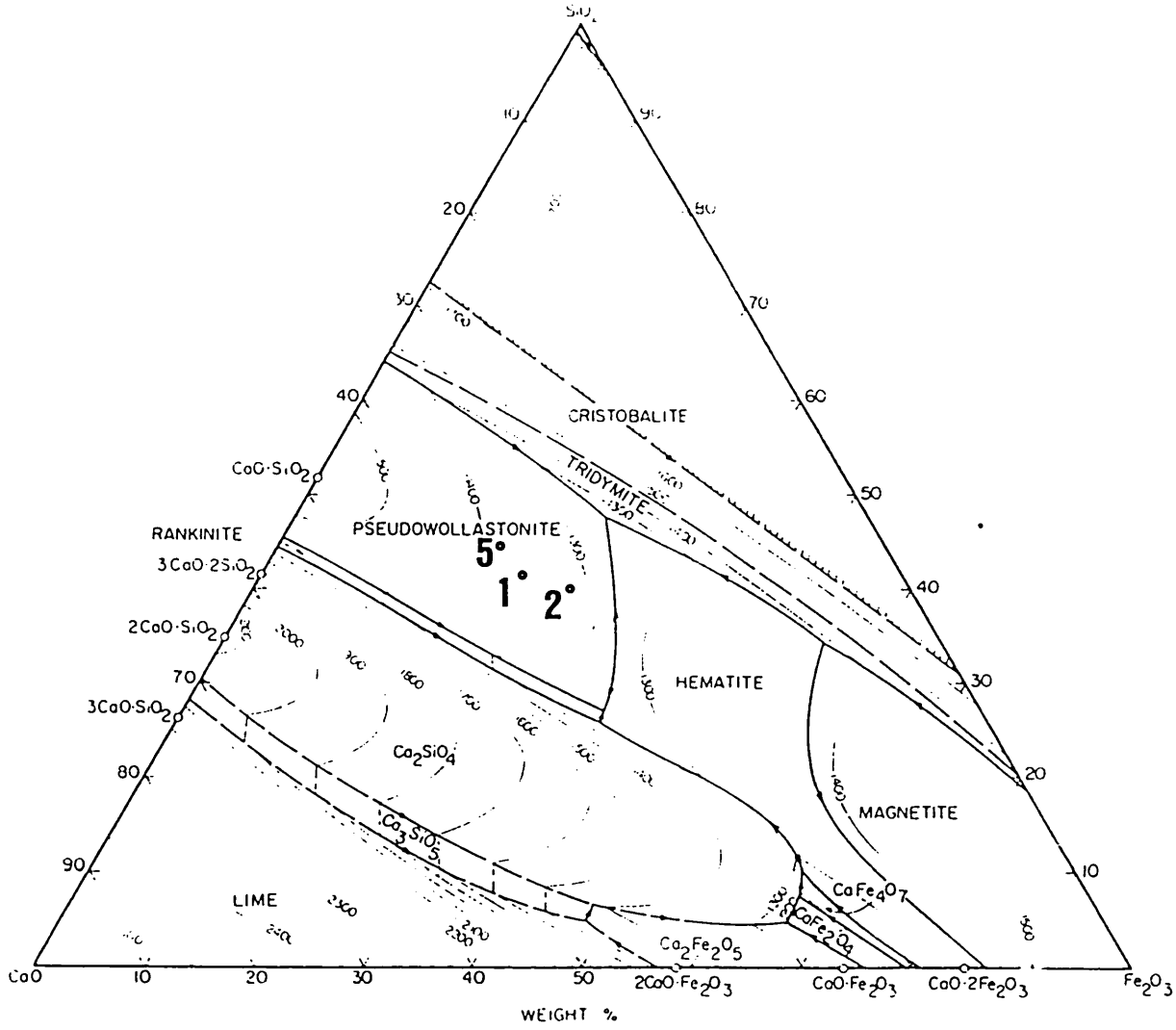

Fig. 4.17 Phase relations in the system CaO-iron oxide-SiO_2 in air (64).

EPMAresults (Plate 12 I)

(Re-calculated from the original data for the system CaO-Fe_2O_3-SiO_2) weight %

No.	Fe_2O_3	CaO	SiO_2	PHASES
1	23.12	35.57	41.31	Pseudowo-llastonite
2	29.18	30.88	39.93	"
5	19.09	36.37	44.55	"

TABLE 4.7 EPMA RESULTS

NO	COMPOSITION (Wt.%)						REMARKS
	Fe_2O_3	FeO	CaO	SiO_2	MgO	MnO	
1	22.69	0	34.92	40.55	0.84	1.00	PLATE 12 I)
2	28.54	0	30.20	39.05	1.09	1.11	"
3	99.24	0	0.05	0 .34	0.04	0.32	"
4	99.01	0	0.26	0 .30	0.11	0.32	"
5	18.60	0	35.44	43.41	1.27	1.29	"
	Fe	FeO	CaO	SiO_2	MgO	MnO	
1	0	57.08	9.45	32.00	0.61	0.86	PLATE 12 II)
2	0	57.92	6 .78	32.23	1.57	1.49	"
3	0	43.12	14.35	41.10	0.37	1.06	"
4	0	31.68	28.09	38.04	1.11	1.08	PLATE 16 I)
5	0	24.36	32.20	41.22	0.90	1.33	PLATE 15 I)
6	0	25.51	32.16	38.77	1.92	1.63	PLATE 16 II)
7	0	20.80	35.13	43.32	0.85	0.91	"
8	0	16.18	36.85	45.13	0.45	1.38	PLATE 16 III)
9	0	97.75	0.04	0.16	0.32	1.74	PLATE 16 I)
10	0	93.89	0.13	0.21	1.37	4.41	PLATE 16 II)
11	98.66	0	0.32	0.59	0.30	0.13	"
12	99.12	0	0.06	0.50	0	0.33	PLATE 16 III)
13	98.58	0	0.33	0.56	0.21	0.31	"

observations.

From these observations, it might be expected that 1% CaO and 2% CaO additions would give similar kientics. The 2% CaO additions may be expected to give slightly lower results, because of the greater quantity of liquid which will be produced causing more pore blockage.
With 5% CaO additions, the liquid is much more basic and is likely to recrystallise more easily and therefore cause

PLATE 12

Digital X-ray mapping of I)hematite grains(CaO 5% added compact sintered at 1300°C for 24 hours in air) and II) iron reduced at (1100-1050)·CaO 2% . EPMA displays of I, II) for a)structure of iron(SEM), b)iron, c)silicon and d)calium.

I)

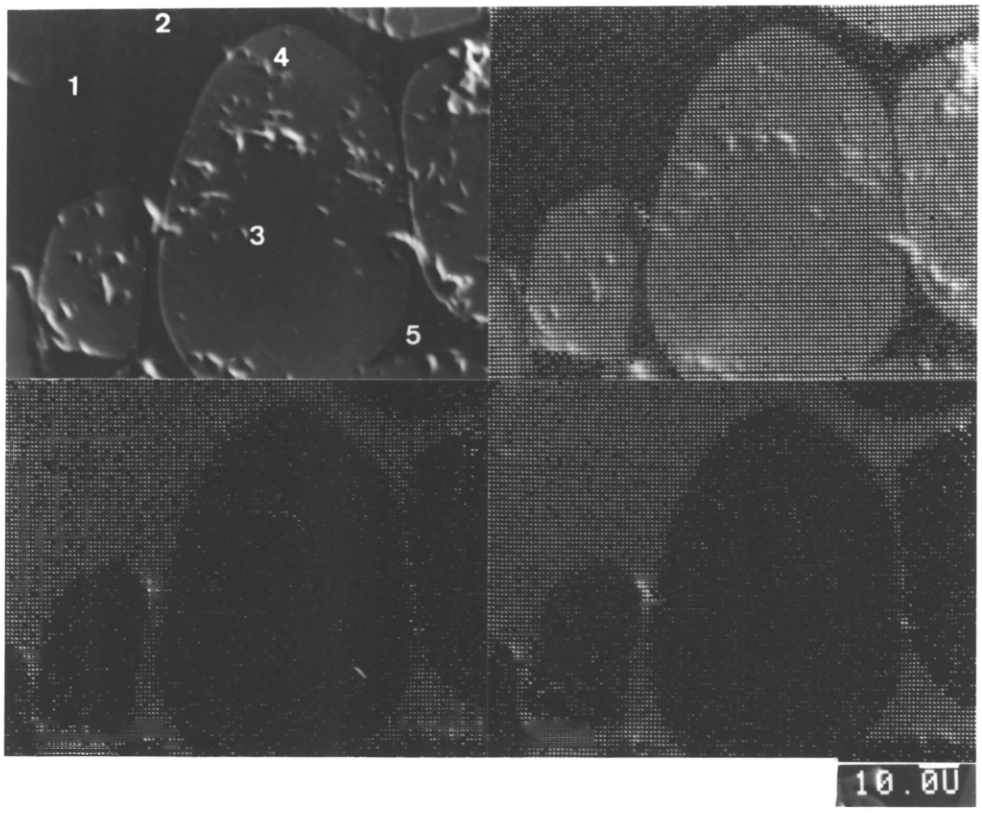

a) b) c) d)

II)

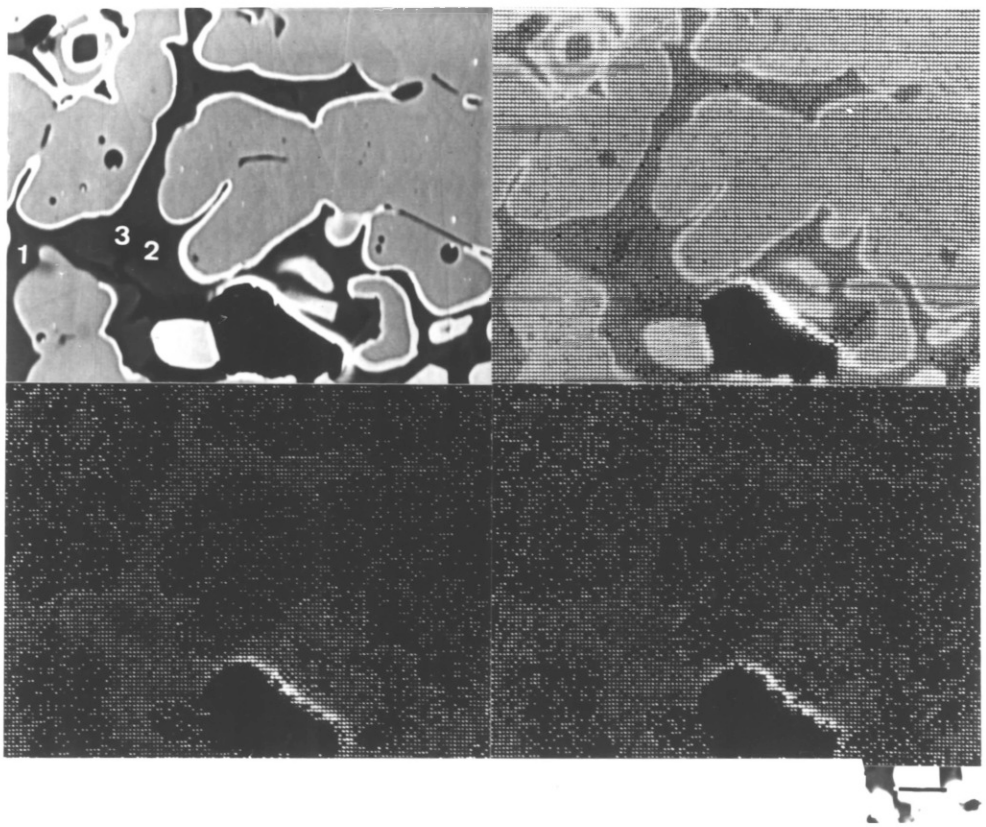

a) b) c) d)

PLATE 13

Micro-structure of a)surface of wustite (SEM) reduced at 950°C, CO/CO_2=1 for 6 hours, b)iron grains reduced at (1100-1100)·CaO 5% and etched with Nital and c)iron reduced at (950-950)·CaO 5% .

a)

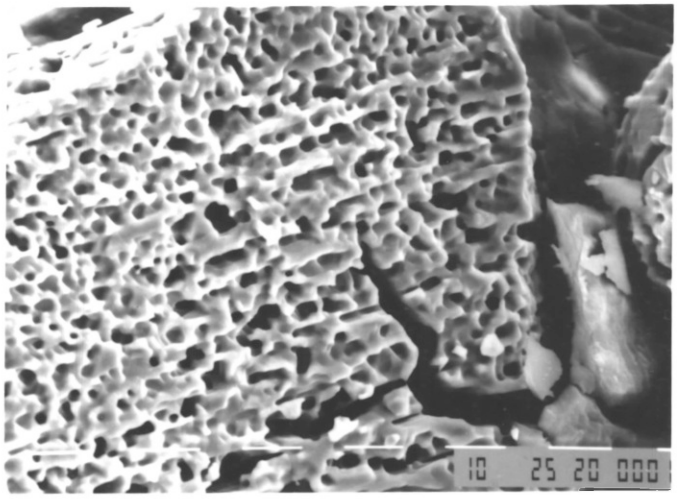

light grey : wustite

black : pore

b)

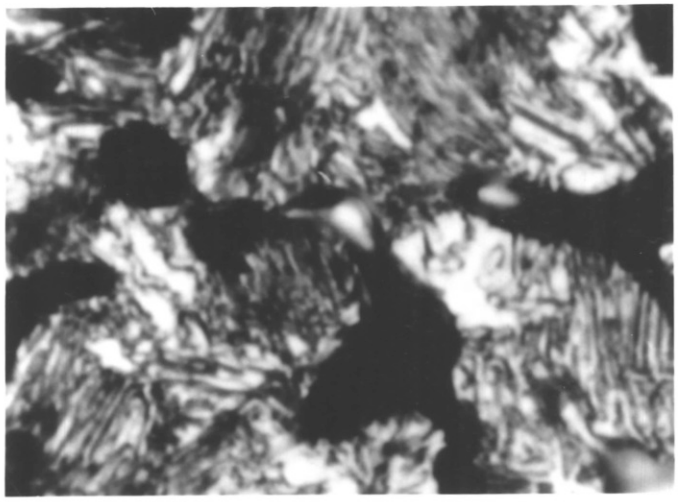

white : ferrite

dark grey : cementite

black : voids

x 1750

c)

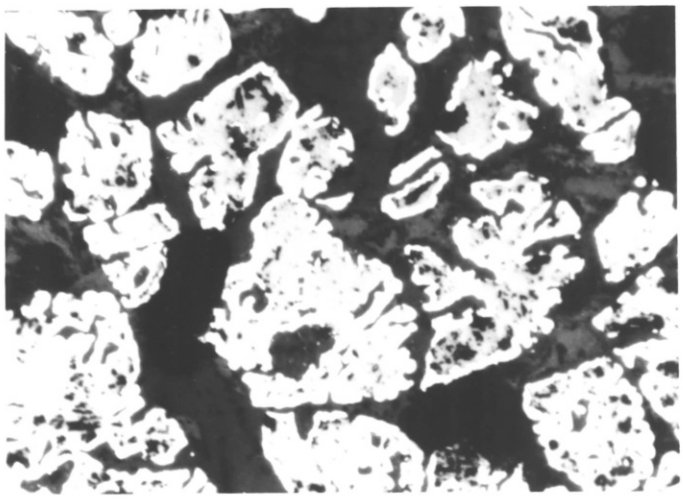

white : iron

light grey : wustite

dark grey : wollastonite

black : voids

x 320

PLATE 14

Micro-structure of iron reduced at a) (1100-950)·CaO 5% , b) (1100-1050)·CaO 5% and c) (1100-1100)·CaO 5% .

a)

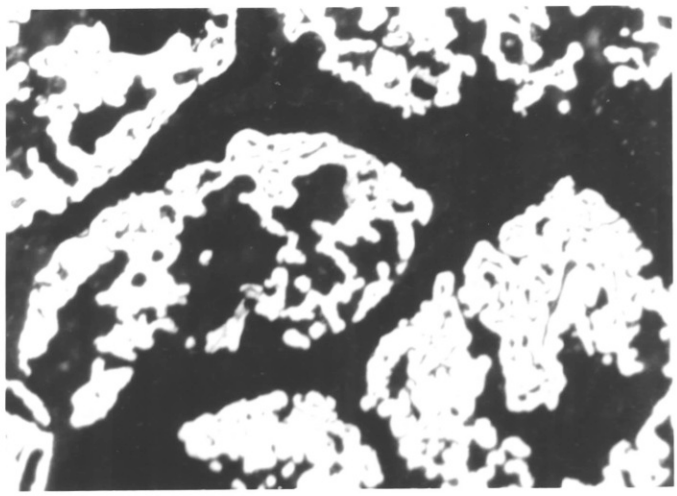

white : iron
dark grey : wollastonite
black : voids

x 320

b)

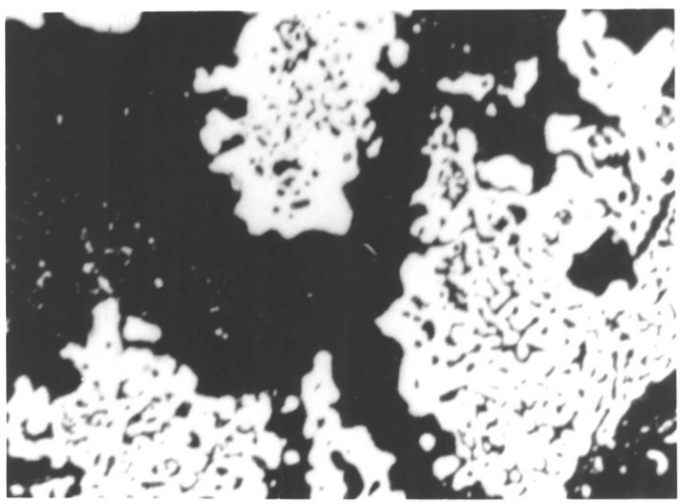

white : iron
dark grey : wollastonite
black : voids

x 320

c)

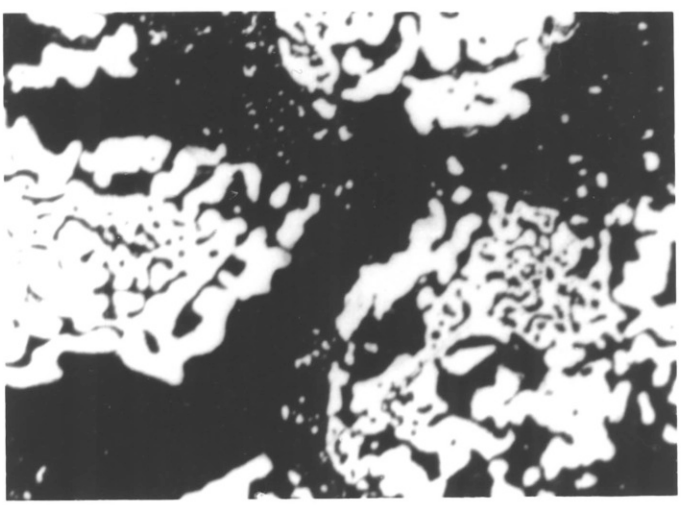

white : iron
dark grey : wollastonite
black : voids

x 320

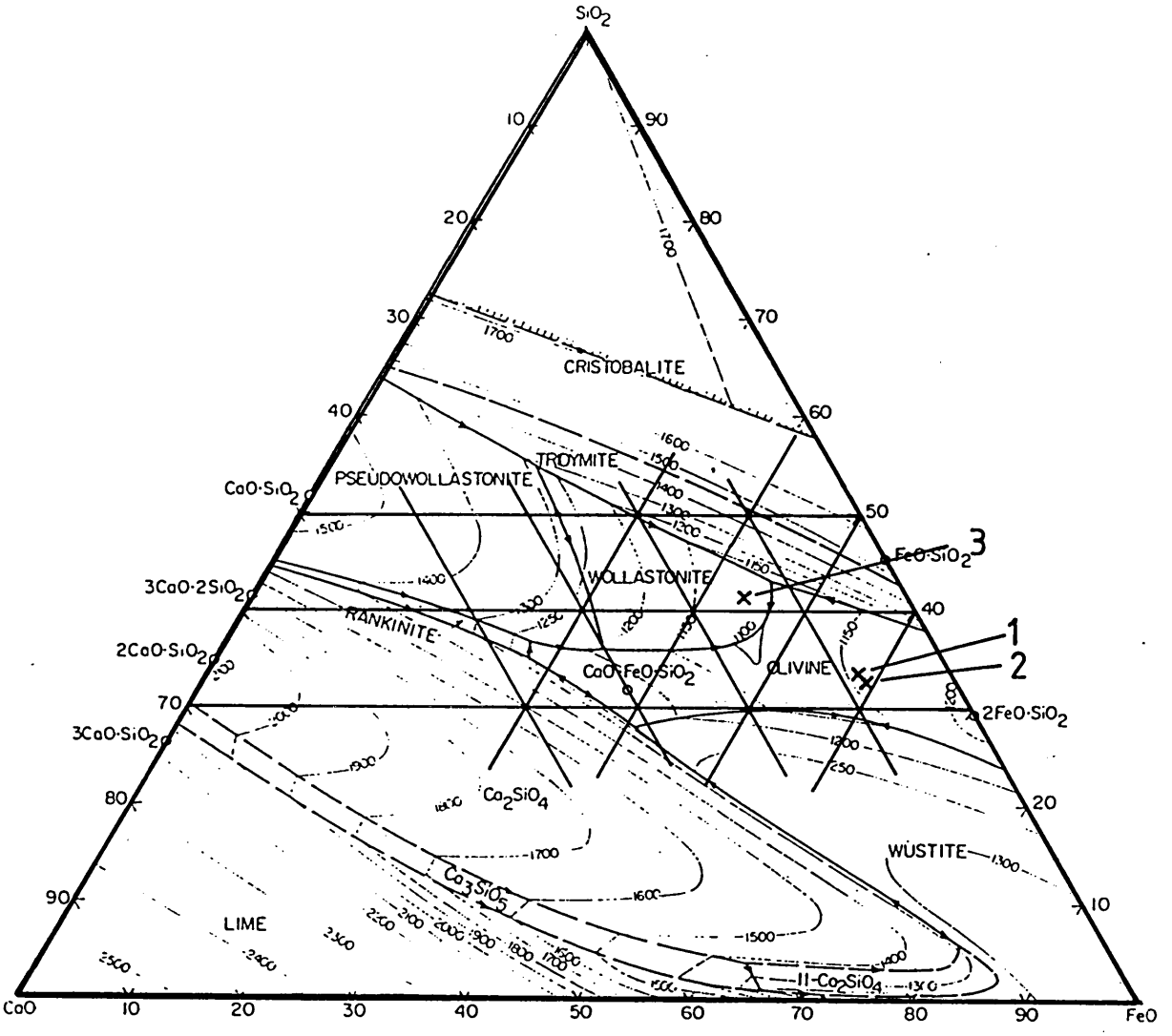

Fig.4.18 Phase relations in the system CaO-iron oxide-SiO_2 in contact with metallic iron(64).

EPMA results

(Re-calculated from the original data for the system CaO-FeO-SiO_2)

weight %

	1	2	3	4	5	6	7	8
CaO	9.6	7.0	14.6	28.7	32.9	33.5	35.8	37.5
FeO	57.9	59.8	43.4	32.4	24.9	36.4	21.2	16.5
SiO_2	32.5	33.2	41.7	38.9	42.2	40.2	43.0	46.0
Experiment	1100 -1050 CaO2%	1100 -1050 CaO2%	1100 -1050 CaO2%	1050 -950 CaO5%	1050 -1050 CaO5%	1050 -1100 CaO5%	1050 -1100 CaO5%	1050 -1100 CaO5%

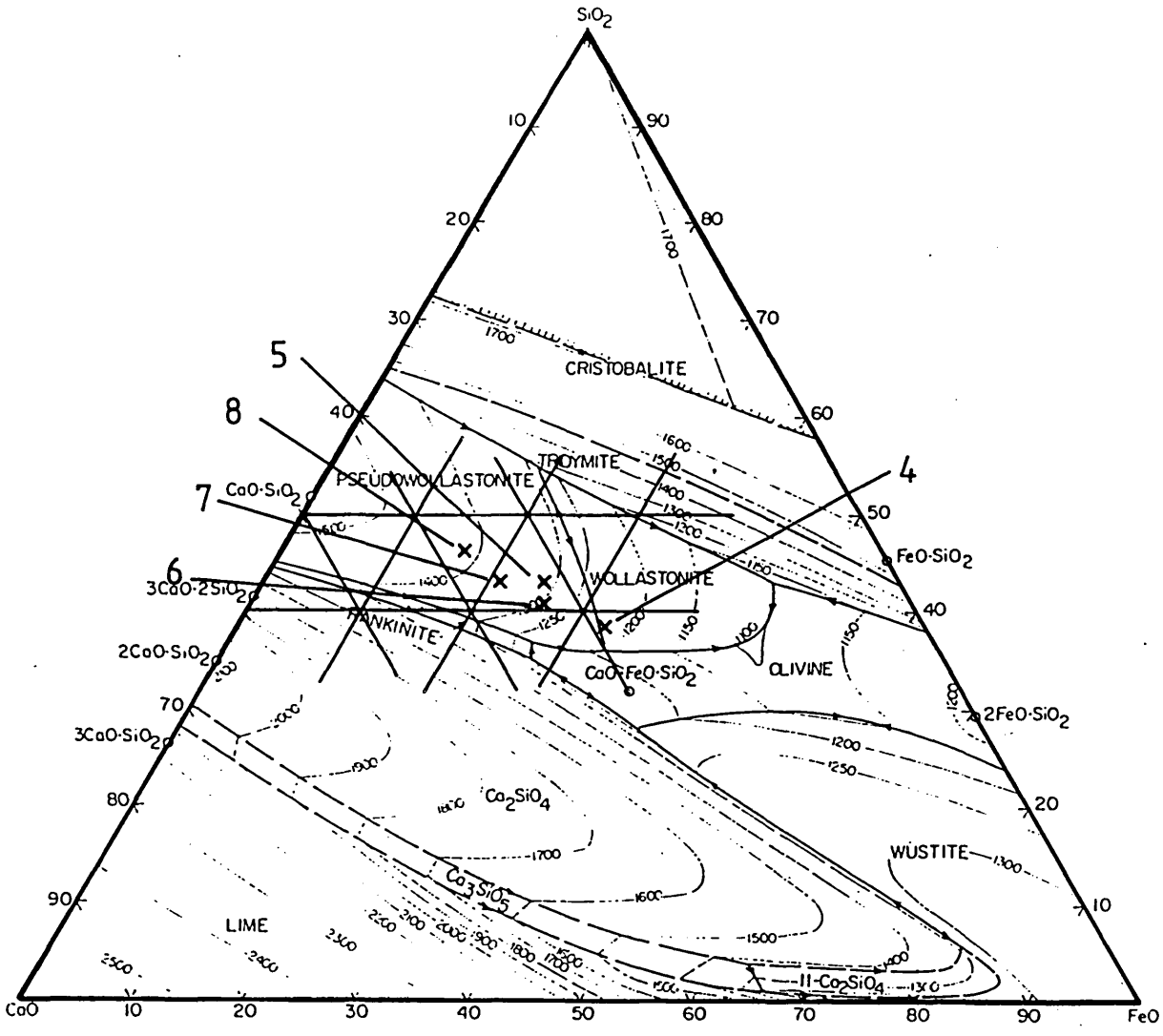

Fig.4.18 Phase relations in the system CaO-iron oxide-SiO_2 in contact with metallic iron(64).

EPMA results

(Re-calculated from the original data for the system CaO-FeO-SiO_2)

weight %

	1	2	3	4	5	6	7	8
CaO	9.6	7.0	14.6	28.7	32.9	33.5	35.8	37.5
FeO	57.9	59.8	43.4	32.4	24.9	36.4	21.2	16.5
SiO_2	32.5	33.2	41.7	38.9	42.2	40.2	43.0	46.0
Experiment	1100 -1050 CaO2%	1100 -1050 CaO2%	1100 -1050 CaO2%	1050 -950 CaO5%	1050 -1050 CaO5%	1050 -1100 CaO5%	1050 -1100 CaO5%	1050 -1100 CaO5%

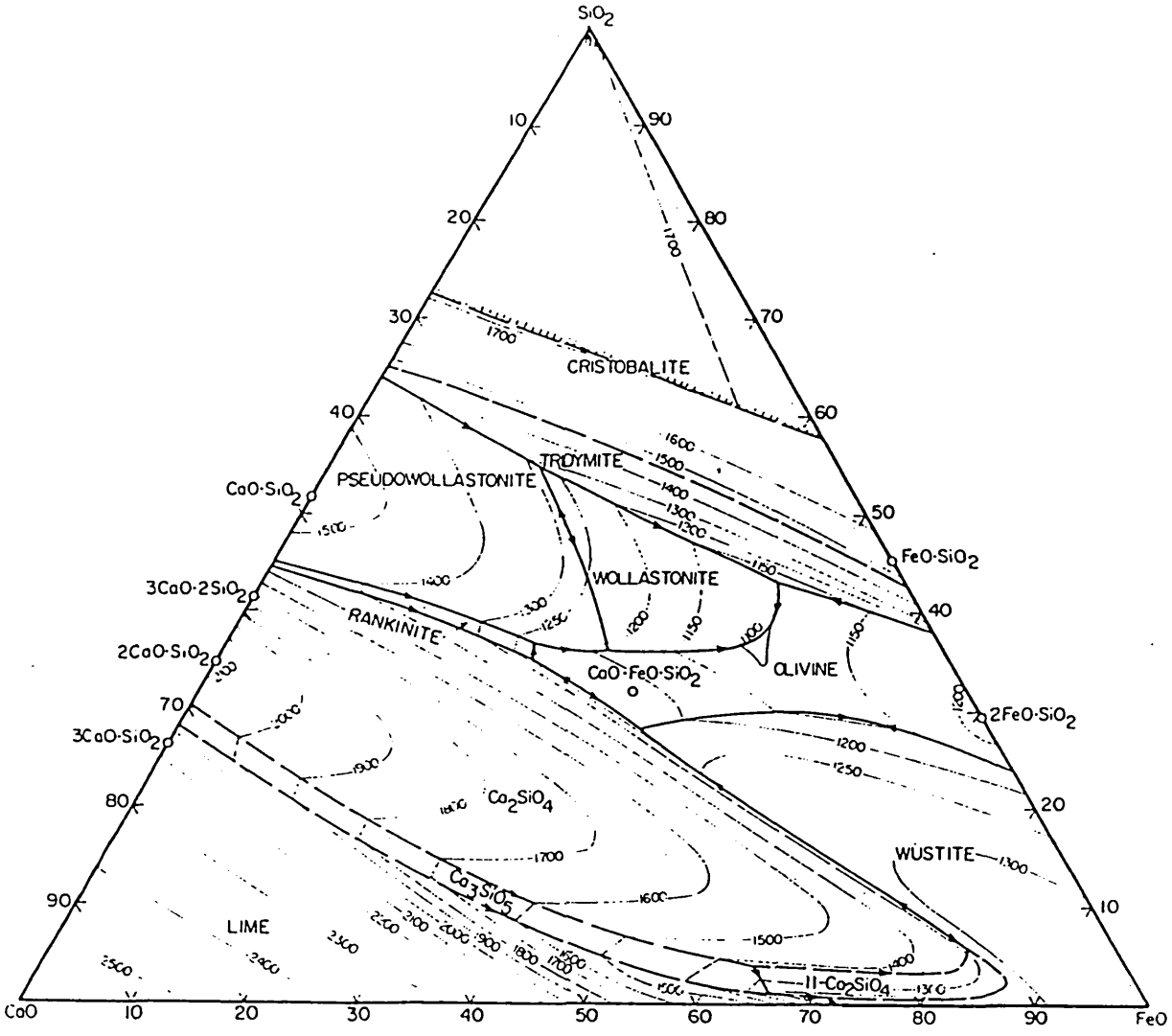

Fig.4.18 Phase relations in the system CaO-iron oxide-SiO_2 in contact with metallic iron(64).

EPMA results

(Re-calculated from the original data for the system CaO-FeO-SiO_2)

weight %

	1	2	3	4	5	6	7	8
CaO	9.6	7.0	14.6	28.7	32.9	33.5	35.8	37.5
FeO	57.9	59.8	43.4	32.4	24.9	36.4	21.2	16.5
SiO_2	32.5	33.2	41.7	38.9	42.2	40.2	43.0	46.0
Experiment	1100 -1050 CaO2%	1100 -1050 CaO2%	1100 -1050 CaO2%	1050 -950 CaO5%	1050 -1050 CaO5%	1050 -1100 CaO5%	1050 -1100 CaO5%	1050 -1100 CaO5%

PLATE 15

Digital X-ray mapping of iron reduced at I) (1050-950)·CaO 5% and II) (1050-1050)·CaO 5% . EPMA displays of I,II) for a)structure of iron(SEM), I,II) for b)iron, I) c) and II) d)silicon and I) d) and II) c)Calcium .

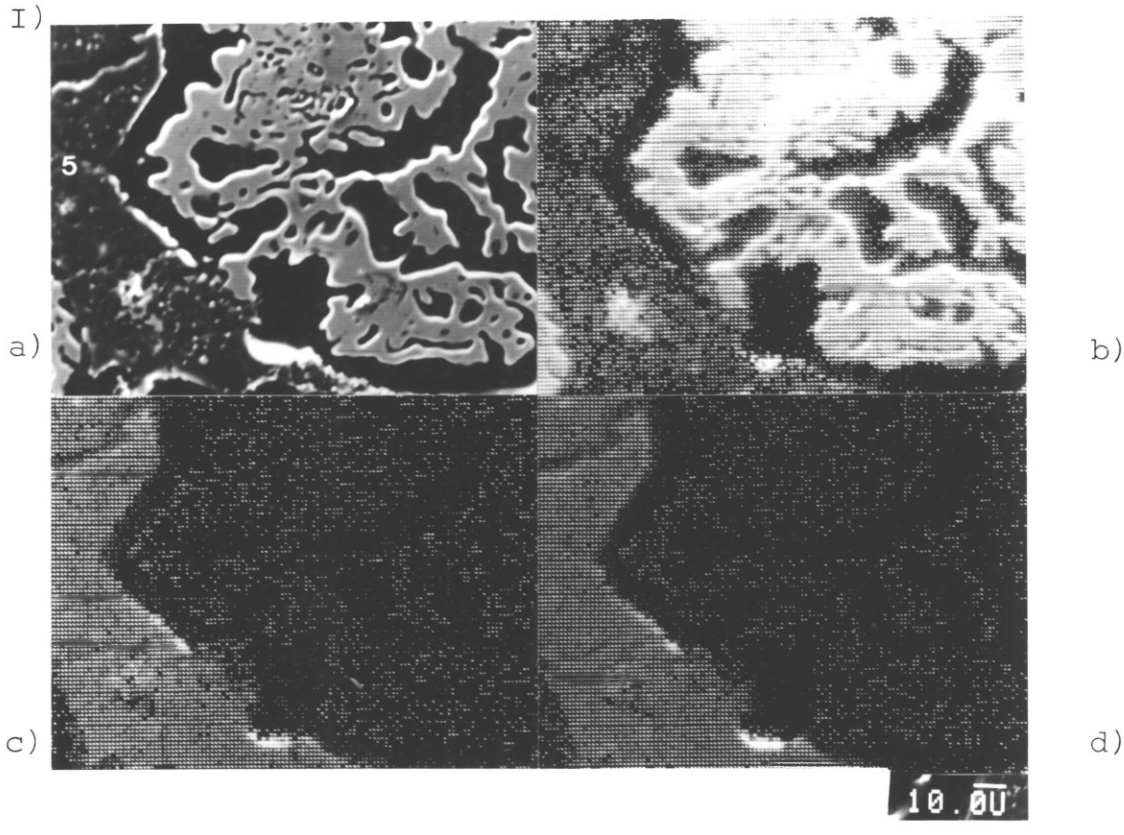

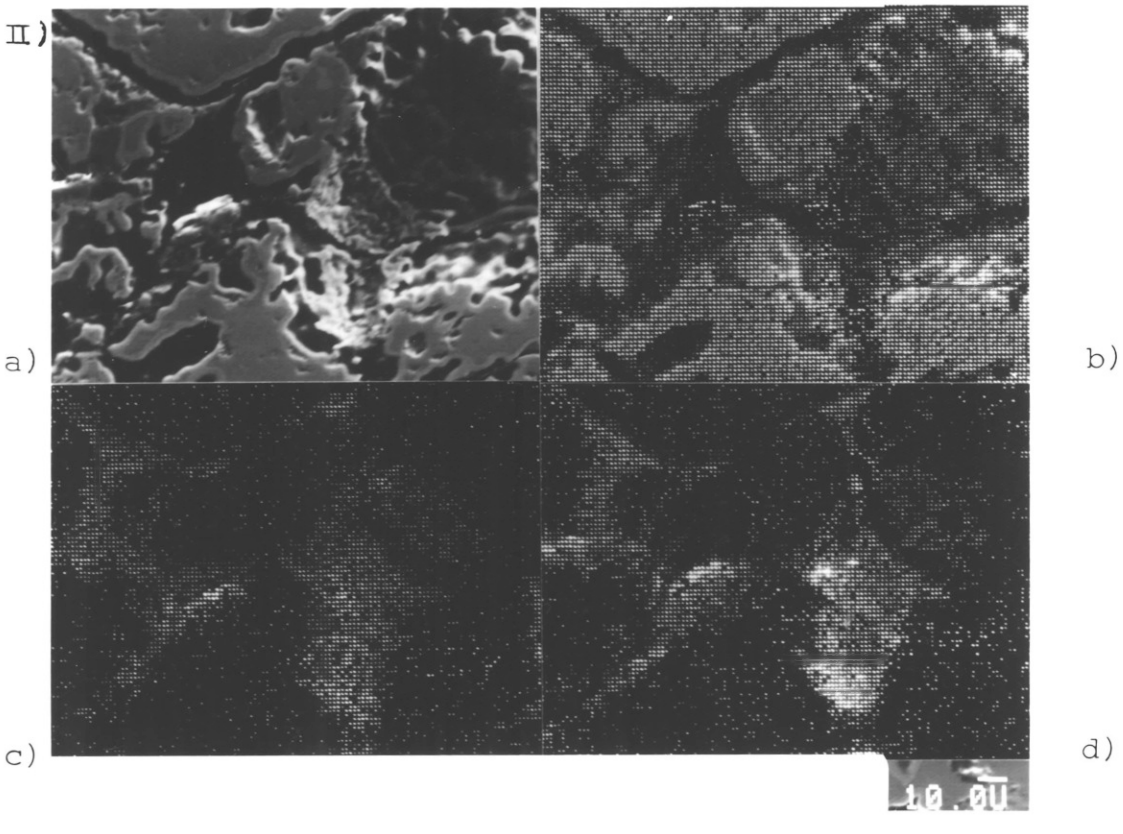

PLATE 16

Micro-structure(SEM) of iron reduced at I) (1050-950)· CaO 5% , II and III) (1050-1100)·CaO 5% .

EPMA displays I),II) and III)a), the analysed points, and III), the ions distribution of b)iron, c)calcium and d)silicon .

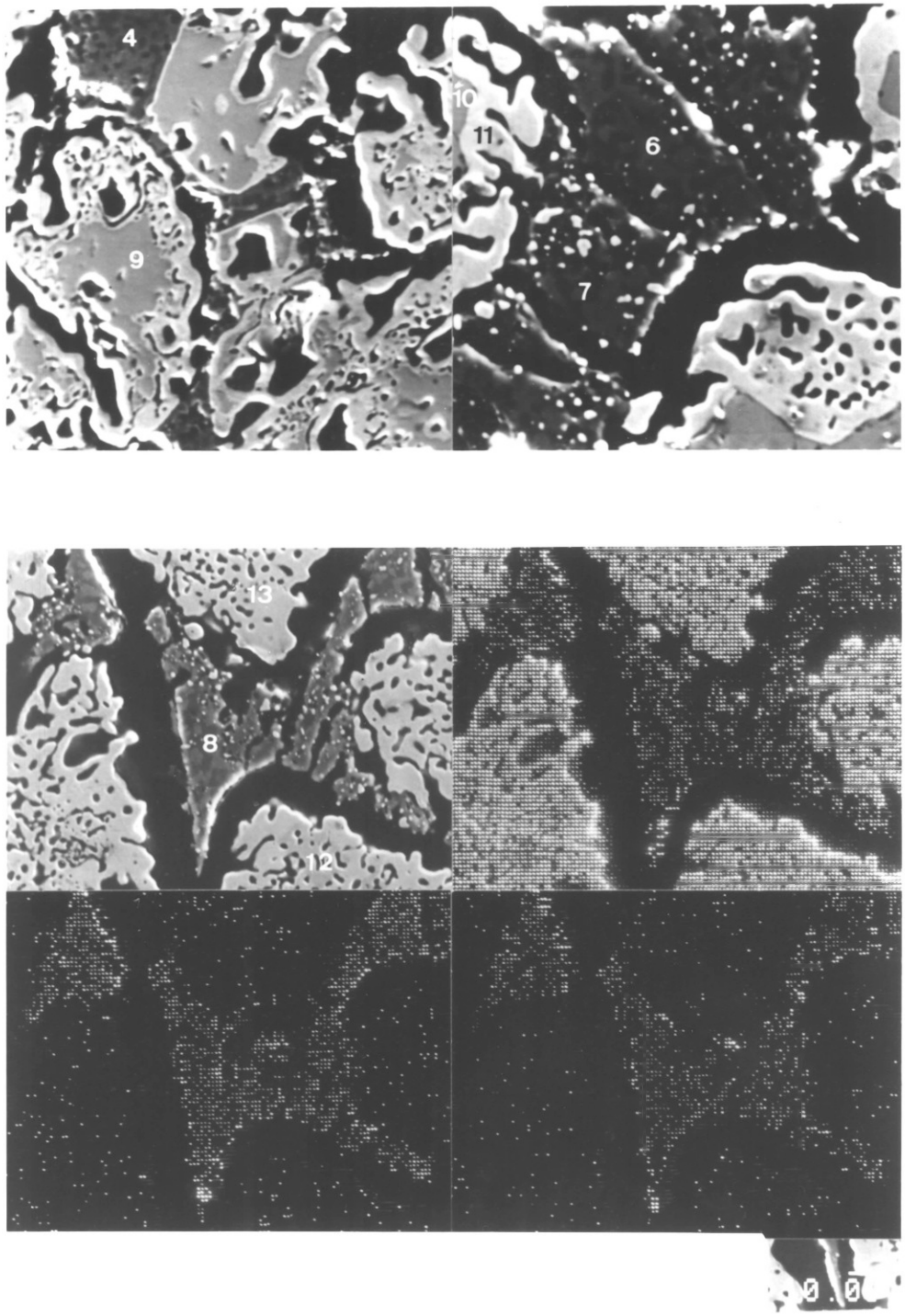

I)

II)

III)

a)

b)

c)

d)

less pore blockage. In addition, with a higher lime concentration in the liquid, some lime dissolution in the iron oxide may occur. Since lime has been reported to increase the rate of iron oxide reduction, both of these factors are expected to give the effect observed for the rate of reduction.

When reduction occurs at 1100°C both to wustite and to iron, the formation of the liquid phase in the CaO-FeO-SiO_2 system at 1100°C is expected to occur. This liquid phase occurs near the $CaO \cdot FeO \cdot SiO_2$ composition. Once this liquid phase forms, it is likely to occupy the interparticle spacing to a greater extent than the $CaO \cdot Fe_2O_3 \cdot SiO_2$ liquid. Due to its lower CaO content, a much greater volume is expected to form and this agrees with the significant reduction in rate observed with 1 and 2% CaO addition when the hematite is formed at 1100°C. Once again, the CaO content in the iron oxide is likely to cause the increase in rate with 5% CaO additions.
Further evidence for the presence of these two liquid phases is produced from the EPMA analyses.

The observations of the reduction of Kirschsteinite are also interesting. Several experiments have been carried out for long reaction times after wustite had been reduced. The XRD pattern for this phase disappeared and carbon deposition was observed at the same time giving a weight gain (see Plate 13b).

Another observation with lime additions relates to the production of iron within the wustite grains. This phenomenon seems to be strongly related to the formation of CaO within the wustite grains. The iron produced appears

as individual grains separated by lime. Sometimes a liquid phase seemed to form between the iron grains on reduction at 1100°C. At 1100°C, this mode of reduction leads to very fast reaction.

4.4. IRON ORE COMPACTS WITH MgO ADDITION

The additions of MgO to iron ore compacts were prepared in the same manner as described in Chapter 3.
The phases present during sintering of the compacted samples were α- Hematite, α- Quartz and magnesioferrite ($MgFe_2O_4$) respectively. During reduction of hematite to wustite, no significant change, such as cracking, was observed. However following reduction, several observations were made which were caused by the MgO in the sample.

4.4.1. EFFECT OF TEMPERATURE

The effects of 1% MgO addition samples on the reduction rate are shown in Fig . 4.19-21. With low temperature reduction (950°C), the reduction rate once again decreased for increased temperature of wustite preparation initially. For reduction at 1050°C, the rates show a gradual decrease for increasing temperature of wustite formation, whilst the rates increased at 1100°C.
At 950°C, the reduction rates show remarkable differences in shape between (950-950)·MgO 1% and the other values by comparison the high temperature reduction are very similar. Increasing the quantity of MgO to 2% produced a series of results which are very similar to 1% MgO additions. In fact, the rates were nearly the same at every temperature for 950°C reduction. At 1050°C and 1100°C, 2% MgO addition results are the same within experimental error and

independent of wustite formation. The low temperature reduction(950°C) shows that the rates seem to be independent of the amount of MgO additions up to 2%.

Figs. 4.25-27 show the reduction rate of the compacts with 5% MgO addition. In all reduction curves, a weight gain is observed in the final stages of reduction. Similar observations were not made in other experiments at such early stages.

In Fig. 4.25, the reduction rate at 950°C shows a remarkable increase compared with 1 or 2% MgO additions, while the reduction rates at higher temperatures (1050,1100°C) show similar behaviour. The reduction rates at 1050 and 1100°C with MgO 5% are remarkably similar.

At low temperatures, the overall rate shown in Fig. 4.25-27-(950-950)·MgO 5% (1050-950)·MgO 5% and (1100-950)· MgO 5%- is higher than the rate with the compacts containing lower MgO additions.

4.4.2. THE EFFECT OF WUSTITE

Fig. 4.19-21 show the effect of wustite produced at different temperatures (950,1050 and 1100°C) with 1% MgO additions. At low temperature (950°C) reduction, the reduction rate decreased significantly by increasing the temperature of wustite preparation, however, the difference became slight at (1100-950) and (1050-950).

The reduction rate at high temperature (1100°C) increased slightly with increased temperature of wustite formation while it decreased slightly at 1050°C.

Similar results to 950°C were observed when wustite prepared at 1050°C and 1100°C was reduced at 1050°C and 1100°C .

A similar effect mentioned above was observed at these temperatures with 2% MgO additions while the reduction at (1100-1100) shows the highest reduction rate.
When 5% of MgO was added (Fig. 4.25-27), the overall reduction rate at low temperatures (950°C) was enhanced for all wustites.

4.4.3. EFFECT OF AMOUNT OF MgO ADDITION

Fig. 4.19,22 and 25 show the effect of the amount MgO addition for wustite produced at 950°C. The overall reduction rate increased with increasing amount of MgO added in proportion to the amount added.
Fig. 4.20,23 and 26 show a similar effect to that observed above, however, the rate slightly decreased at the highest temperature (1100°C) for increased amounts of addition.
With the wustite produced at 1100°C, the reduction rate shows the same effect as the wustite produced at 1050°C (see Fig. 4.21,24 and 27).

Weight gain during reduction

Substantial weight gains was observed at the final stage of reduction at all temperatures when 5% of MgO was added to the compacts.
The weight gain commenced after 92.5% of reduction in the case of reduction at (1100-950).MgO 5%. The reduction at (950-1100)·MgO 5% shows that the weight gain starts after 98.5% of reduction is achieved.

4.4.4. SEQUENCE OF REDUCTION

MgO 1% addition

Table 4.8 shows the XRD results for MgO 1% additions.

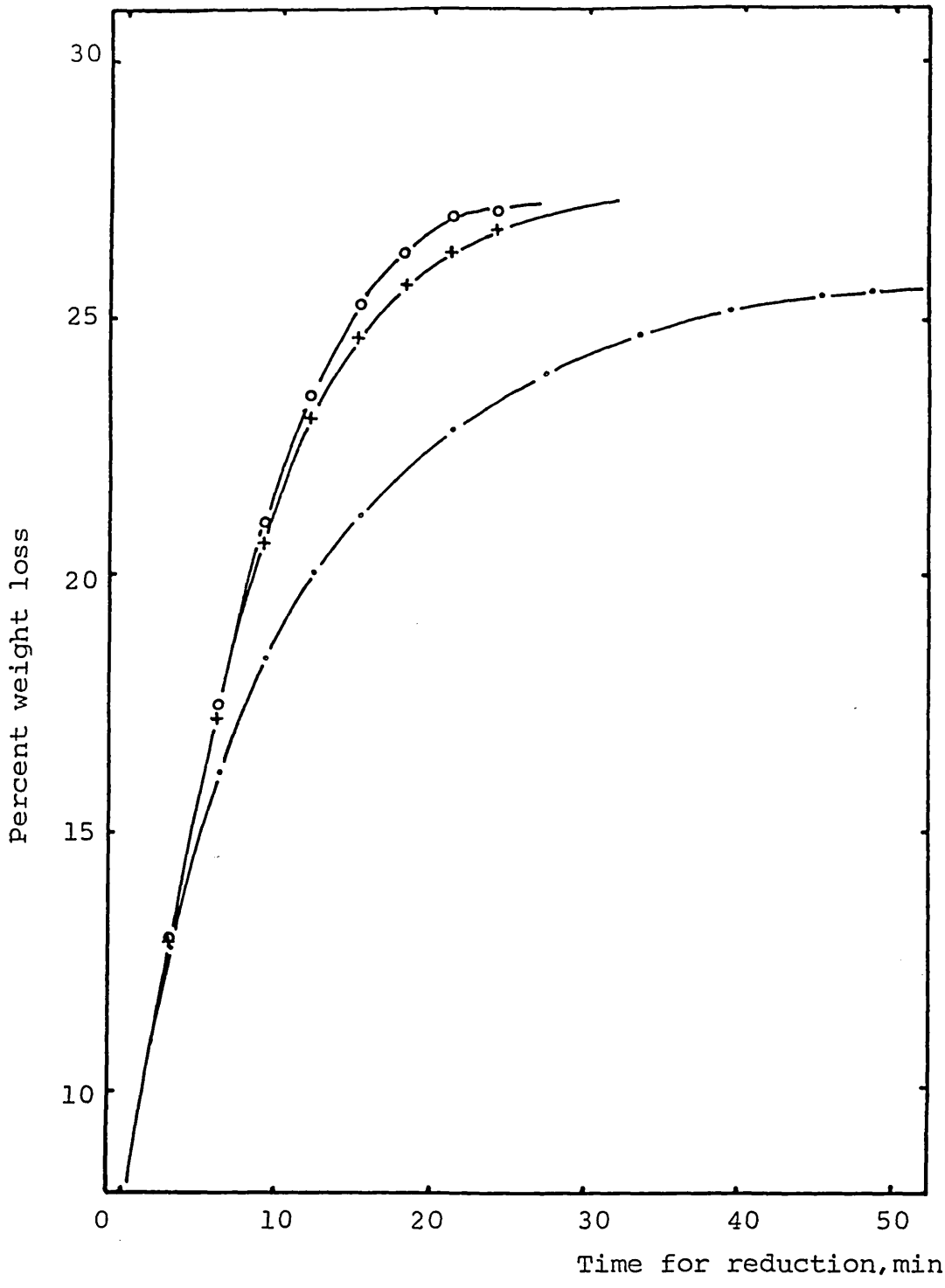

Fig. 4.19- The effect of temperature at 950, 1050 and 1100°C on reduction of wustite compacts pre-reduced at 950°C with MgO 1% additions.

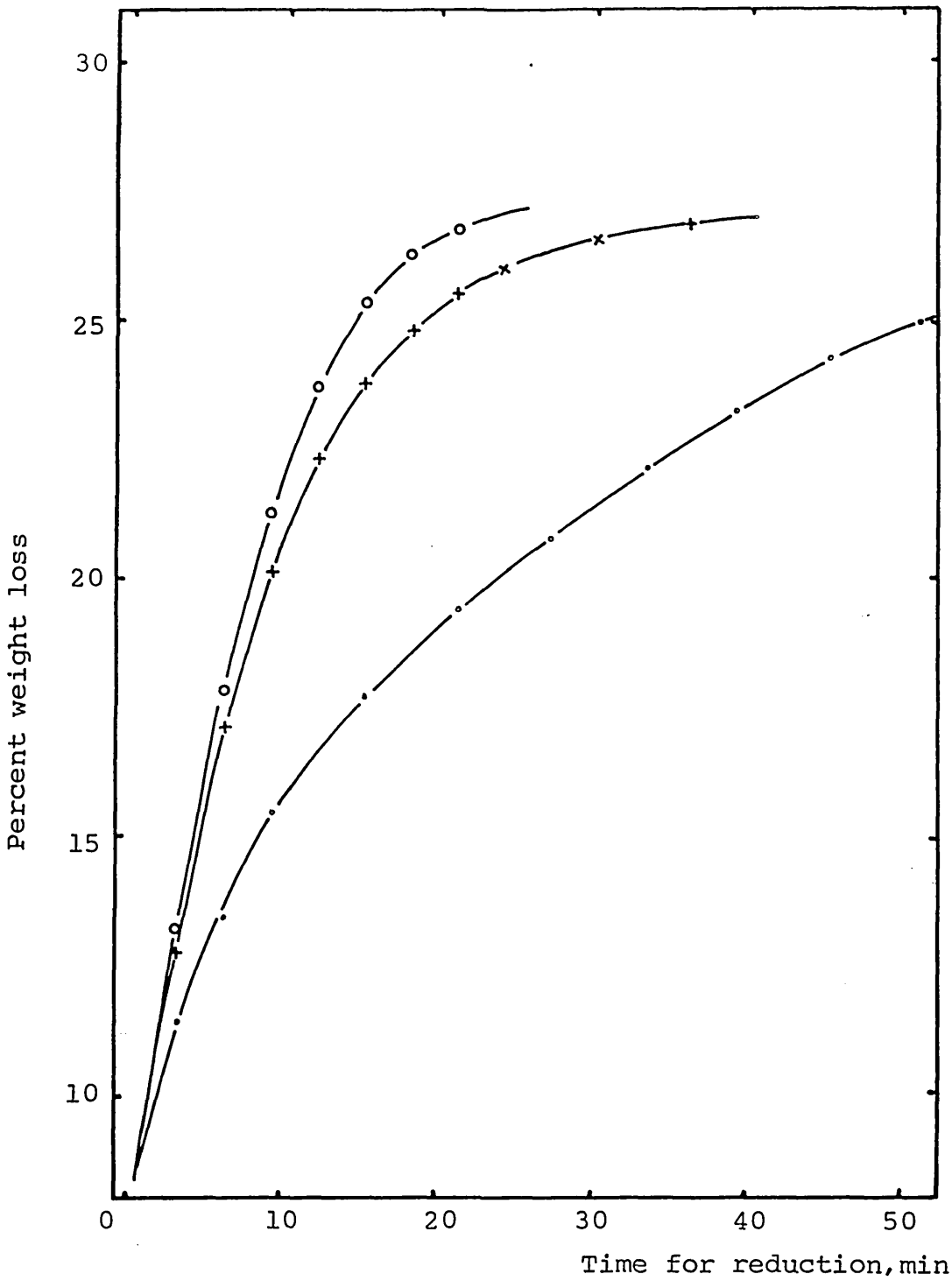

Fig. 4.20- The effect of reduction at 950, 1050 and 1100°C on reduction of wustite compacts pre-reduced at 1050°C with MgO 1% additions.

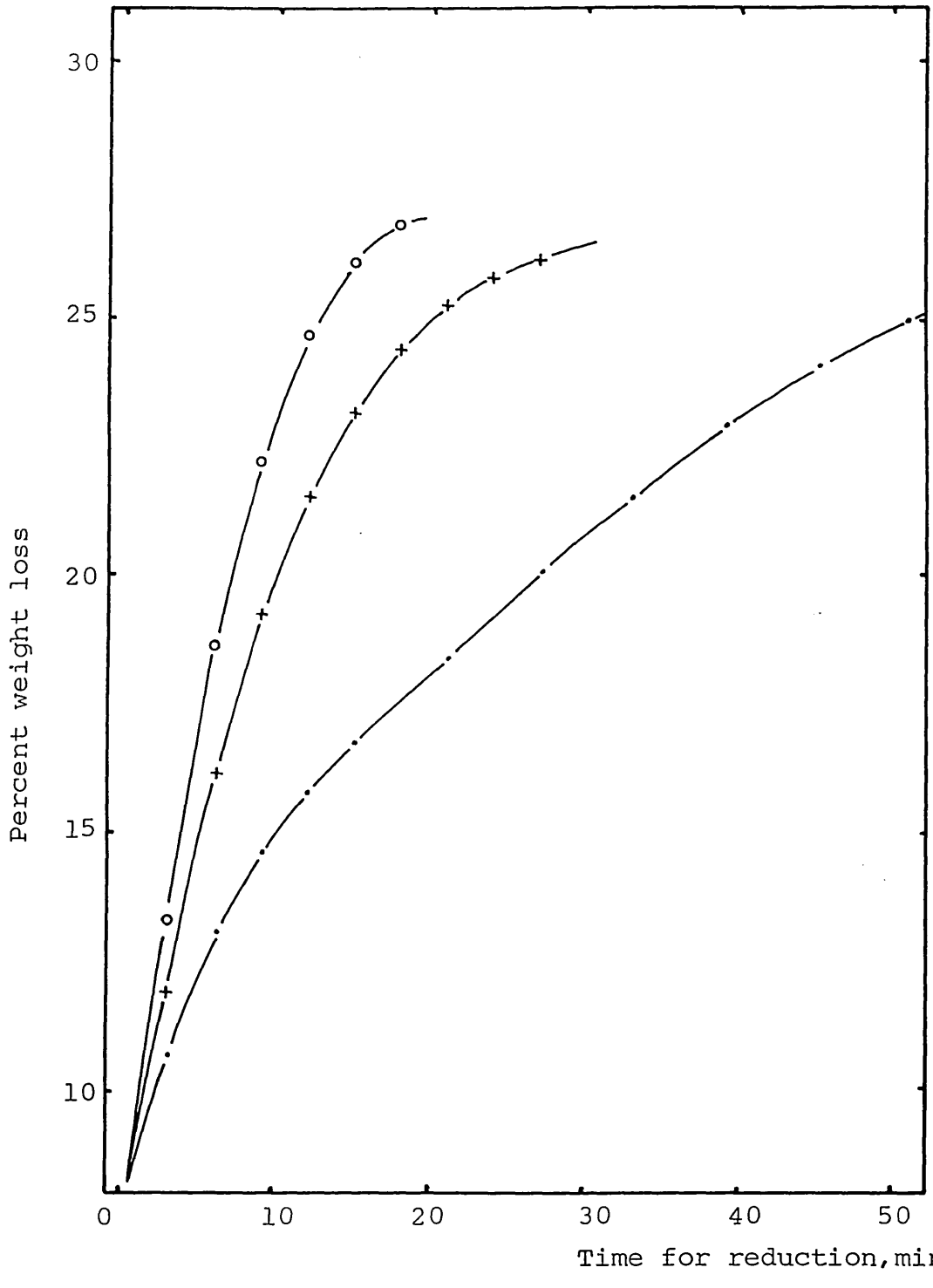

Fig. 4.21- The effect of temperature at 950, 1050 and 1100°C on reduction of wustite compacts pre-reduced at 1100°C with MgO 1% additions.

The phases identified in the samples were Iron, Wustite, α- Cristobalite, Cementite, Magnesioferrite and α- Quartz. From the EPMA results, the remaining unreduced wustite contained more than 4% MgO (see Table 4.11, No 8).
The wustite reflexions in XRD are shifted to indicate an increased unit cell dimension compared with pure wustite. The magnesiowustite has a wide range of variation in concentration and there appears to be almost complete solubility between FeO and MgO (see Fig. 4.28). These features prove that the wustite observed in these samples is magnesiowustite having various MgO contents at different temperatures.
Other phases appearing are α- Quartz and α- Cristobalite. The α- Cristobalite was regarded as appearing by transformation of α- Quartz. Since there is no intermediate phase like fayalite observed in the sample, this phenomenon is possibly slightly different compared to the case of compacts without any additions.
Magnesioferrite was still observed after 98% reduction was achieved.
Cementite was observed in every sample even in the presence of wustite.

MgO 2% addition

Table 4.9 shows the results by XRD and the phases identified after reduction were Iron, Wustite, α- Quartz, α- Cristobalite, Magnesioferrite, Fayalitemagnesian and Clinoenstatite ($MgSiO_3$).
The iron magnesium silicate (Fayalite magnesian) is the orthorhombic modifications and is similar to Fayalite ob-

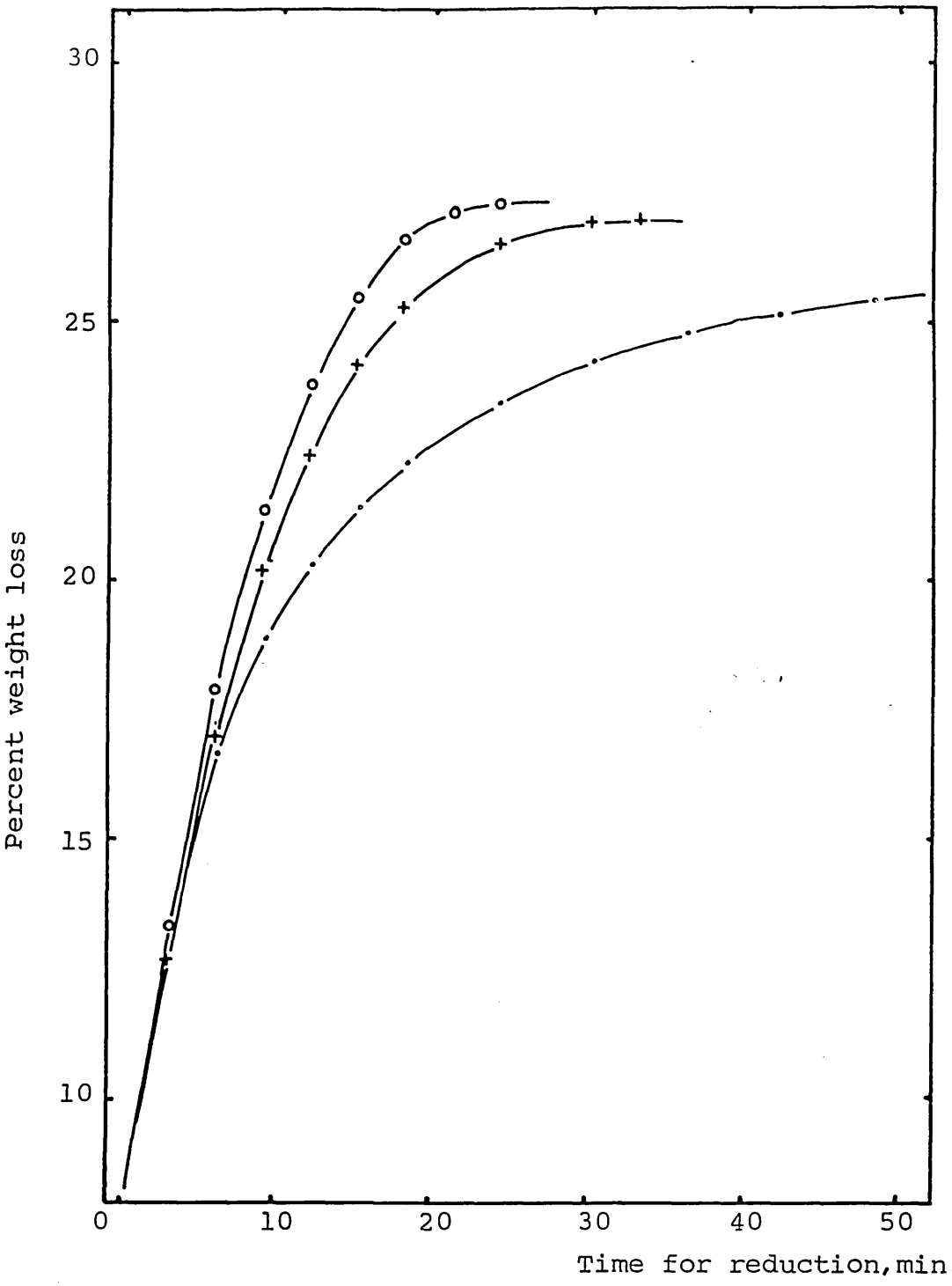

Fig. 4.22- The effect of temperature at 950, 1050 and 1100°C on reduction of wustite compacts pre-reduced at 950°C with MgO 2% additions.

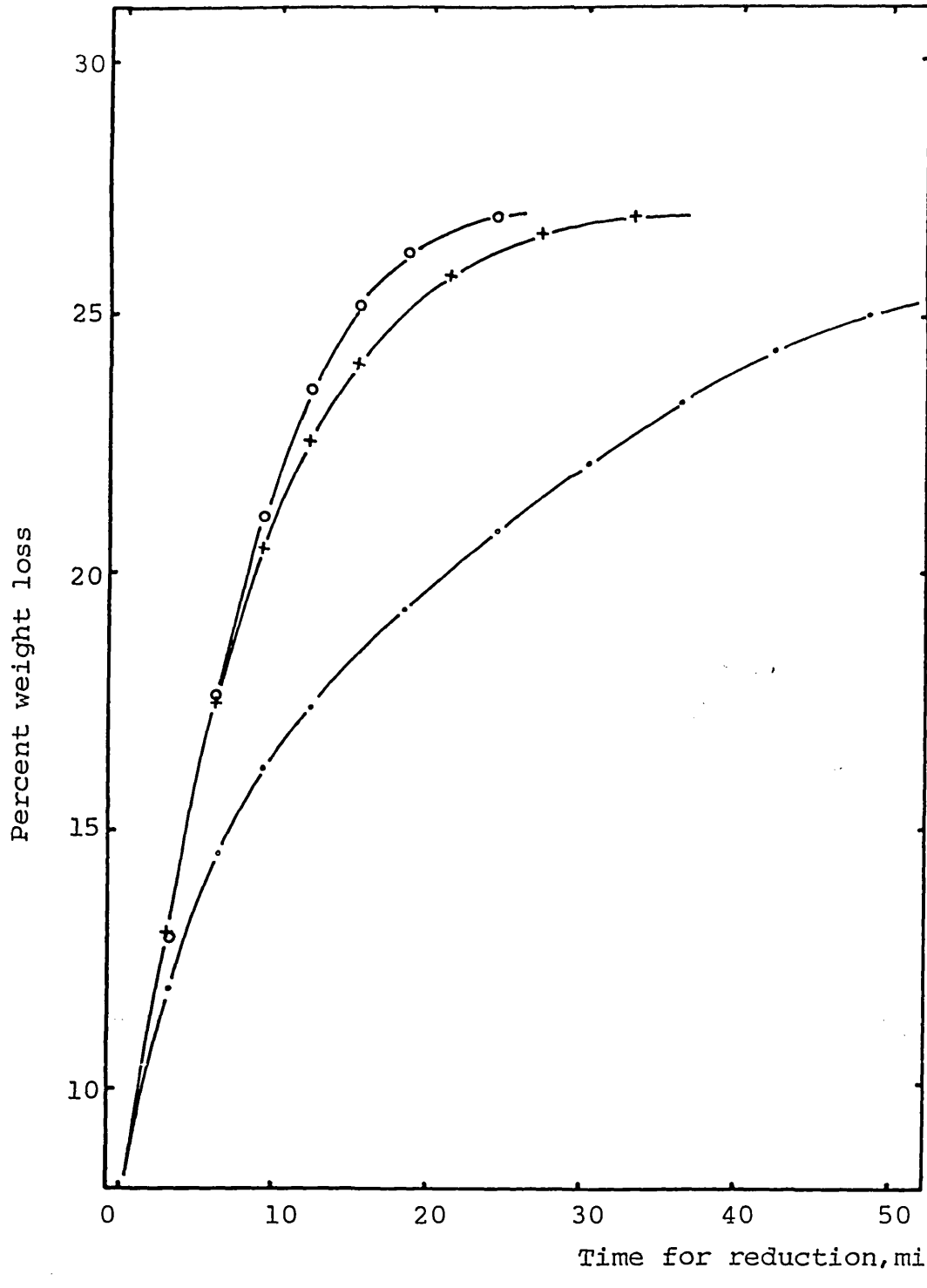

Fig. 4.23- The effect of temperature at 950, 1050 and 1100°C on reduction of wustite compacts pre-reduced at 1050°C with MgO 2% additions.

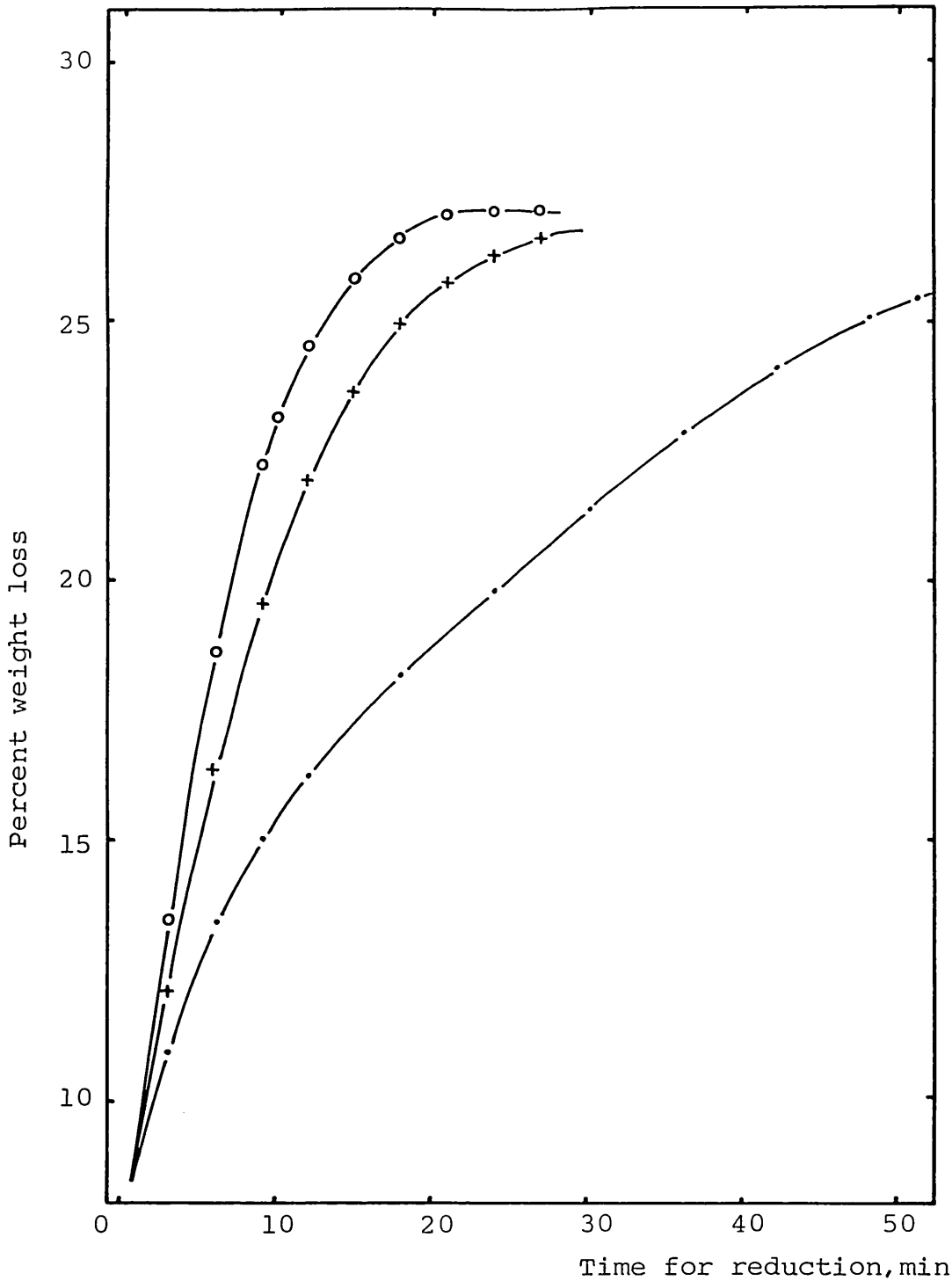

Fig. 4.24- The effect of temperature at 950, 1050 and 1100°C on reduction of wustite compacts pre-reduced at 1100°C with MgO 2% additions.

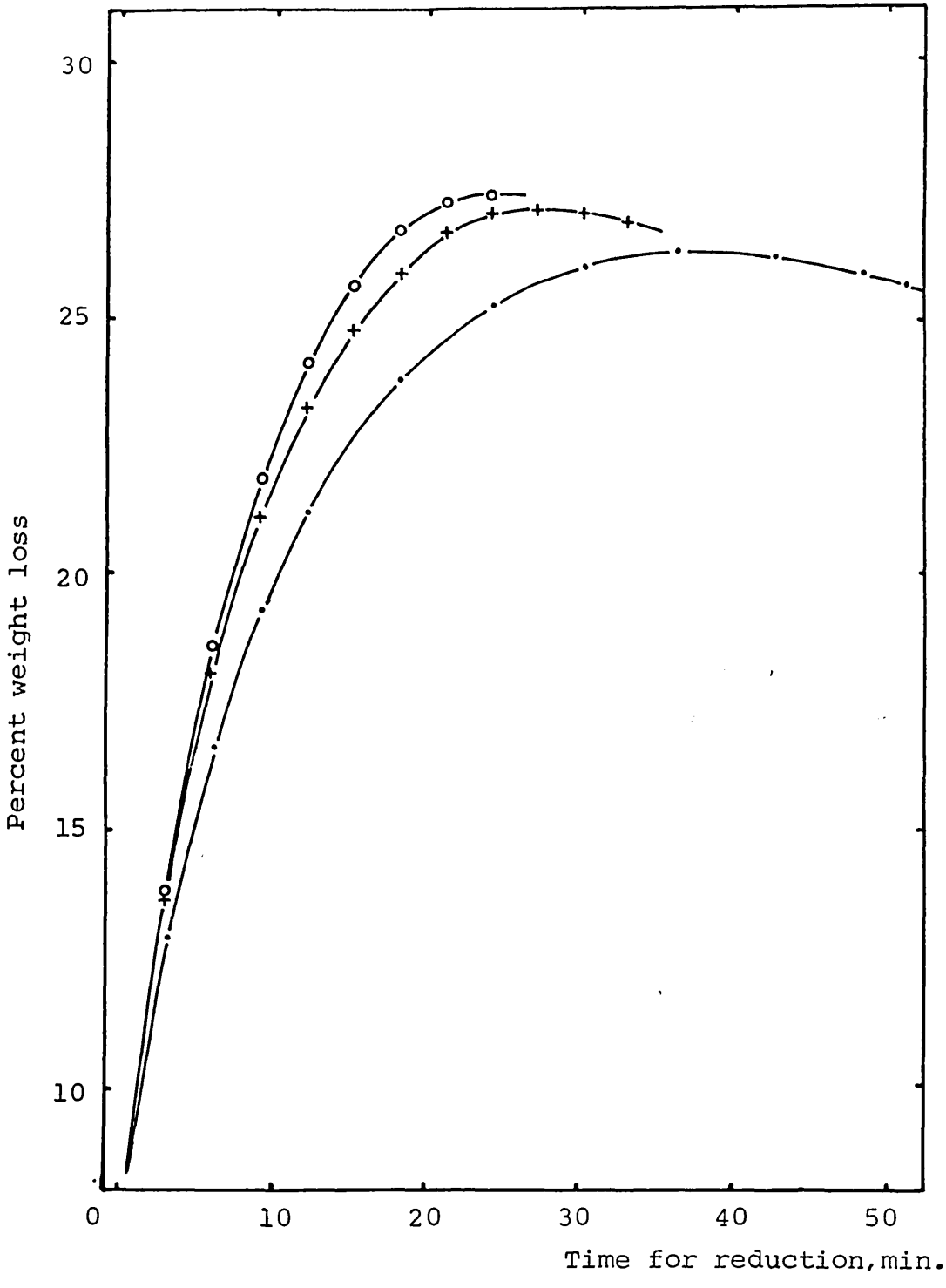

Fig. 4.25- The effect of temperature at 950, 1050 and 1100°C on reduction of wustite compacts pre-reduced at 950°C with MgO 5% additions.

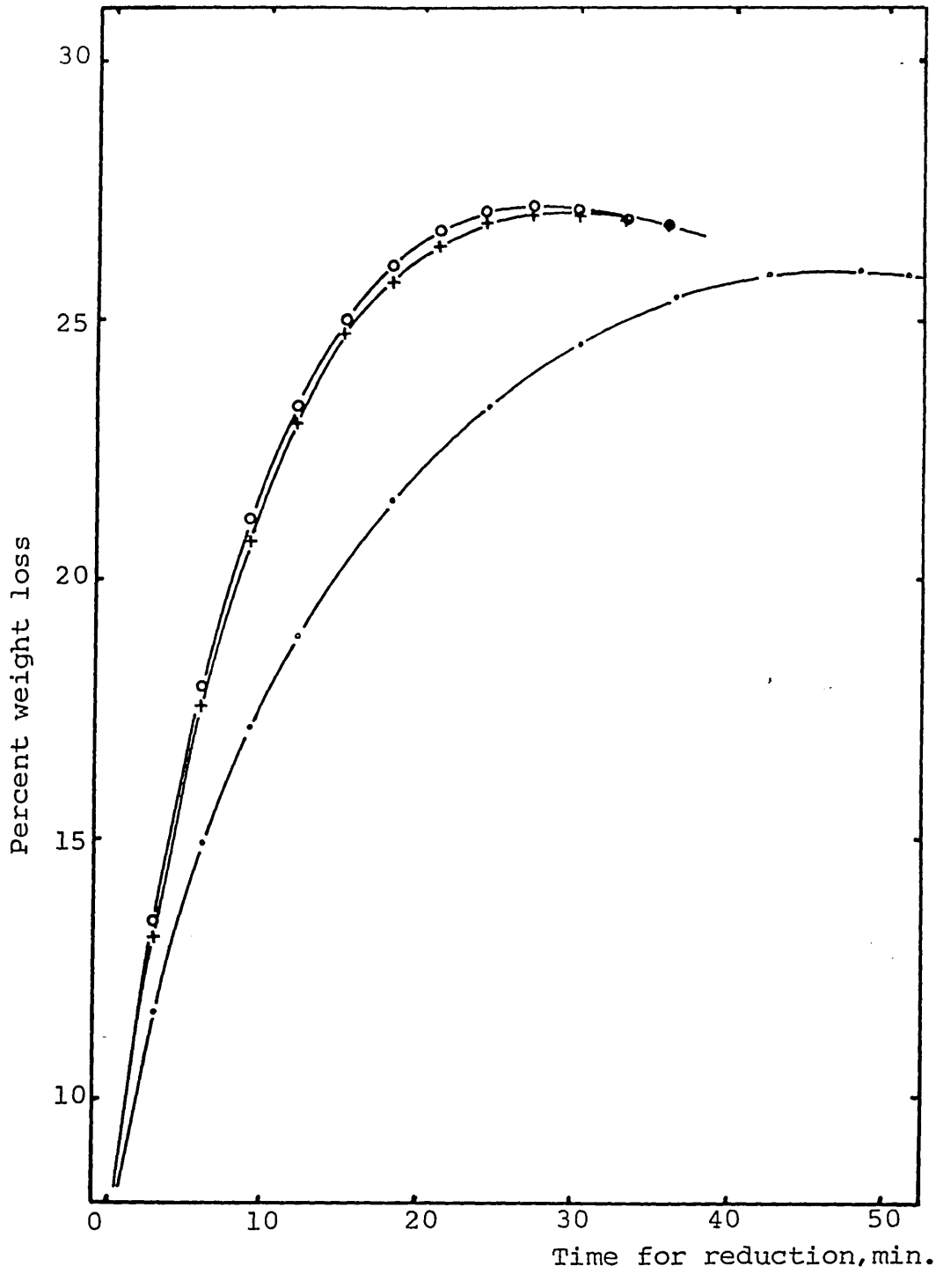

Fig. 4.26- The effect of temperature at 950, 1050 and 1100°C on reduction of wustite compacts pre-reduced at 1050°C with MgO 5% additions.

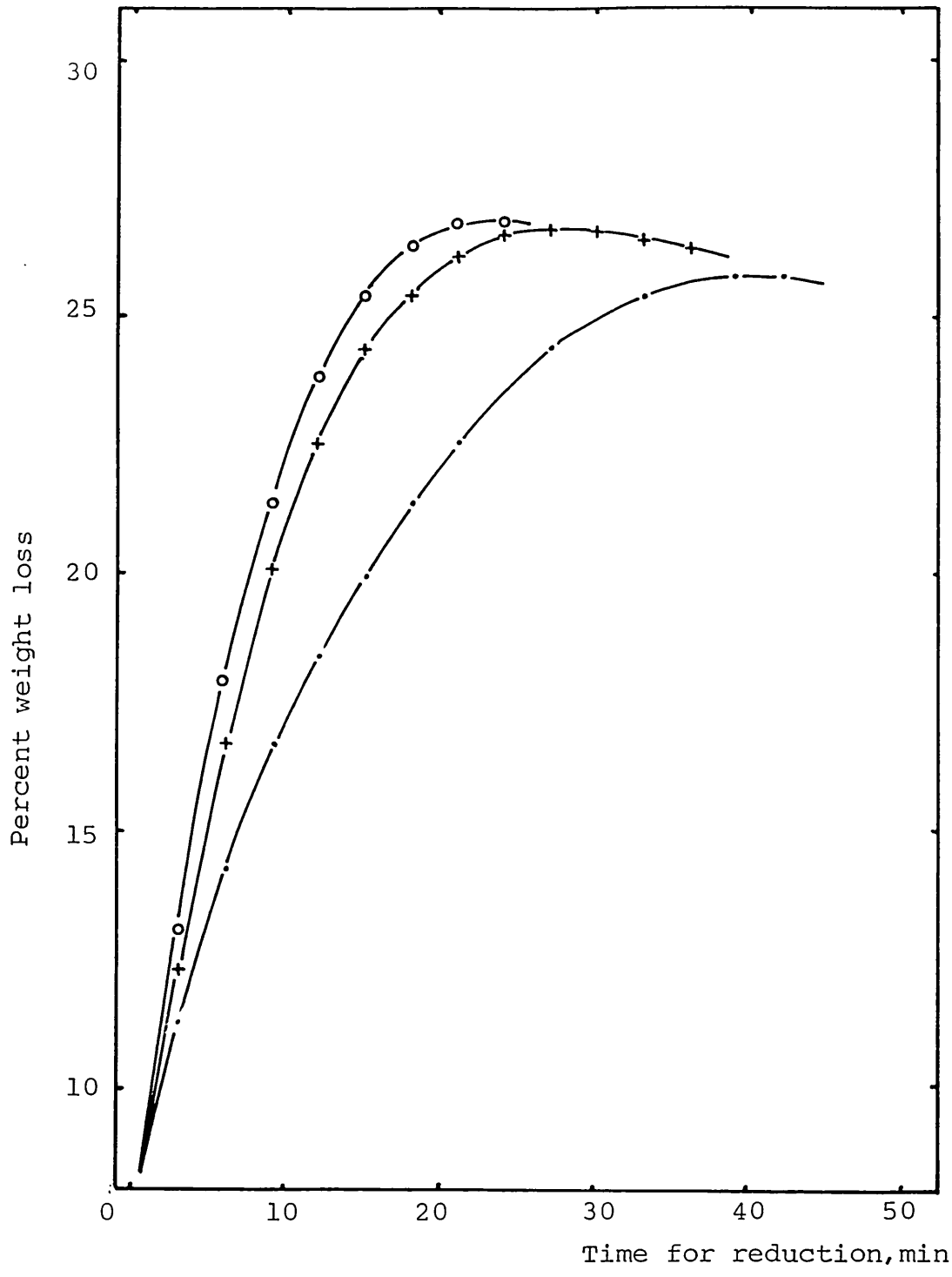

Fig. 4.27- The effect of temperature at 950, 1050 and 1100°C on reduction of wustite compacts pre-reduced at 1100°C with MgO 5% additions.

served in the compacts without additions. This phase was only observed in the sample reduced at (950-1100)·MgO 2%. The α - Quartz phase was observed in the starting material with Magnesioferrite and the intensity decreased by increasing the temperature at which wustite was produced while the α - Cristobalite which seemed to be transformed from α - Quartz gets stronger. The α - Cristobalite was observed in every sample with 2% MgO additions. No relationship with Fayalite magnesian was observed.
The Clinoenstatite, $MgSiO_3$, was also observed in the sample reduced at (1050-1100)·MgO 2% at 98% of reduction.

MgO 5% addition

The phases observed in the starting material (sintered at 1300°C for 24 hours in air) were Hematite, α - Quartz and Magnesioferrite. After reduction at various temperatures, sometimes the hematite was reduced to iron (fully reduced) and wustite and iron (partial reduction). Cementite was also observed in the fully or partially reduced samples and the intensity of cementite reflexions in the XRD got stronger with the degree of reduction (the more reduced, the more cementite present).
Fayalite magnesian, $(Fe,Mg)_2SiO_4$ was identified in the samples reduced at (950-1100), (1050-950) and (1050-1050) and the degree of reduction of each sample was 98%, 93% and 97.8% respectively.
Clinoenstatite, $MgSiO_3$, was observed in every sample (every reduction temperature with the wustite produced at 1100°C) and in the samples reduced at (950-1050) and (1050-1100). The presence of every phase will be mentioned in a later

section and related to the results by EPMA.

4.4.5. MICROSTRUCTURAL CHANGE DURING REDUCTION

Plate 17 shows the photomicrographs of starting materials with MgO additions. The phases in the micrographs mainly divided into two parts, hematite and magnesioferrite. Some of the magnesioferrite grains have planar hematite inside the grains. The XRD results also indicate the presence of magnesioferrite in the starting material. The phase diagram in Fig. 4.28a illustrates the region of formation of magnesioferrite at 1300^{o}C. During cooling, the magnesioferrite (spinel) decomposes into magnesioferrite containing more magnesia and hematite and this hematite phase is precipitated from supersaturated solid solution along the plane (111) as shown in Plate 17.
The amount of magnesioferrite phases increases as the amount of MgO in the compacts increases.
The MgO content in the hematite (or magnesioferrite) grains analysed by EPMA shows that the concentration varies within individual grains from 0 to 6.62% of weight (see Table 4.12).

MgO 1% addition

The microstructural changes after reduction are shown in Plate 18. With low temperature reduction at (1100-950)·MgO 1%, the general shape of the iron grains after reduction (Plate 18a) shows that outer surface of the grains are fractured (Flake like shape) and inside the grains are large pores. However the grains have a thick iron layer (shell) outside and a very porous structure

TABLE 4.8

XRD ANALYSES OF REDUCED SAMPLES OF IRON ORE COMPACTS WITH MgO 1% ADDITION.

REDUCTION PROCEDURE	REDUCTION		PHASES IDENTIFIED
	% Wt.LOSS	TIME, MIN.	
950-950	25.7	60	Fe:VS, W:VW, Q:W, C:VW, CR:MS, M·Fe:VVW
950-1050	27.6	36	Fe:VS, W:VW, Q:W, C:W, CR:MS, M·Fe:VW
950-1100	27.3	25	Fe:VS, Q:W, CR:MS, C:W, M·Fe:VVW
1050-950	26.0	60	Fe:VS, W:VW, Q:W, C:W, CR:MS, M·Fe:VW
1050-1050	27.1	43	Fe:VS, W:VW, Q:W, C:VW, CR:MS, M·Fe:VW
1050-1100	27.4	26	Fe:VS, W:VVW, CR:MS, M·Fe:VVW, C:VVW
1100-950	25.8	60	Fe:VS, CR:MS, M·Fe:W, C:W
1100-1050	26.7	31	Fe:VS, W:VW, Q:M, C:VW, CR:MS, M·Fe:W
1100-1100	27.1	20	Fe:VS, W:VVW, Q:W, CR:MS, M·Fe:VW, C:VW

@ ORDER OF INTENSITY:VS,S,MS,M,MW,W,VW,VVW

Fe : α- Iron

W : Wustite

Q : α- Quartz, SiO_2

CR: α- Cristobalite, SiO_2

C : Cementite, Fe_3C

M·Fe : Magnesio-Ferrite, $MgFe_2O_4$

TABLE 4.9

XRD ANALYSES OF REDUCED SAMPLES OF IRON ORE COMPACTS WITH MgO 2% ADDITIONS.

REDUCTION PROCEDURE	REDUCTION		PHASES IDENTIFIED
	% Wt.LOSS	TIME, MIN.	
950-950	25.8	60	Fe:VS, W:M, Q:M, C:VW, CR:MS, M·Fe:VW
950-1050	27.1	33	Fe:VS, W:VW, Q:M, CR:MS, M·Fe:VW, C:W
950-1100	27.4	24	Fe:VS, C:VVW, CR:MS, M·Fe:VW, FS(Mg):W, Q:M
1050-950	25.7	60	Fe:VS, W:MS, Q:MW, CR:MS, M·Fe:VVW, C:VW
1050-1050	27.0	33	Fe:VS, Q:W, CR:MS, C:VW
1050-1100	27.2	25	Fe:VS, W:VW, Q:MW, C:VW, CR:MS , MS:VVW
1100-950	26.1	60	Fe:VS, W:W, Q:W, CR:MS, C:VW
1100-1050	26.8	29	Fe:VS, W:VVW, Q:W, CR:MS, C:VVW
1100-1100	27.2	21	Fe:VS, Q:W, CR:M, C:VW

@ ORDER OF INTENSITY:VS,S,MS,M,MW,W,VW,VVW

Fe : α- Iron W : Wustite

Q : α- Quartz, SiO_2 CR : α- Cristobalite, SiO_2

M·Fe : Magnesio-ferrite, $MgFe_2O_4$

FS(Mg) : Fayalite magnesian, $(Mg,Fe)_2SiO_4$

MS : Clinoenstatite, $MgSiO_3$

TABLE 4.10

XRD ANALYSES OF REDUCED SAMPLES OF IRON ORE COMPACTS WITH MgO 5% ADDITIONS.

REDUCTION PROCEDURE	REDUCTION		PHASES IDENTIFIED
	% Wt.LOSS	TIME, MIN.	
950-950	26.4	36	Fe:VS, Q:W, CR:MS, W:VW, C:VVW
950-1050	27.2	27	Fe:VS, Q:M, CR:MS, C:VW, MS:VW
950-1100	27.5	24	Fe:VS, Q:M, CR:MS, C:MW, FS(Mg):VVW
1050-950	26.0	36	Fe:VS, W:W, Q:MW, CR:MS, C:W, FS(Mg):VVW
1050-1050	27.2	28	Fe:VS, Q:M, CR:MS, C:W, FS(Mg):VVW
1050-1100	27.4	27	Fe:VS, Q:MW, CR:MS, C:W, MS:VW
1100-950	26.0	43	Fe:VS, W:W, Q:MW, C:W, CR:MS, MS:VVW
1100-1050	26.9	27	Fe:VS, W:VVW, Q:VW, C:W, CR:MS, MS:VVW
1100-1100	27.0	24	Fe:VS, Q:W, CR:MS, C:W, MS:VVW

@ ORDER OF INTENSITY:VS,S,MS,M,MW,W,VW,VVW

Fe: - Iron

W : Wustite

Q : - Quartz, SiO_2

CR: - Cristobalite, SiO_2

M·S: Clinoenstatite, $MgSiO_3$

FS(Mg): Fayalite magnesian, $(Mg,Fe)_2SiO_4$

C : Cementite, Fe_3C

inside the iron shell.

Simple comparison between various grains shows that the thickness of the iron shell (4 μm) is similar. This phenomenon indicates that the porous inner grains was directly related with the unreduced wustite surrounded by a thick iron layer (see Plate 18c).

MgO 2% addition

Plate 19 shows the microstructure of iron reduced at 1050^{o}C with the wustite produced at various temperatures and the overall shape illustrates the temperature of wustite formation was not important. The kinetic analysis mentioned in the last section indicates that both these sets of observations are in agreement (see Fig. 4.22-24).

EPMA results in Plate 20,21 and Table 4.11 show that the distribution of MgO in the iron structure after reduction. The grains in Plate 20a have three different types of iron structure, iron grains that have a porous structure inside (1,2,5), partially reduced wustite covered with a thick iron shell(3) and plain iron grains (4,6). Another phase shown as No. 7 mainly consists of a silica particle which has reacted with FeO and CaO in the sample. Plate 20b also shows grains which contain both these features (porous structure and unreduced wustite).

The EPMA results shown in Table 4.11 reveal that the MgO distribution in the grains differs from one to another. However the concentration of MgO does not vary within any grains even if they have different types of structure (Plate 20b). The left side of this grains illustrates the progress of the reduction. After forming a thick iron

KEY TO PLATE 17-21

PLATE 17 showing the precipitation of hematite from the magnesioferrite grains during cooling and the amount of magnesioferrite increases with increasing amount of MgO.

PLATE 18
PLATE 19 showing microporous structure surrounded by thick iron shell.
The thickness of iron shell shows the same in picture c (comparison between fully reduced grain and partially reduced grain)

PLATE 21 showing MgO distribution in the iron structure and the MgO mainly concentrates in the microporous structure.

PLATE 17

Micro-structure of hematite grains of iron ore compacts with a) 1% MgO , b) 2% MgO and c) 5% MgO addition, sintered at 1300°C for 24 hours in air.

a)

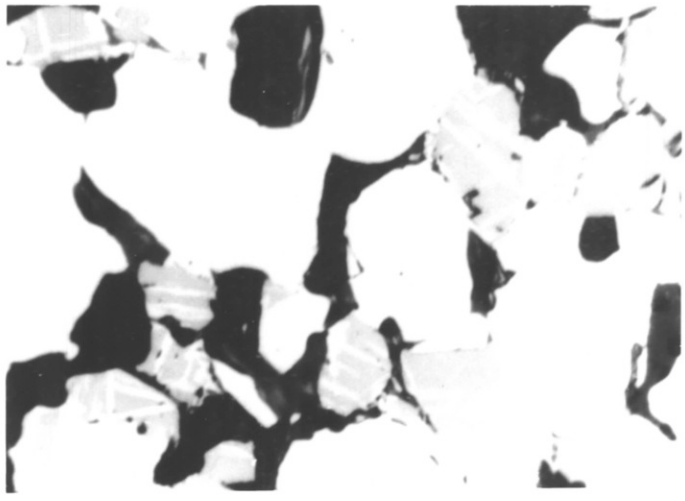

white : hematite
grey : magnesio-ferrite
black : voids

x 320

b)

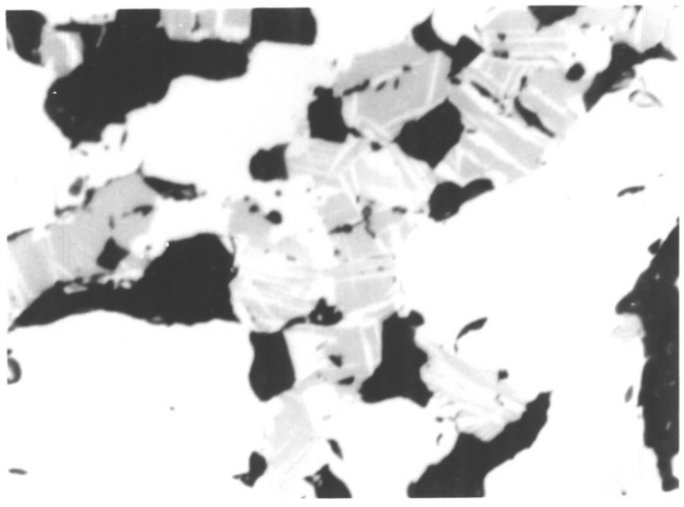

white : hematite
grey : magnesio-ferrite
black : voids

x 320

c)

white : hematite
grey : magnesio-ferrite
black : voids

x 320

layer around the grain, the micropores develop during reduction of the remaining wustite.

Other results by EPMA are shown in Plate 20c and Table 4.11. Analysis of each individual grain, both the iron layer and remaining wustite (or microporous structure), indicates that the MgO concentration is quite distinctive. The analysed group in Plate 20c, 1,2,3,(4,5), (6,7,8) shows the MgO concentration in the unreduced wustite or microporous structure and once again in Plate 21.

MgO 5% addition

Continuous photomicrographs through the specimen were taken from the MgO 5% additions, with 25%, 50% and 75% of reduction respectively. Plate 22a shows the microstructure of iron reduced to 25% and it shows that iron forms on almost every grains throughout the sample. EPMA results illustrate that there is no liquid phase to bind each individual iron oxide grains except a small amount of silicate identified by XRD (Fayalite magnesian, Clinoenstatite). These observations indicate that the influence of any silicate phase on the overall reduction rate is small and the reducing gas can penetrate through the specimen. However, the gradual increase of iron phase in grains near the surface of the specimen was observed with increasing reduction time (Plate 22b,c) and the formation of a thick iron layer was found between the interfaces of reduced iron and unreduced wustite phase.

The microstructures of samples produced at various temperatures are shown in Plate 23. The thickness of the iron shell formed during reduction is 4-4.5 μm and this is the

PLATE 18

Micro-structure of iron reduced at a) (1100-950)·MgO 1% , b) (1100-1050)·MgO 1% and c) (1100-1100)·MgO 1% .

a)

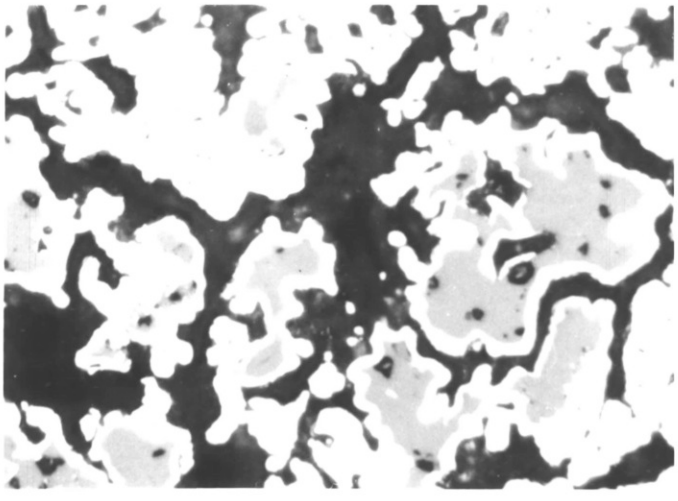

white : iron
light grey : wustite (or magnesio-wustite)
dark grey : α- Quartz
black : voids

x 320

b)

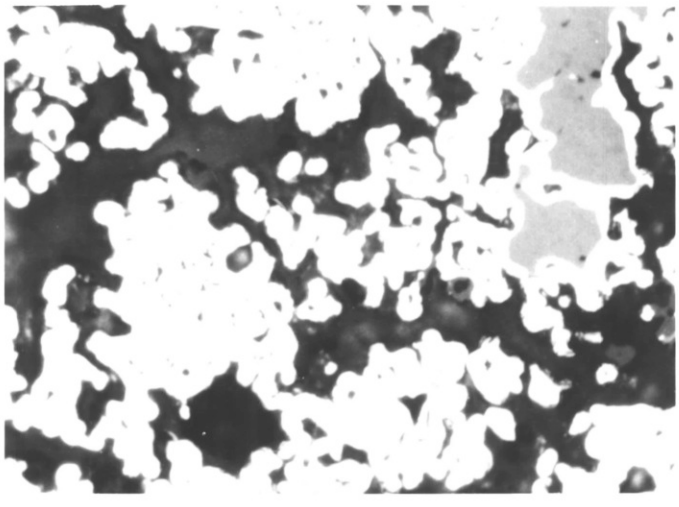

white : iron
light grey : wustite (or magnesio-wustite)
dark grey : α- Quartz
black : voids

x 320

c)

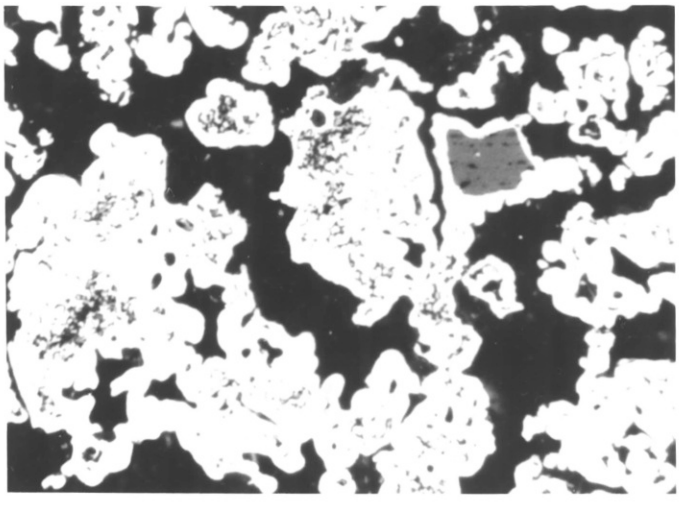

white : iron
light grey : wustite (or magnesio-wustite)
dark grey : α- Quartz
black : voids

x 320

PLATE 19

Micro-structure of iron reduced at a) (950-1050)·MgO 2% , b) (1050-1050)·MgO 2% and c) (1100-1050)·MgO 2% .

a)

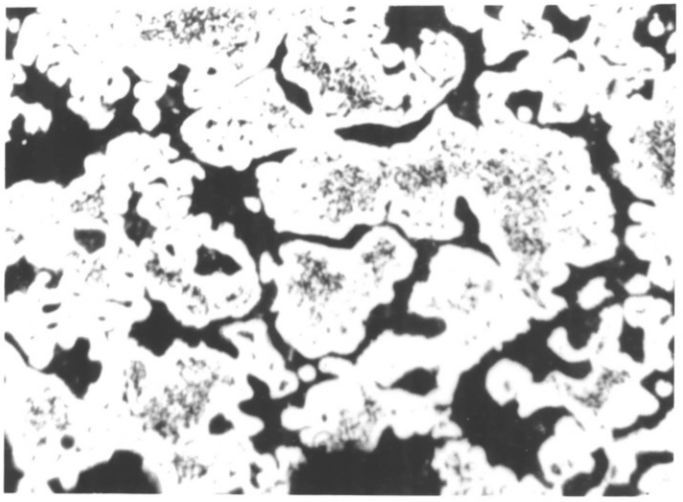

white : iron
black : voids

x 320

b)

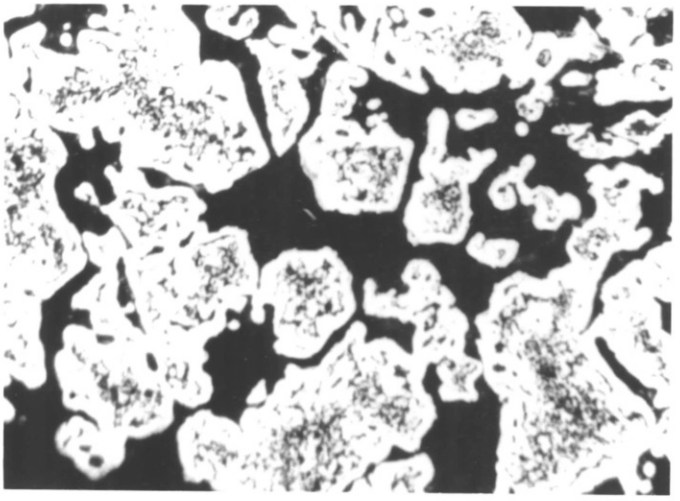

white : iron
dark grey : α- Quartz
black : voids

x 320

c)

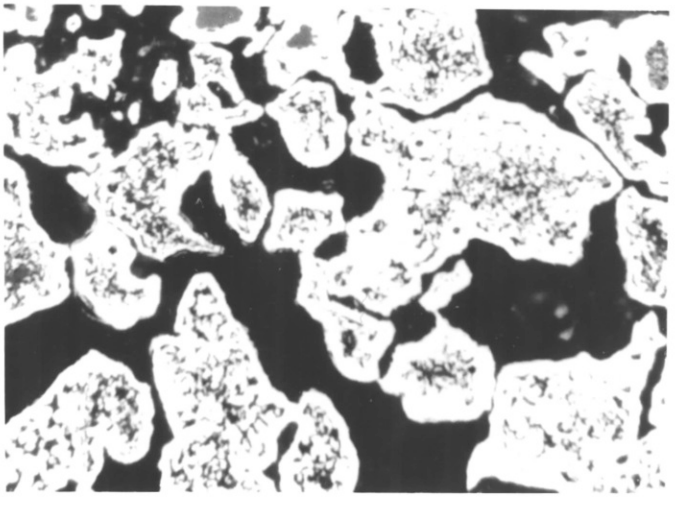

white : iron
light grey : wustite (or magnesio wustite)
dark grey : α- Quartz
black : voids

x 320

TABLE 4.11 EPMA RESULTS

NO.	COMPOSITION (Wt.%)						REMARKS
	Fe	FeO	CaO	SiO_2	MgO	MnO	
1	92.95	0	0.08	0.50	3.92	2.56	PLATE 20 a)
2	97.10	0	0	0.79	1.57	0.53	"
3	0	76.03	1.75	18.64	3.32	0.27	"
4	90.98	0	0.16	5.58	2.91	0.37	"
5	93.30	0	0	0.64	5.09	0.96	"
6	0	70.97	1.39	20.55	5.56	1.54	"
7	0	6.47	2.40	90.67	0.46	0	"
8	0	91.86	0	0.41	4.70	3.03	PLATE 20 b)
9	94.28	0	0	0.75	4.39	0.58	"
1	81.59	0	0	0.51	15.56	2.34	PLATE 20 c)
2	81.17	0	0.02	0.49	15.90	2.42	"
3	0	74.38	0.25	1.51	22.75	1.12	"
4	0	80.03	0	0.63	15.69	3.65	"
5	90.00	0	0.87	3.71	5.01	0.41	"
6	92.05	0	0.17	3.50	3.68	0.60	"
7	0	77.26	0	0.90	17.64	4.20	"
8	94.61	0	0	1.65	3.11	0.64	"
9	99.40	0	0.10	0.38	0.12	0	PLATE 21 I)
10	75.87	0	0.14	0.82	16.00	7.18	"
11	95.19	0	0.08	0.42	1.28	3.03	"
12	94.89	0	0	0.34	2.77	2.00	"
13	99.72	0	0	0.28	0	0	"
14	99.26	0	0.03	0.46	0	0.25	"
15	93.61	0	0.06	0.33	3.48	2.53	"
16	85.57	0	0.27	0.19	10.60	3.36	PLATE 21 II)
17	72.06	0	0.08	0.55	25.33	1.99	"
18	95.38	0	0.01	0.58	3.23	0.79	"
19	97.31	0	0.15	0.24	1.61	0.69	"
20	98.91	0	0.05	0.39	0.37	0.28	"

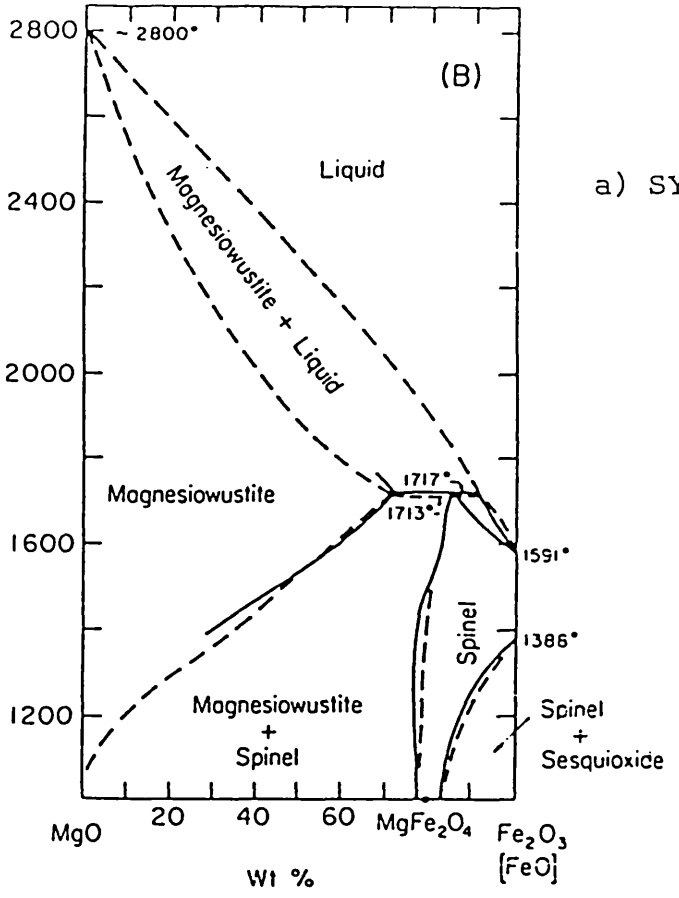

a) SYSTEM $MgO-Fe_2O_3$
IN AIR

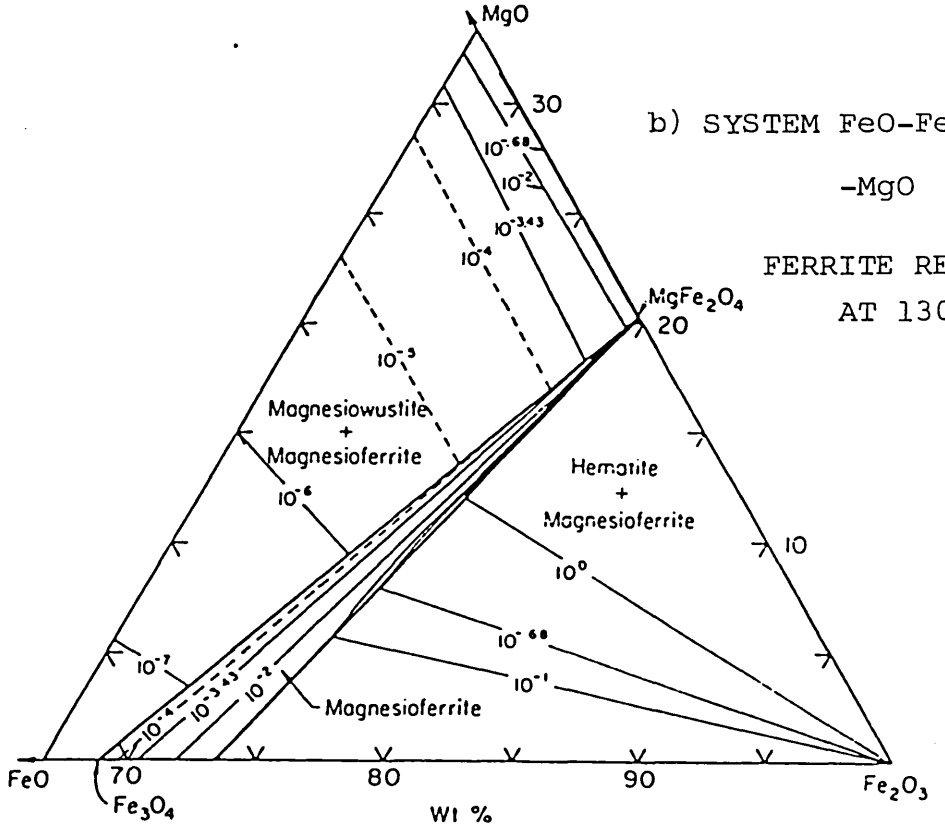

b) SYSTEM $FeO-Fe_2O_3$
$-MgO$

FERRITE REGION
AT 1300°C.

Fig. 4.28 System iron oxide-MgO (64)

same in every samples, see Plate 23. The MgO distribution also shows the same variation about the mean concentration as the results with 1 and 2% of MgO addition (see Plate 25,26) and the MgO level in the middle of the reduced iron grains (microporous structure) is higher than for 1 and 2% MgO additions.

4.4.6. DISCUSSION

The effect of MgO addition on the reduction behaviour was examined in a variety of ways. The present study has shown that the kinetics of reduction, the growth pattern of the iron as the result of fully or partially reduced condition and the behaviour of MgO as additives are complex. Moreover, the reduction rate was also affected by the type of wustite.

Reduction rate

The reduction rate was influenced by several factors such as the reduction temperature, the type of wustite (i.e. the temperature used to produce wustite from hematite) and the amount of MgO addition.

As expected, the reduction rate increased by increasing reduction temperature. The reduction mechanism in this period was determined to be controlled by pore diffusion using a kinetic analysis similar to that developed by Ross (7) and the final stage of reduction seems to be related to the formation of a thick iron layer on wustite grains. The reduction rate was also influenced by the type of wustite. The observed effect of decreasing the reduction rate by increasing the temperature at which wustite was produced may

PLATE 20

Micro-structure(SEM) of iron reduced at a),b) (1100-950)·MgO 2% and c) (1100-1050)·MgO 2% .

The numbers show the points or areas of the analysis.

a)

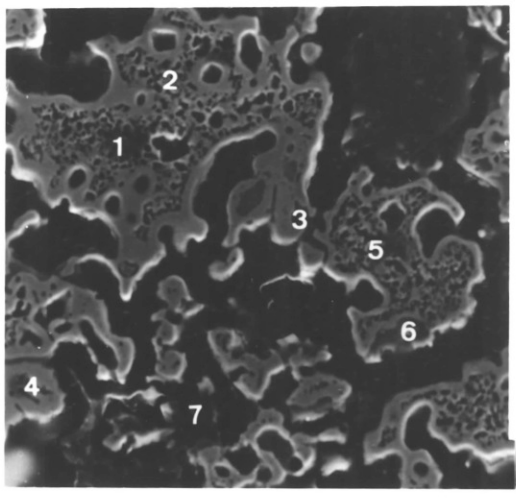

iron : 1,2,4,5

wustite : 3,6

α- Quartz : 7

b)

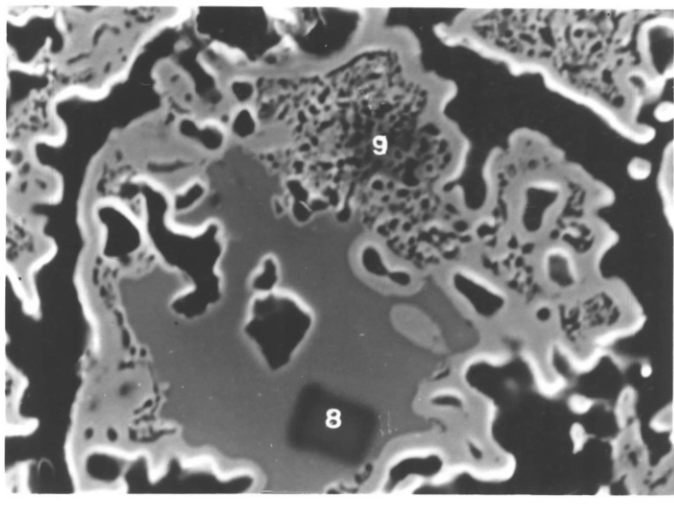

wustite (magnesio-wustite) : 8

iron (micro-pores inside the iron) : 9

c)

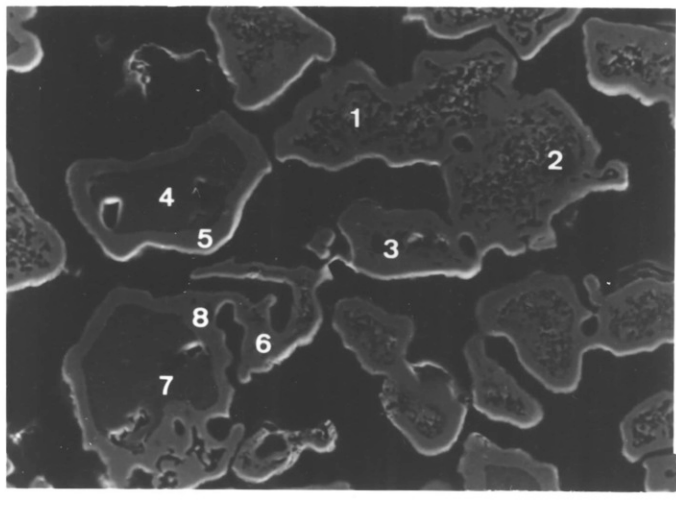

iron : 1,2,5,6,8

wustite (magnesio-wustite) : 3,4,7

PLATE 21

Digital X-ray mapping of iron reduced at I) (1100-1050)· MgO 2% and II) (1100-1100)·MgO 2% . Digital X-ray mapping displays of I), II) for b)iron , c)silicon and d)magnesium .

I)

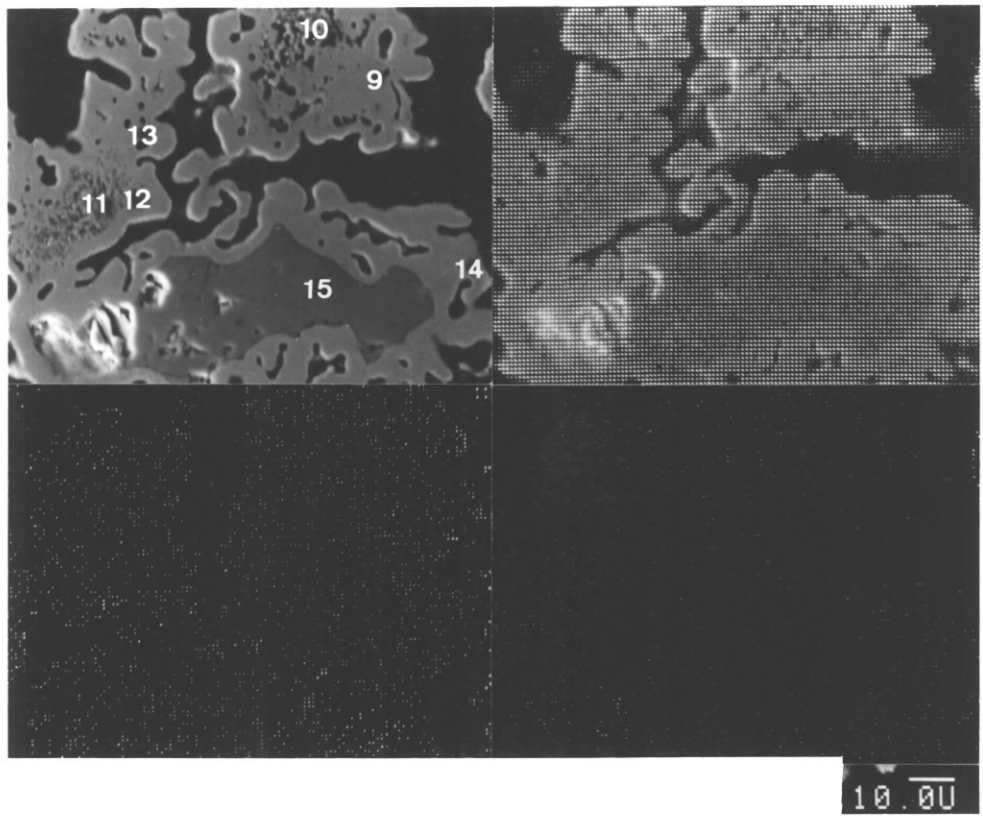

a) b) c) d)

II)

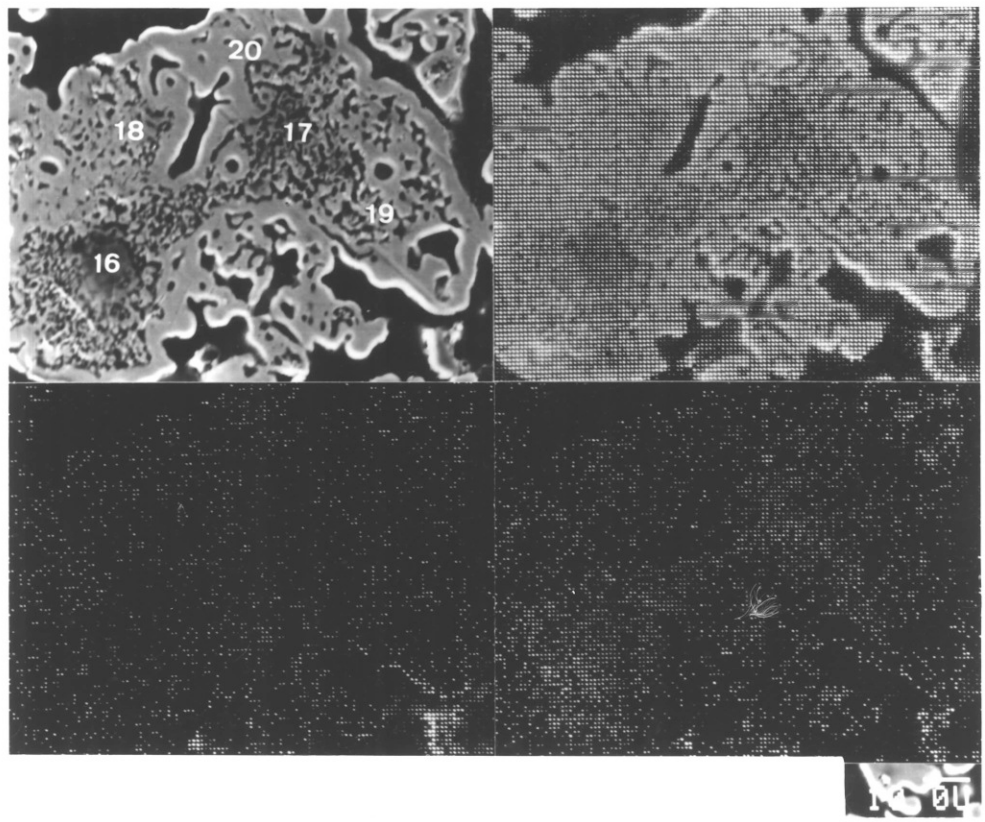

a) b) c) d)

be related to the formation of Iron magnesium silicate (Fayalite magnesian) and Magnesium silicate (Clinoenstatite). The formation of fayalite was discussed in the previous section, however, the formation of fayalite magnesian must be related to the magnesia - silica ratio in the pellets. Since the two phases are similar, e.g. they are both orthorhombic, the formation of fayalite magnesian must be similar to that of fayalite. Using this assumption, the wustite produced at higher temperatures can react more easily with silica in the presence of MgO and forms fayalite magnesian. This fayalite magnesian forms from the surface of wustite grains (Plate 26 I c) and may prevent the access of the reducing gas to the wustite grains. However this effect is less when the reduction temperature from wustite to iron becomes higher. Since it takes 1 hour (from 950^{o}C to 1100^{o}C) and 35 minutes (from 950^{o}C to 1050^{o}C) to change the temperature, fayalite (fayalite magnesian) can be formed more easily during the longer period.

The amount of MgO addition changes the reduction rate such that the higher the concentration, the greater the higher reduction rate. This is more noticeable when 5% of MgO was added and weight gains due to carbon deposition also occurred at an early time.

The carbon deposited by decomposition of carbon monoxide occurs even during reduction. The carbon diffuses into the iron shell and decomposes into cementite and ferrite during cooling. The deposition of carbon on the surface of iron grains seems to be promoted by the presence of MgO. As the presence of cementite was identified in all samples by XRD,

confirming the deposition of carbon.

The behaviour of MgO in the iron grains was rather peculiar. It is shown in Fig. 4.28 that wustite can take unlimited amounts of MgO into solid solutition. When MgO containing compacts were sintered in air, the MgO reacts with hematite and forms magnesioferrite with 6.6% of MgO in the grains. During reduction, magnesiowustite (reduced from magnesioferrite) was reduced to iron and the MgO in this phase was rejected from the iron, as MgO is not soluble in iron. The reduction proceeded from the surface. So the direction of movement of the rejected MgO is the same as the direction of growth of iron layer. The results shown by EPMA also revels that the concentration of MgO increases with reduction time, while virtually no MgO was detected in the iron layer.

4.5. IRON ORE COMPACT WITH DOLOMITE ADDITION

Two types of dolomite were added to the compacts as flux material. Recently several trials were attempted to improve the high temperature characteristics of sinter pellets for the commercial Blast Furnace Operation and reported (77-80) that they could partly control the softening-melting temperature by adding dolomite or serpentine as an MgO source.

However there are doubts about the change of reduction rate before reaching the softening-melting temperature (1150-1300^{o}C). The present investigation of compacts with two different types of dolomite (Thrislington dolomite and Whitewell dolomite) was carried out to study the effect on reduction rate, morphology and the phases present by optical

PLATE 22

Continuous photo-micrographs of iron ore compacts with MgO 5% addition reduced at (1100-1100)·MgO 5%, showing a)25% of reduction, b)50%of reduction and c)75% of reduction proceeded respectively. White(iron), light grey(wustite) dark grey(α-Quartz) and black(voids). x 57

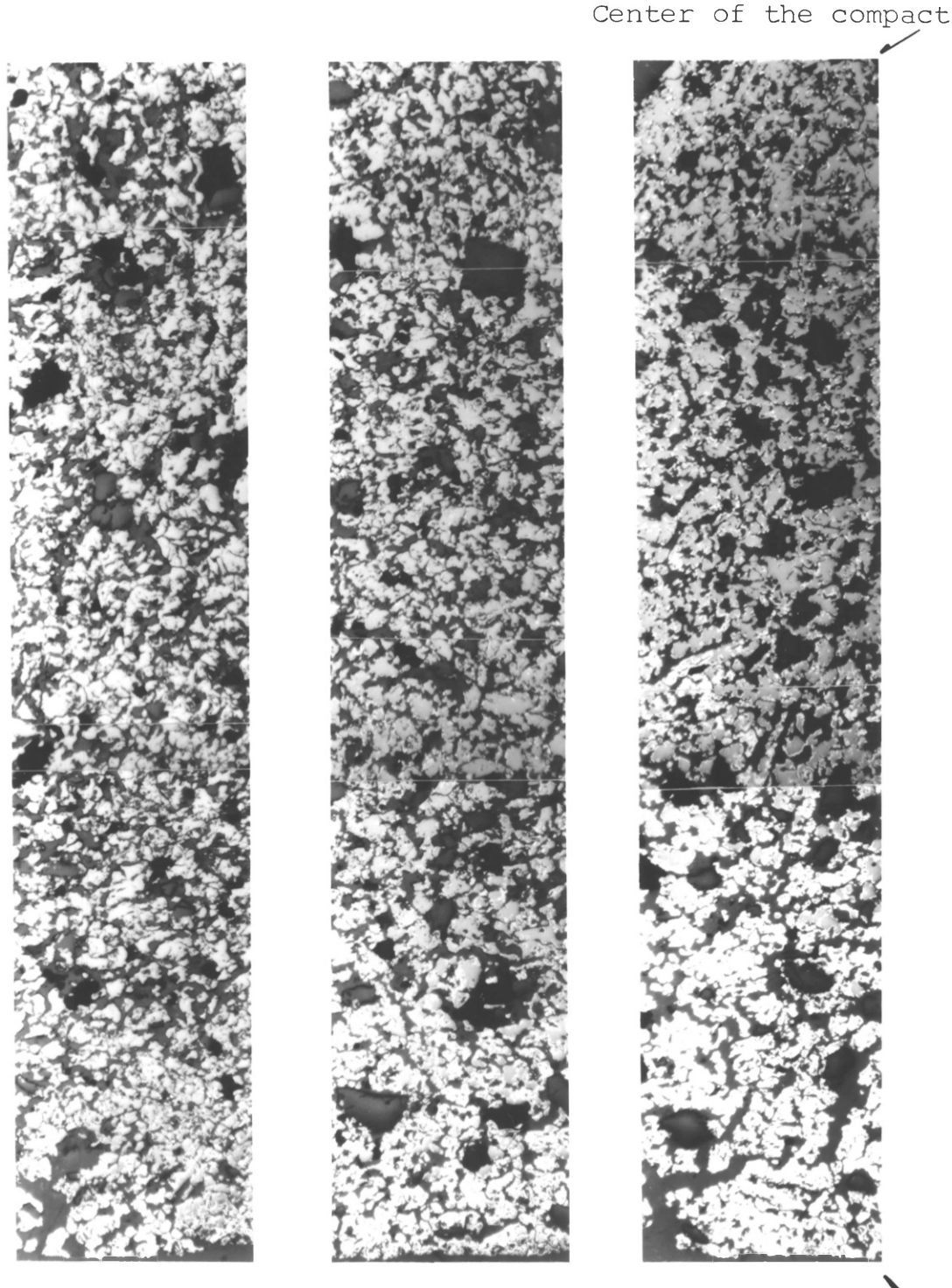

PLATE 23

Micro-structure of iron reduced at a) (1100-950)·MgO 5% , b) (1100-1050)·MgO 5% and c) (1100-1100)·MgO 5% .

a)

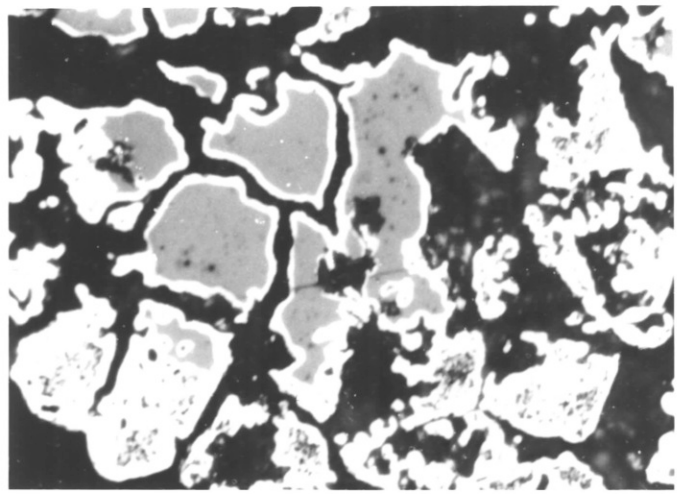

white : iron
light grey : wustite (or magnesio-wustite)
dark grey : α- Quartz
black : voids

x 320

b)

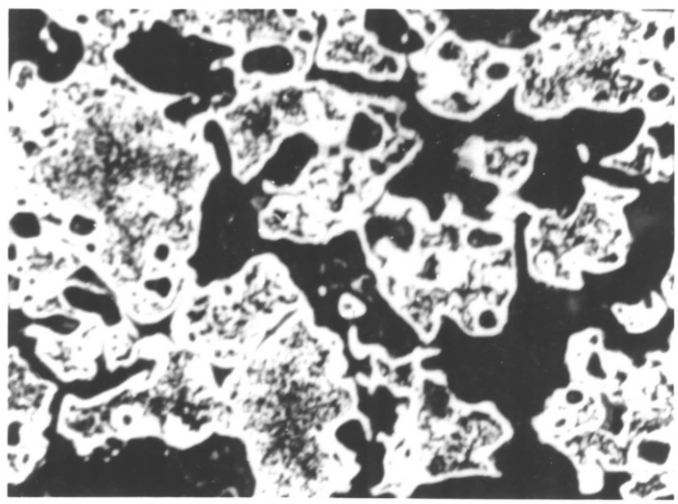

white : iron
dark grey α- Quartz
black : voids

x 320

c)

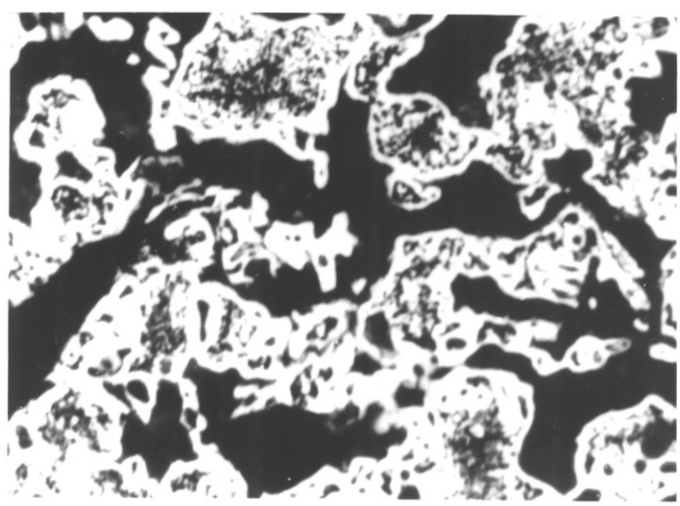

white : iron
dark grey : α- Quartz
black : voids

x 320

TABLE 4.12 EPMA RESULTS

NO	COMPOSITION (Wt.%)						REMARKS
	Fe_2O_3	FeO	CaO	SiO_2	MgO	MnO	
1	98.82	0	0.02	0.54	0.44	0.17	PLATE 24 I)
2	94.66	0	0.11	2.12	2.57	0.54	"
3	96.33	0	0.29	0.70	1.92	0.76	"
4	98.13	0	0.08	0.93	0.02	0.84	"
5	97.52	0	0.06	1.28	1.11	0.03	"
6	96.08	0	0.41	2.80	0.71	0	"
7	99.37	0	0.05	0.19	0.29	0.09	"
8	91.52	0	0.15	0.99	6.62	0.72	"
9	94.09	0	0.12	1.87	3.42	0.49	"
	Fe	FeO	CaO	SiO_2	MgO	MnO	
1	0	1.07	0	98.75	0.11	0.07	PLATE 25 I)
2	72.85	14.74	0.01	12.33	0	0.07	"
3	0	5.89	1.54	91.95	0.42	0.20	"
4	96.21	0	0.07	0.68	2.35	0.70	"
5	98.71	0	0.14	0.55	0.46	0.14	"
6	98.43	0	0.02	1.26	0.29	0	"
7	78.09	0	4.31	0.63	19.78	1.46	PLATE 26 I)
8	72.35	0	0	0.30	25.31	2.04	"
9	94.14	0	0.1	0.47	4.89	0.40	"
10	94.07	0	0.0	0.64	4.79	0.51	"
11	94.53	0	0.03	0.27	4.92	0.25	"
12	98.66	0	0.07	0.32	0.63	0.31	"
13	0	4.07	0.68	94.93	0.31	1.41	"
14	70.54	0	0.01	0.07	25.14	4.23	PLATE 26 II)
15	60.98	0	0.07	0.29	31.82	6.84	"
16	92.83	0	0.02	0.34	5.60	1.21	"
17	98.69	0	0.15	0.88	0.18	0.10	"

PLATE 24

Micro-structure(SEM) of hematite grains compacted with 5% MgO addition and sintered at 1300°C for 24 hours in air , showing I)a)fractured and II) a) polished surface.

Digital X-ray mapping displays of I)and II) for b)iron , c)silicon and d)magnesium.

I)

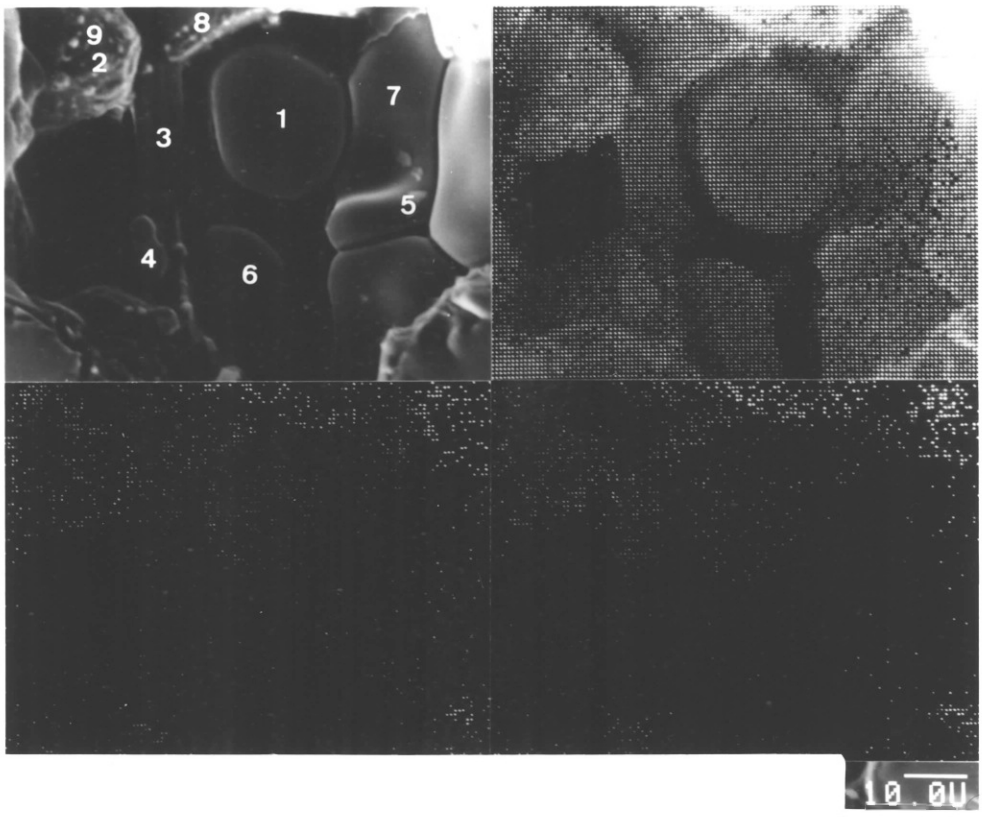

a) b) c) d)

II)

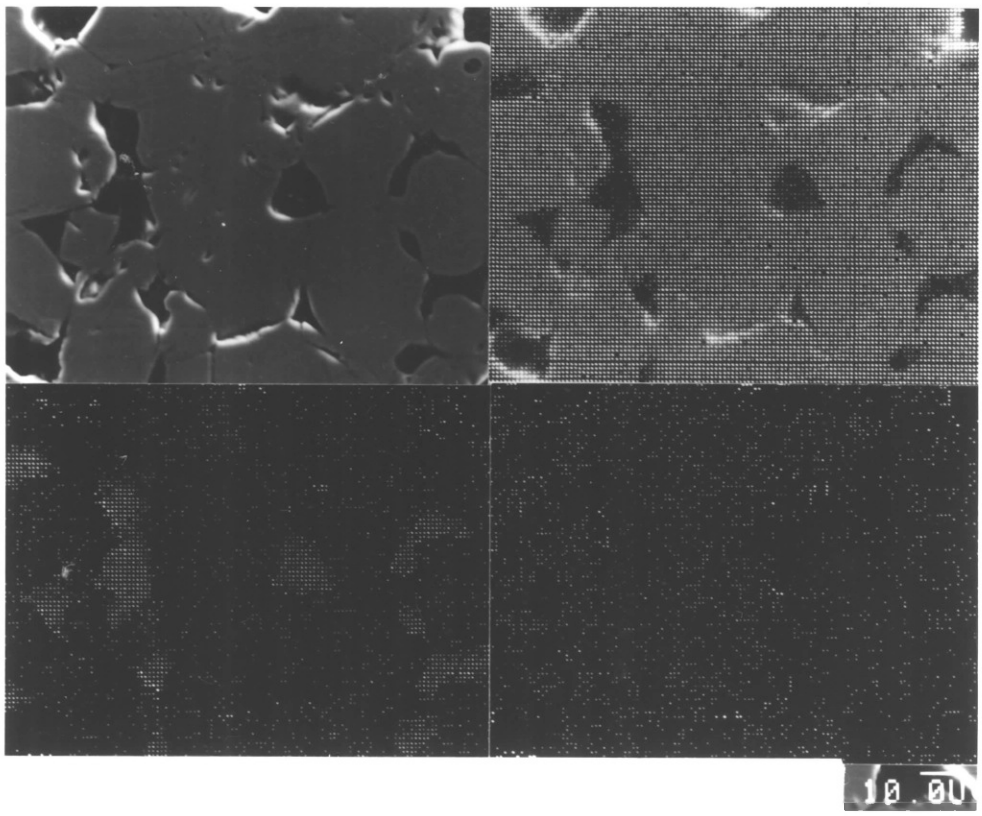

a) b) c) d)

PLATE 25

Micro-structure(SEM) of iron reduced at I,II) a) (1100-950)· MgO 5%. The numbers show the analysed points. Digital X-ray mapping displays of I)and II) for b)iron, c)silicon and d)magnesium.

I)

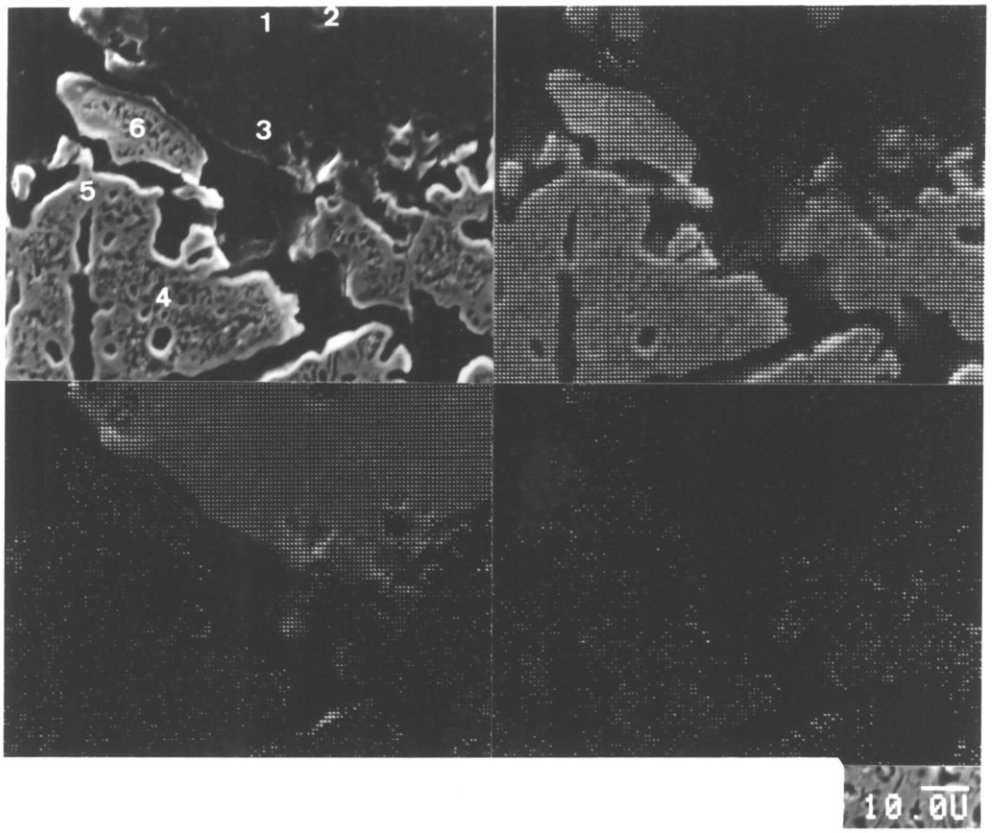

a) b)

c) d)

II)

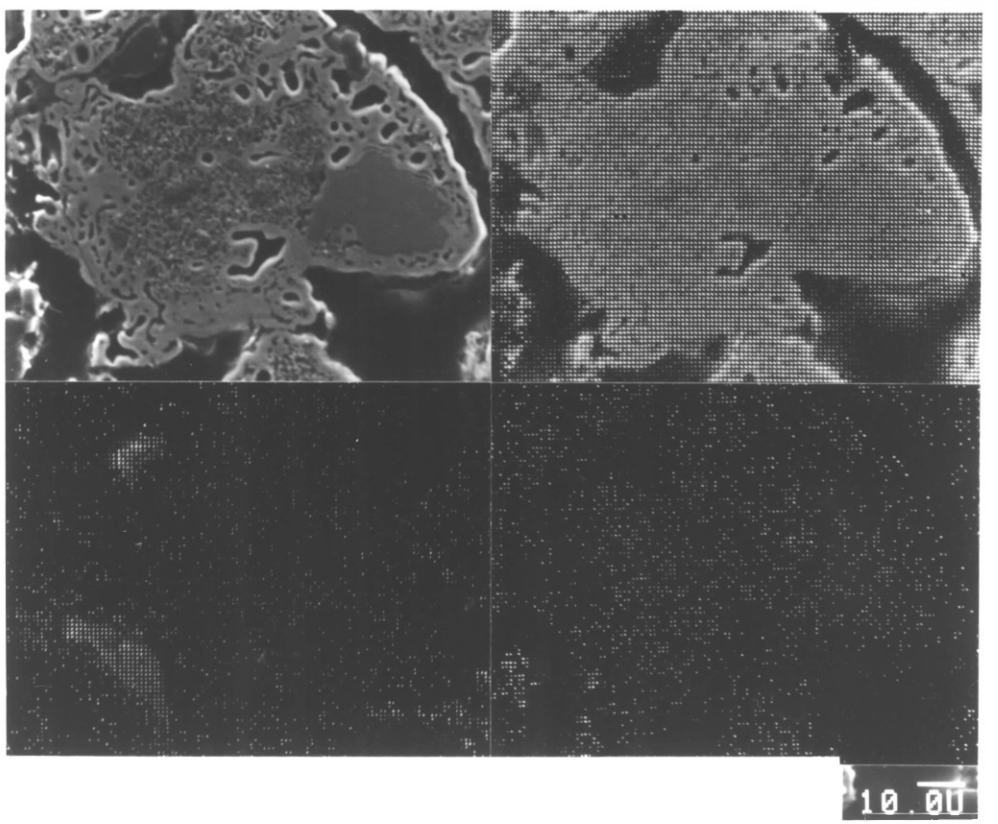

a) b)

c) d)

PLATE 26

Micro-structure(SEM) of iron reduced at I)a) (1100-1050)·MgO 5% and II)a) (1100-1100)·MgO 5% .
Digital X-ray mapping displays of I) and II) for b)iron , c)silicon and d)magnesium.

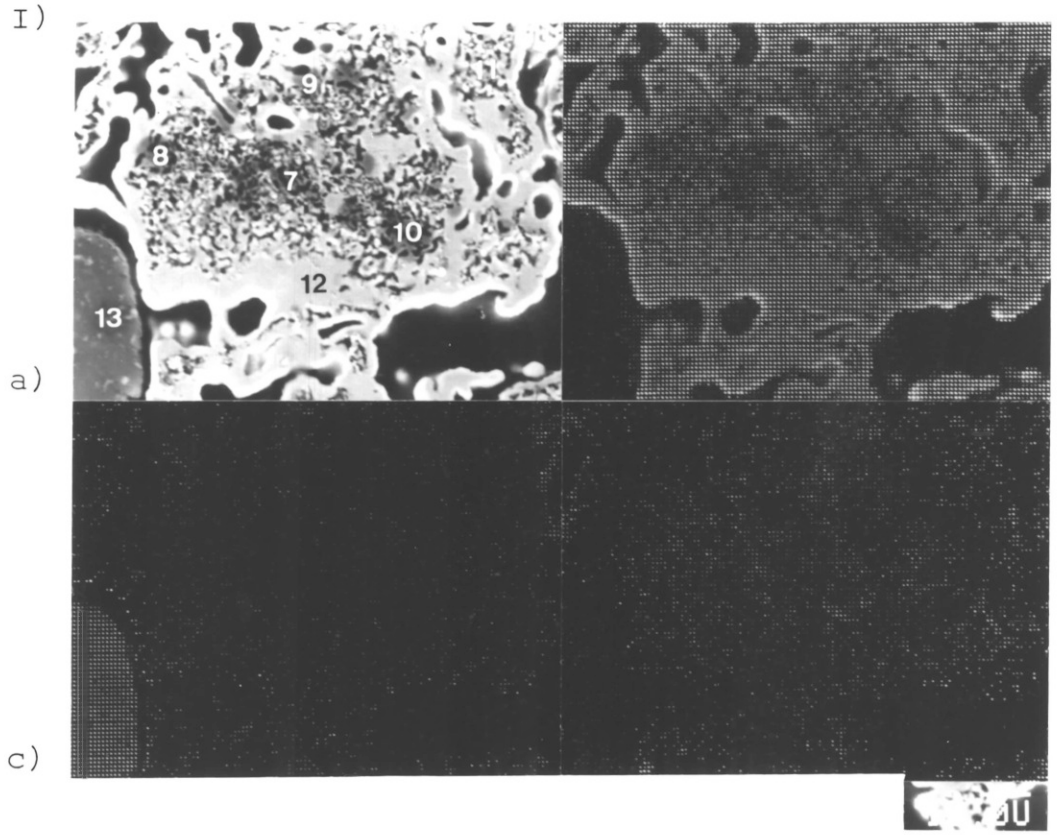

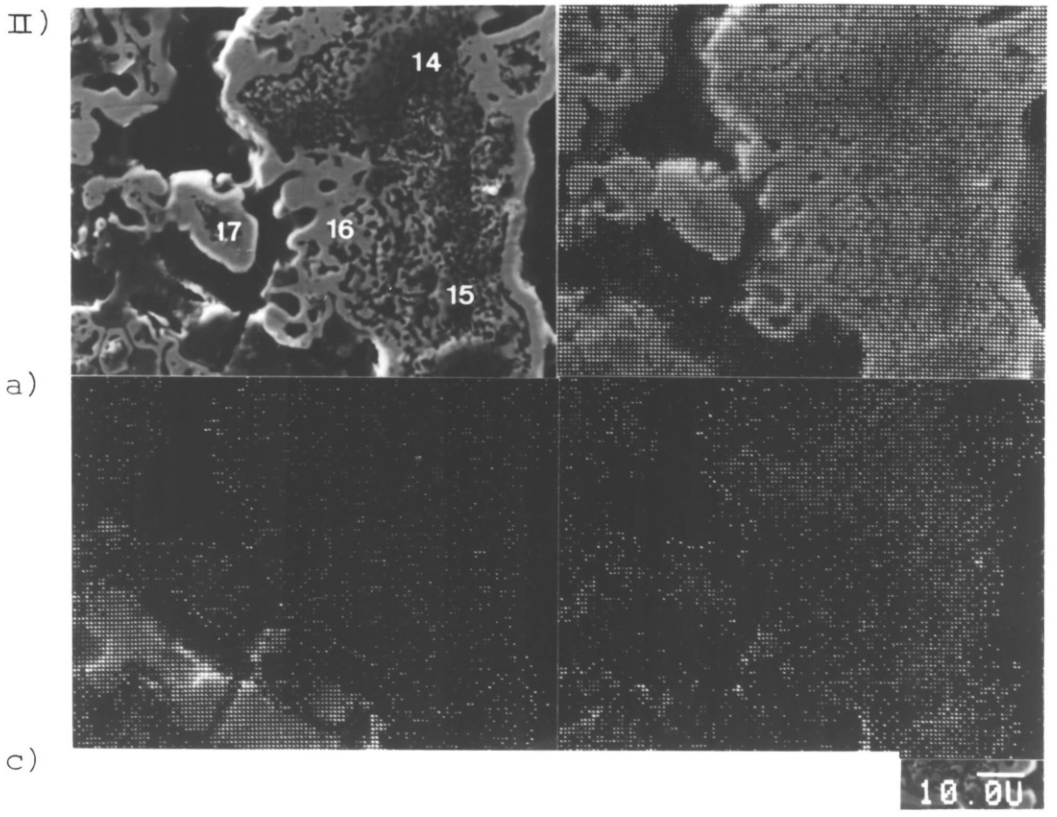

microscopy, EPMA, XRD and porosity by the BET technique. The preparation of the compacts was similar to that used with CaO and MgO additions. The notation is changed slightly to note the raw material source, i.e. , (950 -950)· T.Do 1% or W.Do 1%.

4.5.1. EFFECT OF TEMPERATURE

Thrislington dolomite

The effect of temperature on the rate of reduction was studied by comparing the results between dolomite fluxed compacts and MgO 0.5% CaO 0.5% mixed compacts in the case of 1% dolomite additions. The results are shown in Fig. 4.29-31 (1% dolomite addition), Fig. 4.32-34 (2% dolomite addition) and Fig. 4.35-37 (5% dolomite addition). At the beginning of reduction until 6 minutes at (950-1050)·T.Do 1% and (950-1100)·T.Do 1%, the reduction rates are linear but vary with reduction temperature. However at (950-1100)·T.Do 1%, the reduction rate shows no departure from linearity until 95% of reduction is achieved while at (950-1050)·T.Do 1%, a gradual decrease in reduction rate is observed until 89% reduction when no further reduction occurred. At (950-950)·T.Do 1%, the reduction rate is much slower and after 20 minutes an even slower reduction regime seems to be in operation. At (950-1100)·(0.5% CaO + 0.5% MgO) shows a similar linear initial rate of reduction to (Thrislington dolomite 1%) but probably slightly faster. Similar effects are shown in Fig. 4.29 for reduction at (1050-1050)·T.Do 1% and (1050-1100)·T.Do 1% but the reduction rates are slightly slower and at (1050-1050)·T.Do 1% the initial fast rate

proceeds for a longer time. Whereas the low temperature reduction (1050-950)·T.Do 1% showed a slower rate, the variation of weight loss with time was virtually linear. At each temperature, the reduction rate of wustite, which was produced at high temperature (1100°C) , was observed to be lower at all temperatures and will be described in a later section.

With the addition of 2% Thrislington dolomite to the compacts, the variation of the rate of reduction with conditions of preparation of the wustite and of reduction are very similar. In addition at each temperature of reduction to iron, the rates were observed to be slightly faster than those observed with the lower dolomite additions. At lower temperatures of reduction (950°C), a minimum rate of reduction (see Fig. 4.32-34) is observed.

With 5% Thrislington dolomite addition compacts, the reduction rates are shown in Fig. 4.35-37 and these illustrate that the reduction temperatures both from hematite to wustite and from wustite to iron influence the overall reaction rate. In the reduction at (950-950)·T.Do 5%, two different sintering temperatures were applied to understand the effect of liquid phase formation during the presintering treatment.

The reduction rate with the compacts sintered at low temperature (i.e. 1000°C, 24 hours in air) show that a remarkable increase in reduction rate is achieved such that it is faster than any other compacts reduced at the same temperature. However other compacts which were sintered using normal conditions i.e. 1300°C, 24 hours in air show a far slower reduction rate. Sintering time also affects the

reduction in a similar manner to temperature. The reduction of compacts which were sintered at 1300°C for 90 hours in air occurs at a slower rate at every temperature (see Fig. 4.37, broken line).

Whitewell dolomite

The reduction rates at various temperatures with Whitewell dolomite additions are shown in Fig. 4.38-46 and the rates of reduction were slightly higher than the rates observed with Thrislington dolomite under similar conditions. However the reduction rate at low temperature with 1% Whitewell dolomite addition became the same as the equivalent Thrislington dolomite addition after 15 minutes. For high temperature reduction at (950-1100)·W.Do 1% and (950-1050)·W.Do 1%, similar reduction rate are observed, but a difference of reduction rate is noticed at (1050-1050)·W.Do 1% and (1050-1100)·W.Do 1%. These observations are considered to be related similar to liquid phase formation during reduction of hematite to wustite.
A more profound difference was observed with higher temperature reduction and the difference between the reduction at (1100-1050)·W.Do 1% and (1100-1100)·W.Do 1% becoming greater (see Fig. 4.40).
The reduction behaviour changed when compacts contained more than 2% of Whitewell dolomite where reduction rate depended on the amount of recrystallized magnesioferrite produced from the liquid phase. More details will be described in the sequence of reduction section. In Fig. 4.41, for high temperature reduction (1050°C and 1100°C), the reduction rates are similar. However at lower temper-

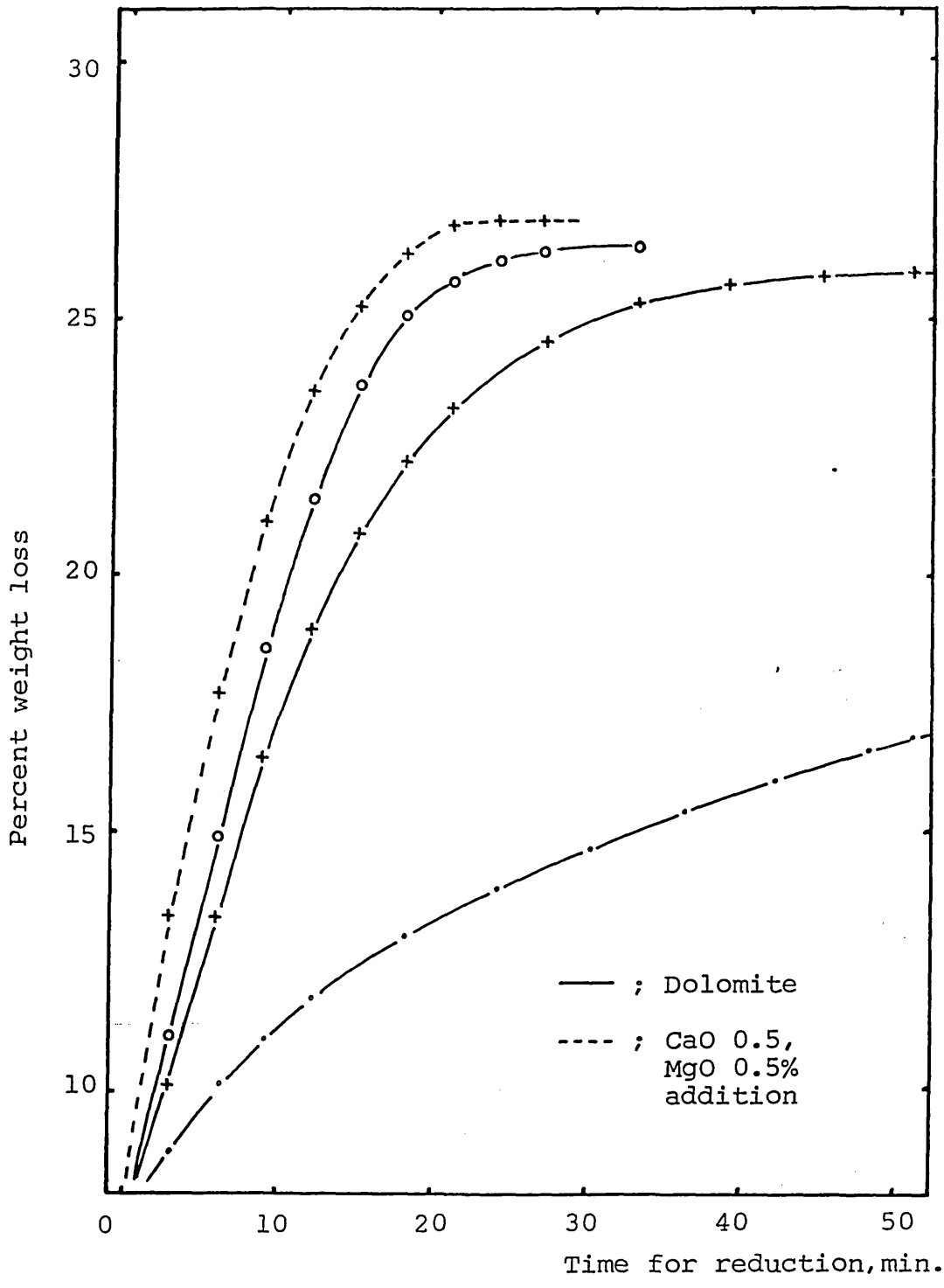

Fig. 4.29- The effect of temperature at 950, 1050 and 1100°C on reduction of wustite compacts pre-reduced at 950°C with Thrislington dolomite 1% additions.

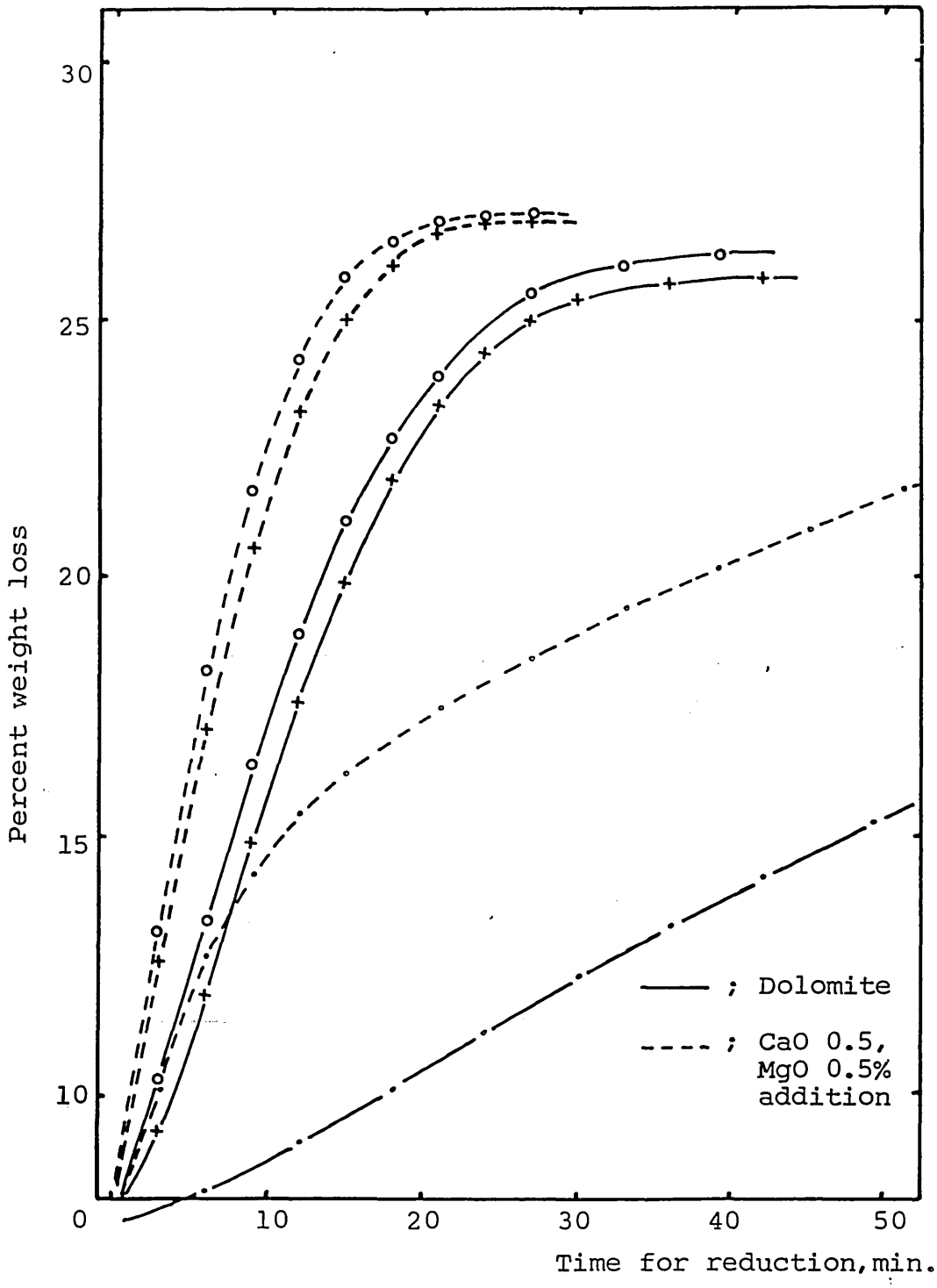

Fig. 4.30- The effect of temperature at 950, 1050 and 1100°C on reduction of wustite compacts pre-reduced at 1050°C with Thrislington dolomite 1% additions.

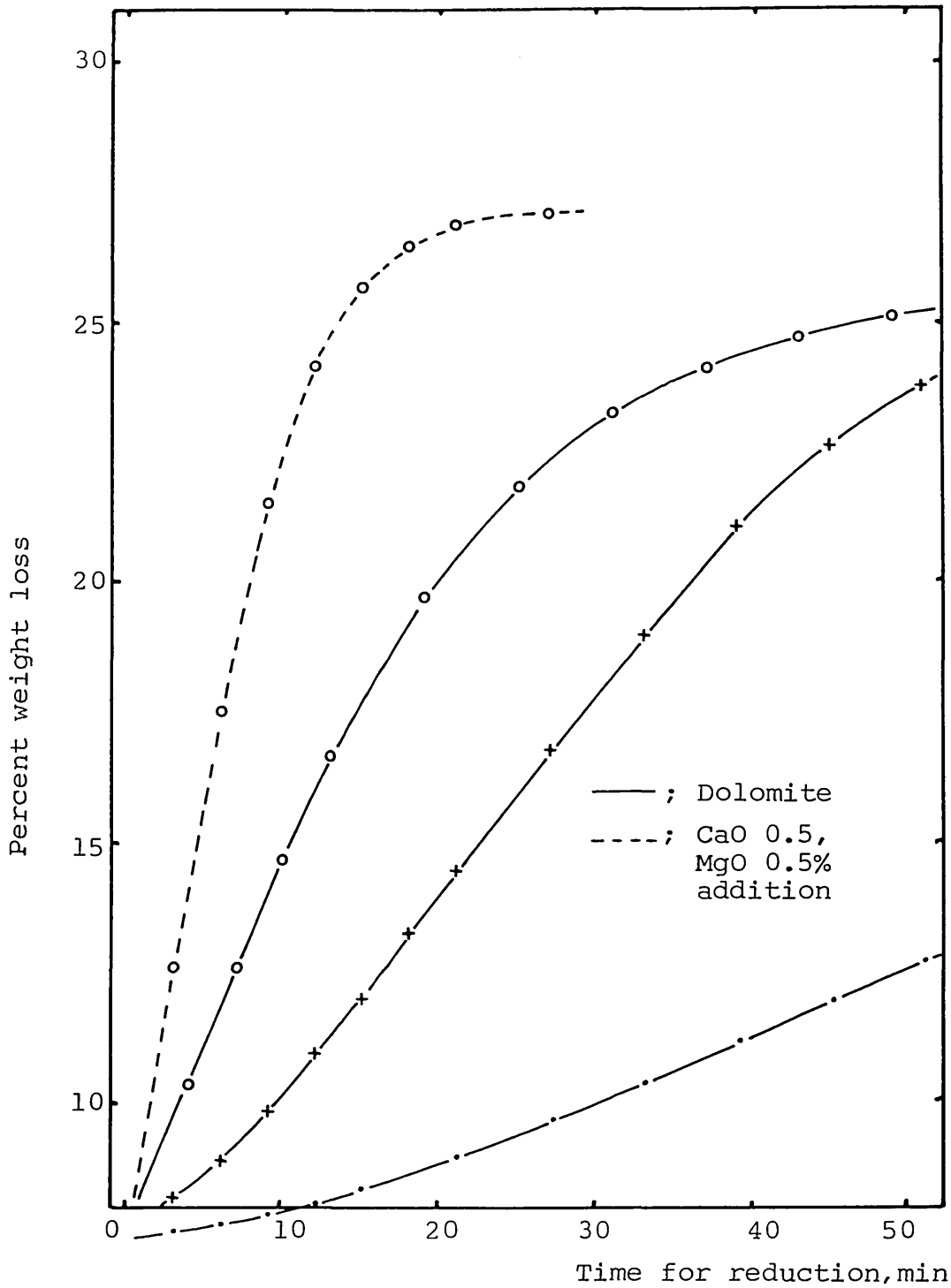

Fig. 4.31- The effect of temperature at 950, 1050 and 1100°C on reduction of wustite compacts pre-reduced at 1100°C with Thrislington dolomite 1% additions.

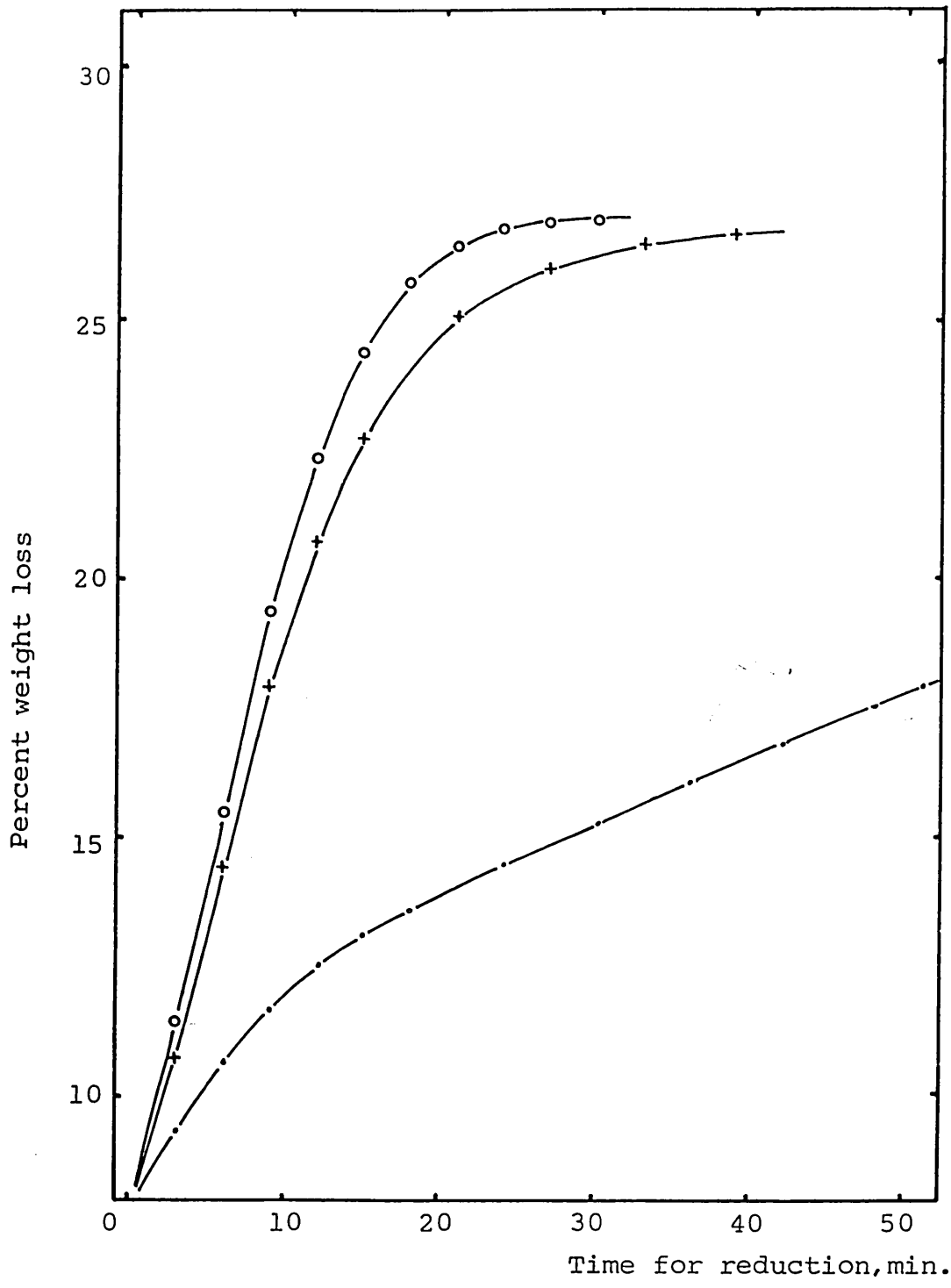

Fig. 4.32- The effect of temperature at 950, 1050 and 1100°C on reduction of wustite compacts pre-reduced at 950°C with Thrislington dolomite 2% additions.

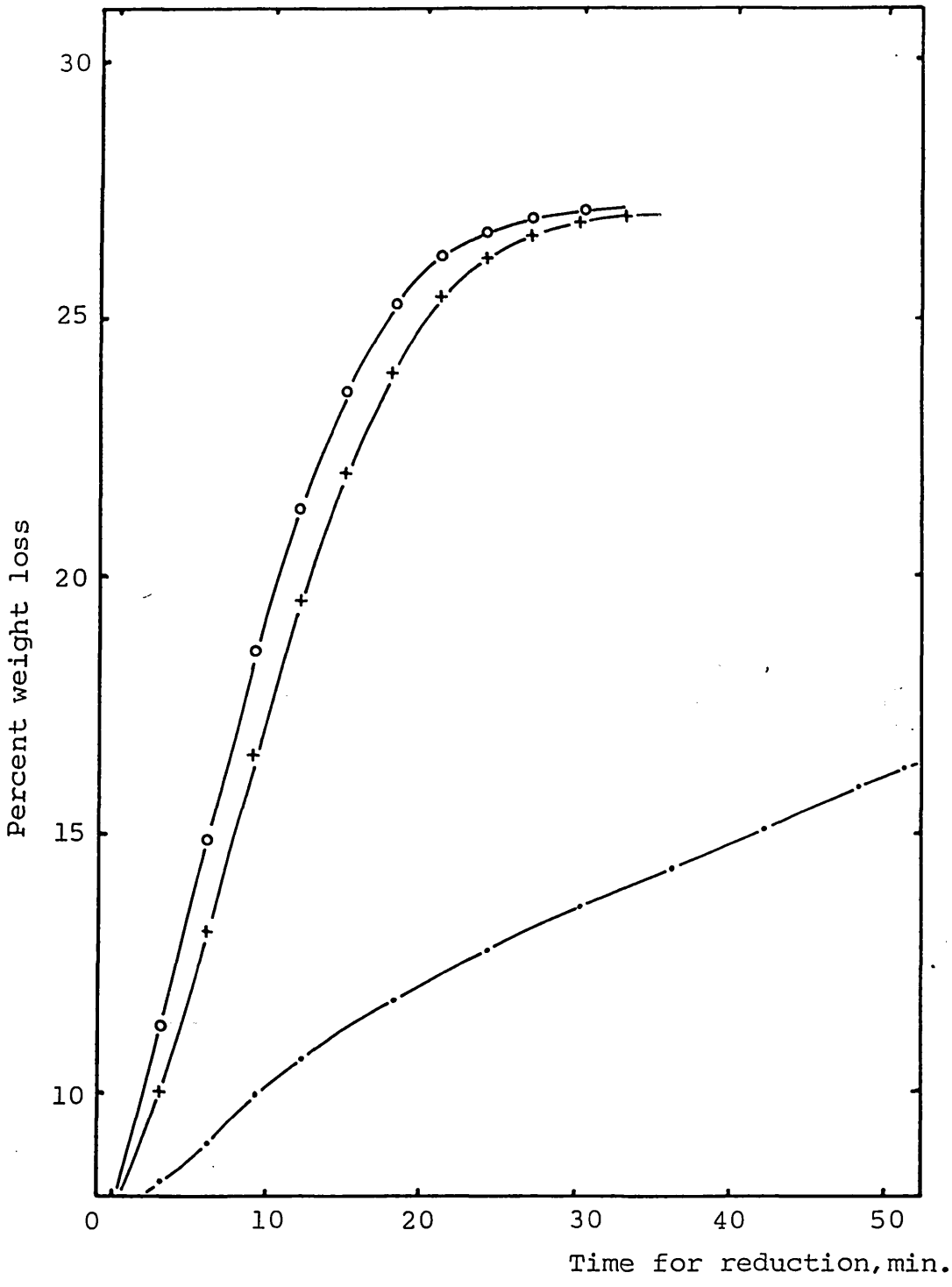

Fig. 4.33- The effect of temperature at 950, 1050 and 1100°C on reduction of wustite compacts pre-reduced at 1050°C with Thrislington dolomite 2% additions.

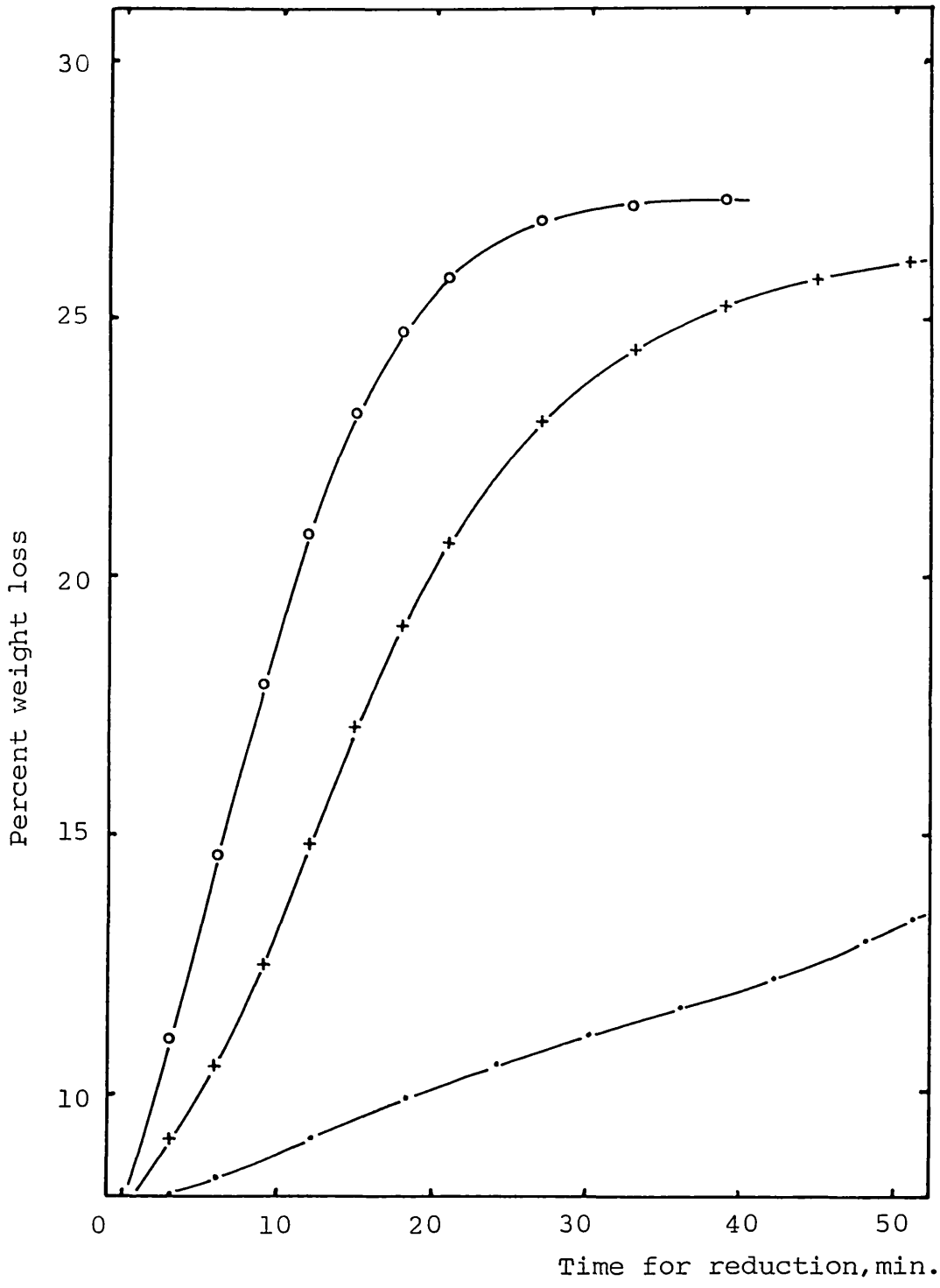

Fig. 4.34- The effect of temperature at 950, 1050 and 1100°C on reduction of wustite compacts pre-reduced at 1100°C with Thrislington dolomite 2% additions.

atures, the state of wustite pre-reduced at different temperatures (from 950°C to 1100°C) causes great differences in reduction rate. This effect is similar to that for 2% CaO addition ones.

Fig. 4.44-46 shows the reduction characteristics of compacts with 5% Whitewell dolomite additions. In essence the results fall into a high temperature and a low temperature group. However the difference between results at each temperature was small and the same characterestics were observed as shown in Fig. 4.14-16. This change with increased dolomite is regarded as being related to an increasing liquidus temperature caused by increasing the amount of dolomite addition.

The effect of temperature on reduction rate with two types of natural dolomite was particularly noticeable at low temperature (950°C). At higher temperatures, the difference were small and could even be said to be the same within experimental error. However at low temperature, the difference is significant with similar reduction behaviour to that shown by CaO additions in the case of Thrislington dolomite.

4.5.2. THE EFFECT OF WUSTITE

The main influence of wustite reduced at various temperatures on reduction rate is quite similar to the effects with another flux materials. The reduction rate is reduced by increasing the reduction temperatures at which wustite was made. However, the reduction rate at the low temperature shows different modes with each type of dolomite.

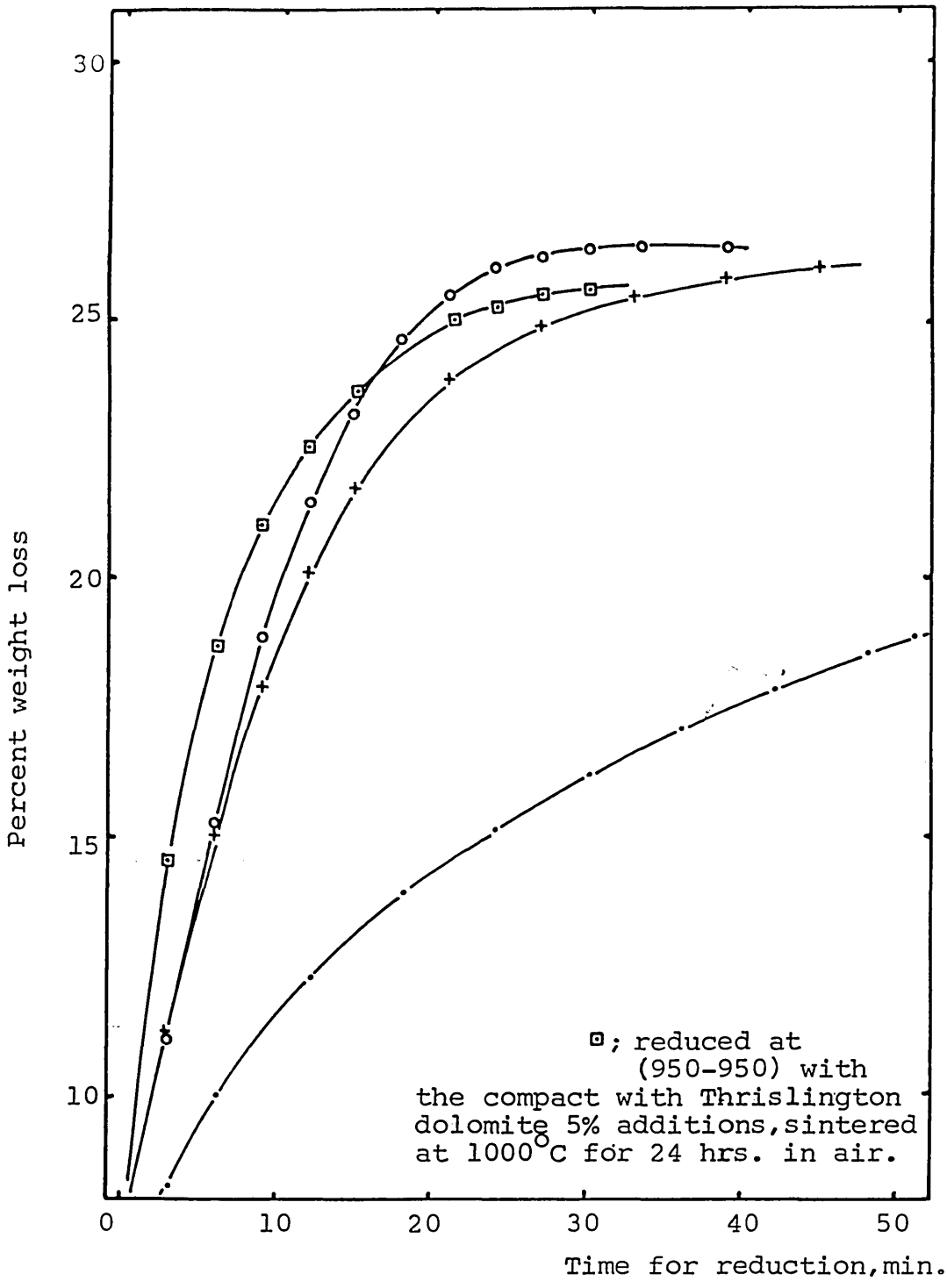

Fig. 4.35- The effect of temperature at 950,1050 and 1100°C on reduction of wustite compacts pre-reduced at 950°C with Thrislington dolomite 5% additions.

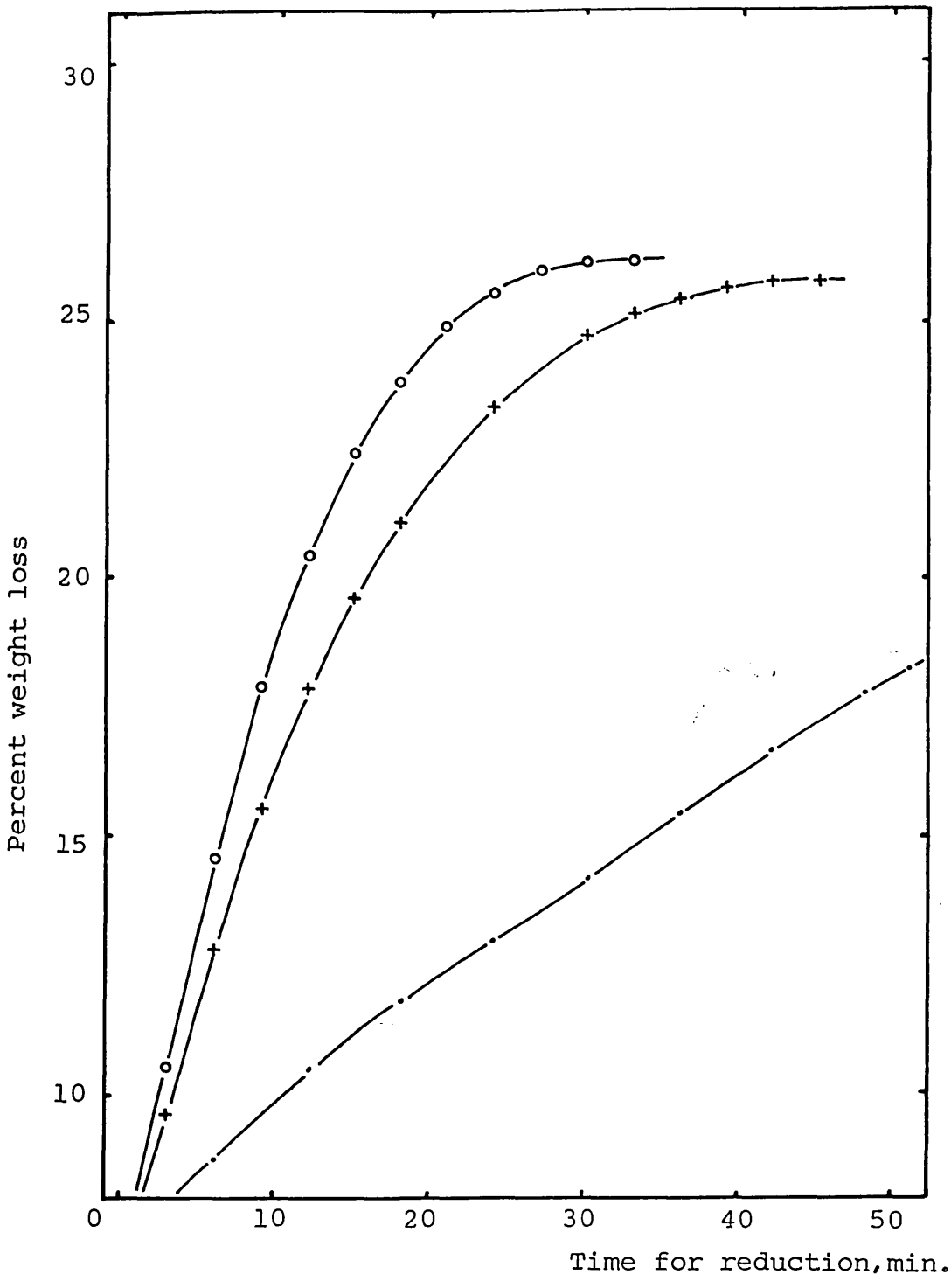

Fig. 4.36- The effect of temperature at 950, 1050 and 1100°C on reduction of wustite compacts pre-reduced at 1050°C with Thrislington dolomite 5% additions.

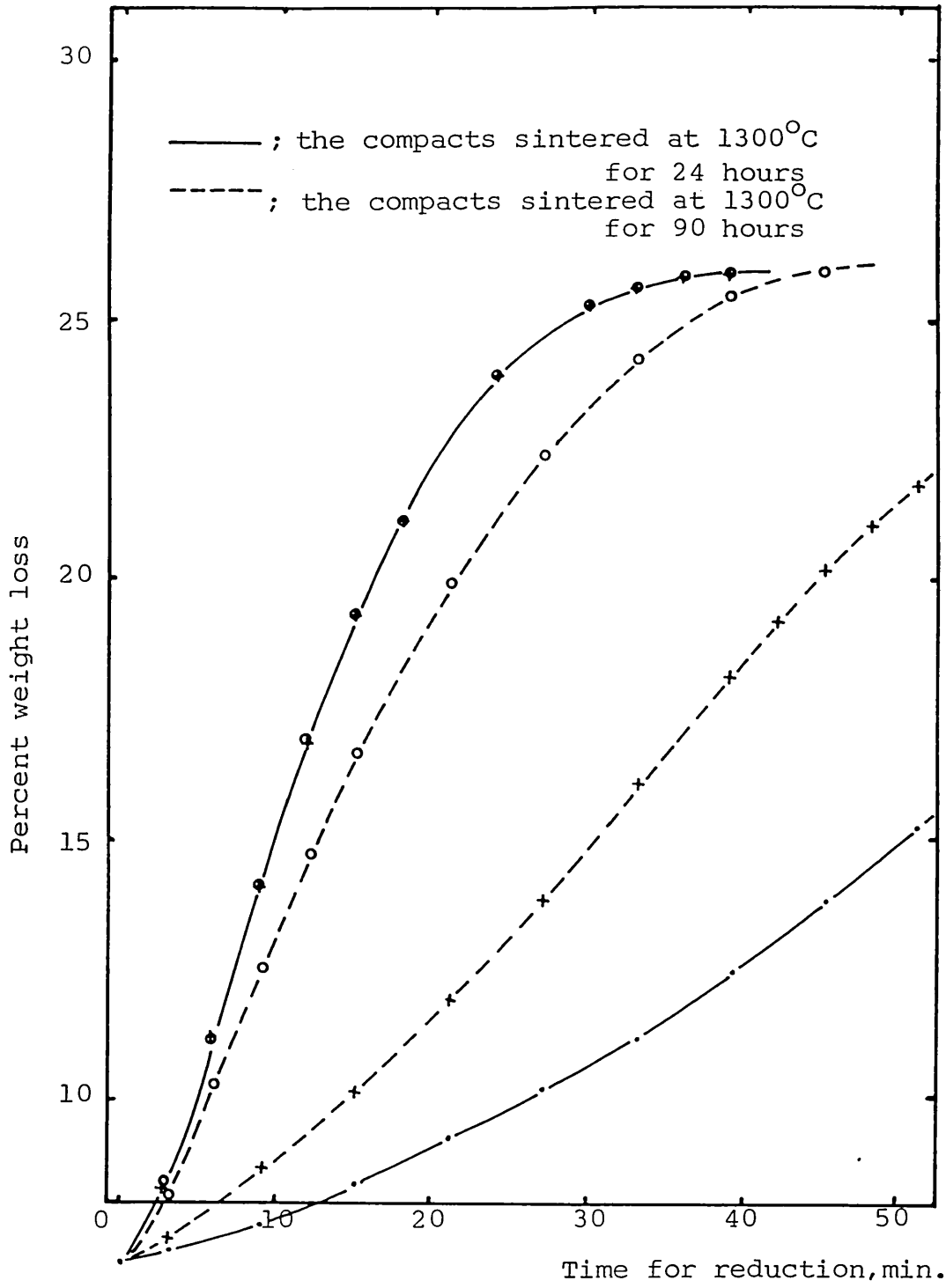

Fig. 4.37- The effect of temperature at 950, 1050 and 1100°C on reduction of wustite compacts pre-reduced at 1100°C with Thrislington dolomite 5% additions.

Thrislington dolomite

Plate 27 shows the liquid phases surrounding the hematite or magnesioferrite grains and the presence of a retangular precipitated phase from the calcium iron magnesium silicate, when the iron ore-dolomite mixture was sintered at 1300°C in air.

During the reduction of wustite, iron oxide dissolved into the liquid phase was reduced to iron and the solidified liquid phase becomes detached from the wustite grains due to shrinkage. Precipitation of wustite from the liquid phase also occurred during reduction depending on the reduction temperature. During reduction from wustite to iron, these different types of wustite were reduced to iron in different ways. Firstly, wustite formed from hematite grains reduce quickly by the same mechanism discussed previously i.e. pore diffusion control. However, other hematite grains which are formed during sintering in the presence of MgO, identified as magnesioferrite, is reduced to wustite. These wustite also contains MgO as the phase diagram shows that wustite can make an unlimited solid solution with MgO. EPMA results show that more than 3% of MgO was detected in the partially reduced wustite (Table 4.19, No 6). The reduction rate of these grains is much faster than the wustite without MgO (i.e. iron reduced from the hematite, light grey in Plate 27).

The magnesiowustite grains form a dense iron shell around the wustite grain. However both types of wustite do not seem to affect the overall reduction rate when compared to MgO additions. The third type of wustite was formed in the liquid phase and was blocked by the liquid phase from contact with

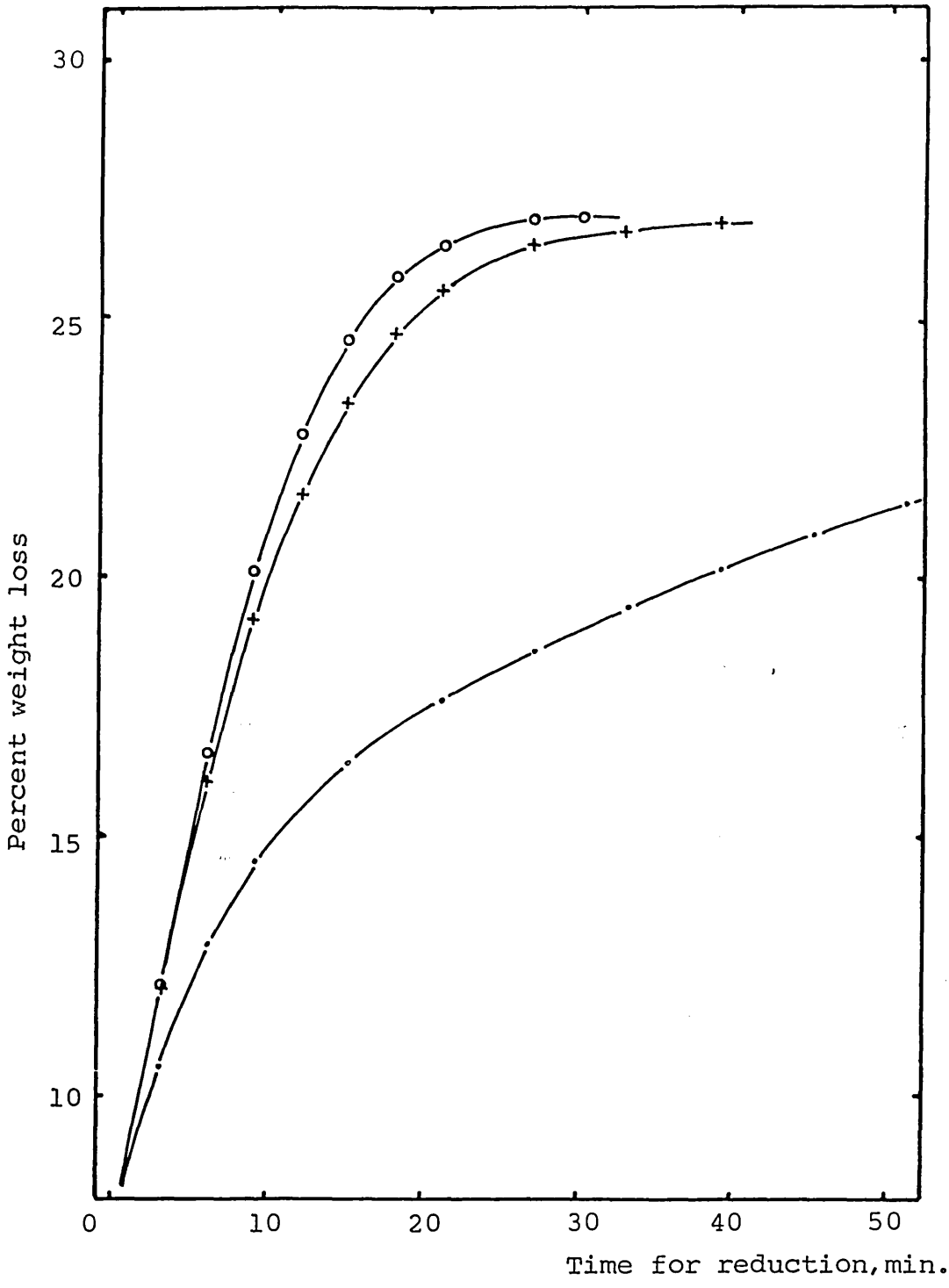

Fig. 4.38- The effect of temperature at 950, 1050 and 1100°C on reduction of wustite compacts pre-reduced at 950°C with Whitewell dolomite 1% additions.

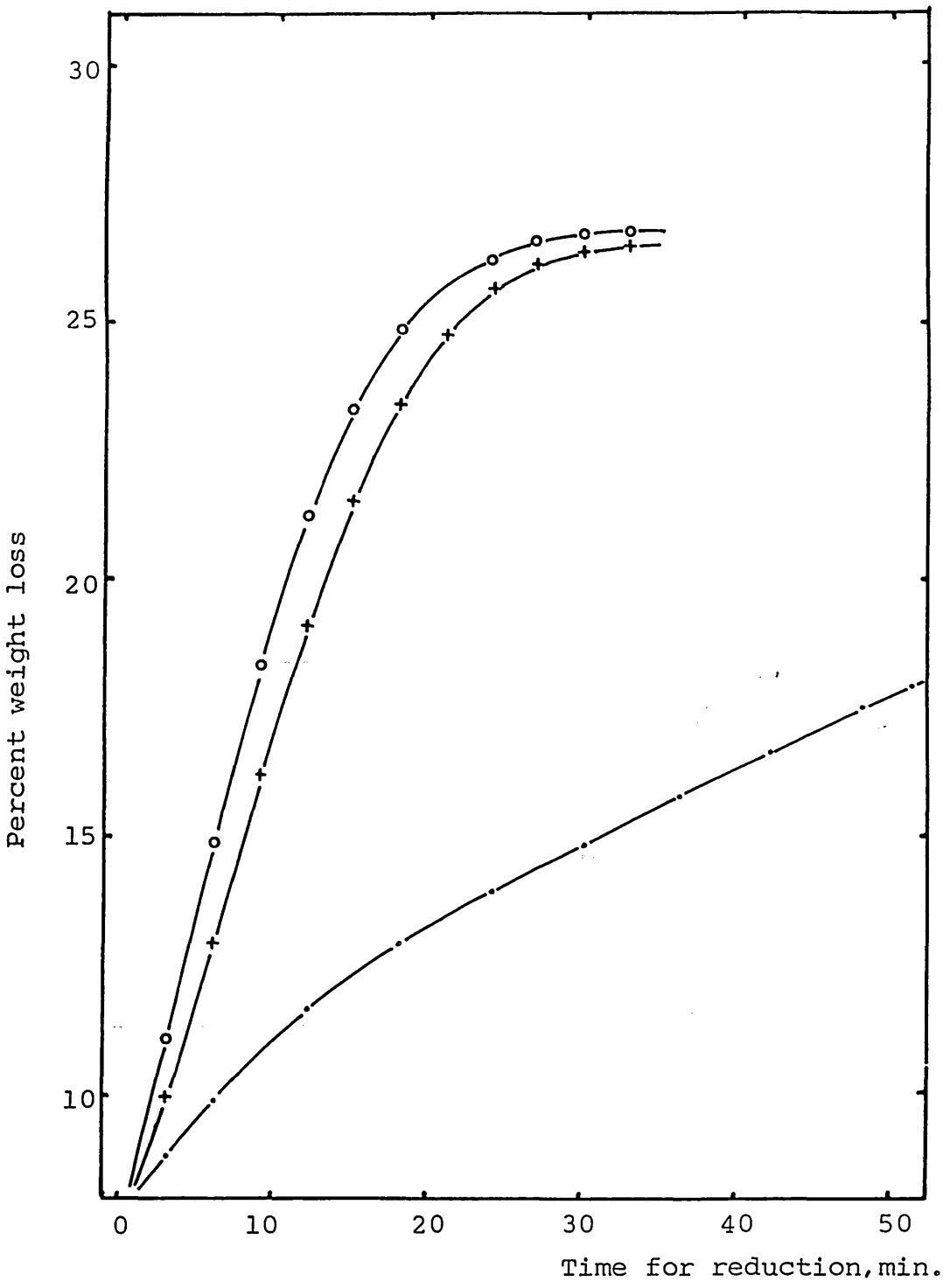

Fig. 4.39- The effect of temperature at 950, 1050 and 1100°C on reduction of wustite compacts pre-reduced at 1050°C with Whitewell dolomite 1% additions.

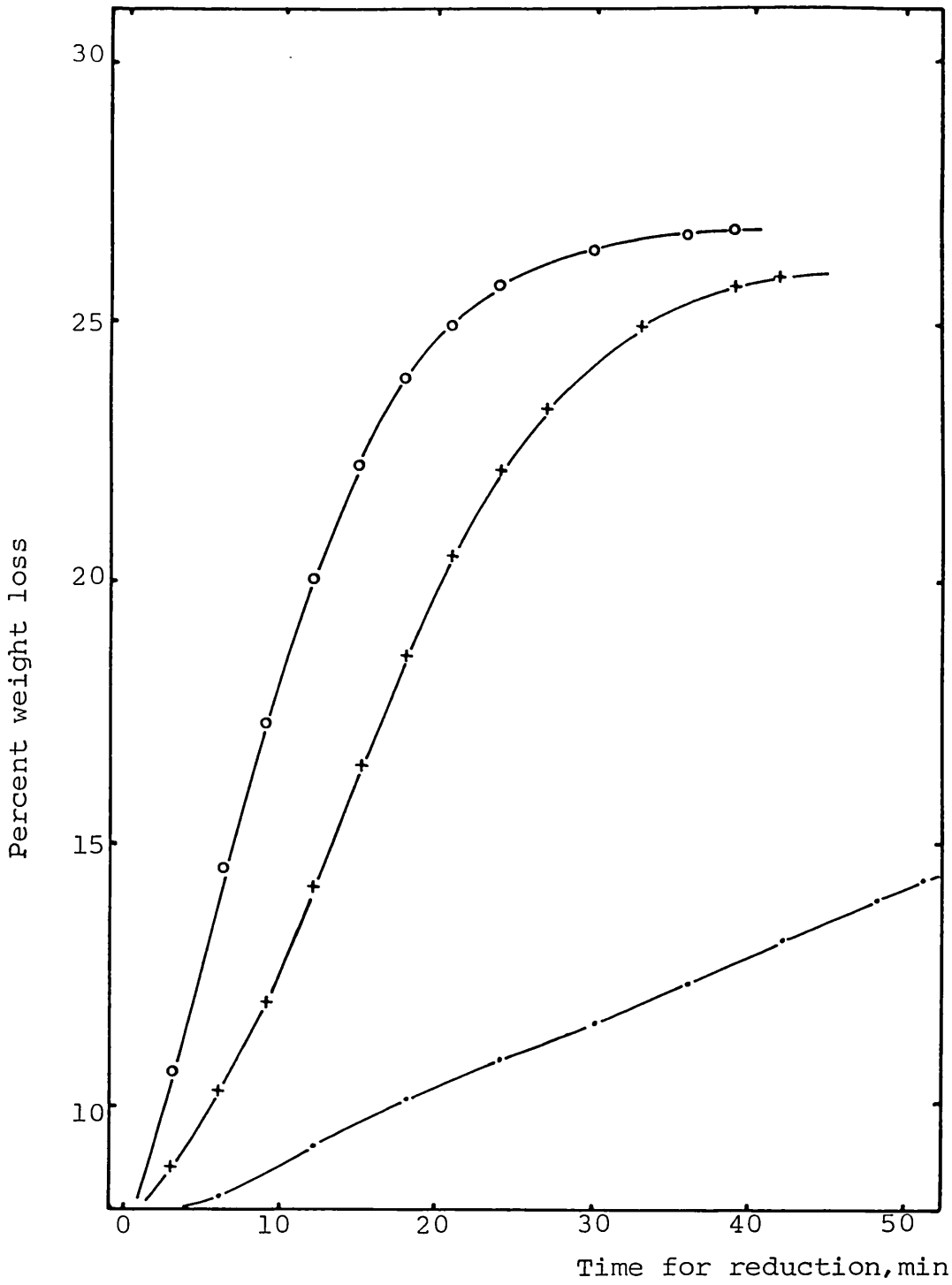

Fig. 4.40- The effect of temperature at 950, 1050 and 1100°C on reduction of wustite compacts pre-reduced at 1100°C with Whitewell dolomite 1% additions.

CO. This type of wustite was slowly dissolved into the liquid phase depending on the reduction temperatures.
When adequate quantities of dolomite are present, the liquid phase is extended.
Most of the kinetic measurements show that the reduction rate slows down at (1100-950). These results are the lowest rate observed for any flux addition.

Whitewell dolomite

Whitewell dolomite additions show similar reduction characteristics to CaO.
Many workers studied the slag formation of dolomite or serpentine in sinter or pellets (81) and they postulated that some of the MgO in the flux materials is very difficult to dissolve and can not produce a liquid phase at certain temperatures compared to other fluxes.
According to the EPMA results, the MgO level in the liquid phase is lower than that observed with Thrislington dolomite, while the MgO level in the iron (center of the iron structure, i.e. microporous structure) is higher than seen with Thrislington dolomite (see Table 4.19, 4.23).
In this aspect, Whitewell dolomite behaves in quite a similar manner to CaO additions except that some MgO diffuses into the hematite grains.

4.5.3. SEQUENCE OF REDUCTION

In the phase diagram (Fig. 2.8), $CaO-MgO-Fe_2O_3-SiO_2$ system can form a liquid phase at 1300°C and this was confirmed by the microstructure of sintered compacts (Plate 27,38). The composition of liquid phase from results of

EPMA (Table 4.21, No 1,4,7) was approximately CaO 27%, MgO 3%, Fe_2O_3 25% and SiO_2 45% by weight.

The phases identified in the dolomite added samples were

α - Hematite, Magnesioferrite and Augite($Ca(Fe,Mg)Si_2O_6$).

Augite is the commonest Pyroxene (65) and in composition it is intermediate between diopside and hedenbergite.

During reduction of these compacts, some of the iron oxide dissolved at 1300°C is reduced easily on the surface of the former liquid phase(at the reduction temperature, this phase was already solid state) and new phases are formed.

The phase relationships for the system CaO-MgO-Iron oxide-SiO_2 in contact with metallic iron have been compiled(64) and main feature of the liquidus phase relations are shown below by means of a " Schairer type " diagram.

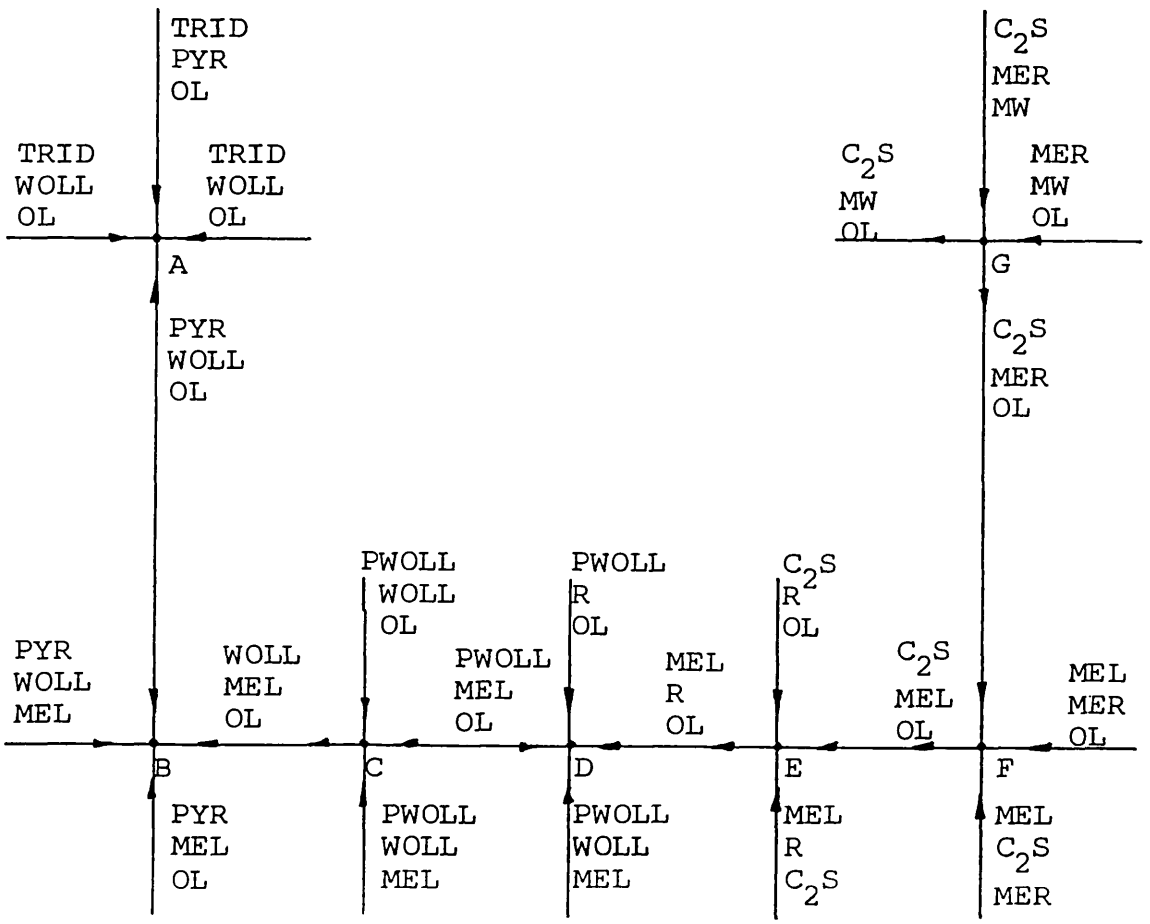

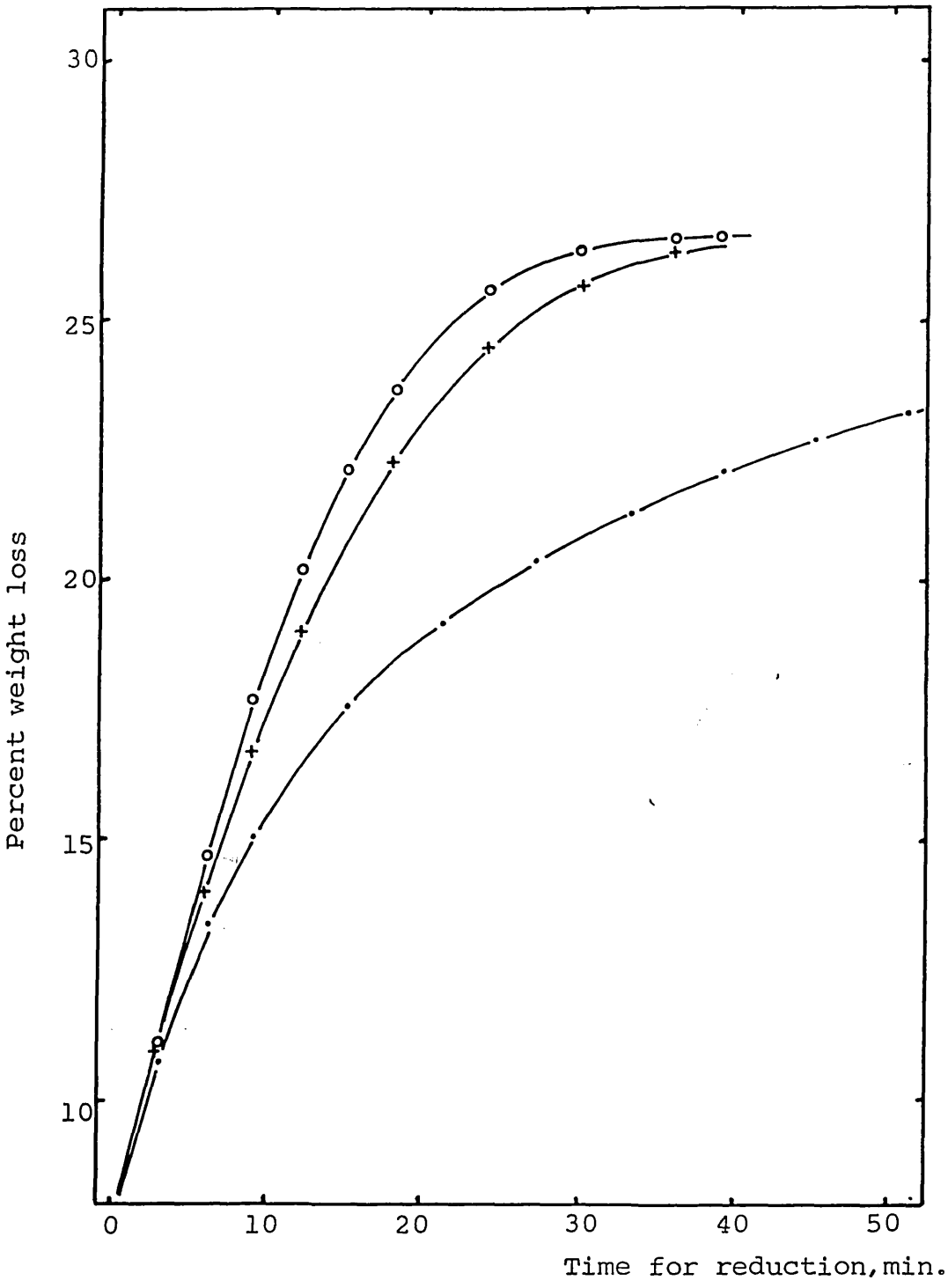

Fig. 4.41- The effect of temperature at 950, 1050 and 1100°C on reduction of wustite compacts pre-reduced at 950°C with Whitewell dolomite 2% additions.

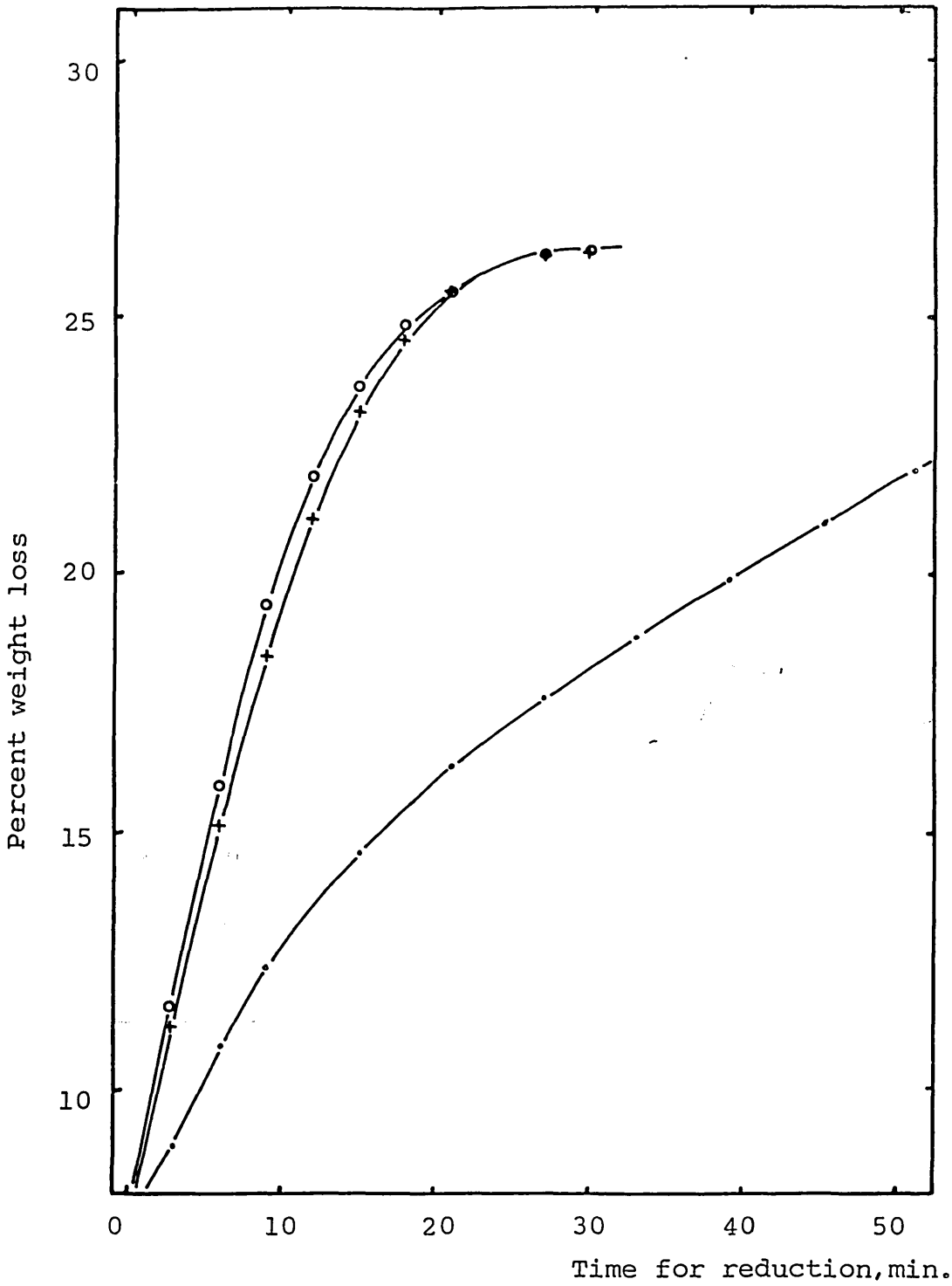

Fig. 4.42- The effect of temperature at 950, 1050 and 1100°C on reduction of wustite compacts pre-reduced at 1050°C with Whitewell dolomite 2% additions.

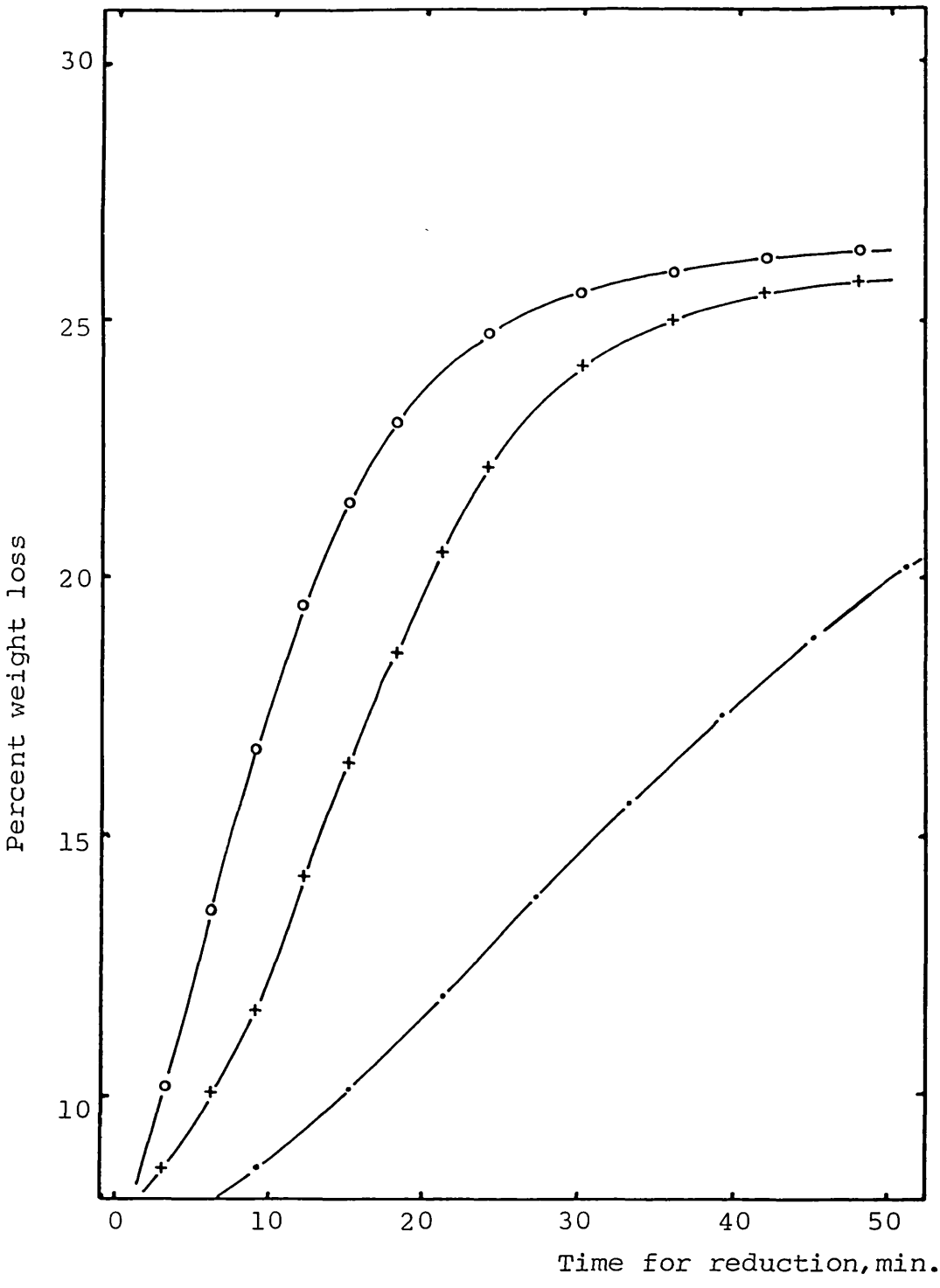

Fig. 4.43- The effect of temperature at 950, 1050 and 1100°C on reduction of wustite compacts pre-reduced at 1100°C with Whitewell dolomite 2% additions.

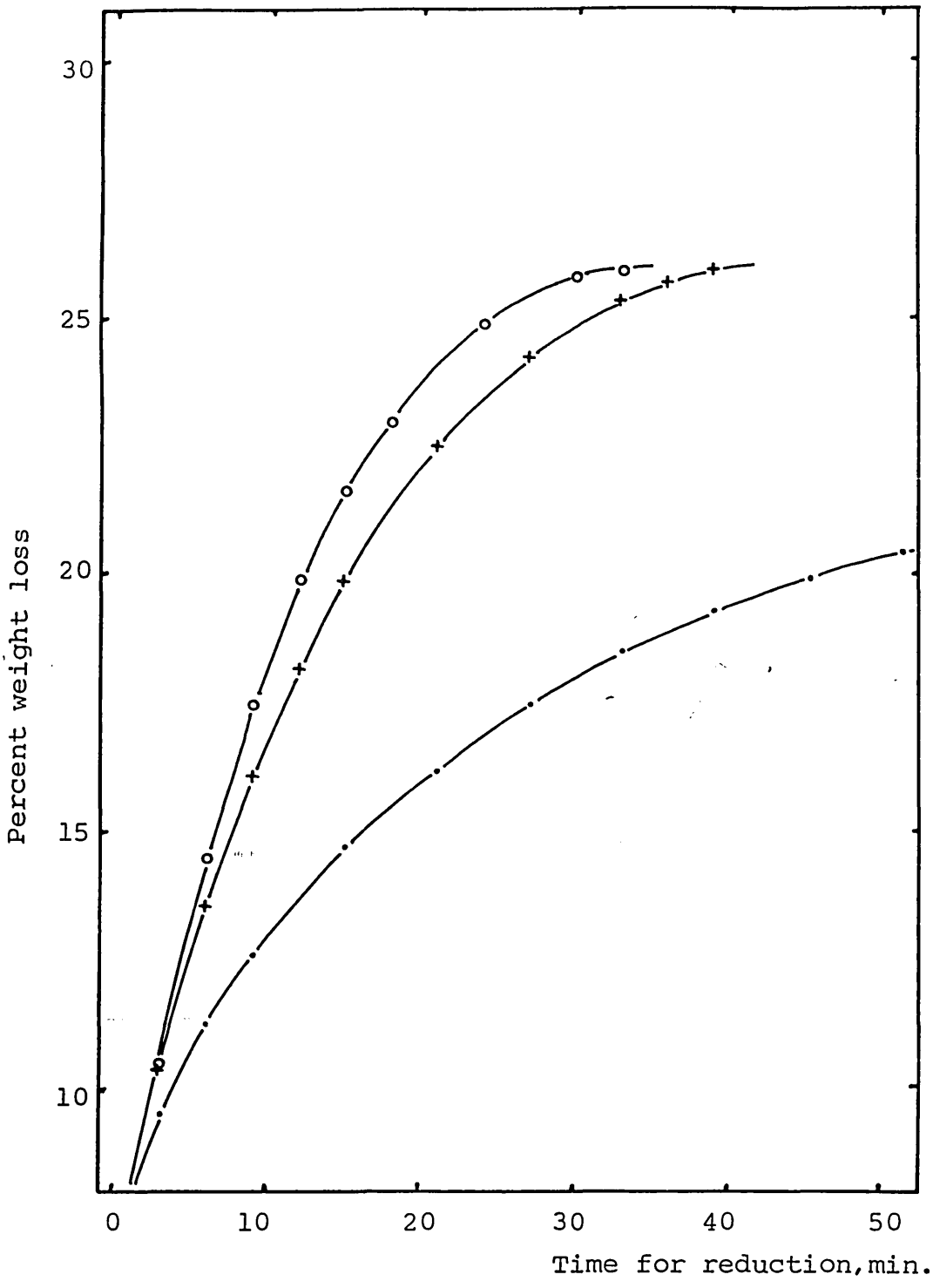

Fig. 4.44- The effect of temperature at 950, 1050 and 1100°C on reduction of wustite compacts pre-reduced at 950°C with Whitewell dolomite 5% additions.

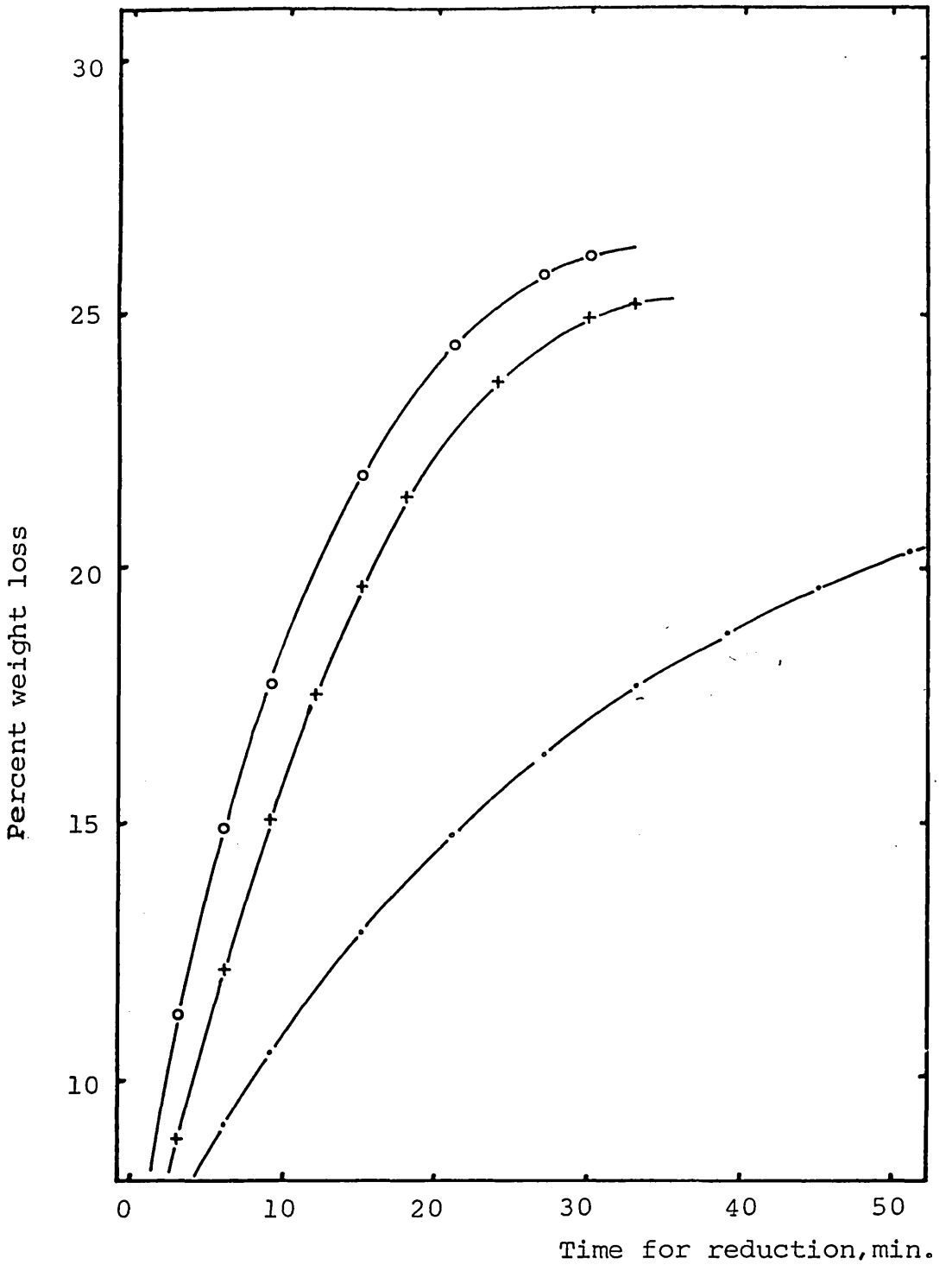

Fig. 4.45- The effect of temperature at 950, 1050 and 1100°C on reduction of wustite compacts pre-reduced at 1050°C with Whitewell dolomite 5% additions.

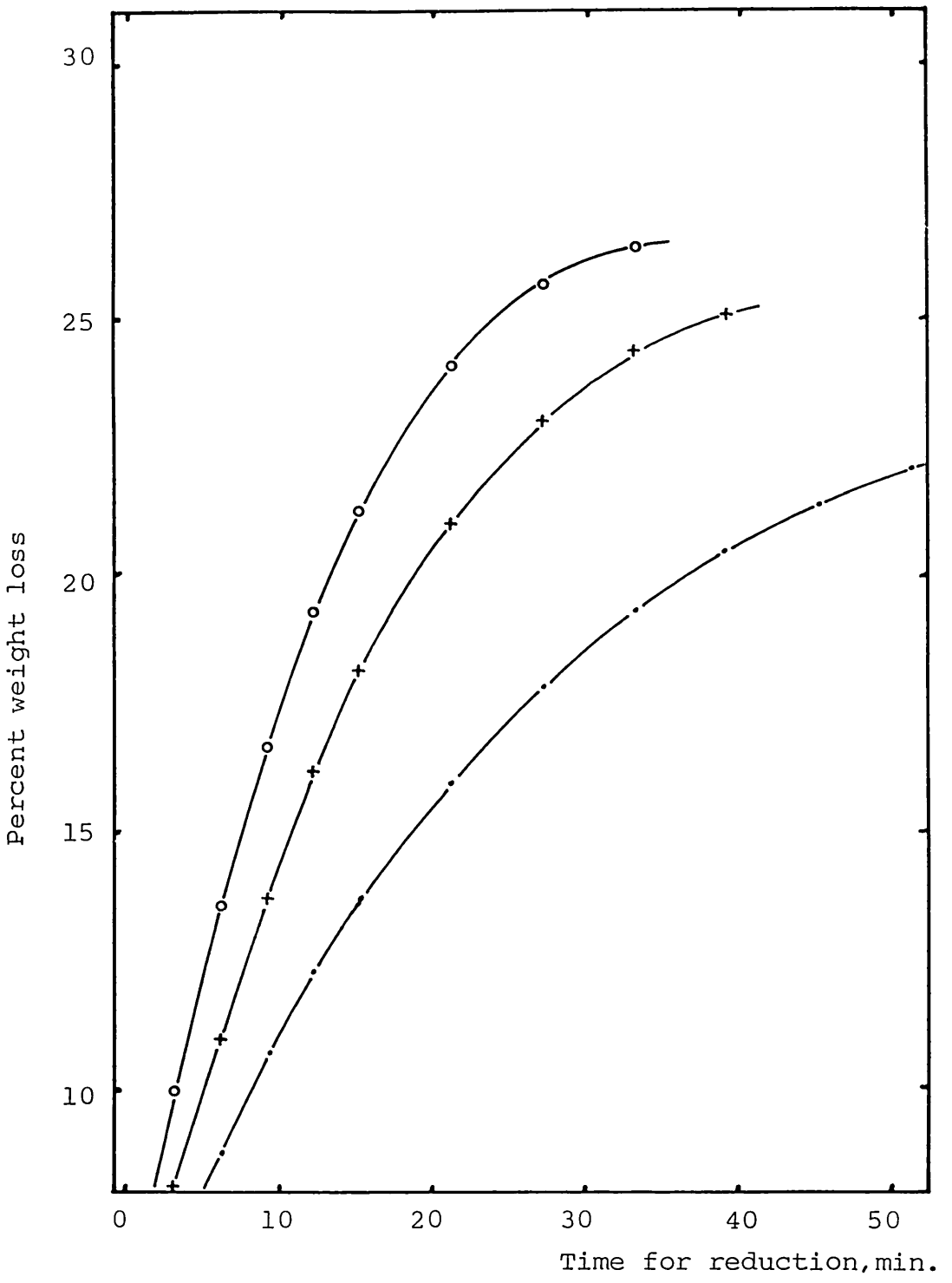

Fig. 4.46- The effect of temperature at 950, 1050 and 1100°C on reduction of wustite compacts pre-reduced at 1100°C with Whitewell dolomite 5% additions.

TRID : Tridymite
PYR : Pyroxene
OL : Olivine
WOLL : Wollastonite
MW : Magnesiowustite
MEL : Melilite
PWOLL : Pseudowollastonite
R : Rankinite
C_2S : Dicalcium silicate
MER : Merwinite

Point	Temperature	Liquid Composition(Wt·%)			
		CaO	MgO	FeO	SiO_2
A	1100	25	8	25	42
B	1125	29	11	20	40
C	1160	35	2	25	38
D	1175	35	4	26	35
E	1180	36	4	27	33
F	1200	41	7	8	44
G	1450	38	17	6	39

According to the EPMA results, some of the liquid phase are near to the composition range of A and C (A:Table 4.21, No 10, Table 4.23, No 14, C:Table 4.21, No 6). This newly formed liquid phase blocks the remaining pores or the gaps which exist between wustite or iron grains and slag matrix. When the reduction proceeds at low temperatures, especially at (1100-950), this factor greatly affects the reduction rate (see Fig. 4.31,34,37) because liquid phase formed at higher temperatures during reduction of hematite to wustite freezes at these low temperatures. However with high temperature reduction (950-1100, 1050-1100, 1100-1100), iron oxide(wustite) was reduced directly from the liquid phase and examples are shown in Plate 28 and 29.

XRD results after reduction shows various phases such as Augite, Hedenbergite ($Ca(Fe,Mg)(SiO_3)_2$) and Diopside ($CaMg(SiO_3)_2$) according to the degree of reduction.

The sequence of reduction of Augite can be demonstrated as follows ;

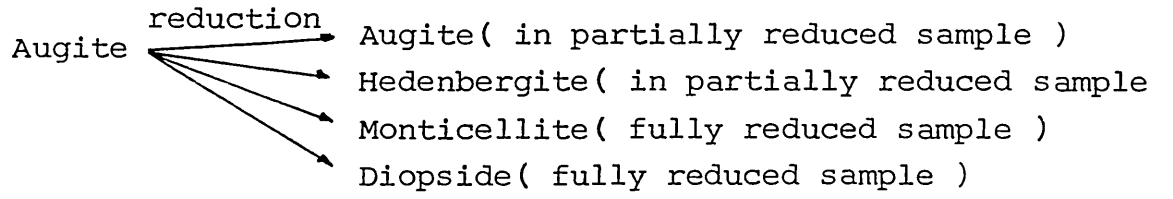

The reduction rate was also affected by the state of liquid phase. The liquid phase that was produced primarily during sintering of compacts has various compositions according to localised element segregation. Since the Fe_2O_3 in the liquid phase was around 25%, the FeO level obviously is not expected to exceed 25%. Within these compositions, liquid phases can be produced at a temperature around 1100°C. Meanwhile reduced iron particles (Plate 28 e,f, Plate 37d,e, Plate 39c, Plate 42a,b,c) in the liquid phase were observed during high temperature reduction and the structure indicates that this iron was formed from the liquid phase at temperatures.

The reduction rate of iron oxide is higher in the liquid than the solid state. This is most pronounced at (950-1100). The wustite is initially produced at a low temperature so there is no newly formed liquid phase. However, as the sample is maintained at high temperature (1100°C), a gradual increase of liquid phase can be related to the decreasing reduction rate and the final iron structures.

Magnesioferrite and Cementite

As mentioned above, magnesioferrite is reduced to the iron by forming a thick iron shell. Once this iron shell forms, the penetration of reducing gas (carbon monoxide) decom-

poses with carbon deposition on the surface of the iron produced. This carbon easily dissolves into the iron at the reduction temperatures and forms a very dense phase. The typical results of cementite formation are shown in Plate 33 and Table 4.13-18. This magnesioferrite was observed when 1% of Thrislington dolomite was added. A comparison of XRD reflexion between magnesioferrite and cementite shows that cementite reflexions become stronger in the presence of magnesioferrite.

Fayalite magnesian

This phase was observed when 1 and 2% of dolomite was added. This observation is similar to that with MgO additions. Since the iron ore contains 4% of silica, this silica did not react with the CaO in the dolomite completely and so formed fayalite magnesian with wustite(magnesiowustite).

Hedenbergite

Hedenbergite only was identified when 1% of Thrislington dolomite was added and reduced at (1100-950). This was the lowest reduction rate observed with any dolomite addition.

4.5.4. STRUCTURAL CHANGE DURING REDUCTION

Morphology of iron structures after reduction partially or fully at various temperatures was studied by optical microscopic and electron microscopic methods.

Four distinctive iron structures were observed with additions of dolomite, both Thrislington and Whitewell.

TABLE 4.13

XRD ANALYSES OF REDUCED SAMPLES OF IRON ORE COMPACTS WITH THRISLINGTON DOLOMITE 1% ADDITIONS.

REDUCTION PROCEDURE	REDUCTION		PHASES IDENTIFIED
	% Wt.LOSS	TIME, MIN.	
950-950	17.6	60	Fe:VS, W:S, Q:MW, A:M, CR:MW, C:VW
950-1050	26.0	60	Fe:VS, W:W, Q:VW, CR:W, C:W, M·Fe:W, D:MW
950-1100	26.5	33	Fe:VS, W:VW, Q:VW, D:W, C:VVW
1050-950	17.0	60	Fe:VS, W:W, Q:M, C:M, M·Fe:MW, FS(Mg):W
1050-1050	25.9	45	Fe:VS, W:W, Q:VW, C:W, M·Fe:VW, A:MW, FS:W
1050-1100	26.4	40	Fe:VS, W:W, Q:VW, C:VW, Hed:MW, FS:VW
1100-950	14.0	60	Fe:VS, W:S, Q:VW, C:W, Hed:W, FS:MW
1100-1050	25.1	60	Fe:VS, W:MW, Q:VVW, C:W, A:W, FS(Mg):MW
1100-1100	25.6	60	Fe:VS, W:W, C:W, D:W

@ ORDER OF INTENSITY: VS,S,MS,M,MW,W,VW,VVW

Fe : α- Iron
W : Wustite
Q : α- Quartz, SiO_2
CR: α - Cristobalite, SiO_2
C : Cementite, Fe_3C
A : Augite, $Ca(Mg,Fe)Si_2O_6$
M·Fe : Magnesio Ferrite, $MgFe_2O_4$
D : Diopside, $CaMg(SiO_3)_2$
FS(Mg) : Fayalite Magnesian, $(Fe,Mg)_2SiO_4$
Hed : Hedenbergite, $Ca(Fe,Mg)(SiO_3)_2$

TABLE 4.14

XRD ANALYSES OF REDUCED SAMPLES OF IRON ORE COMPACTS WITH THRISLINGTON DOLOMITE 2% ADDITIONS.

REDUCTION PROCEDURE	REDUCTION		PHASES IDENTIFIED
	% Wt.LOSS	TIME, MIN.	
950-950	19.4	60	Fe:VS, W:S, CR:W, C:VW, A:W, FS(Mg):VVW
950-1050	26.8	41	Fe:VS, CR:W, C:VW, TR:MW, A:VVW
950-1100	27.1	30	Fe:VS, W:S, Mont:MW, TR:MW
1050-950	17.3	60	Fe:VS, W:S, CR:W, TR:MW, C:VVW, Mont:W, A:W
1050-1050	27.2	34	Fe:VS, W:VVW, Q:VW, A:W, CR:VW, FC:VW, TR:MW
1050-1100	27.3	31	Fe:VS, W:MW, Q:VW, CR:VW, A:VW, TR:MW
1100-950	14.5	60	Fe:S, W:S, Q:VVW, C:VW, CR:VVW, Mont:W, A:VVW
1100-1050	26.4	60	Fe:VS, W:M, Q:VW, A:W, CR:VW, C:VW, Mont:W
1100-1100	27.4	39	Fe:VS, Mont:MW, Q:VW, CR:VW, C:VVW, A:VW

@ ORDER OF INTENSITY:VS,S,MS,M,MW,W,VW,VVW

Fe : α- Iron
W : Wustite
Q : α- Quartz
CR : α- Cristobalite
C : Cementite
A : Augite, $Ca(Mg,Fe)Si_2O_6$
FS(Mg) : Fayatite Magnesian $(Fe,Mg)_2SiO_4$
Mont : Monticellite, $CaMgSiO_4$
TR : Tridymite, SiO_2

TABLE 4.15

XRD ANALYSES OF REDUCED SAMPLES OF IRON ORE COMPACTS WITH THRISLINGTON DOLOMITE 5% ADDITIONS.

REDUCTION PROCEDURE	REDUCTION		PHASES IDENTIFIED
	% Wt.LOSS	TIME, MIN.	
950-950	19.5	60	Fe:VS, W:S, D:VW, C:VW
950-1050	26.1	47	Fe:VS, W:MW, C:VW, D:W, Mont:W
950-1100	26.5	33	Fe:VS, W:VVW, C:VVW, D:W, Mont:W
1050-950	19.9	60	Fe:VS, W:S, C:VVW, A:VW, Mont:W
1050-1050	25.9	46	Fe:VS, W:VVW, C:VVW, Mont:W, A:VW
1050-1100	26.3	33	Fe:VS, C:VW, A:VW, Mont:W
1100-950	17.5	60	Fe:VS, W:M, C:VW, A:VW, Mont:MW
1100-1050	26.1	39	Fe:VS, W:VVW, C:VW, Mont:W, A:VW
1100-1100	26.1	39	Fe:VS, C:W, A:W, Mont:W

@ ORDER OF INTENSITY:VS,S,MS,M,MW,W,VW,VVW

Fe : α- Iron

W : Wustite

Q : α- Quartz, SiO_2

CR: α- Cristobalite, SiO_2

A : Augite, $Ca(Mg,Fe)Si_2O_6$

Mont : Monticellite, $CaMgSiO_2$

D : Diopside, $CaMg(SiO_3)_2$

C : Cementite, Fe_3C

Thrislington dolomite

Microstructures of the starting material(1,2 and 5% Thrislington dolomite addition) are shown in Plate 27. The compacts consist of hematite grains, liquid phase (identified as Augite) and magnesioferrite(some of this phase was observed and have formed in the liquid phase by recrystallization upon cooling and some formed in hematite grains by reaction with MgO.

From the results of EPMA(see Table 4.21), the MgO concentration in the recrystallized magnesioferrite was around 4% and this was a little higher than that in the liquid phase around hematite grains. The overall shape of recrystallized magnesioferrite is recognized by the rectangular form or sharp edged grains in the liquid phase (see Plate 27c). Plate 28a,c and e show the iron structure reduced at different temperatures with the wustite made at the same temperature(1100^{o}C). After low temperature reduction from wustite to iron, the wustite was reduced from the surface of the grains or perimeter of the pores inside the grains. The kinetic observations and the iron structures agree well with each other with respect to the variation of surface area caused by the sintering of wustite grains as determined by comparison of the grain size of wustite made at low(Plate 28b) and high(Plate 28a) temperatures. At high temperature, the general shape of the iron structure can be divided into essentially two distinct types. Plate 28c,d shows the structure of porous iron inside the grains surrounded by the thick layer of iron shell. According to the EPMA results in Table 4.19, it was revealed that the porous grains contains high MgO(8%)

TABLE 4.16

XRD ANALYSES OF REDUCED SAMPLES OF IRON ORE COMPACTS WITH WHITEWELL DOLOMITE 1% ADDITIONS.

REDUCTION PROCEDURE	REDUCTION		PHASES IDENTIFIED
	% Wt.LOSS	TIME, MIN.	
950-950	22.3	60	Fe:VS, W:S, C:VW, TR:MW, FS(Mg):VW
950-1050	26.9	41	Fe:VS, C:VW, TR:MW, A:VVW
950-1100	27.0	30	Fe:VS, C:VVW, W:VW, TR:W, D:VW
1050-950	19.0	60	Fe:VS, W:S, C:VVW, TR:W, FS(Mg):W
1050-1050	26.7	33	Fe:VS, W:VW, C:VW, D:VW, TR:MW, FS(Mg):VVW
1050-1100	27.0	33	Fe:VS, W:VVW, C:VVW, TR:MW, D:W
1100-950	15.4	60	Fe:VS, W:S, C:VW, TR:MW, FS(Mg):MW
1100-1050	26.1	45	Fe:VS, W:W, C:W, TR:W, FS(Mg):W
1100-1100	27.0	40	Fe:VS, W:VW, C:VVW, TR:VW, D:W

@ ORDER OF INTENSITY:VS,S,MS,M,MW,W,VW,VVW

Fe : α- Iron W : Wustite

TR : Tridymite, SiO_2 C : Cementite, Fe_3C

A : Augite, $Ca(Mg,Fe)Si_2O_6$

FS(Mg) : Fayatite Magnesian, $(Fe,Mg)_2SiO_4$

D : Diopside, $CaMg(SiO_3)_2$

TABLE 4.17

XRD ANALYSES OF REDUCED SAMPLES OF
IRON ORE COMPACTS WITH WHITEWELL DOLOMITE 2% ADDITIONS.

REDUCTION PROCEDURE	REDUCTION		PHASES IDENTIFIED
	% Wt.LOSS	TIME, MIN.	
950-950	23.9	60	Fe:VS, W:MW, C:VW, FS(Mg):VW, A:W
950-1050	26.6	41	Fe:VS, W:W, C:VW, FS(Mg):VW, A:W
950-1100	26.8	39	Fe:VS, W:W, C:W, FS(Mg):VW, A:VW
1050-950	23.2	60	Fe:VS, W:M, C:W, FS(Mg):M, A:W
1050-1050	26.4	30	Fe:VS, W:W, C:W, FS(Mg):MW, A:VW
1050-1100	26.4	30	Fe:VS, W:VW, C:W, A:VW, FS(Mg):VW
1100-950	21.6	60	Fe:VS, W:MW, C:MW, A:W, FS(Mg):VVW
1100-1050	25.9	51	Fe:VS, W:VW, C:VW, FS(Mg):VW, A:W
1100-1100	26.5	48	Fe:VS, W:VW, C:VW, FS(Mg):VW, A:W

@ ORDER OF INTENSITY : VS,S,MS,M,MW,W,VW,VVW.

Fe : α- Iron
W : Wustite
C : Cementite, Fe_3C
FS(Mg) : Fayalite Magnesian, $(Fe,Mg)_2SiO_4$
A : Augite, $Ca(Mg,Fe)Si_2O_6$

TABLE 4.18

XRD ANALYSES OF REDUCED SAMPLES OF IRON ORE COMPACTS WITH WHITEWELL DOLOMITE 5% ADDITIONS.

REDUCTION PROCEDURE	REDUCTION		PHASES IDENTIFIED
	% Wt.LOSS	TIME, MIN.	
950-950	21.1	60	Fe:VS, W:W, C:VW, Q:MW, A:W, Mont:W
950-1050	26.2	43	Fe:VS, W:VVW, C:VVW, Mont:W, A:W
950-1100	26.1	33	Fe:VS, W:VW, C:VW, A:W, Mont:W
1050-950	21.0	60	Fe:VS, W:MW, C:VVW, A:W, Mont:MW
1050-1050	25.5	36	Fe:VS, C:W, Mont:VW, A:W
1050-1100	26.4	34	Fe:VS, C:VW, Mont:W, A:W
1100-950	22.9	60	Fe:VS, W:W, C:VW, A:VW, Mont:MW
1100-1050	25.4	41	Fe:VS, C:VVW, Mont:W, Q:W, A:W
1100-1100	26.7	35	Fe:VS, C:VVW, Mont:W, A:W

@ ORDER OF INTENSITY:VS,S,MS,M,MW,W,VW,VVW

Fe : α - Iron

Q : α - Quartz, SiO_2

A : Augite, $Ca(Mg,Fe)Si_2O_6$

Mont : Monticellite, $CaMgSiO_4$

W : Wustite

C : Cementite, Fe_3C

while the outside iron shell has virtually no MgO. This result indicates that MgO diffuses to the center during reduction.

The other type of iron structure can be observed after higher(1100°C) temperature reduction. This iron structure consisted of two types, one is that just mentioned above(1050°C) and the other is reduced from the liquid phase(see Plate 28e,f, Plate 8,9,10c).

Plate 29 shows the microstructure of iron reduced with 2% Thrislington dolomite. As a result of more flux addition, more liquid phase is formed during sintering and the reduced iron was fully or partly surrounded by the liquid phase(Plate 29a,b). The reduction rate(Fig. 4.34) also indicates the difficulties of penetration of gas through the liquid phase. However the microstructure in Plate 29c shows that this iron structure was formed from the liquid phase like Plate 28e and f. This result is similar to CaO 1 and 2% additions during reduction at 1100°C and almost all the iron reduced is interconnected.

Because of these observations, the role of the liquid phase must be considered as follows.

1. The liquid phase was formed during sintering with magnesioferrite recrystallized from the liquid during cooling.

   Thus, a change of composition occurred and the liquid phase was in close contact with wustite grains during reduction of hematite to wustite(Plate 30, Plate 27c).

2. Another type of liquid phase was formed during reduction to wustite by dissolving wustite at temperatures higher than 1050°C.

KEY TO PLATE 27-37

PLATE 27 showing hematite grains attacked by calcium magnesium silicate and two distinct type of magnesioferrite, one combined with hematite by diffusion of magnesia to hematite and the other recrystallized from the magnesia rich liquid phase(rectangular grains).

PLATE 28 e) and f) shows that the iron is reduced from the liquid phase

PLATE 32 e) shows the formation of magnesium silicate inside the micropores.

PLATE 33 showing the cementite in the iron shell formed outer grains.

PLATE 34 II and III shows the nucleation of iron from the surface of the magnesioferrite grains.

PLATE 37 a) the magnesioferrite grains surrounded by liquid phase shows no progress of reduction while the other type of grains show fully reduced already.

PLATE 27

Micro-structure of hematite grains of iron ore compacts with a)1% Thrislington dolomite, b)2% Thrislington dolomite and c)5% Thrislington dolomite addition, sintered at 1300°C for 24 hours in air .

a)

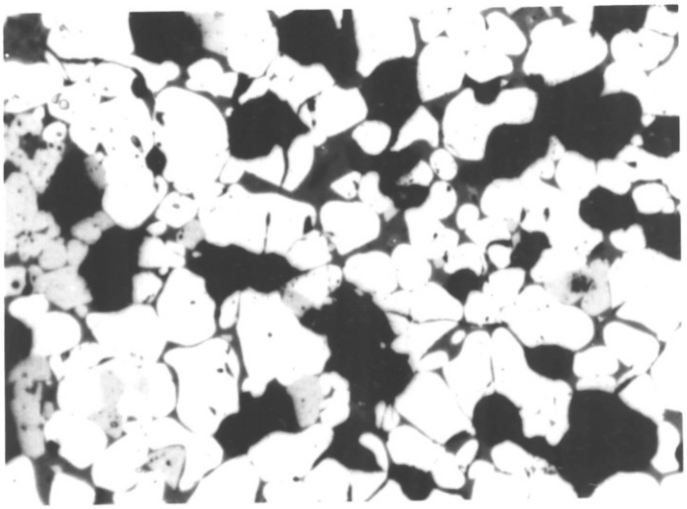

white : hematite
grey : magnesio-ferrite
dark grey : calcium iron magnesium silicate
black : voids

x 120

b)

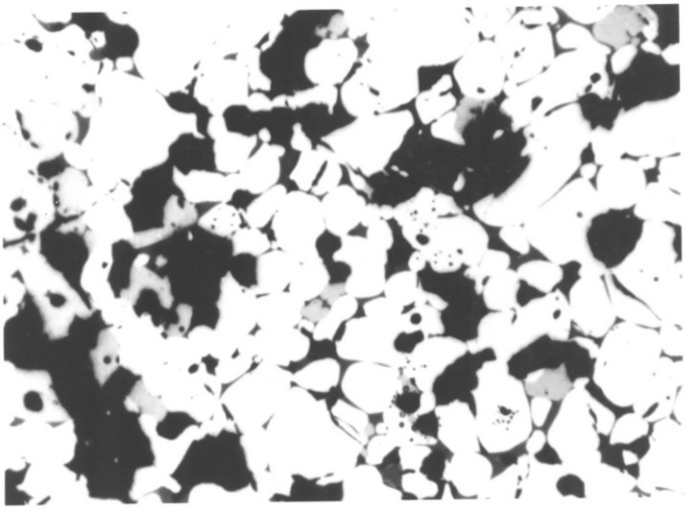

white : hematite
grey : magnesio - ferrite
dark grey : calcium iron magnesium silicate
black : voids

x 120

c)

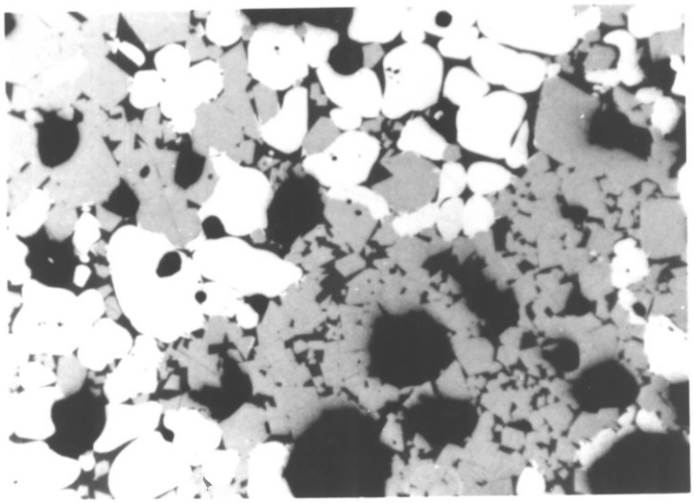

white : hematite
grey : magnesio-ferrite
dark grey : calcium iron magnesium silicate
black : voids

x 120

Because of the increasing amount of the FeO in the liquid phase, more liquid could be formed(Plate 28 e,f and Plate 29c).

On the aspect of reducibility of wustite, reduction of iron is more likely to proceed in the liquid state than the solid state which presents the penetration of reducing gas(Plate 29a,b and Plate 30). The kinetic results also support this general assessment. When the reduction is delayed due to reasons liquid phase surrounding the wustite or thick iron layer formation in the wustite grains, decomposition of carbon monoxide must be considered. In the reduction condition adapted during these experiment, deposition of carbon on the surface of the iron layers occurred at every temperature. This carbon diffuses into the iron layer. The observed results by XRD also indicate that precipitation of cementite in the ferrite occurred during cooling of the specimen. A typical microstructure of cementite is shown in Plate 33 by etching with Nital. The intensity of cementite reflexions also show (Table 4.13-15) that cementite can be formed in the presence of wustite. However this factor is related to the liquid phase formed during sintering since more cementite was observed in the fully reduced samples during reduction of iron ore powder or compacts without flux materials. The behaviour of MgO in the wustite has similar characteristics to that observed with MgO additions. Table 4.19 shows the results of point analyses by EPMA. No. 6 in Plate 31b has the MgO concentration of 3.45% and this wustite(magnesiowustite) grains is isolated from the iron

reduced nearby.

With further reduction of this type of wustite, a fine iron structure was produced with pores inside. High concentrations of MgO were observed associated with these pores(see Table 4.19, No 2, 4.20, No 10,14,15).

This phenomenon further confirms that MgO in the wustite (magnesiowustite) was rejected during reduction.

Another analysis was carried out to see the concentrated site of MgO after reduction of this type of wustite.

Plate 32e shows the detail of the area analysed in Plate 32d, No 15 and the results(Table 4.20) strongly indicates that the MgO concentrates in the pores as both silicates (Plate 32e) or MgO clusters(Plate 35 I).

As expected, more recrystallized magnesioferrite and liquid phase were formed when 5% of Thrislington dolomite was added and the reduction rate was also affected by this phenomenon. This was mentioned in the last section. However by increasing dolomite addition, more MgO was observed in the unreduced wustite or pores produced especially in the case of recrystallized magnesioferrite. Plate 34 II,III shows the difficulties of reduction according to the relationship of hematite or magnesioferrite grains with the liquid phase.

Visual demonstration of the distribution of elements in the iron structure after reduction illustrates(Plate 35II and Plate 36II) that CaO and SiO_2 appear on the same sites while MgO distributes more freely through the specimen. However some of the iron that dissolved in the liquid phase is a kind of iron silicates(confirmed by XRD as fayalite magnesian) and more MgO is concentrated in the site of

PLATE 28

Micro-structure of iron reduced at a) (1100-950)·T.D.1% , b) (950-950)·T.D.1% , c) (1100-1050)·T.D.1% , d) (950-1050)·T.D.1% , e) (1100-1100)·T.D.1% and f) (950-1100)·T.D.1% . white(iron), light grey(wustite), dark grey(calcium-iron-magnesium silicate) and black(voids). x 320

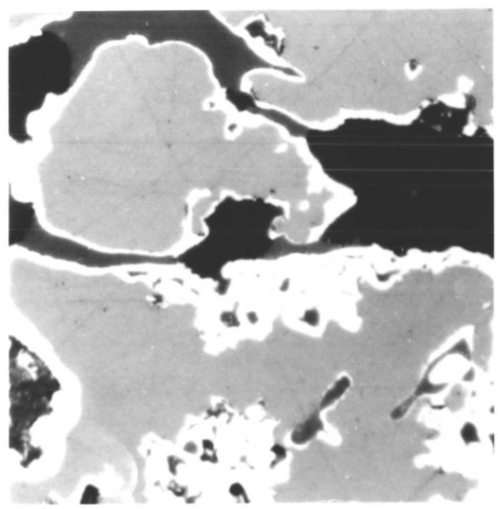

a)

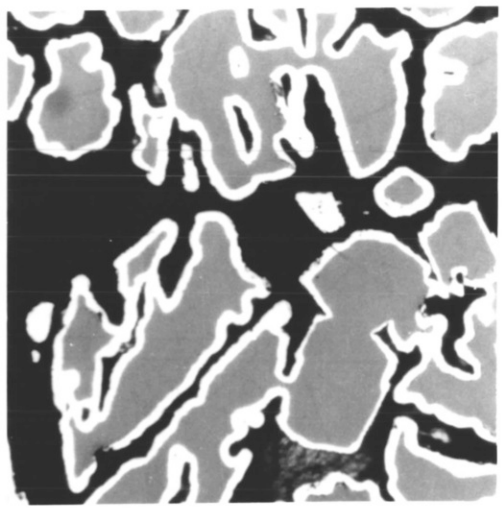

b)

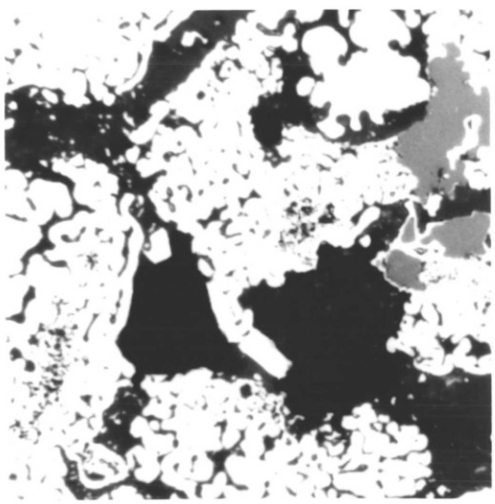

c)

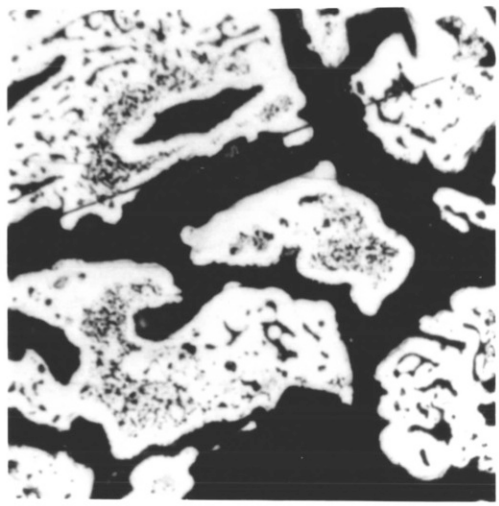

d)

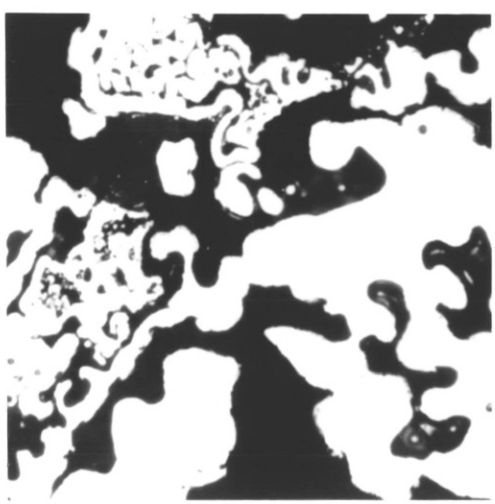

e)

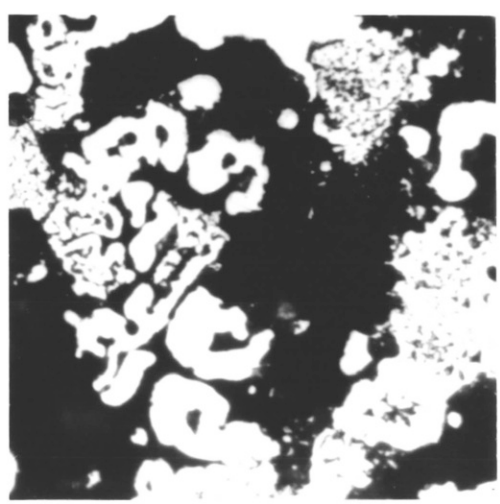

f)

PLATE 29

Micro-structure of iron reduced at a) (1100-950)·T.D. 2% , b) (1100-1050)·T.D.2% and c) (1100-1100)·T.D.2% .

a)

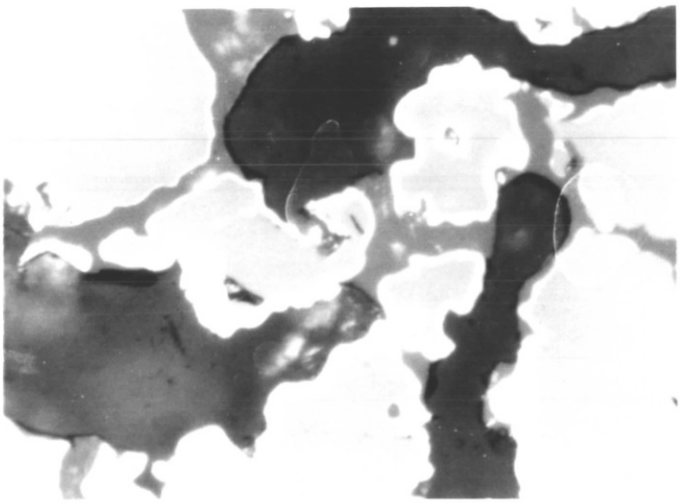

white : iron
light grey : wustite
dark grey : calcium iron magnesium silicate
black : voids

x 320

b)

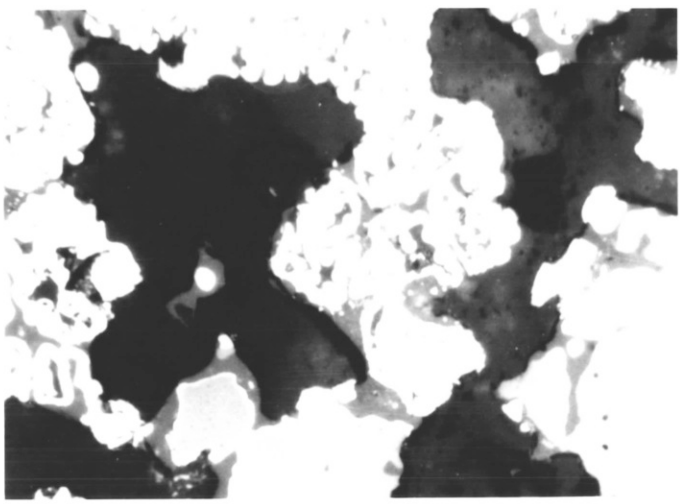

white : iron
light grey : wustite
dark grey : calcium iron magnesium silicate
black : voids

x 320

c)

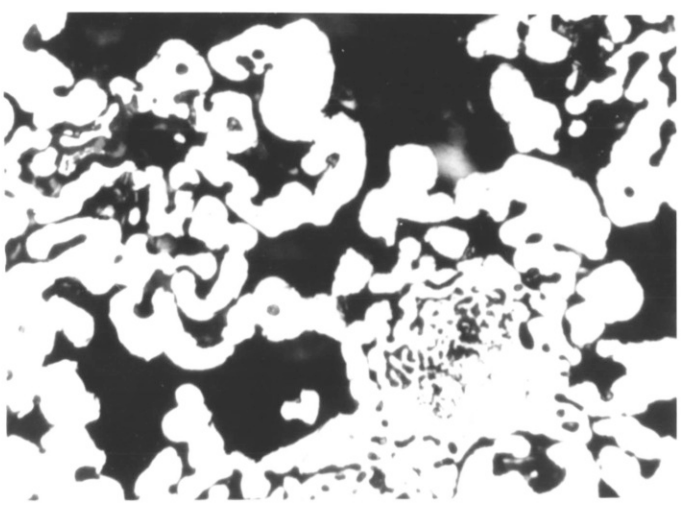

white : iron
dark grey : calcium iron magnesium silicate
black : voids

x 320

PLATE 30

Micro-structure of iron reduced at a) (950-950)·T.D.5% , b)(1050-950)·T.D.5% and c) (1100-950)·T.D.5% .

a)

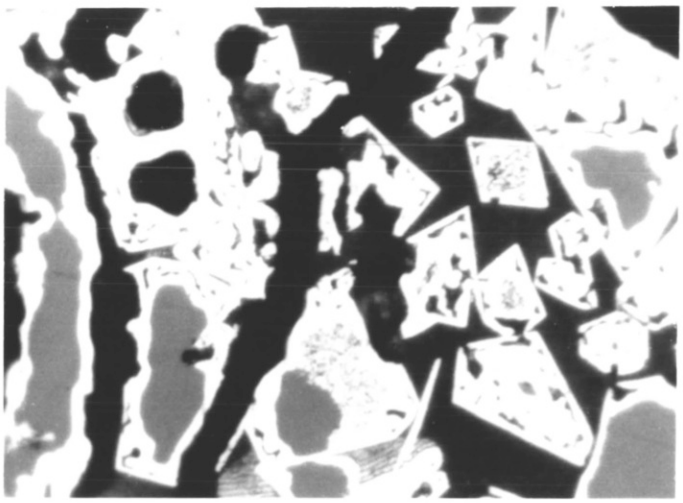

white : iron

grey : wustite (or magnesio-wustite)

dark grey : calcium iron magnesium silicate

black : voids

x 320

b)

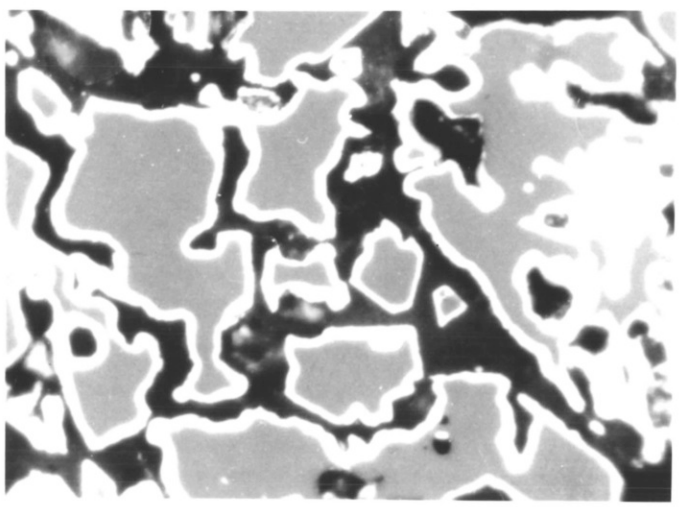

white : iron

grey : wustite (or magnesio-wustite)

dark grey : calcium iron magnesium silicate

black : voids

x 320

c)

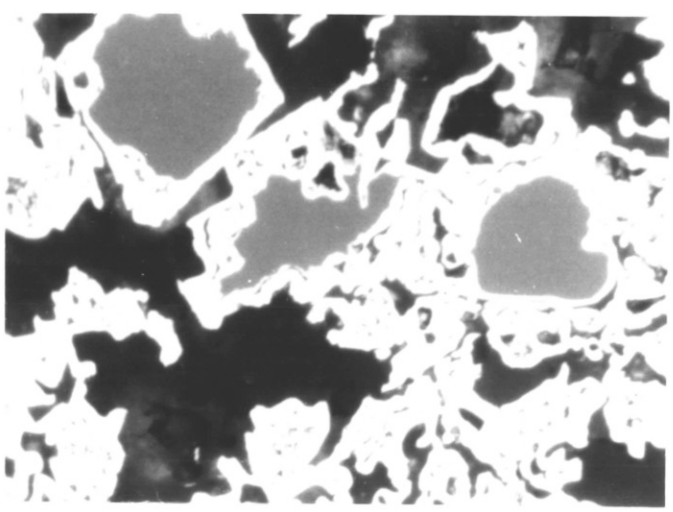

white : iron

grey : wustite (or magnesio-wustite)

dark grey : calcium iron magnesium silicate

black : voids

x 320

the pores.

Plate 37 shows the comparison of iron structures produced by reducing samples having different sintering periods. More liquid phase was observed for long sintering times as expected and the reduction rate was reduced accordingly. Plate 37e shows the iron structure formed from the liquid phase created during reduction as small particles in the liquid phase.

This indicates that the original liquid phase is now solid. This explains the retardation of the overall rate of reduction. As that liquid phase forms during sintering and did not produce any new liquid phase at the reduction temperatures with this composition.

Whitewell dolomite

Plate 38 shows Whitewell dolomite additions sintered at 1300^{o}C in air for 24 hours(a:1%, b:2% and c:5% Whitewell dolomite addition) and the hematite grains in the compacts have similar shapes to those seen with CaO or Thrislington dolomite additions.

When 1% Whitewell dolomite was added, the hematite grains were partially dissolved by the Calcium magnesium silicate (see Plate 38a), however, in the case of 2 and 5% Whitewell dolomite additions, magnesioferrite from the liquid phase was observed(Plate 38b,c) just like Thrislington dolomite additions.

Precipitation of hematite during cooling was also observed in the liquid phase pool(see Plate 38c) similar to CaO additions(see Plate 7c).

Plate 39 and 41 show the microstructual change during re-

TABLE 4.19 EPMA RESULTS

NO	COMPOSITION (Wt.%)						RESULTS
	Fe	FeO	CaO	SiO_2	MgO	MnO	
1	99.81	0	0	0.19	0	0	PLATE 31 a)
2	92.14	0	0.08	0.11	7.68	0	"
3	99.78	0	0	0.22	0	0	"
4	99.17	0	0.16	0.18	0.50	0	PLATE 31 b)
5	99.53	0	0.05	0.21	0.21	0	"
6	0	96.39	0	0.17	3.45	0	"
7	99.74	0	0	0.03	0.23	0	"
8	91.65	0	1.37	6.03	0.95	0	"
9	0	55.13	3.84	34.63	6.40	0	PLATE 31 c)
10	0	56.88	4.02	32.85	6.42	0	"
11	98.41	0	0.11	0.53	0.95	0	"
12	0	97.79	0	0.48	1.73	0	"
13	99.50	0	0	0.14	0.36	0	"
14	0	97.98	0.18	0.25	1.59	0	"

duction at different temperatures. According to the analysis(EPMA results in Plate 44 I, II), the MgO content in the iron grains has different values. In Plate 39a the typical structure is formed from hematite grains and the other structure shown in Plate 39b is that formed from recrystallized or MgO diffused hematite grains(magnesioferrite). In Plate 39a, some grains are already fully reduced whilst nearby grains are only partially reduced. The MgO level shown in Table 4.22 indicates that partially reduced grains have virtually no MgO, however, the remaining type(fully reduced porous grains that have an iron shell outside) shows high MgO(more than 7% of

TABLE 4.20 EPMA RESULTS

NO.	COMPOSITION (Wt.%)						REMARKS
	Fe	FeO	CaO	SiO_2	MgO	MnO	
1	0	93.84	0.05	0.71	5.39	0	PLATE 32 a)
2	93.05	0	0.11	0.61	6.23	0	"
3	85.82	0	0.01	0.33	13.84	0	"
4	0	36.09	10.90	40.82	12.19	0	"
5	0	47.08	6.67	35.27	10.98	0	"
6	96.98	0	0.58	0.73	1.71	0	"
7	0	97.04	0.01	0.40	2.54	0	PLATE 32 b)
8	98.41	0	0.07	0.34	1.18	0	"
9	98.03	0	0.21	0.75	1.01	0	"
10	94.29	0	0.03	0.21	4.14	1.33	PLATE 32 c)
11	99.11	0	0.16	0.32	0.25	0.16	"
12	99.40	0	0.15	0.45	0	0	"
13	99.56	0	0.05	0.11	0.28	0	PLATE 32 d)
14	42.24	21.64	4.50	18.10	13.52	0	"
15	77.99	0	2.32	10.21	9.48	0	"
16	82.65	0	1.37	4.33	1.37	10.28	"
17	0	48.47	4.31	25.42	21.80	0	PLATE 32 e)
18	99.88	0	0.01	0.08	0.03	0	"

MgO) contents in the grains.

This factor illustrates that reduction is more likely to proceed with the grains having MgO than primary hematite (partially reduced iron grains in Plate 39a,b).

Plate 39c shows the type of iron structure that consists of iron reduced from the newly formed liquid phase and MgO containing hematite reduced at 1100°C. In Plate 41, the same mode is shown as in Plate 39. However,

PLATE 31

Micro-structure(SEM) of iron grains reduced at a) (950-1100)·T.D.1% , b) (1050-1100)·T.D.1% and c) (1100-1100)·T.D.1%.

The numbers in the photo-micrographs show the analysed points or areas by EPMA .

a)

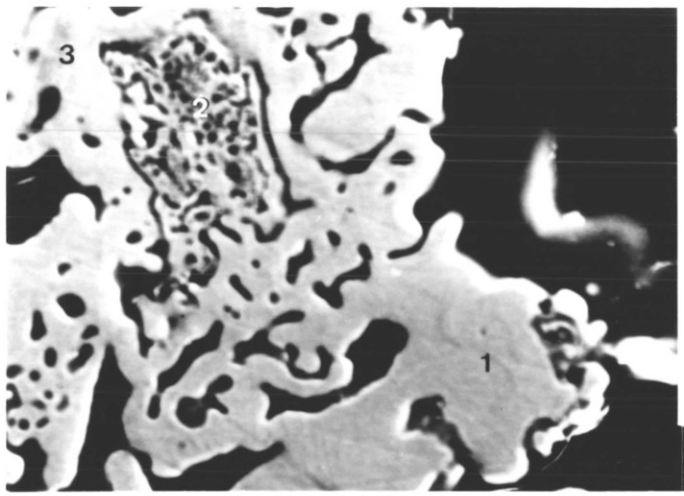

iron : 1,3(white)
iron with magnecia concentrates : 2 (white with microporous black voids)
black : voids

b)

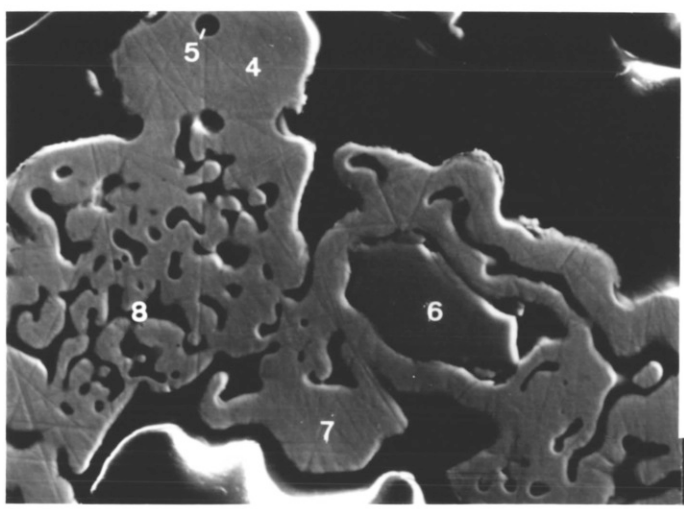

iron : 4,5,7,8 (white)
wustite(magnesiowustite) : 6
black : voids

c)

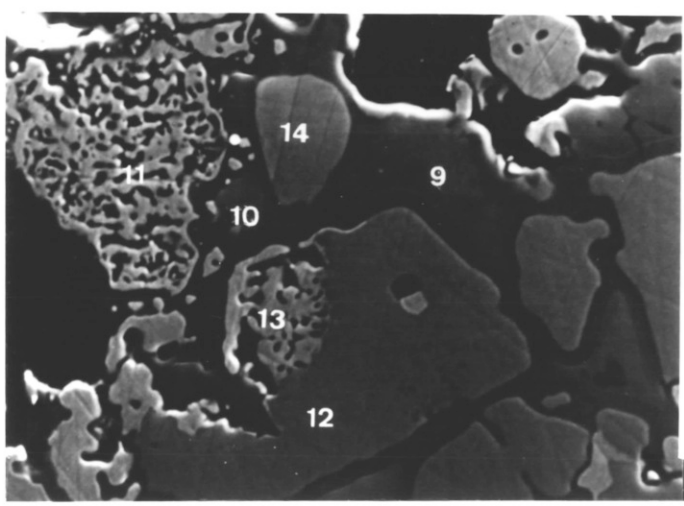

iron : 11,13 (white)
wustite : 12,14 (grey)
calcium iron magnesium silicate :9,10(dark grey)
black : voids

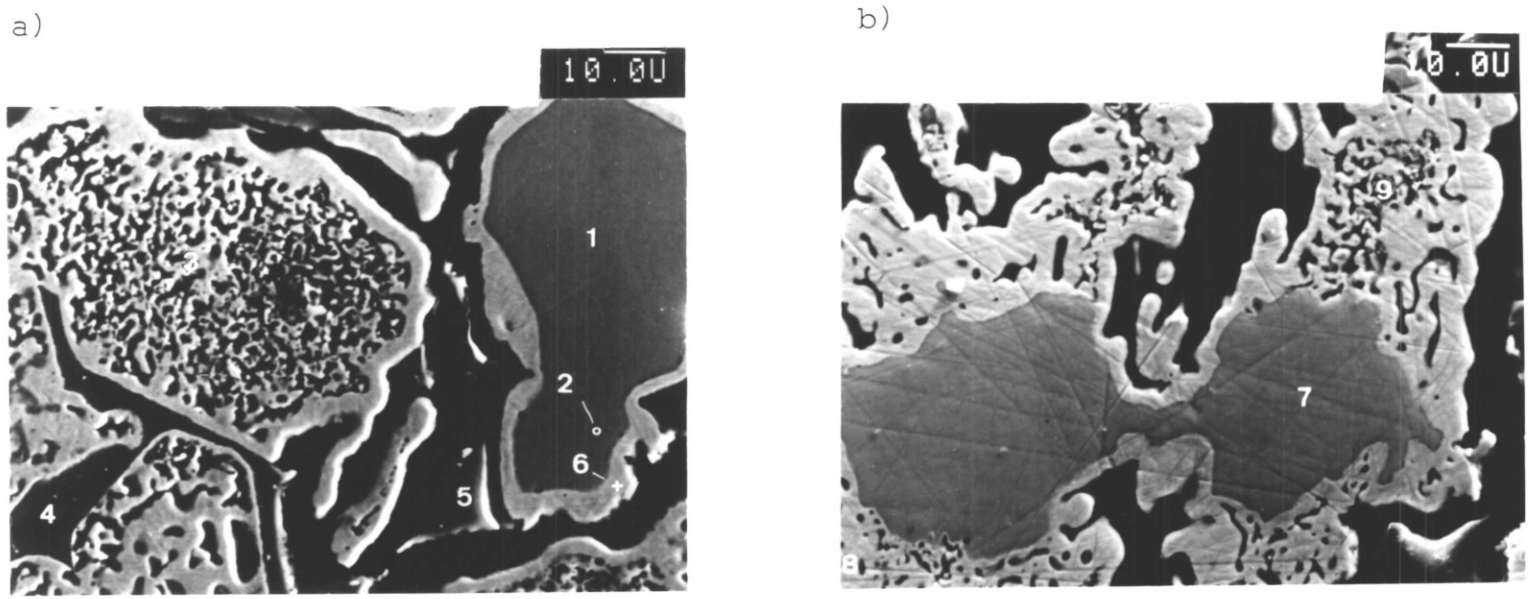

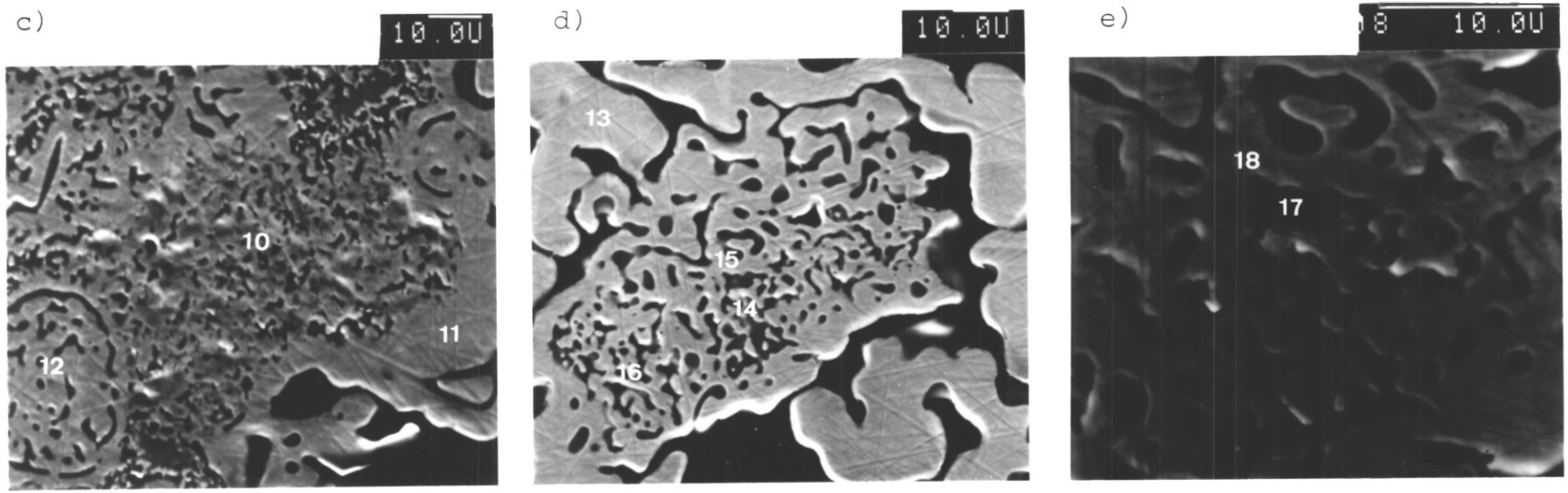

PLATE 32

Microstructure(SEM) of iron reduced at a)(950-1050)·T.D.2% b)(950-1100)·T.D.2% and c,d,e)(1100-1100)· T.D.2% . Picture e)is the magnified area of No. 15 in d).

PLATE 33

Micro-structure of iron reduced at (950-1100)· T.D.2% .
Each micro-structure of iron is a lamellar mixture of ferrite(white) and cementite(darker).
The polished surface was etched with Nital.

a)

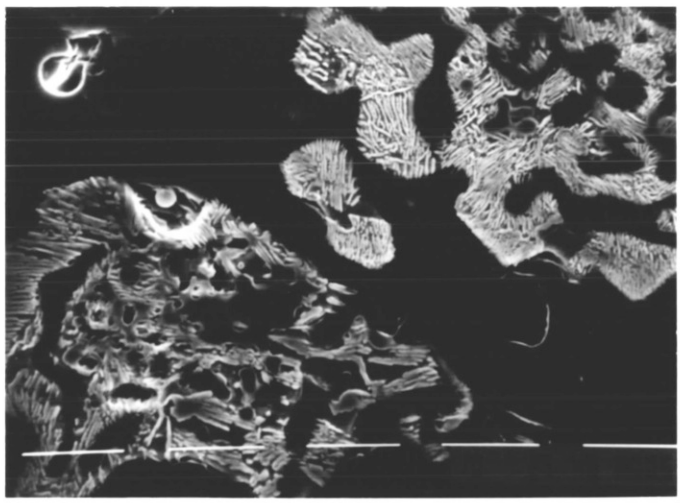

ferrite : white
cementite : dark

b)

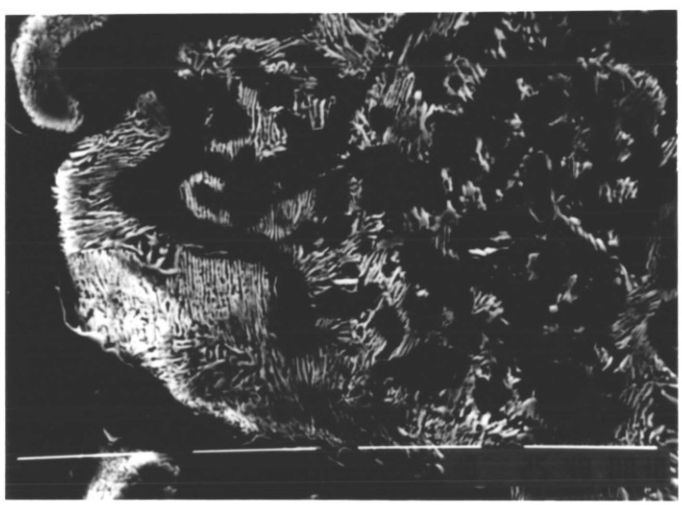

ferrite : white
cementite : dark

c)

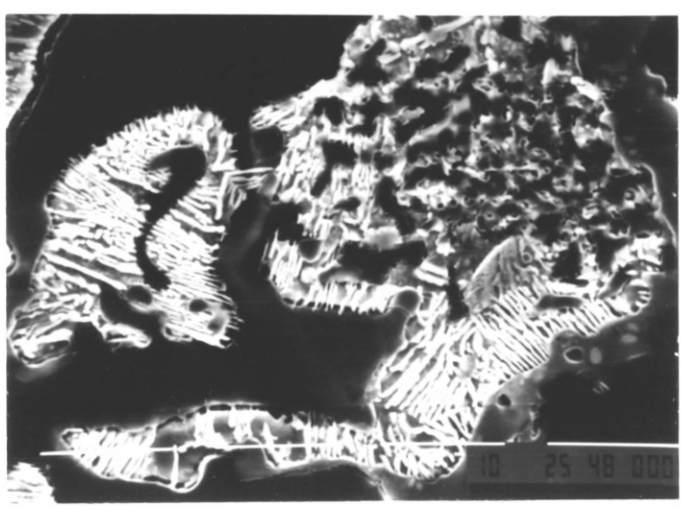

ferrite : white
cementite : dark

TABLE 4.21 EPMA RESULTS

NO.	COMPOSITION (Wt.%)						REMARKS
	Fe_2O_3	FeO	CaO	SiO_2	MgO	MnO	
1	24.95	0	26.38	45.27	2.94	0.46	PLATE 34 I)
2	94.26	0	0.46	0.76	0.75	0.77	"
3	94.38	0	0.47	0.56	3.72	0.86	"
4	25.75	0	25.91	44.94	2.72	0.70	"
5	99.00	0	0.12	0 .61	0.15	0.13	"
6	99.30	0	0.10	0.40	0	0.21	"
7	25.33	0	26.55	45.08	2.62	0.42	"
8	94.83	0	0.19	0.80	3.45	0.72	"
	Fe	FeO	CaO	SiO_2	MgO	MnO	
1	0	94.20	0.04	0.20	5.56	0	PLATE 34 IV)
2	0	93.91	0.15	0.22	5.73	0	"
3	98.76	0	0.32	0.17	0.76	0	"
4	0	19.82	32.04	46.84	1.30	0	"
5	0	93.47	0.16	0.27	6.10	0	"
6	0	25.22	28.48	43.88	2.42	0	"
7	85.92	0	0.17	0.26	13.64	0	"
8	76.86	0	0.07	0.19	21.30	1.58	PLATE 35 I)
9	77.62	0	0.24	0.24	20.78	1.11	"
10	0	22.11	24.81	43.66	8.10	1.32	PLATE 35 II)
11	74.02	0	0	0	22.76	3.21	PLATE 36 I)
12	96.78	0	0.22	0.38	2.61	0.0	"
13	74.42	5.94	0.38	5.09	13.97	0.21	"
14	87.37	0	0	1.01	10.21	1.40	PLATE 36 II)
15	98.73	0	0.04	0.38	0.69	0.17	"
16	95.43	0	1.46	1.65	0.30	1.17	"
17	66.40	12.23	4.70	10.23	4.37	2.07	"
18	95.35	0	0.30	1.30	2.44	0.60	"
19	12.16	35.45	15.33	29.65	5.34	2.05	"
20	99.29	0	0.05	0.29	0.36	0	"
21	96.96	0	0.04	0.24	2.45	0.31	"
22	98.91	0	0.06	0.30	0.56	0.17	"

PLATE 34

Micro-structure(SEM) of I)hematite grains of iron ore compact with 5% Thrislington dolomite. EPMA displays of I)for b)iron, c)calcium and silicon and d)magnesium .

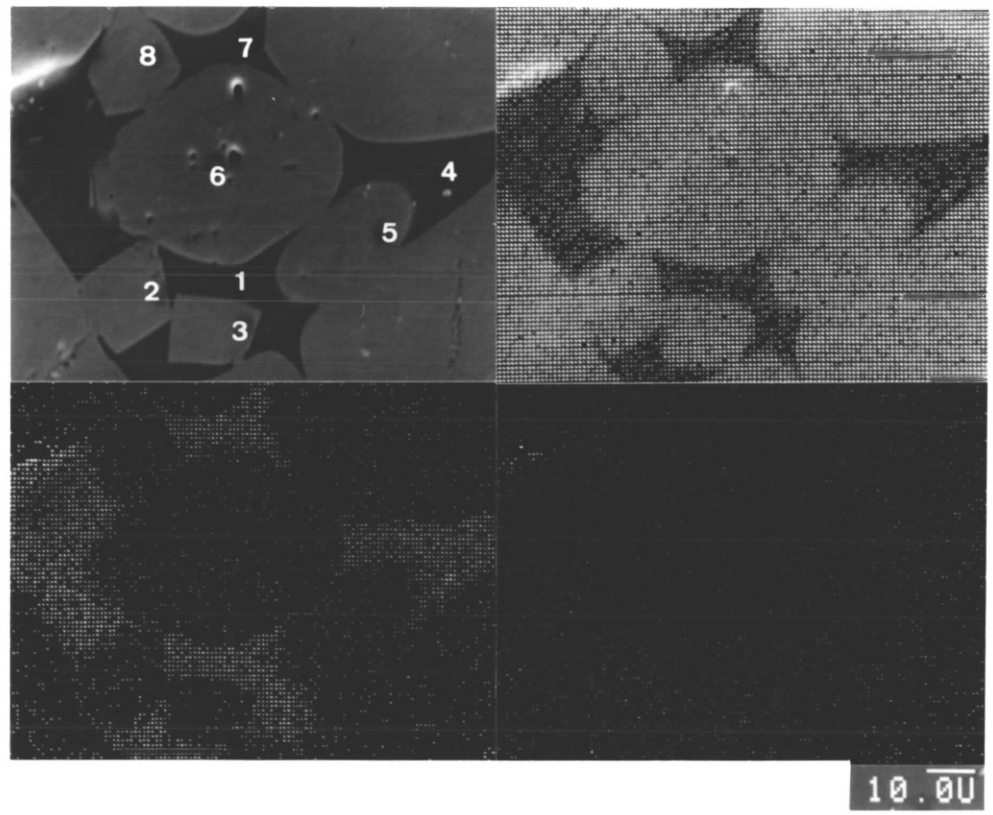

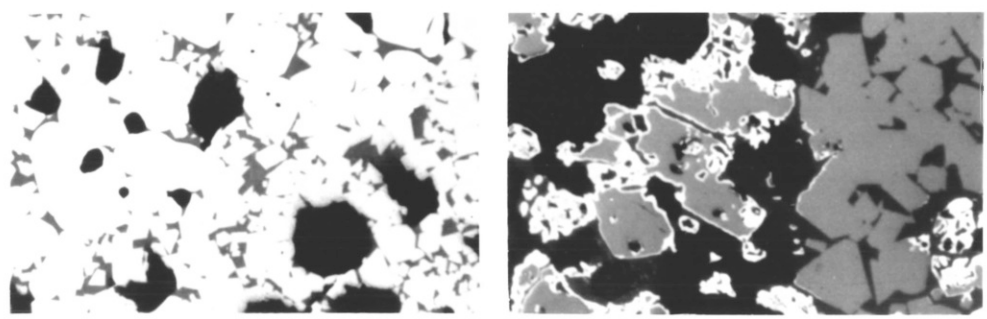

X 98

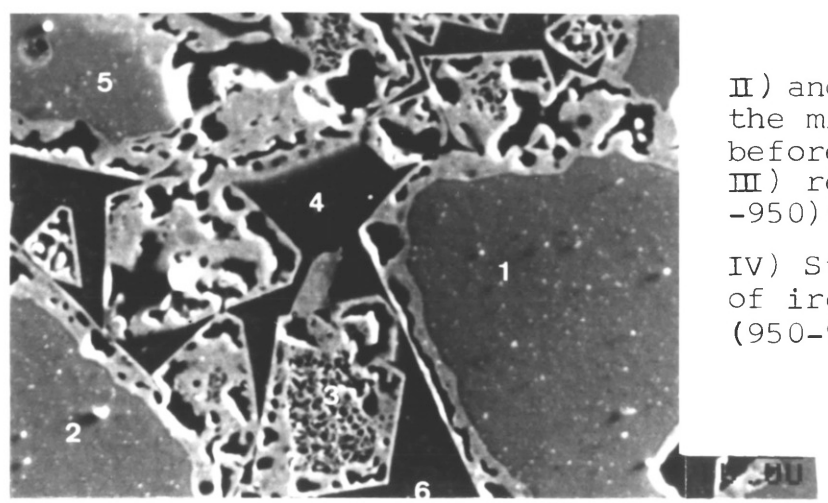

II) and III) show the microstructures before II) and after III) reduction(1100 -950)·T.D.5%.

IV) Structure(SEM) of iron reduced at (950-950)·T.D.5%.

PLATE 35

Micro-structure(SEM) of iron reduced at (950-1050)·T.D.5%,
I)iron grains and II) liquid phase.

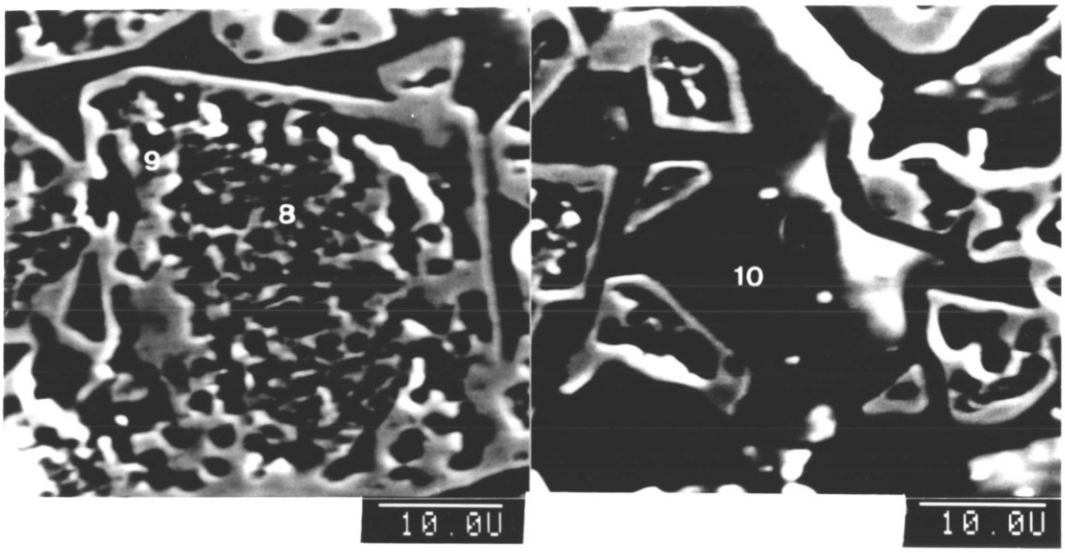

I)

II)

III)

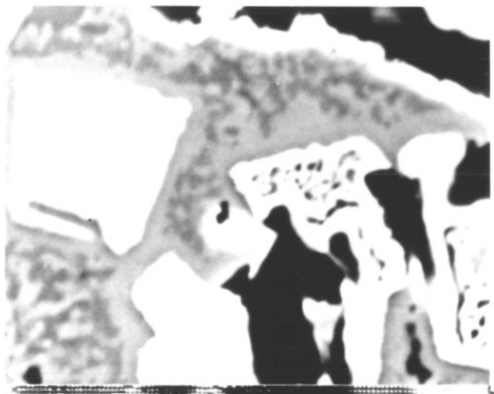

Digital X-ray mapping displays of III)(1050-950)· T.D.5% for b)iron, c)magnesium , d)calcium and e)silicon .

a)

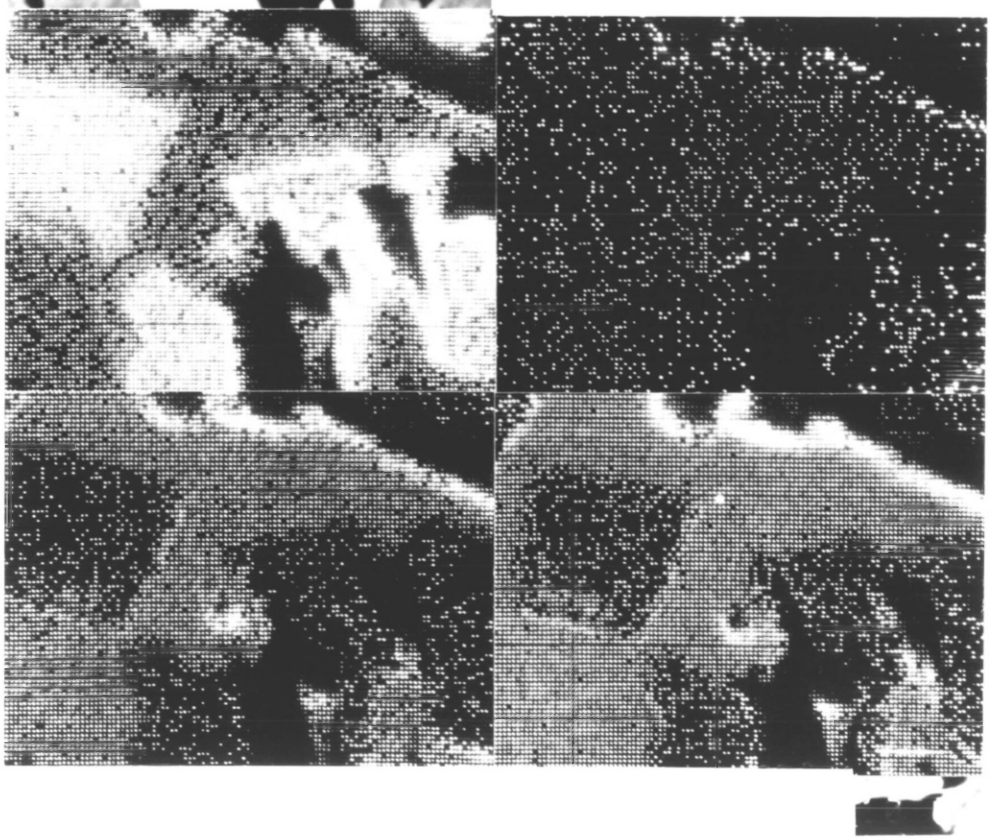

b)

c)

d)

e)

PLATE 36

Micro-structure (SEM) of iron reduced at I) (1050-1100) · T.D.5% and II) (1100-1100)· T.D.5% .

The numbers in I,II) show the analysed points by EPMA and Digital X-ray mapping in II) displays b)iron, c)calcium and silicon and d)magnesium.

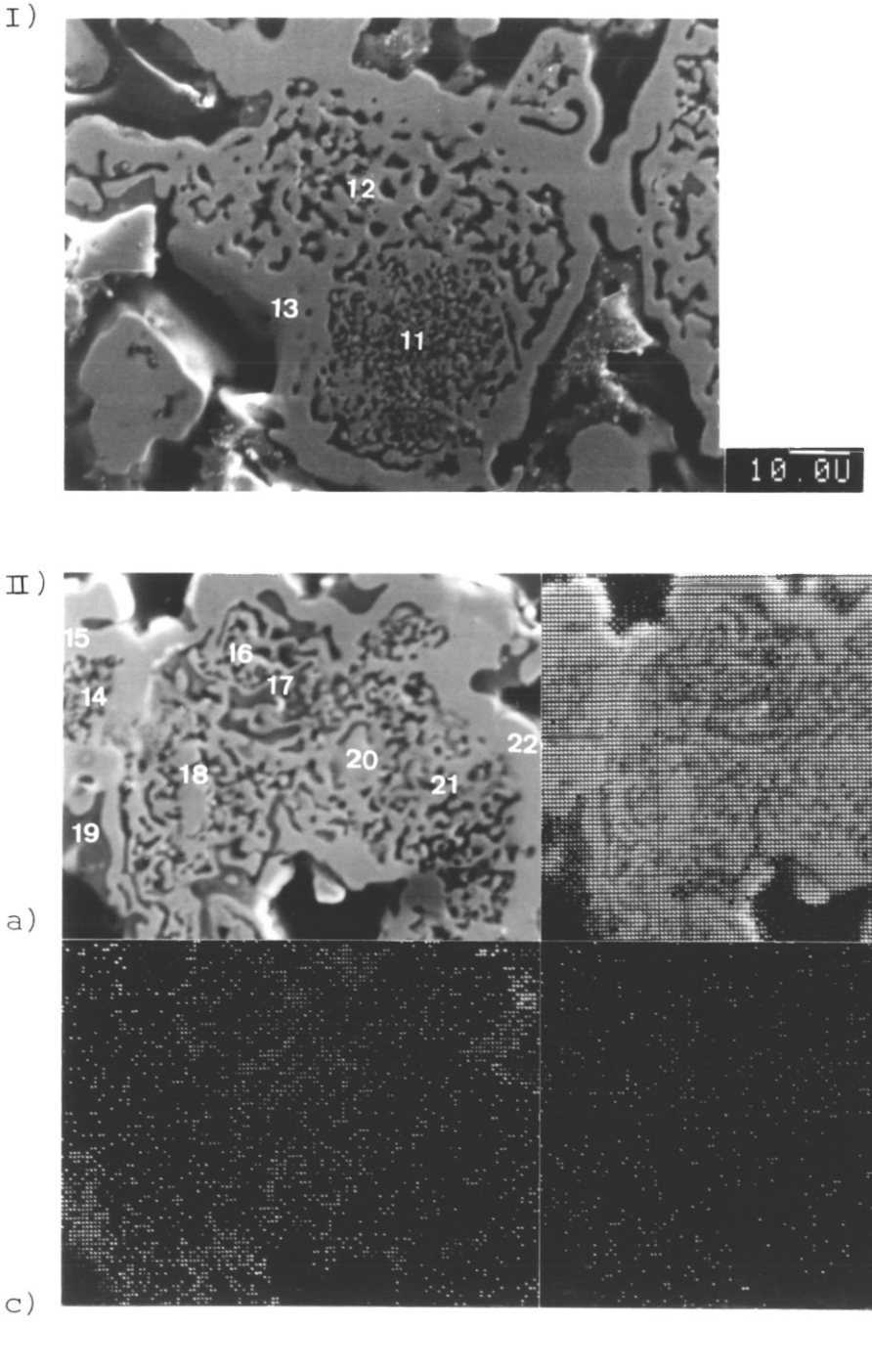

at (1100-950)·W.Do 1% reduction, the wustite grains were reduced very slowly (see Fig. 4.40) caused by the liquid phase newly formed during wustite production. At low temperature, this phase is now solid, iron can not be produced such as that seen in Plate 41c. This liquid phase formed during wustite formation sealed most of the wustite grains and retarded the reduction.

When 2% of Whitewell dolomite was added to the compacts, the reduction rate as shown in Fig. 4.41-43 increased at high temperature (1050, 1100°C). Plate 42a,b shows two distinct iron structures in the same sample reduced at (950-1100)·W.Do 2%. One, reduced from the liquid phase produced at 1100°C and the other from the original liquid phase formed during sintering (dotted shapes are iron). These micrographs show the presence of the original liquid phase on one side and the new liquid phase formed at 1100°C on the other side.

Plate 40 shows the microstructure of iron reduced at (1100-1100)·W.Do 5% and indicates that the reduction was strongly influenced by the liquid phase. In Plate 3, reduction occurred throughout the specimen from the beginning(first observation at 25% reduction).

4.6. GENERAL DISCUSSION

The kinetics of reduction of various types of iron ore compacts, with or without flux materials, were extensively studied. The reduction was carried out with CO in the temperature range 950-1100°C. Many studies have been completed with and without flux additions.

Most of the present work has concentrated primarily on the

PLATE 37

Micro-structure of iron reduced at a)(1100-950)·T.D.5% , b,c)(1100-1050)·T.D.5% and d,e)(1100-1100)·T.D.5% .

Where starting materials of experiments were sintered at 1300°C in air for a,b,d) 24 hours and c,e) 90 hours.

x 320

a)

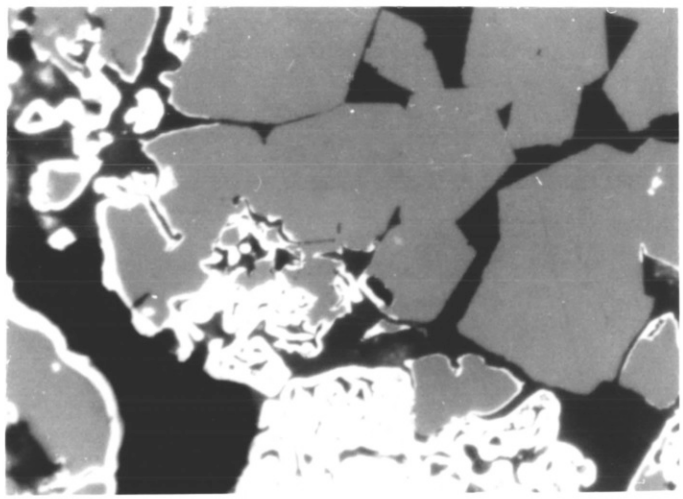

white : iron

grey : wustite (or magnesio-wustite)

dark grey : calcium iron magnesium silicate

black : voids

b)

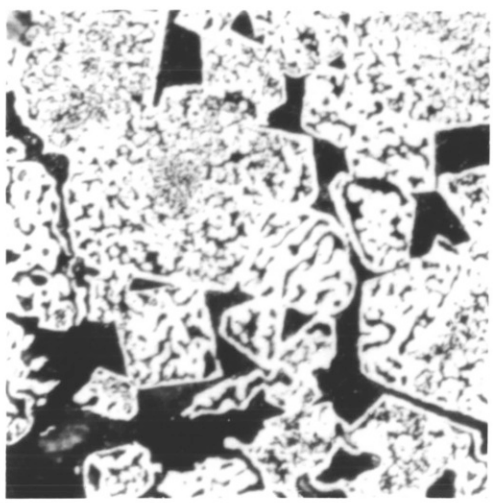

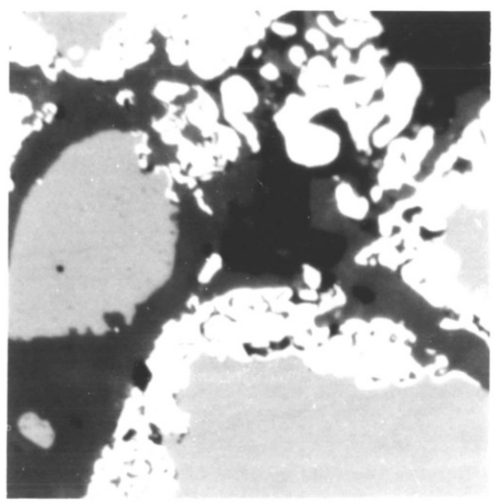

c)

d)

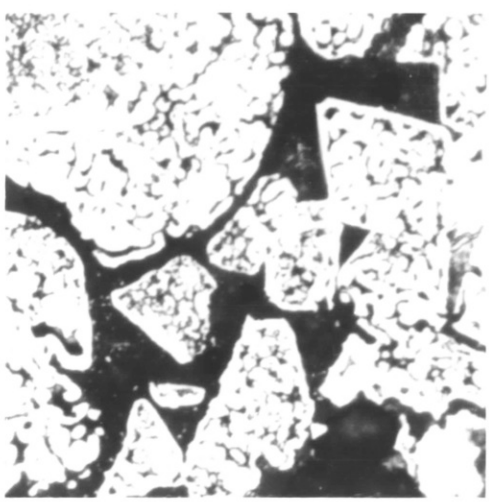

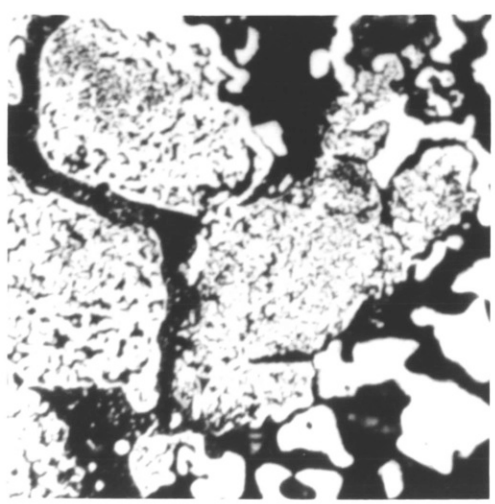

e)

kinetics of reduction with their major interest in understanding the variation of reduction with time and temperature in terms of chemical kinetic or mass transport mechanisms.

Much less attention has been placed on the important microstructural changes which occur upon reduction. It was considered that for some systems, these microstructural factors may be important and could even influence the mechanisms of reaction.

It was decided to place considerable emphasis on these factors in the present study in the hope that some new light might be shed to improve our understanding of these important reactions.

To this end, many of the partially and fully reduced iron oxide samples have been studied systematically using optical and electron microscopy and X-ray diffraction.

The study commenced with the reduction of Carol Lake concentrate powder and compacts. It was intended that this information should act as a basis for comparison with the compacts containing flux additions. The first surprising observation was that the concentrate powder reduced at a lower rate than compacts especially at low temperatures. The experimental procedure was to produce wustite by reduction at a predetermined temperature and while leaving the specimen in the furnace in an inert atmosphere, the temperature was adjusted to the final reduction temperature. The reason for the anomalous behaviour of powder and compacts was found when some samples were examined after wustite production. In all cases with powder specimens,

KEY TO PLATE 38-46

PLATE 39 a) shows that the iron layer produced after reduction has the similar thickness.

PLATE 41 c) showing the iron reduced from the liquid phase.

PLATE 42 the iron structure indicates that more liquid phase formed in the surface than the center of the pellet.

PLATE 47 showing the nucleation iron with various type of flux material.
a) without addition
b)MgO 5%
c)Whitewell dolomite 5% addition

PLATE 48 showing the CaO rich calciowustite precipitats from the wustite grains heated at various temperature and cooled afterwards.

PLATE 38

Micro-structure of hematite grains of iron ore compacts with a)1% Whitewell dolomite, b)2% Whitewell dolomite and c)5% Whitewell dolomite addition, sintered at 1300^{o}C for 24 hours in air.

a)

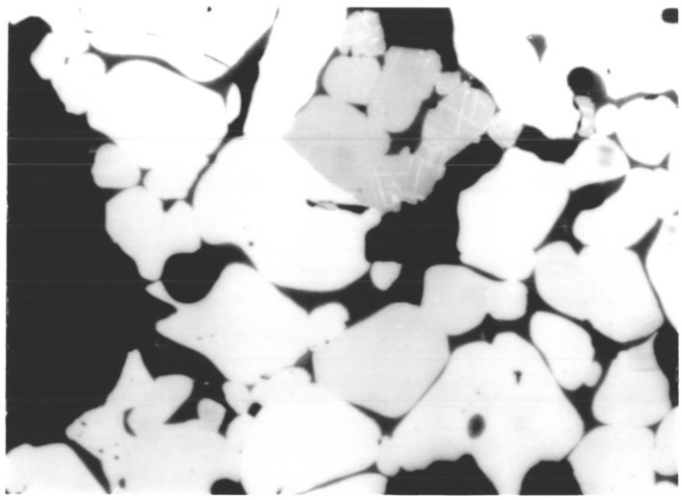

white : hematite
light grey : magnesio-ferrite
dark grey : calcium iron magnesium silicate
black : voids

x 256

b)

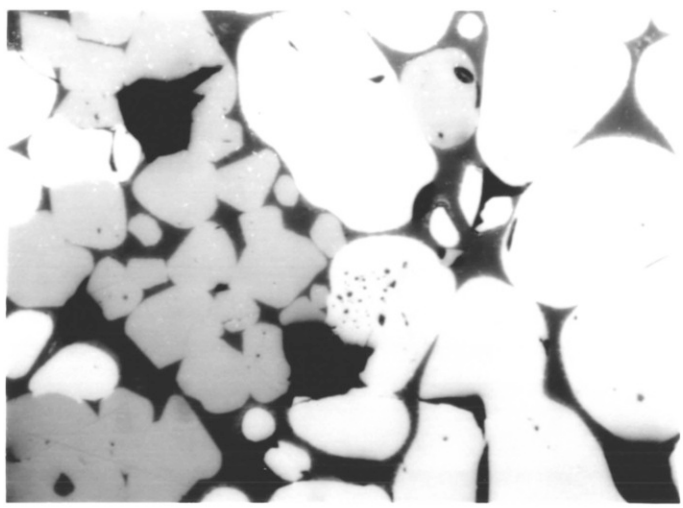

white : hematite
light grey : magnesio-ferrite
dark grey : calcium iron magnesium silicate
black : voids

x 256

c)

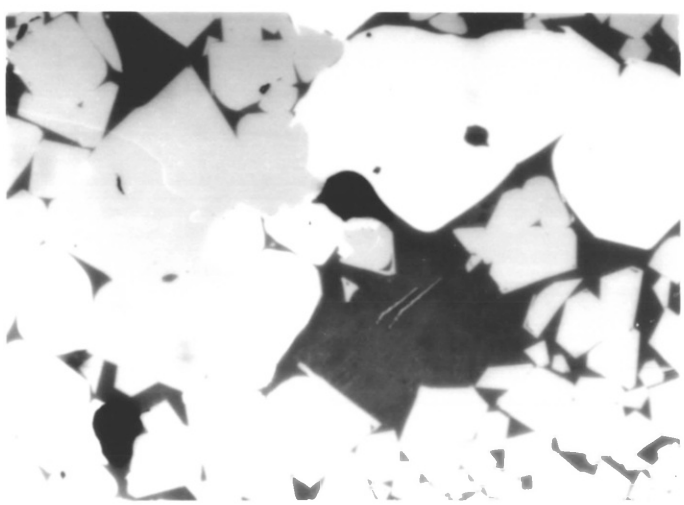

white : hematite
light grey : magnesio-ferrite
dark grey : calcium iron magnesium silicate
black : voids

x 256

PLATE 39

Micro-structure of iron reduced at a) (1050-950)·W.D. 1% , b) (1050-1050)·W.D. 1% and c) (1050-1100)· W.D.1% .

a)

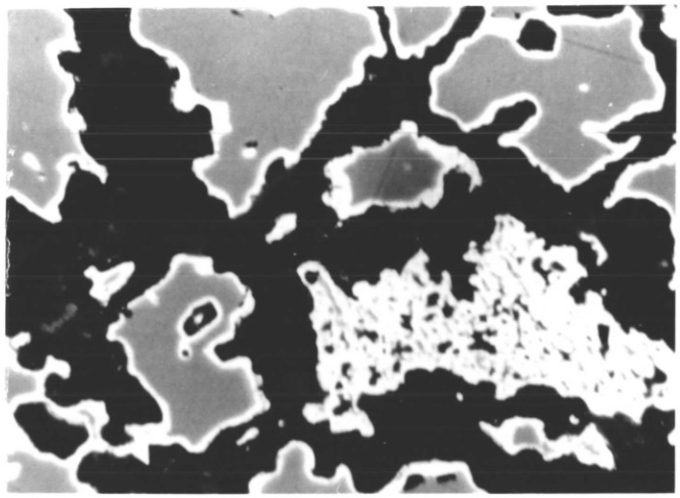

white : iron
grey : wustite
dark grey : calcium iron magnesium silicate
black : voids

x 320

b)

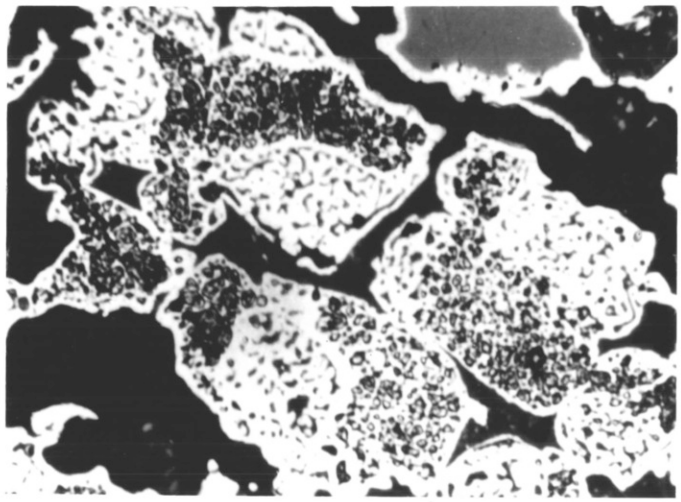

white : iron
grey : wustite
dark grey : calcium iron magnesium silicate
black : voids

x 320

c)

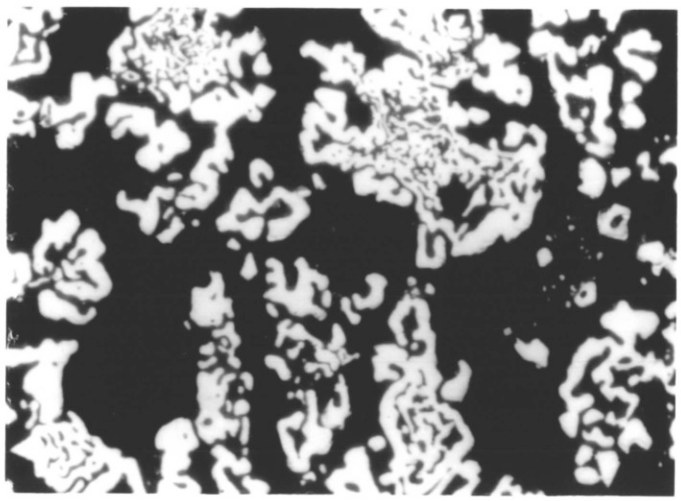

white : iron
dark grey : calcium iron magnesium silicate
black : voids

x 320

it was found that significant sintering had occurred with stronger sintering related to the higher temperature of wustite formation. In this light, the powder results were explicable.

With the compacts contrary to the sintering that had occurred with the powder specimens, swelling and cracking of the pellets had occurred. Particularly severe cracking occurred with the compacts reduced at 1050°C. Upon closer examination of the reduction reaction to wustite, it was noticed that the initial reduction was very slow until sufficient weight loss to be equivalent to magnetite formation occurred. At that time, a very fast final reduction phase happened such that complete reaction happened in an additional 5 minutes. This latter fast sequence obviously occurred after the severe cracking was complete allow easy gas access. It seems that the severe cracking and swelling is related to the early formation of wustite from magnetite. Swelling upon reduction at 950°C and 1100°C was less severe. Unfortunately, there is no explanation for this observation but it was totally reproducible.

With the compacts, the presence of fayalite was observed under all reduction conditions. In addition, the presence of cristobalite was noted. Whereas, cristobalite is the stable silica modification in the temperature ranges studied, its formation from quartz was totally unexpected. In the past, the presence of cristobalite with quartz in these temperature ranges has been attributed to the presence of some amorphous silica in the ore. In the present case, this

PLATE 40

Continuous photo-micrographs of iron ore compacts with Whitewell dolomite 5% addition reduced at (1100-1100)·W.D. 5%, showing a)25%, b)50% and c)75% of reduction proceeded respectively. white(iron), light grey(wustite), dark grey(calcium iron magnesium silicate) and black(voids).
x 57

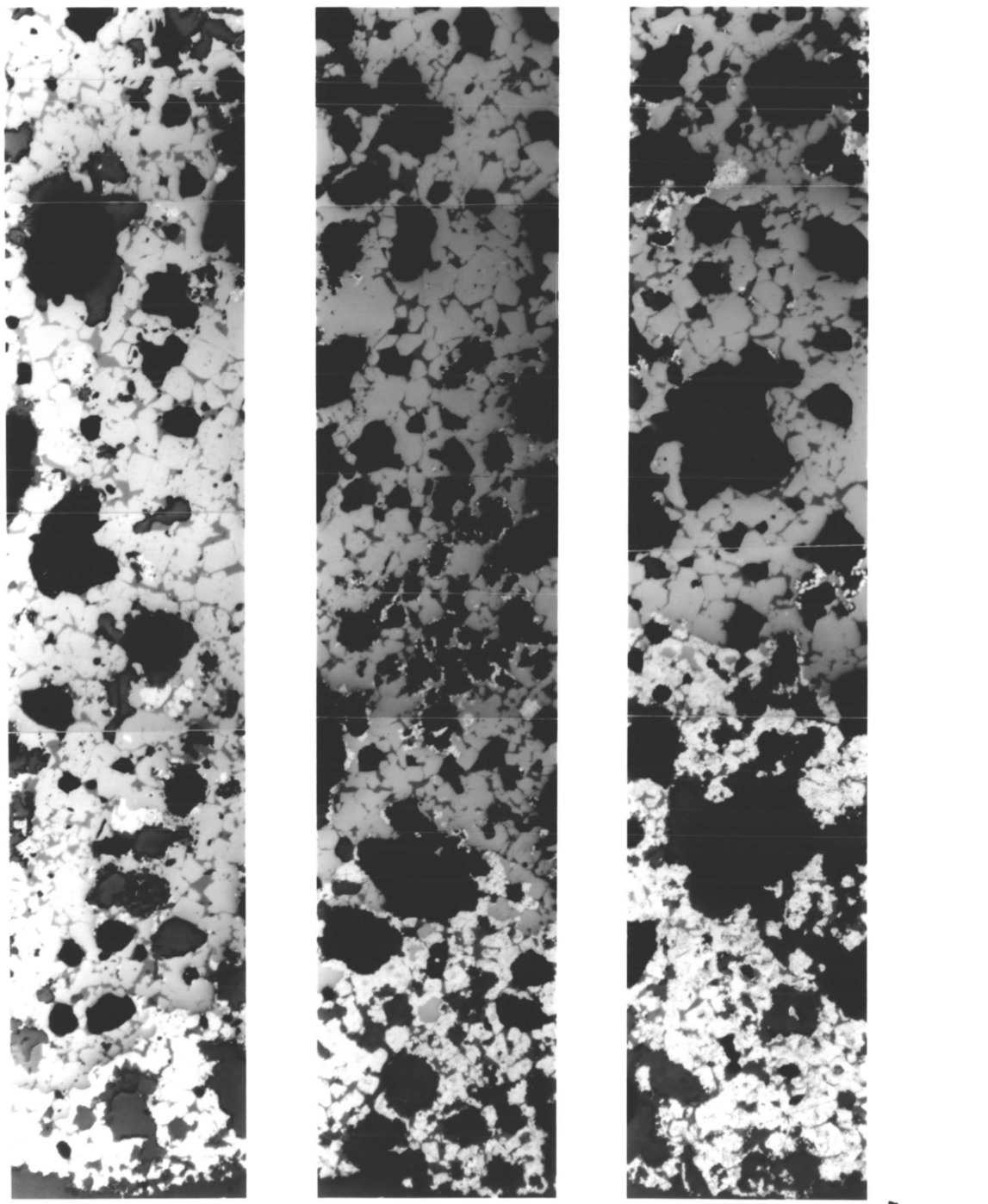

PLATE 41

Micro-structure of iron reduced at a) (1100-950)·W.D.1% , b) (1100-1050)·W.D.1% and c) (1100-1100)·W.D.1% .

a)

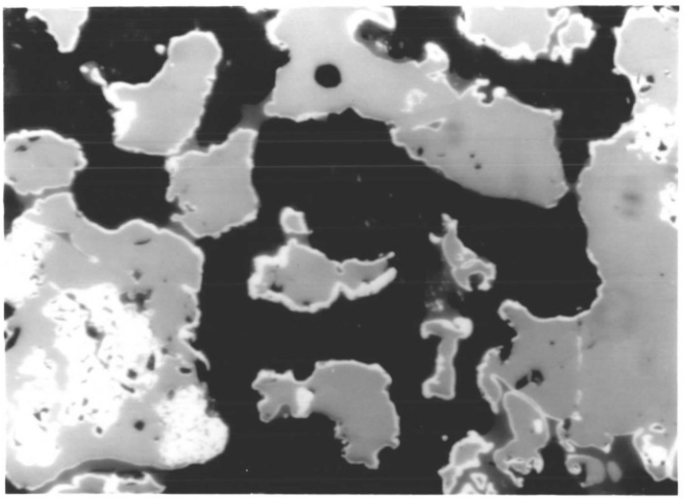

white : iron
light grey : wustite
dark grey : calcium iron magnesium silicate
black : voids

x 256

b)

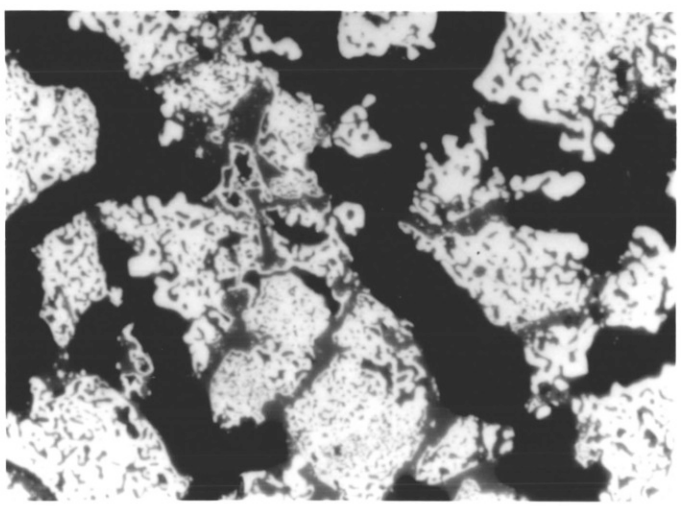

white : iron
dark grey : calcium iron magnesium silicate
black : voids

x 256

c)

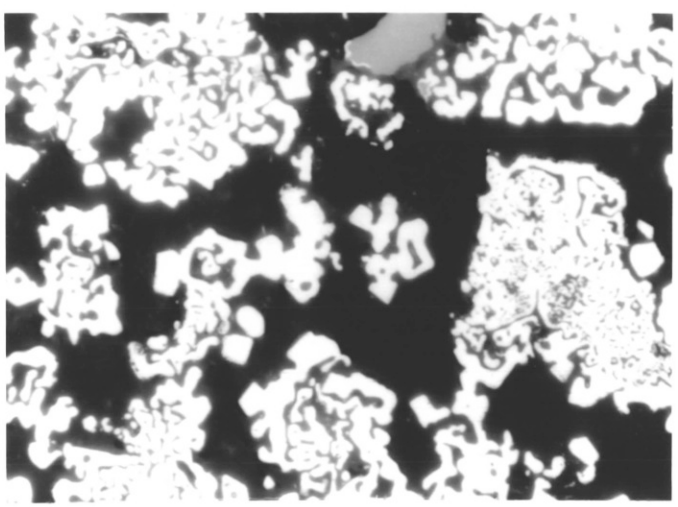

white : iron
dark grey : calcium iron magnesium silicate
black : voids

x 256

PLATE 42

Micro-structure of iron reduced at a,b) (950-1100)·W.D.2% and c) (1100-1100)·W.D.2%.

a)was taken from the middle of the specimen and b)was taken from the surface of the specimen .

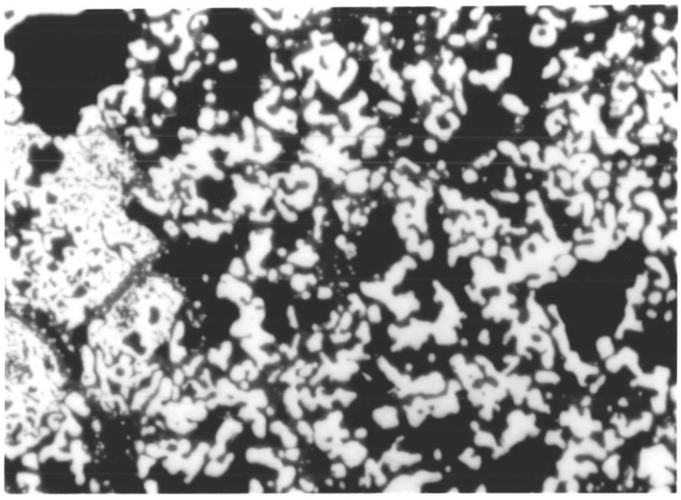

white : iron
dark grey : calcium iron magnesium silicate
black : voids

a) x 256

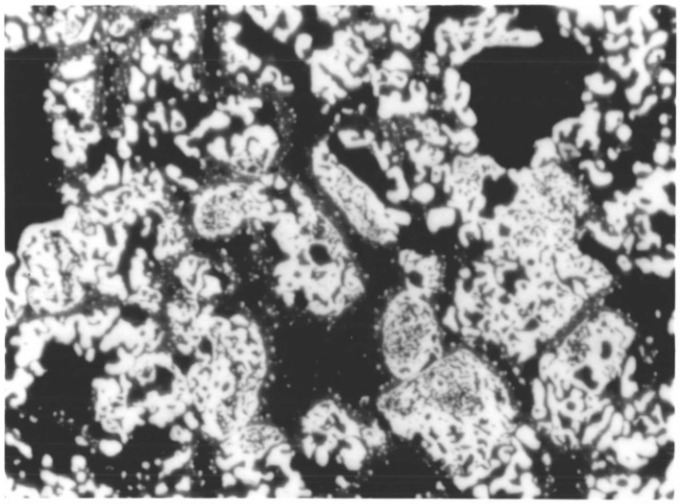

white : iron
dark grey : calcium iron magnesium silicate
black : voids

b) x 256

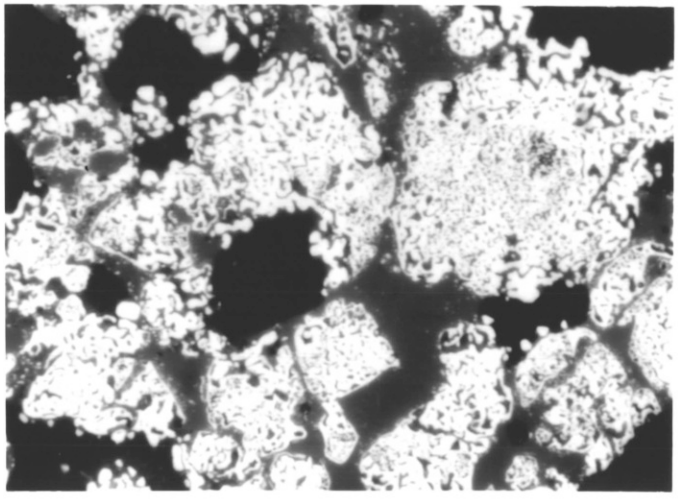

white : iron
dark grey : calcium iron magnesium silicate
black : voids

c) x 256

PLATE 43

Micro-structure of iron reduced at a) (1050-950)·W.D.5% , b) (1050-1050)·W.D.5% and c) (1050-1100)·W.D.5%.

a)

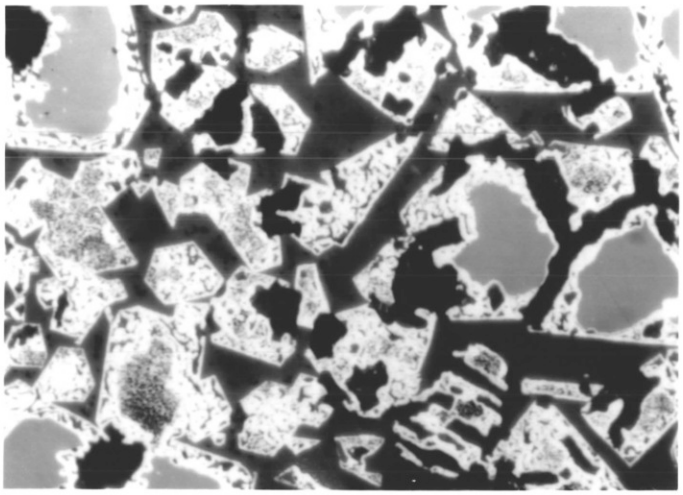

white : iron
light grey : wustite (or magnesio-wustite)
dark grey : calcium iron magnesium silicate
black : voids

x 128

b)

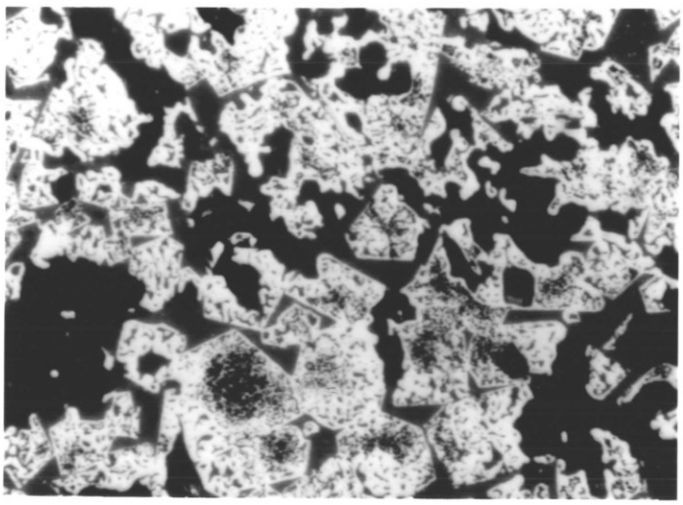

white : iron
light grey : wustite
dark grey : calcium iron magnesium silicate
black : voids

x 128

c)

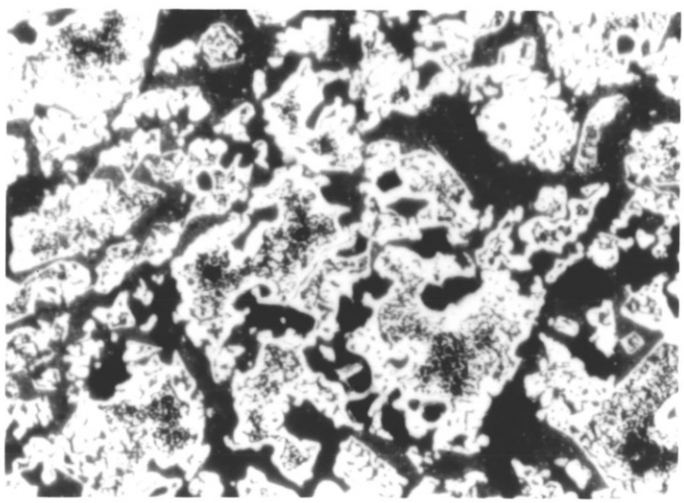

white : iron
dark grey : calcium iron magnesium silicate
black : voids

x 128

is not totally acceptable as in several cases, the cristobalite appears to form at the expense of quartz. Even accounting for the fact that some cristobalite forms by reduction of fayalite after long reaction times, this process can not account for all the observations. It was considered that oxygen potential may be the critical factor in the transformation especially as the literature data are related to quartz-cristobalite conversion in air at high temperatures. However a few experiments with differing oxygen potential failed to confirm the hypothesis. However, it does appear that the presence of iron oxide impurity can in some way catalyse the transformation but much more detailed study is required.

For samples of Carol Lake concentrate, the studies of the rate of reduction fell into two distinct groups. The experiments in which the final reduction in CO was carried out at 1050°C and 1100°C and those at 950°C. At the higher temperatures, rapid reduction occurred for about 10 minutes with little temperature effect followed by a slower reduction process until complete reaction was achieved. At 950°C, the reaction was much slower and after about 20 minutes a slower almost linear rate was observed. Theses results seemed to indicate that a distinct change in mechanism occurred between 950°C and 1050°C. Some understanding of the variation in reduction rates came from the optical microscopic studies. It was noted that even after 25% reduction at all temperature, reduction was proceeding throughout the specimen indicating access of reducing gas to the centre fo the specimen. However

TABLE 4.22 EPMA RESULTS

NO	COMPOSITION (Wt.%)						REMARKS
	Fe	FeO	CaO	SiO_2	MgO	MnO	
1	0	19.91	10.77	64.73	3.19	1.39	PLATE 44 I)
2	0	44.68	9.21	43.59	1.22	1.30	"
3	0	97.89	0	0.51	0.41	1.18	"
4	0	97.05	0.03	0.42	1.24	1.26	"
5	0	98.36	0	0.25	0.30	1.09	"
6	97.62	0	0.08	0.05	1.23	1.01	PLATE 44 II)
7	89.05	0	0.44	1.54	8.29	0.67	"
8	92.56	0	0.20	0	5.37	1.87	"
9	98.17	0	0	0	1.68	1.56	"
10	93.40	0	0.25	1.03	4.05	1.27	"
11	71.06	0	0.03	0.47	8.79	19.64	"
12	83.12	0	0.14	0.01	7.77	8.96	"
13	99.70	0	0	0.10	0	0.20	"
14	99.01	0	0.13	0.61	0.13	0.11	"
15	90.01	0	0.03	0.61	7.56	1.78	"
16	0	52.23	4.41	31.45	9.12	2.78	"
17	0	99.55	0.05	0.25	0	0.14	"

it was noticed that nucleation of iron was only spasmodic over the wustite grain surface. At higher temperatures, nucleation over the whole surface of the wustute grains throughout the specimen was achieved in a few minutes. However at 950°C, this state of affairs was not achieved until more than 20 minutes had elapsed. This problem of nucleation of iron on the wustite grain surface was important in the kinetics of reaction. In addition, the iron formed at 1050°C and 1100°C was much more porous in

PLATE 44

Micro-structure(SEM) of iron reduced at I)(950-950)·W.D.1% and II) (950-1050)·W.D.1% .

Digital X-ray mapping displays of I) and II) for b)iron , c)calcium, silicon and d)magnesium.

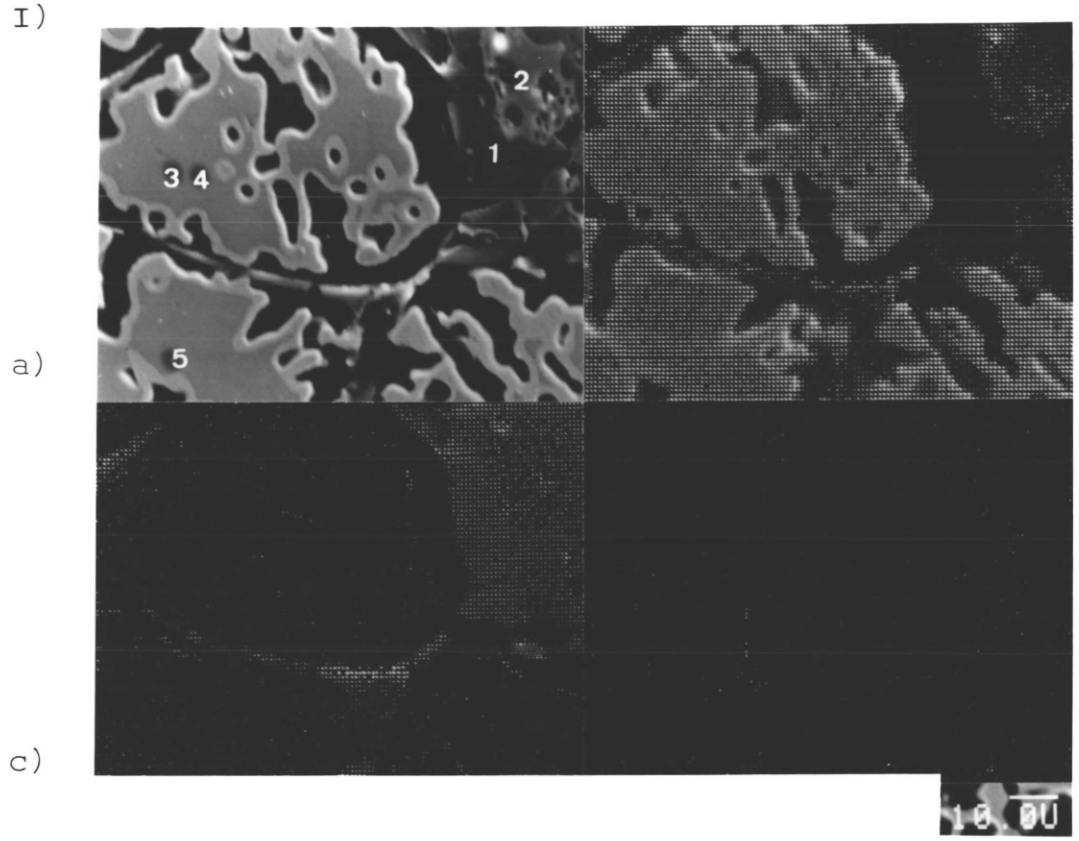

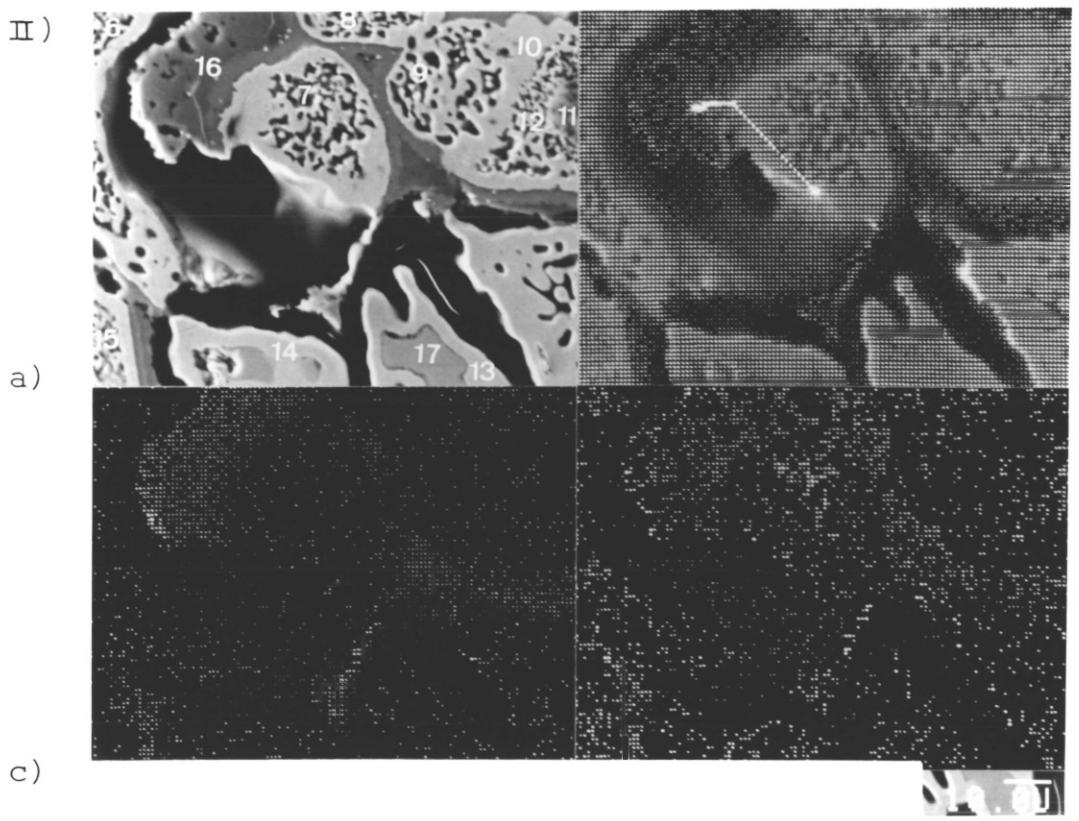

TABLE 4.23 EPMA RESULTS

NO.	COMPOSITION (Wt.%)						REMARKS
	Fe	FeO	CaO	SiO_2	MgO	MnO	
1	82.86	6.47	1.47	5.41	2.43	1.36	PLATE 45 I)
2	79.11	7.65	1.52	6.40	3.40	1.92	"
3	84.67	5.80	1.58	4.85	1.75	1.35	"
4	0	1.59	0.32	98.04	0	0.04	"
5	0	1.99	0	97.69	0.29	0.04	"
6	63.70	14.69	3.31	12.29	3.79	2.22	"
7	97.99	0	0	0.19	1.22	0.61	PLATE 45 II)
8	72.40	0	0.18	0.37	22.77	4.28	"
9	0	44.69	6.03	35.37	9.82	4.10	"
10	0	50.83	8.28	30.54	6.82	3.52	"
11	84.57	0	0.04	0.18	9.16	6.06	PLATE 46 a)
12	98.34	0	0.20	0.14	0.35	0.96	"
13	81.53	0	0.16	0.17	13.41	4.73	"
14	0	31.23	14.57	45.77	6.56	1.88	"
15	99.24	0	0	0.04	0.57	0.14	"
16	87.30	0	0.19	0.29	9.45	2.77	"

nature than that produced at 950°C. As expected the samples at 1100°C were more porous than those at 1050°C. At 950°C when complete iron nucleation had occurred on all the wustite grains, this iron layer appeared to be quite dense. This time essentially coincides with the onset of the apparent linear reduction rate. It seems probable that the reduction becomes controlled by oxygen diffusion through the dense iron layer, a process which is known to be considerably slower than porous gas diffusion or surface chemical kinetics which probably control at the

PLATE 45

Micro-structure(SEM) of iron reduced at I,II) (950-1100) ·W.D.1% .

The numbers in I)and II)a) show the analysed points by EPMA .

Digital X-ray mapping displays of II) for b)iron, c)calcium, silicon and d)magnesium .

I)

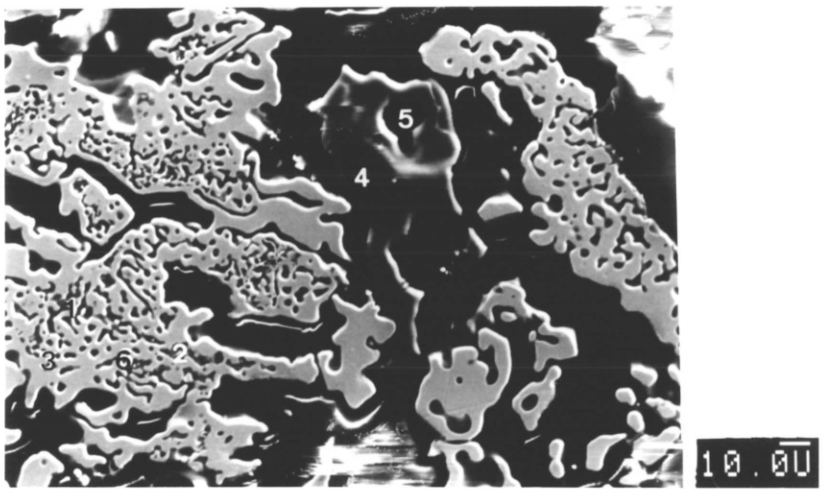

II)

a)

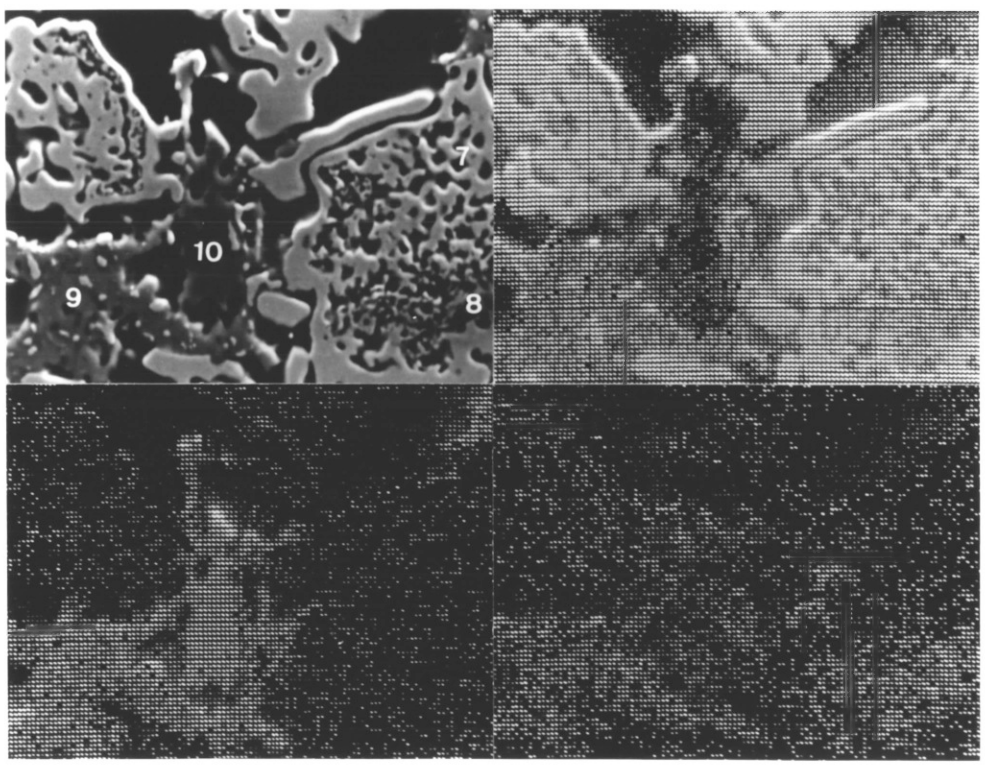

b)

c)

d)

PLATE 46

Micro-structure(SEM) of iron reduced at (1050-1050)·W.D.1%.

Digital X-ray mapping displays of a) for b)iron , c)magnesium, d)calcium and e)silicon.

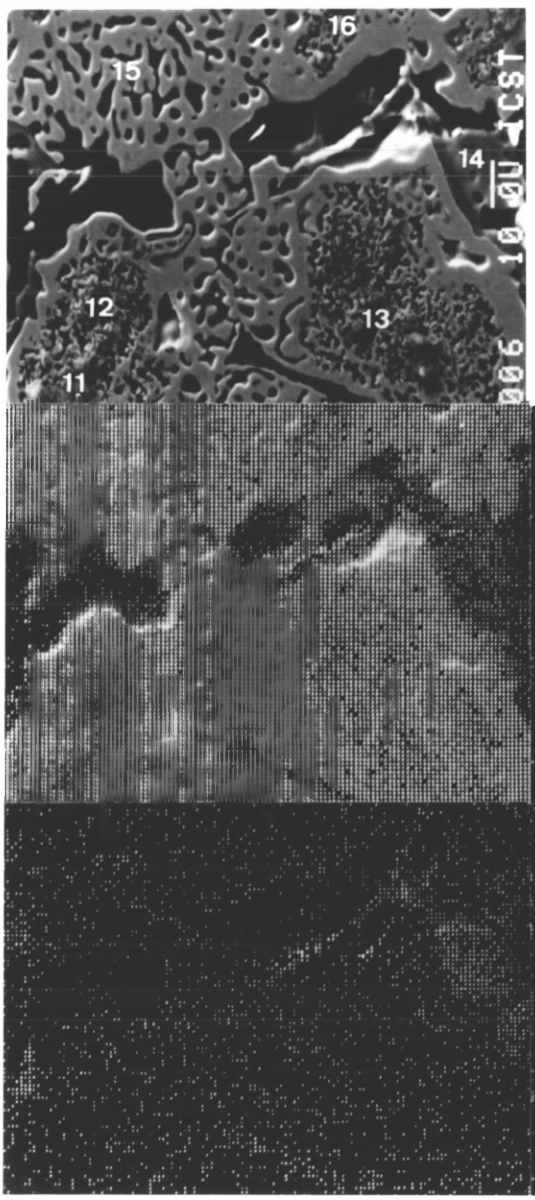

a)

b)

c)

d)

e)

higher temperature.

With lime additions to the iron oxide, a liquid phase was observed to form at the sintering temperature of 1300°C in air. The volume of liquid increased as the quantity of lime increased as expected.
Optical micrographs of the specimens showed that the iron oxide grains were rounded as dissolution into the liquid phase proceeded. Inspection of the $CaO-SiO_2-Fe_2O_3$ phase diagram showed the presence of a liquid phase field near $CaO \cdot Fe_2O_3$ and initially it was thought that the liquid must be of this composition. It was a surprise therefore when the X-ray diffraction analysis showed the absence of calcium ferrite and quartz but the presence of wollastonite. Another inspection of the phase diagram revealed that a liquid phase field existed in the pseudowollastonite region at this temperature. Obviously the liquid formed on sintering was associated with this area.
Thus lime reacts preferentially with silica even though its concentration is small and forms a liquid phase in the pores of the pellet influenced the subsequent reduction rates.
In general with the 5% CaO additions, some similarity in the rates was observed with the original pellets with the rates slightly lower due to a reduction in gas access due to the presence of the silicate phase in the pores.
However, for specimen with 1 and 2% CaO addition in which wustite was produced at 1100°C, a significant decrease in rate of reduction was observed at low temperatures.
The use of EPMA analysis gave results which showed that

the liquid region associated with 5% CaO additions were related to the intial liquid formation on sintering.
With 2% CaO additions the analysis of the apparent liquid by EPMA showed the presence of a liquid composition equivalent to the small liquid phase field associated with the region between $CaO \cdot FeO \cdot SiO_2$ and $FeO \cdot SiO_2$ which was liquid at $1100^{o}C$.
The presence of this new liquid region affected the reduction kinetics with 1 and 2% CaO additions.
With 5% CaO additions, X-ray diffraction analysis revealed the presence of the phase $CaO \cdot FeO \cdot SiO_2$ during the late stages of reduction at which time it was reduced and formed wollastonite. At this stage in the reduction excessive carbon deposition occurred and strong cementite was formed.
The lime additions broadly cause a reduction in rate up to 2% due to the formation of a liquid phase on forming wustite at $1100^{o}C$. Up to this composition, nearly all the lime is associated with the liquid phase.
For 5% CaO additions, a small increase in reduction rate is observed. This is probably due to the presence of CaO in solid solution in the wustite phase.

When MgO was added as flux addition, the results were contrary to the effect of lime. Whereas no liquid phase was formed on sintering as expected as the liquidus temperatures in the ternary system are too high, substantial quantities of magnesioferrite were observed with unchanged silica. As lime has apparently reacted preferentially with silica, and since magnesium silicate has a more negative free energy of formation than magnesium

ferrite, this was not expected. However the formation of magnesioferrite is obviously due to the preponderance of hematite present and the well known effect of magnesia forming solid solutions with iron oxides. In addition, the ease of diffusion of the small magnesium within the iron oxide lattice also helps.

One interesting observation was the presence of hematite precipitation in the magnesio-ferrite grains. The precipitation occurs because the range of stability of the magnesioferrite phase moves to higher magnesia contents at lower temperatures. Obviously on cooling, segregation occurs and the hematite seems to form preferentially on sub-grain-boundaries or in a specific crystallographic direction. This precipitation of hematite possibly plays an important role in the reduction.

Upon reduction, magnesia additions give faster rates at all temperatures than the Carol Lake compacts or these with lime additions. The rate of reduction at all temperatures increases with increasing magnesia content. The most significant effect is that due to 5% addition at 950^{o}C. The presence of phases in the olivine range are observed by X-ray diffraction with increasing magnesia additions.

Near to complete reduction, the phase Clinoenstatite is characterised.

As the magnesia content increases, the proportion of magnesioferrite in the specimen increases and is proportional to the rate of reduction, i.e. faster reduction is observed with great proportions of magnesioferrite in the

sintered material. Upon reduction to wustite, these grains form magnesiowustite. The metallographic examination shows that complete nucleation of iron round each magnesiowustite grain occurs very quickly in contrast to the normal wustite grains especially at low temperatures.

It is felt that this easy nucleation may be related to the tendency of magnesioferrite to segregate such that a thin film of hematite is formed at the surface. Since the wustite production is achieved in about 15 minutes, it seems probable that magnesium equilibration may not be completely achieved in the magnesiowustite phase.

The nucleation of iron from a thin film of wustite at the edge of each grain is then assisted by a surface energy term. This rapid nucleation on magnesiowustite grains is responsible for the significant increase in rate of reduction particularly at low temperatures. The magnesiowustite grains reduce rapidly with the formation of a dense iron shell at the outside of each grain.

EPMA evidence is provided which shows clearly that magnesia diffuses away from the iron rim. It is obvious that magnesia diffusion is very rapid. After an iron layer about 4-5 μm is provided, the reduction progresses with the formation of a porous iron and magnesia mixture in the centre of the grains.

Because of the dense nature of the iron, significant carbon deposition occurs in the specimens before complete reduction is achieved. The addition of magnesia leads to rapid reduction because no liquid phase is formed in

PLATE 47

Micro-structure of partially reduced iron, showing a)25% and b)50% reduced iron ore compacts(without addition) , c) and d)50% reduced iron ore compacts(MgO 5% addition) and e)25%, f)50% reduced iron compacts(Whitewell Dolomite 5% addition). x 256

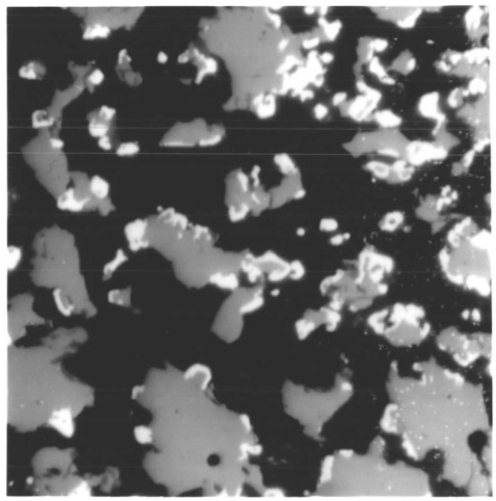

a)

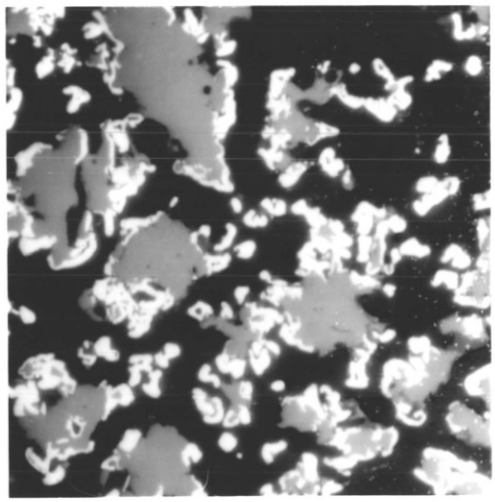

b)

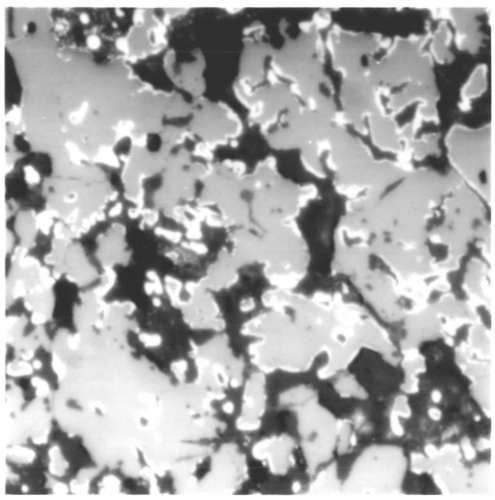

c)

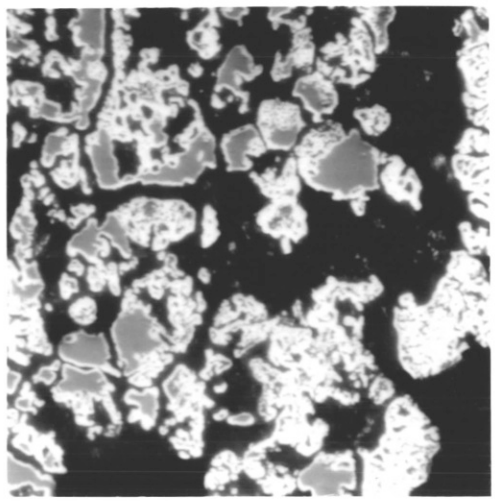

d)

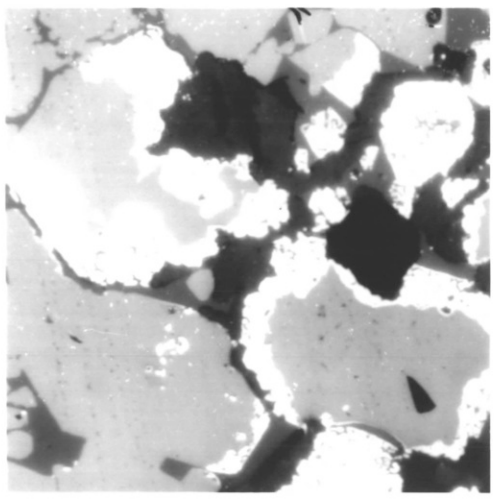

e)

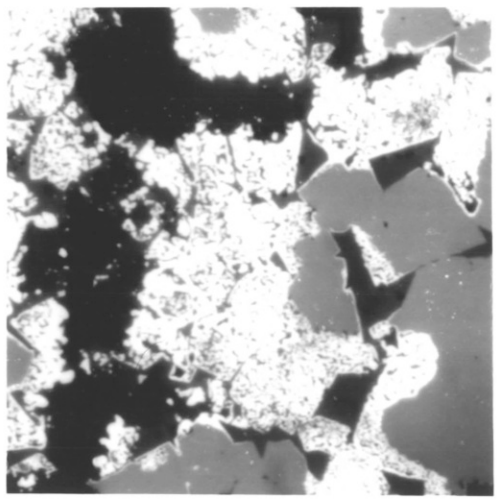

f)

the intergranular spaces and because magnesiowustite is reduced more rapidly than wustite. This latter effect is mostly due to the ease of iron nucleation over the whole surface.

Finally dolomite additions were studied with the hope that the lime would tie the silica while the magnesia would be associated with iron oxide and assist reduction. Essentially dolomite additions produced effects which can be related to both lime and magnesia. A liquid phase is formed during sintering but its composition lies in the $CaO-MgO-Fe_2O_3-SiO_2$ phase field. EPMA analysis indicates that the concentration of magnesia is small. In addition magnesioferrite grains are produced. Of particular interest is the observation of magnesioferrite grains which are crystallized from this liquid phase. Upon wustite formation at 1100°C, the formation of another liquid in the $CaO-MgO-FeO-SiO_2$ system is observed and produces similar effects to the corresponding liquid in the lime system. Upon reduction a series of quaternary and ternary phases is observed which were crystallized from the glass and then changed as iron oxide was reduced.

The sintering temperature for dolomite additions was shown to have a significant effect on the rate of reduction especially when liquid phase formation is formed.

The results of the present investigation indicate that flux additions in which a liquid phase is formed on sintering create problems on the reducibility of this ore at temperatures below about 1000°C. It is perhaps significant that this is broadly the temperature of the thermal

reserve zone in the blast furnace where wustite is starting to be reduced to iron. Better reducibility with flux additions can be obtained by avoiding liquid phase sintering, thus this will only be achieved by some sacrifice in strength. For good blast furnace operation, these conditions must be balanced.

It is felt that the present investigation has been rewarding in that a contribution has been made to the understanding of the role of flux additions especially the metallographic and structural aspects. It has been possible to correlate some of these aspects with variations in the rate of reduction. Sufficient information has been gathered to indicate that kinetic investigations must be carried out in conjunction with metallography, structural identification and microanalysis if a complete, understanding is to be achieved. Unfortunately this thesis like so many others, does not give a complete picture but it is considered that some progress has been made.

PLATE 48

Micro-structure of wustite grains reduced in CO/CO_2=1 for 6 hours at a)950°C , b)1050°C and c)1100°C.

The starting materials used were CaO 5% added compacts.

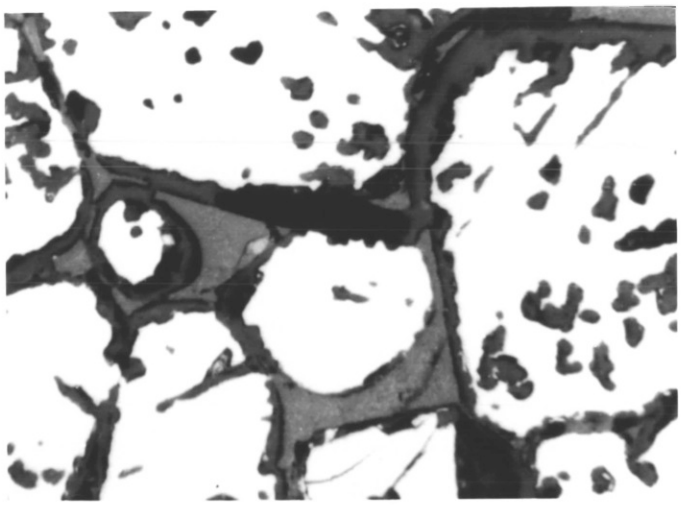

white(light grey) : wustite

grey : wollastonite (The colour was getting darker by the increasing amount of FeO dissolved).

black : voids

a) x 320

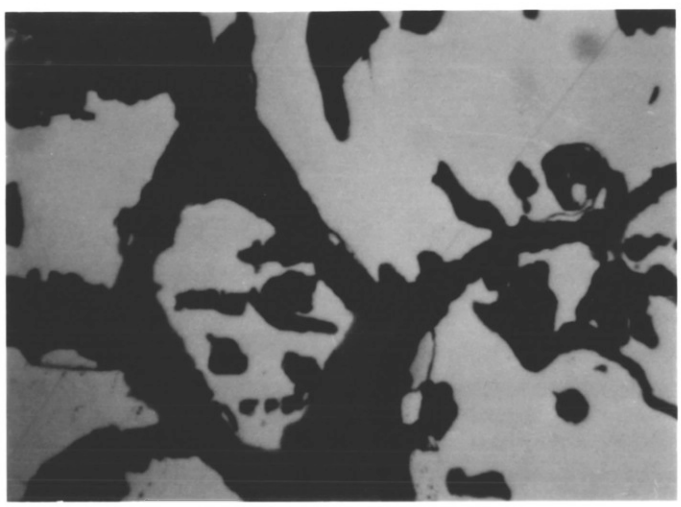

b) x 320

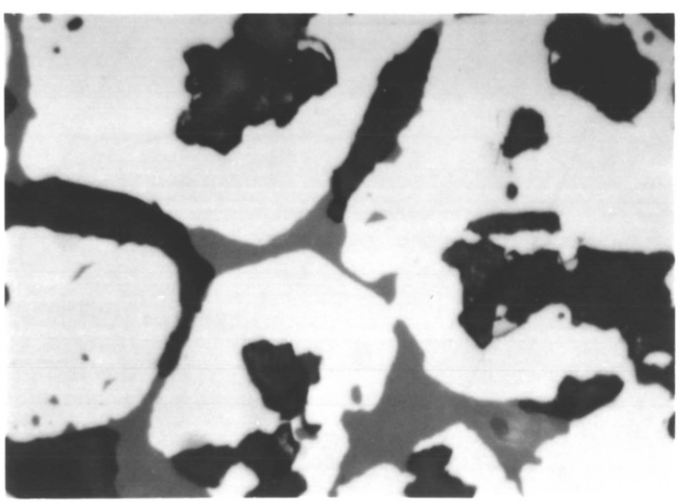

c) x 320

CHAPTER 5

CONCLUSIONS

CHAPTER 5

CONCLUSIONS

On the basis of the experimental results the following conclusions can be drawn

1. The reduction rate at low temperature with Carol Lake iron ore powder is slightly lower than that with compacted iron ore because of factors involved in the early stage of sintering during preparation of wustite at higher temperatures.

2. In the reduction of iron ore powder, the reduction rates show two distinct groups and indicate that a distinct change in mechanism occurred between 950°C and 1050°C.

3. The reduction at 950°C with iron ore compacts shows a linear rate of reduction caused by the formation of a thick iron layer on the surface of wustite and leads to the reduction being controlled by oxygen diffusion through the dense iron layer.

4. Calcium ferrite was not observed during reduction with lime addition compacts but wollastonite and kirschsteinite appeared by preferential reaction between lime and silica.

5. The reduction rate decreased significantly with low temperature reduction of 1 and 2% lime additions compacts by forming a liquid phase, during preparation

of wustite at 1100°C, blocking the pores in the following reduction. 5% lime additions increase the liquidus temperature and forms no liquid phase during reduction.

6. A small increase in reduction rate is related to the presence of CaO in solid solution in the wustite phase.

7. Magnesioferrite was formed during sintering and on reduction on adding MgO to the compacts. This phase seems to promote easy nucleation of iron possibly related to the tendency of magnesia to segregate leaving a thin film of reactive hematite to form at the surface.

8. The magnesioferrite grains reduce rapidly with the formation of a dense iron shell at the outside of each grain(4-5 μm) and significant carbon deposition occurs in the specimens(especially with 5% MgO addition) before complete reduction is achieved due to the formation of the dense iron layer around unreduced magnesiowustite particles.

9. Magnesioferrite grains which are crystallized from the liquid phase(Augite, $CaO-MgO-Fe_2O_3-SiO_2$ phase field) with dolomite additions show peculiar MgO behaviour due to the diffusion of MgO from the surface of the iron shell formed.

10. Transformation of cristobalite was observed during reduction except with lime and dolomite additions and this is considered to be related to the presence of iron oxide impurity and oxygen potential.

REFERENCES

1. J.O.Edstrom JISI Nov 1953 289-304

2. W.M.McKewan Trans. AIME Vol 218 1960 2-6

3. W.M.McKewan Trans. AIME Vol 224 1962 387-393

4. M.Ridgion JISI May 1962 389-399

5. N.A.Warner Trans. AIME Vol 230 1964 163-176

6. R.H.Spitzer, F.S.Manning and W.O.Philbrook Trans. AIME Vol 236 1966 726-742

7. B.B.L.Seth and H.U.Ross Trans. AIME Vol 233 1965 180-185

8. Y.Ono Trans. ISIJ Vol 8 1968 377-381

9. Von Bogdandy and H.J.Engell The Reduction of Iron ores Springer Verlog New York 1967

10. W.M.McKewan Trans AIME Vol 212 1958 791

11. R.H.Spitzer, F.S.Manning and W.O.Philbrook Trans. AIME Vol 242 1968 618-625

12. E.T.Turkdogan and J.V.Vinters Metallurgical Transactions Vol 2 1971 3176-3188

13. E.T.Turkdogan and J.V.Vinters Metallurgical Transactions Vol 2 1971 3189-1396

14. E.T.Turkdogan and J.V.Vinters Metallurgical Transactions Vol 3 1972 1561-1574

15. Y.K.Rao Metallurgical Transactions Vol 2 1971 1439-1447

16. H.O.Lien, A.E.El-Mehairy and H.U.Ross JISI 1971 541-545

17. S.Y.Ezz and K.A.Shehata Trans. Inst. Min. Met 1973 c38-c45

18. Okura Tetsu-to-Hagane 1974 No 2 3-10

19. S.Kondo Tetsu-to-Hagane 1974 No 9 1261-1270

20. H.S.Lee Tetsu-to-Hagane 1975 No 15 3041-3049

21. J.Szejeky, M.Choudhary and Y.El-Tawil Metallurgical Transaction Vol 8B 1977 639-643

22. H.U.Ross Agglomeration 77 Chap. 19 336-355

23. E.T.Turkdogan Metallurgical Transactions Vol 9B 1978 163-179

24. Joseph.T.L Trans. AIME 1936 Vol 120 72-98

25. S.T.Rostovtsev and V.P.Zhohson Izvestiya vvz Chernaya Metallurgiya 1980(10) 5-8

26. Rokuro Kuwano Tetsu-to-Hagane 66 1980 No. 12 1622-1628

27. P.C.Hayes and P.Grieveson Vol 12B 1981 579-587

28. Wiberg.M Discussion of the Faraday society No 4 1948 23-233

29. I.Fujita. Trans. ISIT Vol 20 1980 547

30. Munekazu Ohmi Trans. ISIJ Vol22 1982 66-74

31. H.U.Ross Direct reduced Iron, Metal socity 1978 9-34

32. B.B.L.Seth JISI 1969 1104-1109

33. B.B.L.Seth and H.U.Ross Canadian Metallurgical Quarterly Vol 15 1966 315-328

34. S.Watanabe Sumitimo J 77 1965 323-330

35. R.H.Tien and E.T.Turkdogan Metallurgical Transaction Vol 3 1972 2039-2048

36. J,Szekely and H.Y.Sohn Gas-solid reaction Academic Press 1976

37. L.L.Van Reijen Delft Progress Report 1980 5 292-302

38. E.T.Turkdogan Can. Metallurgical Quarterly Vol 12 No 1 1973 9-21

39. H.U.Ross Can. Metallurgical Quarterly Vol 4 No 1 1965 97-111

40. R.L.Bleifuss Trans AIME 247 225-231 1970

41. B.G.Baldwin JISI 1954 312-316

42. El-Geassy and S.Y.Ezz Iron and Steel International 1977 329-332

43. J.Burgess B.H.P CRL internal report Effect of burden softening temperature on B.F gas distribution 1979

44. P.C.Hayes and P.Grieveson British Steel Corp. Research Fellowship final report 1975

45. A.Muan Trans. AIME Vol 218 1960 1112-1119

46. E.T.Turkdogan Trans. AIME Vol 221 1961 546-553

47. P.C.Hayes Unpublished re rt 1982

48. L.Himmel and R.F.Mehl J.Metalls 5 1953 827-843

49. H.K.Kohl and H.J.Engell Arch Eisenhuttenwes 34 1963 411-418

50. C.Wagner Ztsch. fur physikalische

51. S.Rosenberg Arch. Eisenhuttenwes 44 1973 No 9 637-649

52. J.Harkki Helsinki University of Technology Inst. of Process Metallurgy B11-B13

53. L.S.Darken and R.W.Gruuy J.Am.Chem. Soc. 1945 Vol 67

54. I.Fujita Agglomeration 77 Chap.44

55. Y.Iguchi Tetsu-to-Hagane 65 1979 No 12 1692-1701

56. J.O.Edstrom and G.Bitsianes Trans. AIME 1955 760-765

57. A.Poos and A.Decker CRM Report(second part) 1968

58. A.Poss and A.Decker CRM Report(third part) 1968

59. M.Tigerschiold JISI 177 1954 13-24

60. K.Sato Tetsu-to-Hagane 55 1969 No 13 1107-1118

61. R.Isumi Iron making Research 272 1971 1-22

62. J.O.Edstrom Jernkontorets Ann. 1956 Vol 140

63. H.von Ende and K.Grebe Stahl U. Eisen 91 815 1971

64. A.Muan, E.F.Osborn Phase equilibria among oxides in steel making Pergamon Press Ltd. 1965

65. L.G.Berry Element of Mineralogy Freeman and Co.1968

66. F.Matsuno Tetsu-to-Hagane 64 1978 No 10 1499-1508

67. I.Fujita Tetsu-to-Hagane 66 1980 No 1 1830-1839

68. M.Sasaki Tetsu-to-Hagane 59 1973 No 9 1209-1217

69. K.S.Goto Metallurgical Transaction B Vol 12B 1981 449-454

70. I.Fujita Tetsu-to-Hagane 66 1980 No 13 1840-1849

71. S.E.Khalafallaand Weston Trans. AIME Vol 239 Oct. 1967 1494-1499

72. A.Schneider Arch. Eisenhuttenwes 50 1979 No 7 283-288

73. I.Fulita Tetsu-to-Hagane 66 1980 Nol 1830-1839

74. E.Overkett and J.Willems Stahl u. Eisen 18 Sept. 1966 1122

75. A.G.Verduch Journal of the American Ceramic Society Vol 41 No 11 1958 427-432

76. K.Kunii Tetsu-to-Hagne 52 No 9 1966 1364

77. K.Narita Trans ISIJ Vol 21 1981 862-869

78. K.Kanbara Tetsu-to-Hagane 52 No 9 1966 1348

79. I.Fujita Tetsu-to-Hagane 66(1980) No 13 1840-1849

80. M.Sasaki Tetsu-to-Hagane 59(1973) No 9 1209-1217

81. R.Isumi Iron making research 272 1971 1-22

82. J.Berggren Scan J. Met. 4 75 140 1975

83. David H.Speidel Journal of the American Ceramic Society 1976 Vol 50 No 5

84. John J. Friel et al Metallurgical Transactions B Vol 1113 1980 233-243

85. S.K.Gupta Ph D Thesis Uni.of London 1982

86. C.E.Wicks and F.E.Block Bulletin 605 Bureau of Mines United States Government Printing Office.

ACKNOWLEDGEMENT

I wish to express my sincere gratitude with my every words to my supervisor, Professor P.Grieveson for his excellent supervision, most useful discussions and encouragement throughout the course of this work.

I am also glad to acknowledge the helpful suggestions that I have had with Dr.P.Rogers.

I wish to thank Mr.M.Andrews for his ready help, Miss.P.Martins and her staff for the production of numerous plates.
I also wish to express my thanks to my collegues of the John Percy Research Group for valuable discussion. In particular, I am grateful to Mr.A.Jha for his interest and suggestions.

I would like to thank Pohang Iron and Steel Company for financial support and generous approval for my study.

Finally, I am indebted to my father-in-law who died during my studying, my parents, my wife, my mother-in-law and all members of my family, especially Mr.J.W.Hwang for their unending moral support throughout the entire duration of the project.